CATALYTIC OXIDATION OF SULFUR DIOXIDE BY HETEROGENEOUS COBALT-PHTHALOCYANINE

Thesis by

Pui-Kwan Andrew Hong

In Partial Fulfillment of the Requirements

for the Degree of

Doctor of Philosophy

California Institute of Technology

Pasadena, California

1988

(Submitted August 3, 1987)

ACKNOWLEDGEMENTS

I shall always remember my greatest advisor, Michael Hoffmann, who allowed me lots of freedom to pursue what interested me, supported me all the way throughout my graduate education, guided me when I side-tracked. I shall never forget many others who helped me. And in particular, I want to thank Detlef Bahnemann, Scott Boyce, Kit-Yin Ng, Dana Roth, and Sylvia Yuen.

Support for this work was provided by the U.S. Environmental Protection Agency.

ABSTRACT

Various homogeneous and hybrid cobalt phthalocyanines were developed. They were shown to be effective catalysts for the catalytic degradation of many aqueous pollutants. The catalytic activity of these systems was attributed to their ability to activate molecular oxygen. Semiconductor titanium dioxide was found to be useful both as solid support and photocatalyst. The electron relay property of cobalt phthalocyanine on the photoactive TiO_2 surface was elucidated. The homogeneous and heterogeneous kinetics and mechanisms for the catalytic oxidation of aqueous sulfur dioxide were studied.

TABLE OF CONTENTS

LIST OF FIGURES

LIST OF TABLES

LIST OF REFERENCES

Chapter 1

Overview

The removal of organic and inorganic pollutants from industrial and domestic wastewater effluents, contaminated soils, and groundwater is currently of great concern. Even though high-temperature incineration and microbial degradation are seen as alternatives, chemical oxidation remains the primary pathway for the degradation of many undesirable substances. However, oxidation of pollutants by strong oxidants such as chlorine, ozone, hydrogen peroxide, and permanganate is cost-intensive and in many cases these reagents are inherently hazardous. Oxidation by molecular O_2, which is readily available, appears to be both cost-effective and safe. However, autoxidation (i.e., the reaction of reductants with molecular O_2) is generally slow in the absence of catalysis. The kinetic limitations can be understood from the standpoint of electronic spin-state restrictions. In the ground state of $O_2(^3\Sigma_g^-)$, two electrons of parallel spin occupy each of the two degenerate π-antibonding valence orbitals. Conversely, the ground-state valence electrons of most inorganic and virtually all organic compounds conform to spin multiplicities of zero. Therefore, to surmount the activation energy barrier and hence achieve desirable reaction kinetics, the electronic configurations of reductants and/or oxygen must be altered. This is generally achieved through catalysis.

Homogeneous metal-phthalocyanine complexes have been shown to be effective catalysts for the autoxidation of a variety of substrates such as aldehydes, aromatic hydrocarbons, ascorbic acid, hydrazine, hydroxylamine, hydrogen sulfide, mercaptans, phenols, and sulfur dioxide.[1] As a frame of reference, we refer to a homogeneous catalyst as a catalyst that is soluble in the aqueous phase. However, a major

disadvantage associated with homogeneous catalysis involves the problem of separating the catalyst from the reaction medium following the desired reactions. This drawback may be overcome by attachment of the catalyst to the surface of a solid support. In this case, hybrid catalysts can be recovered by coarse filtration. We shall use the term "heterogeneous" or "hybrid" catalyst to refer to a catalyst supported on an insoluble solid substrate.

The principal objectives of this research were to develop catalytic systems suitable for the oxidative degradation of aqueous pollutants and to investigate the kinetics and mechanisms of these systems. Particular emphasis has been directed toward supported catalysts capable of activating molecular O_2 and/or reductants and to the understanding of the resulting physico-chemical processes. In particular, the catalyzed autoxidation of sulfur(IV) to sulfur(VI) with homogeneous and hybrid catalysts has been studied in detail.

Pathways for S(IV) oxidation are of great interest because of the important role that SO_2 plays in cloud-, fog-, rainwater acidification.[2] The oxidation of aquated sulfur dioxide (Eq. 1) is known to proceed via either 1-electron radical or 2-electron non-radical pathways.

$$HSO_3^- + \frac{1}{2} O_2 \longrightarrow HSO_4^- \qquad (1)$$

Backstrom proposed the following free-radical chain mechanism for metal-catalyzed autoxidation of S(IV):[3]

$$M^{n+} + SO_3^{2-} \longrightarrow M^{(n-1)+} + SO_3^{\cdot -} \qquad (2)$$

$$SO_3^{\cdot -} + O_2 \longrightarrow SO_5^{\cdot -} \qquad (3)$$

$$SO_5^{\cdot -} + SO_3^{2-} \longrightarrow SO_5^{2-} + SO_3^{\cdot -} \qquad (4)$$

$$SO_5^{2-} + SO_3^{2-} \longrightarrow 2SO_4^{2-} \qquad (5)$$

$$2SO_3^{\cdot -} \longrightarrow S_2O_6^{2-} \qquad (6)$$

This mechanism has been modified by others to account for photolytic initiation or to include other chain carriers such as $SO_4^{\cdot -}$, $O_2^{\cdot -}$, $HO_2^{\cdot}$, and $HO^{\cdot}$.[4] Non-radical mechanisms have also been proposed; they involve the formation of an inner-sphere complex as a prelude to 2-electron transfer oxidation of S(IV):[5]

$$M^{n+} + SO_3^{2-} \rightleftharpoons MSO_3^{(n-2)+} \qquad (7)$$

$$MSO_3^{(n-2)+} + SO_3^{2-} \rightleftharpoons M(SO_3)_2^{(n-4)+} \qquad (8)$$

$$M(SO_3)_2^{(n-4)+} + O_2 \rightleftharpoons M(SO_3)_2O_2^{(n-4)+} \qquad (9)$$

$$M(SO_3)_2.O_2^{(n-4)+} \longrightarrow M^{n+} + 2SO_4^{2-} \qquad (10)$$

Two-electron oxidation of S(IV) has also been observed with oxidants such as H_2O_2 and O_3:[6]

$$HSO_3^- + H_2O_2 \longrightarrow H^+ + SO_4^{2-} + H_2O \qquad (11)$$

$$HSO_3^- + O_3 \longrightarrow H^+ + SO_4^{2-} + O_2 \qquad (12)$$

In general, there are large discrepancies in the reported reaction orders of the reactants and in the observed rate laws for metal-catalyzed S(IV) autoxidation.[2,7]

Metal-phthalocyanine complexes, because of their well-defined geometry and chemical behavior, have been used in this work as an active homogeneous catalyst for the autoxidation of S(IV). Because of its reversibility in binding reductants and molecular oxygen, $Co^{II}TSP$ is found to be the most active catalyst and is the focus of further kinetic and mechanistic studies. The $Co^{II}TSP$ complex has been subsequently attached to solid supports such as silica gel, polystyrene/divinylbenzene copolymer, and titanium dioxide surfaces. The resulting hybrid catalysts are shown to be, as their homogeneous counterparts are, catalytically effective for the oxidation of a variety of substrates.

Autoxidation via heterogeneous catalysis inevitably involves physical processes such as adsorption-desorption, pore diffusion in a permeable solid, in addition to the chemical steps. In order to investigate the complex kinetics involved in heterogeneous catalysis, it is important to first elucidate the homogeneous kinetics; perturbation due to physical processes can then be included. Both homogeneous and heterogeneous kinetics and mechanisms are presented in this thesis. Chapters 2 to 4 discuss homogeneous pathways and Chapters 5 to 7 address heterogeneous ones including photo-assisted processes.

Chapter 2 presents the results of homogeneous autoxidation of aquated sulfur dioxide as catalyzed by various transition metal-phthalocyanines. The order of catalytic activity among different metal complexes (i.e. $Co^{II} > Fe^{II} > Mn^{II} > V^{IV} \simeq Ni^{II} \simeq Cu^{II}$) follows a trend that reflects the relative capacity of the complex's central metal atom to bind molecular O_2 reversibly. An ordered-ternary complex model for S(IV) oxidation is proposed. In this mechanism, the sulfito-cobalt(III)-superoxide complex, $(SO_3)Co^{III}TSP(O_2^{\cdot -})^{4-}$, forms when monomeric Co(II)TSP binds, with each of its two apical coordination sites, one sulfite and one oxygen molecule. This reactive complex subsequently adds on an additional sulfite molecule to form the ternary activated complex, $(SO_3)Co^{III}TSP(O_2^{\cdot -})(SO_3)^{6-}$. The rate-limiting step involves a two-electron transfer from the second sulfite molecule to the sulfito-cobalt(III)-superoxide system while one electron shuttles back from oxygen to the metal center, followed by hydrolysis to yield S(VI) and a sulfito-cobalt(II)-peroxide. The catalytic sequence is closed by the release of peroxide to solution as H_2O_2.

The results of S(IV) oxidation under very low catalyst concentration ([CoTSP]=0.25 μM) show a pronounced induction period, followed by rapid depletion of the substrate. This behavior suggests a free-radical pathway. However, spectrophotometric and ESR methods have been employed to verify the 2-electron transfer mechanism proposed in Chapter 2. The results of these studies are presented in Chapter 3. The induction period is found to correspond to the formation of the active $(SO_3)Co^{III}TSP(O_2^{\cdot -})^{4-}$ complex in the beginning of the reaction. The depletion rate of S(IV) increases as the active complex is formed; the rate reaches a maximum when the active complex has built up to its

highest concentration. After this point, the reaction can simply be described as a bimolecular reaction between the active complex and the S(IV) molecule. The findings support the proposed mechanism and suggest that the active complex reacts with a second sulfite ion without the formation of a ternary activated complex of sufficiently long life to be kinetically significant. Direct evidence for the active complex is obtained from both spectrophotometric and ESR measurements.

Chapter 4 attempts to relate laboratory kinetics to the oxidation of atmospheric SO_2. SO_2 is released to the atmosphere primarily during fuel combustion processes, and until recently has been thought to be removed by oxidation through homogeneous gas-phase reactions involving hydroxyl ($HO^{\cdot}$) and hydroperoxyl ($HO_2^{\cdot}$) radicals. However, the rates of these reactions are not sufficiently fast to explain the high formation rate of sulfate, especially under humid conditions and at night when little radical species can be photolytically generated. These discrepancies have led to the recognition of an additional non-photolytic pathway for S(IV) oxidation occurring in a condensed phase such as fog and clouds.[8] In liquid aerosol systems, it is of interest that dissolved organic molecules may act as complexing agents for metal. For example, benzoic acid and 2-hydroxybenzoic acid, which are liquid-phase autoxidation products of benzaldehyde and 2-hydroxybenzaldehyde, respectively, are suitable complexing agents. In the presence of trace transition metals (e.g., Fe, Zn), the resulting metal-organic chelates may provide, in a fashion parallel to CoTSP, active centers for the activation of molecular O_2; this would result in the non-photolytic production of H_2O_2, $HO_2^{\cdot}$, and $HO^{\cdot}$ and hence would add to the complex interrelated network of SO_2 oxidation in the atmosphere.

The preceding chapters concentrated on elucidating the catalytic activity of the homogeneous complexes. Based on these findings, the remainder of the thesis is devoted to understanding heterogeneous kinetics and mechanisms. Chapter 5 reports on the reactivities of silica gel and polystyrene/divinylbenzene copolymer-supported Co(II)-phthalocyanine catalysts. These hybrid organometallic complexes are shown to be effective catalysts toward the autoxidation of various reductants such as sulfur dioxide, sulfide, mercaptoethanol, cysteine, and hydrazine. Elements of heterogeneous catalysis in permeable solids, which involve physical pore diffusion in addition to chemical reaction steps, are considered and integrated to build an analytical model. The hybrid metal complexes showed lower catalytic activity than their homogeneous analogs; this was attributed to diffusion limitations within internal pores. Furthermore, the relative efficiency of various catalysts, which are linked to the surface either through direct complexation of the metal center or through covalent bonding of a peripheral group on the macrocyclic ligand, indicated the relative capacity of the hybrid complexes to activate molecular oxygen; this ability depends on the nature of the complexing ligand located trans to dioxygen. The hybrid catalysts have been shown to retain their catalytic activity for longer periods of time than their homogeneous counterparts.

Chapters 6 and 7 examine the photo-catalytic aspects of some of our heterogeneous catalysts. The hybrid catalyst used is Co(II)TSP covalently linked to the surface of a photoactive semiconductor such as titanium dioxide. Upon absorption of a photon with energy that exceeds the band-gap energy ($\lambda \leq 380$ nm for TiO_2), an electron from the filled

valence band of the semiconductor is promoted to the empty conduction band, leaving behind a hole in the valence band. The result is the separation of charges with redox potential E = -0.2 V for the conduction band electron and E = 3.0 V for the valence band hole. In principle, this potential energy can be utilized in driving redox reactions on the particle surface. However, in the absence of electron or hole scavengers, the recombination of the separated charges is very fast; this often results in a low quantum efficiency for redox reactions. The role of CoTSP on a TiO_2 surface is to function as an electron relay. The CoTSP complex, because of its ability to reversibly undergo multiple oxidation state changes, can capture the conduction band electron as created, thus leaving a hole available for oxidation of a substrate. Robust, inexpensive, and non-toxic TiO_2 solid not only provides a support for CoTSP, but also offers potential means of exploiting readily available near-UV irradiation in the oxidative degradation of hazardous pollutants.

Chapter 6 reports on the novel synthesis, characterization, and reactivity of the hybrid catalyst, TiO_2-CoTSP. Upon irradiation with band-gap energy, the hybrid catalyst changes from its original blue color to yellow under anoxic conditions both as dry powder and in aqueous suspension. This indicates that the surface bound Co(II)TSP is reduced to Co(I)TSP by the photo-generated conduction band electron. The photochemical reduction is fully reversible in the presence of molecular oxygen. Hydrogen peroxide is produced upon illumination of an aerated aqueous suspension of the hybrid catalyst. H_2O_2 is formed by molecular O_2 that is coordinated to the metal center of CoTSP and is subsequently reduced by conduction band electrons. In addition,

indirect evidence suggests that H_2O_2 forms via the oxidation of H_2O by holes. Under prolonged irradiation, H_2O_2 concentration reaches a limiting value; this steady-state concentration arises because of destruction. H_2O_2 can be further reduced to H_2O at CoTSP sites or further oxidized to O_2 by valence holes. Quantum yields for O_2 reduction approach unity and indicate that the hybrid electron relay system is extremely active. Furthermore, the hybrid catalyst fully retains its reactivity after prolonged exposure to extreme alkaline and acidic conditions. Due to its high quantum efficiency and chemical stability, TiO_2-CoTSP appears to be a potent oxidation catalyst.

Chapter 7 presents the kinetics and mechanisms of the photocatalytic oxidation of S(IV) with hybrid TiO_2-CoTSP in aqueous suspension. Upon band-gap illumination of the semiconductor, TiO_2, conduction band electrons and valence band holes are separated; the electrons are channeled to the bound Co(II)TSP complex, resulting in the reduction of dioxygen while the holes react with adsorbed S(IV) to produce S(VI) in the form of sulfate. The involvement of S(V) radicals indicates that the reaction proceeds via successive one-electron transfers. Quantum yields in excess of unity were observed and attributed to the desorption of $SO_3^{\cdot -}$ from the TiO_2 surface and subsequent initiation of a homogeneous free-radical chain reaction. The two-electron oxidation mechanism, which was established previously for the homogeneous case, operates at CoTSP sites but with smaller significance when compared to the solution phase chain reaction. A complex heterogeneous kinetic model is formulated to blend together processes such as photon absorption by the solid, species adsorption to the surface, redox reactions on the surface, 2-electron oxidation of

S(IV) at CoTSP sites, and 1-electron free radical chain reactions in solution. This model is then verified experimentally. The principal objectives of this chapter are to provide further insight into the photochemical properties of TiO_2-CoTSP hybrid catalyst and to examine in greater detail the mechanisms for the heterogeneous photocatalytic oxidation of S(IV).

Hybrid photocatalysts such as TiO_2-CoTSP possess great potential for degradation of undesirable contaminants. As $CHCl_3$ oxidation experiments show, the valence hole of TiO_2 is an extremely powerful oxidant for polychlorinated hydrocarbons. By-product H_2O_2 that results from photo-reduction of O_2 is also very effective in this regard.

References

1. References 3-14 cited in Chapter 5.

2. (a) Jacob, D.; Hoffmann, M. *J. Geophys. Res.* **1983**, 88, 6611.

   (b) Hoffmann, M.; Jacob, D. In *Acid Precipitation: SO_2, NO, and NO_x Oxidation Mechanisms: Atmospheric Considerations*, Calvert, J. Ed.; Butterworth: Boston, 1984; p. 101.

3. Backstrom, H. *Z. Phys. Chem.* **1934**, *25B*, 122.

4. (a) Hayon, E.; Treinin, A.; Wilf, J. *J. Am. Chem. Soc.* **1972**, 94, 47.

   (b) Huie, R.; Neta, P. *Environmental Health Perspectives*, **1985**, 64, 209.

   (c) Huie, R.; Neta, P. *J. Phys. Chem.* **1984**, 88, 5665.

   (d) McElroy, W. *Atmos. Environ.* **1986**, 20, 323.

5. (a) Bassett, J.; Parker, W. *J. Chem. Soc.* **1951**, 1540.

   (b) Freiberg, J. *Atmos. Environ.* **1975**, 9, 661.

6. (a) Hoffmann, M.; Edwards, J. *J. Phys. Chem.* **1975**, 79, 2096.

   (b) McArdle, J.; Hoffmann, M. *J. Phys. Chem.* **1983**, 87, 5425.

   (c) Hoffmann, M. *Atmos. Environ.* **1986**, 20, 1145.

7. (a) Hoffmann, M.; Boyce, S. In *Advances in Environmental Science and Technology*, Vol. 12, Schwartz, S. Ed.; John Wiley & Sons: New York, 1983, p. 147. And references cited therein.

   (b) References 1-24 cited in Chapter 2.

8. Jacob, D. J. Report No. AC-2-85; California Institute of Technology: Pasadena, CA, 1985.

Chapter 2

Catalysis of the Autoxidation of Aquated Sulfur Dioxide by Homogeneous Metal Phthalocyanine Complexes

Scott Boyce, Michael Hoffmann, Andrew Hong, Lorraine Moberly

Environ. Sci. Tech. 1983, 17, 602-611.

Catalysis of the Autoxidation of Aquated Sulfur Dioxide by Homogeneous Metal–Phthalocyanine Complexes

Scott D. Boyce, Michael R. Hoffmann,* P. Andrew Hong, and Lorraine M. Moberly

Department of Environmental Engineering Science, W. M. Keck Laboratories, California Institute of Technology, Pasadena, California 91125

■ The autoxidation of sulfur dioxide to sulfate in aqueous solution has been examined over the pH range 4–13 in the presence of water-soluble transition metal-4,4′,4″,4‴-tetrasulfophthalocyanine complexes, MTSP (where M = Fe^{II}, Mn^{II}, Co^{II}, Ni^{II}, Cu^{II}, and V^{IV}). Experimental rate data have been analyzed in terms of a Michaelis–Menten kinetic expression derived from a bisubstrate kinetic model. The rate law and spectroscopic measurements indicate that the reaction proceeds via the formation of an activated complex in which O_2 and two molecules of SO_3^{2-} are reversibly bonded to the catalytic center. Relative reactivity is determined by the ability of the central metal atom to reversibly bind molecular oxygen. Analysis of the spectroscopic data suggests that photoassisted catalysis arises from the absorption of light by a ternary activated complex.

Introduction

Numerous attempts have been made to characterize the kinetics and mechanisms of the metal-catalyzed autoxidation of sulfur dioxide in aqueous solution (*1–20*). Results obtained from previous studies show considerable disagreement as to the rate, rate law, and pH dependence of this reaction (*21–24*). The reaction rate is sensitive to catalysis by a wide variety of transition-metal ions such as Mn^{2+}, Fe^{3+}, Co^{2+}/Co^{3+}, and Cu^{2+}. The catalytic autoxidation of SO_2 dissolved in atmospheric water droplets represents a viable pathway for the formation of sulfate (*25*), while oxygenation of S^{IV} in aquatic environments plays a fundamental role in the natural sulfur cycle (*26, 27*).

Hoffmann and Jacob (*28*) describe in detail inconsistencies reported by other investigators. There is general agreement that the homogeneous reaction rate exhibits a zero-order dependence on $[O_2]$, but observed kinetic orders in substrate and metal-ion concentration vary from zero to two for reactions carried out under similar concentration conditions. The majority of experimental data indicates that the kinetics of sulfite oxidation conform to a simple empirical rate law which is first order in both $[S^{IV}]$ and $[M^{n+}]$. However, Barron and co-workers (*2, 5*), Bengtsson and Bjerle (*3*), and Mishra and Srivastava (*17, 18*) have each reported a nonintegral dependence on reductant (three-halves order) and catalyst (half order) concentration.

Three types of reaction mechanisms have been proposed to account for the catalytic activity of transition metals in solution. These mechanisms include free-radical chain processes involving a sequence of one-electron transfer steps following thermal initiation (*29*), heterolytic mechanisms in which metal–sulfite complexation precedes the inner-sphere transfer of two electrons from S^{IV} to oxygen (*30*), and photoassisted pathways whereby homolytic oxidation of sulfite is promoted through the absorption of light by either the substrate, the metal catalyst, or a metal–substrate adduct (*31–34*).

In order to investigate the reaction of aquated SO_2 with molecular oxygen in a well-defined catalytic system, water-soluble metal–phthalocyanine, M(PC), complexes were employed. Phthalocyanines are macrocyclic tetrapyrrole compounds that readily form square-planar complexes in which the metal center is bonded to the four pyrrole nitrogen atoms of the ligand as depicted in Figure 1. Cobalt(II)-4,4′,4″,4‴-tetrasulfophthalocyanine, Co^{II}-TSP, has been shown to be an effective catalyst for the autoxiation of hydrogen sulfide (*23*), cysteine (*35, 36*), hydrazine (*37*), and hydroxylamine (*38*). The properties of M(PC) derivatives have been compared to those of catalase, oxidase, and oxygenase enzymes (*36, 39–46*). The results of the current investigation should clarify several fundamental aspects of the mechanism for the catalytic autoxidation of S^{IV} in aqueous media. From a commerical standpoint, the oxidation of SO_2 and other S-containing reductants in the presence of either homogeneous or heterogeneous transition-metal complexes may provide convenient and economical methods for sulfur pollution control (*23, 47*).

Experimental Procedures

Materials. The monosodium salt of 4-sulfophthalic acid was obtained by neutralization of a 50% aqueous solution of 4-sulfophthalic acid (Eastman) with 15 N NaOH and purified by recrystallization from absolute ethanol. All other chemicals utilized in the preparation of the metal–phthalocyanine catalysts were of reagent grade.

Analyses. Microanalyses were performed by Galbraith Microanalytical Laboratories, Inc., of Knoxville, TN. ^1H NMR spectra were recorded on a Varian Model EM 390 nuclear magnetic resonance spectrometer.

Synthesis of Catalysts. The tetrasodium salt of cobalt(II)-4,4′,4″,4‴-tetrasulfophthalocyanine dihydrate, Co^{II}TSP, was synthesized from sodium 4-sulfophthalate, ammonium chloride, urea, ammonium molybdate, and cobalt(II) sulfate heptahydrate according to the procedure

 0013-936X/83/0917-0602$01.50/0

$$2SO_3^{2-} + O_2 \xrightarrow{\text{catalyst}} SO_4^{2-}$$

catalyst = M–4,4',4'',4'''–tetrasulfophthalocyanine

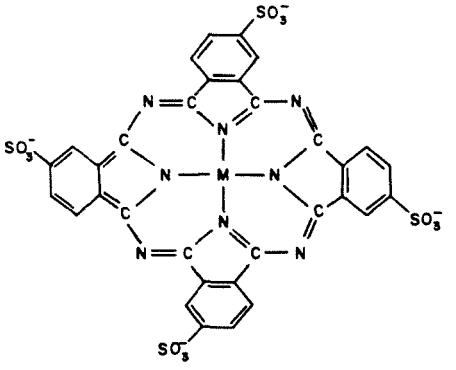

M = Fe^{II}, Mu^{II}, Co^{II}, Ni^{II}, Cu^{II}, V^{III}

Figure 1. Generalized stoichiometric relationship for the aqueous phase autoxidation of sulfite as catalyzed by homogeneous transition metal–phthalocyanine complexes.

described by Weber and Busch (*48*). The initial product was treated successively with NaCl, 0.1 N NaOH, and 80% aqueous ethanol in the prescribed manner. Pure Co^{II}TSP was obtained by extracting the solid with absolute ethanol for 4 h in a Soxhlet apparatus. The blue crystalline complex was then dried in vacuo over P_2O_5 prior to analysis.

Tetrasulfophthalocyanine complexes containing manganese(II), iron(II), nickel(II), copper(II), and vanadium(IV) were prepared from appropriate metal salts by using analogous procedures. The structure of each catalyst was characterized by elemental analysis and through a comparison of ^1H NMR and UV/VIS spectra with published reference data (*38*, *48*).

Buffers. Tris(hydroxymethyl)aminomethane hydrochloride (TRIS-HCl) (Sigma), 2-[[tris(hydroxymethyl)-methyl]amino]ethanesulfonic acid (TES) (Sigma), monobasic sodium phosphate (Mallinckrodt), dibasic sodium phosphate (Mallinckrodt), tribasic sodium phosphate (Mallinckrodt), sodium borate (Mallinckrodt), sodium chloride (Mallinckrodt), and sodium hydroxide (Mallinckrodt) were used to prepare the pH buffer solutions. Sodium perchlorate (G. Frederick Smith) was employed to maintain the ionic strength constant at μ = 0.4 M. Deionized water (18 MΩ cm resistivity) obtained from a Milli RO-4/Milli Q purification system (Millipore) was utilized in the preparation of all reagent solutions. The water was deoxygenated by purging with N_2 prior to the preparation of the Na_2SO_3 solutions.

Kinetic Data. Kinetic data were obtained from two different analytical procedures. In one set of experiments $[S^{IV}]$ was determined by monitoring the UV absorption spectrum (λ_{max} 212 nm) of the reaction solution as a function of time. Optical absorption data were collected with a Hewlett-Packard Model 8450A UV/vis spectrophotometer. The reactions were performed at 25 ± 1 °C directly in Teflon-stoppered quartz spectrophotometer cells (2- or 10-cm pathlength).

In another set of experiments, the oxidation of S^{IV} was followed by continuous measurement of changes in O_2 concentration as a function of time. Dissolved oxygen was determined potentiometrically by using an Orion Model 97-08-00 O_2 electrode coupled to an Orion Model 901 Ionanalyzer/Model 951 digital printer system. The pH of the reaction mixture was monitored simultaneously with an Orion Model 91-62 combination pH electrode. The dissolved oxygen and pH electrodes were interfaced to the Ionanalyzer through an Orion Model 605 electrode switch.

These reactions were conducted in a water-jacketed, glass and Teflon reactor with a total volume of 2.0 L. The design and operation of the batch reactor system have been described previously by Hoffmann and Lim (*47*). To minimize the potential catalytic effect of trace-metal contaminants, all glassware was washed with phosphate-free detergent (Alconox), soaked in 5.2 N HNO_3, and then rinsed several times with deionized water.

In a typical experiment, a 2.0 L volume of buffer solution containing the appropriate catalyst was transferred to the reactor system. Air (Matheson), oxygen (Matheson), or a controlled N_2/O_2 mixture was purged through the solution with constant stirring for 30 min. After saturation, the reaction was sealed from the atmosphere. A constant temperature of 25 (±0.1) °C was maintained by using a Haake Model FK-2 water circulation system and temperature controller.

To initiate the reaction, a known volume of a stock sulfite solution was added to the buffer/catalyst mixture. Sulfite concentrations, $[S^{IV}]$, ranged from 5×10^{-5} to 5×10^{-3} M. Dissolved oxygen varied from 2.5×10^{-4} to 1.2×10^{-3} M. Addition of the disodium salt of ethylenediaminetetraacetic acid (EDTA) (Sigma) reduced the potential catalytic effect of residual trace-metal contaminants during control reactions (*49*). Mannitol, sodium cyanide (NaCN), and EDTA were used selectively as free-radical and trace-metal inhibitors.

Analyses for sulfate were conducted by using the standard $BaCl_2$ turbidimetric procedure (*50*). Hydrogen peroxide was detected as a kinetic intermediate by measuring the decrease in the fluorescence intensity of scopoletin dye (6-methoxy-7-hydroxy-2*H*-1-benzopyran-2-one) in the presence of horseradish peroxidase as described by Perschke and Broda (*51*). Aliquots of the reaction solution were collected during the course of experiments for analysis of SO_4^{2-} and H_2O_2. Fluorescence spectra were recorded with an Aminco-Bowman spectrofluorometer.

Results

The reaction of sulfur dioxide with oxygen in aqueous solution proceeds according to the following stoichiometry:

$$2S^{IV} + O_2 \rightarrow 2S^{VI} \qquad (1)$$

where $[S^{IV}] = [SO_2 \cdot H_2O] + [HSO_3^-] + [SO_3^{2-}]$ and $[S^{VI}] = [H_2SO_4] + [HSO_4^-] + [SO_4^{2-}]$. Addition of water-soluble cobalt(II)–, iron(II)–, and manganese(II)–tetrasulfophthalocyanine complexes accelerated reaction 1 under neutral and alkaline pH conditions. Another frequently observed, but low-yield reaction product, is dithionate, $S_2O_6^{2-}$ (*52*). However, dithionate was not detected in any of the reaction solutions containing M^{II}TSP catalysts.

Reaction kinetics were studied under pseudo-order conditions with respect to substrate concentration (i.e., $[O_2]_0 \gg [S^{IV}]_0$) at constant pH and ionic strength. The observed rate constant, k_{obsd}, for each reaction was calculated from linear least-squares analyses of sulfite concentration $[\ln ([S^{IV}]_t/[S^{IV}]_0)]$ vs. time plots.

Reaction Orders. The kinetic data obtained from a typical series of experiments are summarized in Figure 2. At the principal wavelength for light absorption due to SO_3^{2-} (λ_{max} 212 nm), Beer's law ($A = \epsilon lc$) was found to be valid over a broad range in $[S^{IV}]$ as reported by Hayon and co-workers (*31*). Under the reaction conditions specified in Figure 2, the observed pseudo-first-order rate constants

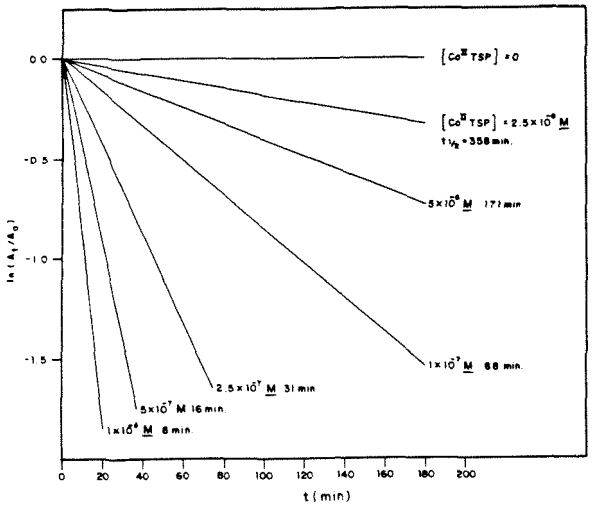

Figure 2. Pseudo-first-order plots of ln (A_t/A_0) (λ 212 nm) for the reaction of S^{IV} with O_2. $[S^{IV}]_0 = 1 \times 10^{-4}$ M, $[O_2]_0 = 1.2 \times 10^{-3}$ M, and $[Co^{II}TSP]_0 = 2.5 \times 10^{-8}$–$2.5 \times 10^{-6}$ M, pH 9.2 (borate buffer); $\mu = 0.4$ M, $T = 25 \pm 1$ °C.

ranged from 3.3×10^{-5} s^{-1} at $[Co^{II}TSP]_0 = 2.5 \times 10^{-8}$ M to 5.2×10^{-3} s^{-1} at $[Co^{II}TSP]_0 = 2.5 \times 10^{-6}$ M ($0.985 \leq R^2 \leq 0.999$). No decrease in $[S^{IV}]$ was observed after 12 h in the absence of catalyst. First-order kinetic behavior in total sulfite concentration was also observed for reactions carried out at pH 6.7 and over the entire pH range under study.

The linearity of ln (A_t/A_0) vs. time can be accepted as evidence of a first-order rate dependence on $[S^{IV}]$. Additional support for this conclusion was obtained from a series of experiments in which the rate of change of $[O_2]$ was monitored potentiometrically at different initial values of $[S^{IV}]$. The amperometric response of the O_2 electrode is a linear function of the dissolved oxygen concentration (*53*). Analysis of this data by the van't Hoff method of initial rates (*54*) confirmed that the reaction was nearly first order in reductant. For example, the slopes of linear plots of $-d[O_2]_0/dt$ vs. $[S^{IV}]_0$ were equal to 1.18 (R^2 = 0.9893) at pH 6.7 and 1.25 R^2 = 0.9580) at pH 9.2. A moderate degree of scatter in the experimental data could account for the values of greater than one. These results suggest that a potential source of variability in previously reported empirical rate laws for the oxidation of SO_2 may originate from the selective fitting of experimental measurements to a narrow range of concentration conditions.

The dissolved oxygen electrode response ($i_\infty \alpha [O_2]$) decreased linearly with time during reactions in which $[O_2]_0 \gg [S^{IV}]_0$. This observation indicated that the apparent reaction order in oxygen concentration was zero. Additional evidence of zero-order kinetic behavior was acquired through the spectrophotometric determination of k_{obsd} at a variety of initial oxidant concentrations (2.5×10^{-4} M $\leq [O_2]_0 \leq 1.2 \times 10^{-3}$ M). In this case, the observed first-order rate constants remained unchanged within the limits of experimental error (±5%). When the initial pseudo-order reaction conditions were adjusted in a fashion such that $[S^{IV}]_0 \gg [O_2]_0$, an apparent exponential decay in $[O_2]$ was observed. This result suggests a shift to a first-order rate dependence on oxygen when sulfite is in excess.

From a least-squares regression analysis of the rate data presented in Figure 2, the rate of oxidation of S^{IV} was determined to be first order in cobalt(II)–phthalocyanine over the concentration range 2.5×10^{-8} M $\leq [Co^{II}TSP]_0 \leq 2.5 \times 10^{-6}$ M. In contrast, the kinetic measurements

Table I. Effect of pH on k_{obsd}[a]

pH	buffer system	k_{obsd} (s^{-1})
4.1	0.1 M NaH_2PO_4 0.3 M $NaClO_4$	no reaction
6.7	0.1 M NaH_2PO_4 0.1 M Na_2HPO_4	2.56×10^{-4}
7.7	0.2 M TES 0.1 M NaOH 0.3 M $NaClO_4$	3.22×10^{-5}
8.4	0.1 M TRIS 0.1 M TRIS-HCl 0.3 M $NaClO_4$	4.53×10^{-5}
9.2	0.1 M NaB_4O_7 0.1 M $NaClO_4$	5.27×10^{-5}
10.1	0.1 M Na_2CO_3 0.1 M $NaHCO_3$	3.47×10^{-5}
11.5	0.044 M Na_2HPO_4 0.044 M Na_3PO_4	4.17×10^{-5}
12.9	0.1 M NaCl 0.1 M NaOH 0.2 M $NaClO_4$	7.03×10^{-5}

[a] $[S(IV)]_0 = 5 \times 10^{-5}$ M, $[O_2]_0 = 2.5 \times 10^{-4}$ M, and $[Co^{II}TSP]_0 = 1 \times 10^{-6}$ M; $\mu = 0.4$ M, $T = 25.0 \pm 0.1$ °C.

collected from reactions occurring in phosphate buffer or neutral pH showed a nonintegral rate dependence on $[Co^{II}TSP]_0$.

pH Dependency. A summary of the experimental rate data presented in Table I shows a complex pH dependency for the kinetics of S^{IV} oxidation. In general, the rate of reaction appeared to increase with increasing hydroxide concentration over the pH range 4–13. However, the observed trend is obscured by a number of secondary factors such as general-base catalysis and inhibition due to competitive complexation of buffering reagents such as TRIS and TES to cobalt(II). The increase in the reaction rate between pH 4.1 and pH 9.2 corresponds approximately to the acid dissociation of bisulfite ion to form SO_3^{2-} (pK_a = 6.7 at T = 20 °C and μ = 0.1 M) (*55*). As the fraction of S^{IV} present as sulfite increases, the rate of reaction is enhanced. This behavior suggests that SO_3^{2-} is the principal reactant species in aqueous solution.

In a related study, Hoffmann and Lim (*47*) reported that the rate of the autoxidation of HS^- in the presence of $Co^{II}TSP$ increased significantly under strongly alkaline conditions (pH 9–12). Acceleration of the reaction was attributed to the enhanced catalytic efficiency of the dioxygen complex $Co^{III}TSP(O_2^{-}\cdot)^{3-}$ [relative to $Co^{III}TSP(O_2^{-}\cdot)^{2-}$] formed by deprotonation of a pyrrole N atom of the phthalocyanine ligand. Boucher (*56*) recently suggested that coordination of O_2 by $Co^{II}TSP$ at high pH may be controlled by the acid dissociation of a water molecule attached to the metal center. With an increase in the pH of the reaction medium, the remaining solvent molecules within the coordination sphere of the cobalt–phthalocyanine complex are replaced by hydroxyl groups resulting in an enhancement of the stability of monomeric species such as $(HO)Co^{II}TSP^{3-}$ and $(HO)Co^{III}TSP(O_2^{-}\cdot)^{3-}$. From ligand field theory, the bonding of OH^-, a strong σ-electron donor, in an axial coordination site would raise the energy of the $3d_{z^2}$ $3d_{xz}$, and $3d_{yz}$ atomic orbitals on Co^{II} to a level which would promote stronger bonding with the π^*-molecular orbitals of appropriate symmetry on O_2 (*57*). This change in catalyst speciation may account for a further increase in the rate of sulfite oxidation by O_2 between pH 10 and 13.

Relative Reactivity of MTSP Complexes. The reactivity of $Co^{II}TSP$ is significantly greater than that of the other homogeneous phthalocyanine catalysts. According to the data presented in Table II, the order of catalytic

Table II. Effect of a Variation in the Central Metal Atom on the Rate of Autoxidation of S^{IV} [a]

metal-tetrasulfophthalocyanine	k_{obsd} (s^{-1}) × 10^4
Co^{II}	18.30
Fe^{II}	2.23
Mn^{II}	0.24
Cu^{II}	~0
Ni^{II}	~0
V^{IV}	~0

[a] $[S^{IV}]_0 = 1 \times 10^{-4}$ M, $[O_2]_0 = 1.2 \times 10^{-3}$ M, and $[MTSP]_0 = 1 \times 10^{-6}$ M, pH 9.2 (borate buffer); μ = 0.4 M, T = 25 ± 1 °C.

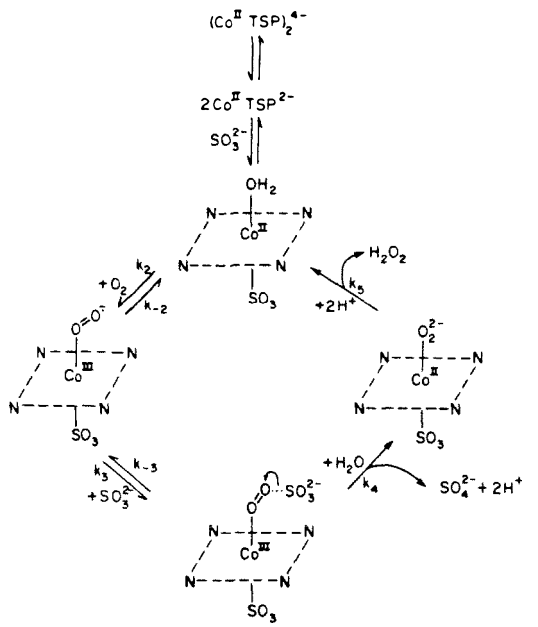

Figure 3. Schematic representation of the proposed bisubstrate complexation reaction mechanism for the catalytic autoxidation of sulfite in aqueous solution.

activity, $Co^{II} > Fe^{II} > Mn^{II} > V^{IV} \simeq Ni^{II} \simeq Cu^{II}$, follows a general sequence that reflects the relative capacity of each square-planar transition-metal complex to reversibly coordinate O_2 (*56*). Tetra- and pentacoordinate low-spin complexes of cobalt(II), iron(II), and manganese(II) have been shown to function as dioxygen carriers in organic and aqueous solvent systems (58, *59*), whereas square-planar nickel(II) ($3d^8$ low spin) and copper(II) ($3d^{10}$) derivatives do not form stable dioxygen adducts. Similar trends in the catalytic properties of metal–phthalocyanines have been reported previously by Kropf et al. (*60*, *61*) for the liquid-phase autoxidation of aromatic hydrocarbons and by Kothari and Tazuma (*62*) for the oxygenation of phenols.

Discussion

The catalytic activity of transition metal–phthalocyanine complexes in aqueous solution was documented initially by Cook (*39*, *40*) for the decomposition of H_2O_2 and the oxidation of HI, later by Wagnerova and co-workers (*35*, *37*, *38*) for the autoxidation of hydrazine, hydroxylamine, and cysteine, and by Hoffmann and Lim (*47*) for the oxidation of H_2S. These investigators suggested that the catalytic properties of metal–phthalocyanines were characteristic of an oxidase. Wagnernova et al. (*37*) reported that the kinetics of oxidation reactions catalyzed by

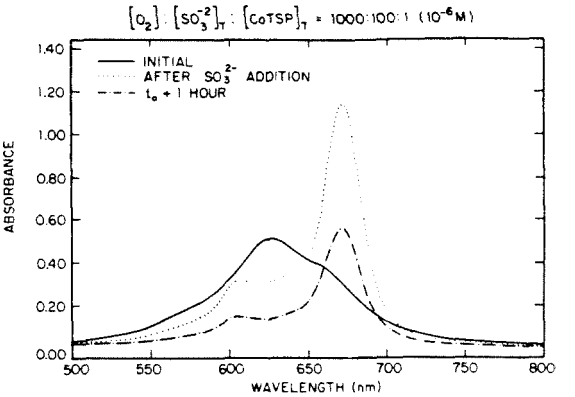

Figure 4. Changes in the visible absorption spectrum of $Co^{II}TSP$ during the catalytic autoxidation of sulfite. $[S^{IV}]_0 = 1 \times 10^{-4}$ M, $[O_2]_0 = 1.2 \times 10^{-3}$ M, and $[Co^{II}TSP]_0 = 1 \times 10^{-6}$ M, pH 6.7; μ = 0.4 M, T = 25 ± 1 °C.

$Co^{II}TSP$ conformed to a Michaelis–Menten rate law. The experimental evidence obtained in this study is indicative of enzymelike kinetics for the catalytic autoxidation of S^{IV}. A well-known characteristic of enzymatic reactions is the variability of reaction order with respect to the concentrations of substrate and catalyst (*63*). For example, the order in substrate can vary between zero and one. In order to interpret the observed reaction kinetics of sulfite oxidation within this framework, a bisubstrate complexation model has been proposed.

The mechanism proposed for the kinetics of the autoxidation of S^{IV} between pH 6.7 and pH 9.2 is an ordered-ternary complex pathway (*64*) which is depicted schematically in Figure 3 and consists of the following elementary steps:

$$(Co^{II}TSP)_2^{4-} \overset{K_d}{\rightleftharpoons} 2Co^{II}TSP^{2-} \quad (2)$$

$$Co^{II}TSP^{2-} + SO_3^{2-} \overset{K_1}{\rightleftharpoons} (SO_3)Co^{II}TSP^{4-} \quad (3)$$

$$(SO_3)Co^{II}TSP^{4-} + O_2 \underset{k_{-2}}{\overset{k_2}{\rightleftharpoons}} (SO_3)Co^{III}TSP(O_2^{-}\cdot)^{4-} \quad (4)$$

$$(SO_3)Co^{III}TSP(O_2^{-}\cdot)^{4-} + SO_3^{2-} \underset{k_{-3}}{\overset{k_3}{\rightleftharpoons}} (SO_3)Co^{III}TSP(O_2^{-}\cdot)(SO_3)^{6-} \quad (5)$$

$$(SO_3)Co^{III}TSP(O_2^{-}\cdot)(SO_3)^{6-} + H_2O \xrightarrow[\text{slow}]{k_4} (SO_3)Co^{II}TSP(O_2^{2-})^{6-} + SO_4^{2-} + 2H^+ \quad (6)$$

$$(SO_3)Co^{II}TSP(O_2^{2-})^{6-} + 2H^+ \xrightarrow[\text{rapid}]{k_5} (SO_3)Co^{II}TSP^{4-} + H_2O_2 \quad (7)$$

$$H_2O_2 + SO_3^{2-} \xrightarrow[\text{rapid}]{k_6} SO_4^{2-} + H_2O \quad (8)$$

The theoretical rate expression for this mechanism was derived by using the method of King and Altman (*65*), which is based on a standard determinant procedure for solving a system of nonhomogeneous linear equations. Reactions 2 and 3 represent the formation of the active catalytic center $(SO_3)Co^{II}TSP^{4-}$, from the dimer of cobalt(II)–phthalocyanine (*66*, *67*). This sequence of reactions is consistent with the observed changes in the spectrum of $Co^{II}TSP$ (Figure 4) that indicate a shift in the position of the monomer/dimer equilibrium, monomer (λ_{max} 636 nm)/dimer (λ_{max} 670 nm), upon coordination of a substrate molecule to the metal center at an axial pos-

ition either above or below the plane of the macrocyclic ring. Complexation of sulfite by $Co^{II}TSP$ in an axial coordination site enhances the subsequent uptake of molecular oxygen as written in eq 4. Carter et al. (*68*) have studied the reversible binding of dioxygen to cobalt(II) chelates of the general form $Co^{II}(L)(B)$ where L refers to a quadridentate Schiff base or porphyrin ligand and B designates an axial base. The authors concluded that as the π-electron-donating ability of B increased, the electron density on the cobalt atom would be enhanced and that this would, in turn, strengthen the "π-back-bonding" interaction between Co and O_2. Rollman and Chan (*69*) reported that the imidazole complex of $Co^{II}TSP$ underwent rapid reaction with O_2, whereas the corresponding pyridine derivative did not. Similar trends in the bonding of dioxygen to $Co^{II}TSP$ have been observed previously by Cookson and co-workers (*70*) and Przywarska-Boniecka and Fried (*71*). In addition, studies of the catalytic properties of Co^{II}-substituted heme have demonstrated that the electronic properties of B affect both the formation constant and reversibility of oxygen transfer (*59*).

Electron spin resonance spectroscopic studies on 1:1 $Co^{II}TSP$–dioxygen adducts have been shown to be consistent with the formulation of the structure of the oxygenated complex as cobalt(III)–superoxide (*69*, *70*). Consequently, the intermediate that is produced by reaction 4 is considered to be a mixed ligand superoxo–$Co^{III}TSP$ complex in which $O_2^{-}\cdot$ and SO_3^{2-} are bonded to the metal center at opposite axial coordination sites. Subsequently, this O_2 adduct reacts with an additional molecule of substrate to form the ternary activated complex $(SO_3)Co^{III}TSP(O_2^{-}\cdot)(SO_3)^{6-}$. The rate-limiting step of the reaction involves photoassisted electron transfer from SO_3^{2-} to the sulfito–cobalt–phthalocyanine–dioxygen system and hydrolysis of the bound SO_3 to yield SO_4^{2-} and a $Co^{II}TSP$–peroxide complex as shown in Figure 3. After protonation, O_2^{2-} is released to solution as hydrogen peroxide which either disproportionates to water and oxygen under the catalytic influence of $Co^{II}TSP$ (*44*, *45*) or reacts directly with additional sulfite by means of a two-electron redox process (eq 8) (*57*). Hydrogen peroxide was detected at a steady-state concentration of $\leq 10^{-7}$ M as an intermediate reduction product of oxygen.

In the proposed mechanism, the active catalytic center is the complex $(SO_3)Co^{II}TSP^{4-}$. The catalytic cycle begins and ends with this species. The initial steps leading to the formation of $(SO_3)Co^{II}TSP^{4-}$ (reactions 2 and 3) are assumed to be in rapid equilibrium and are ignored in the preliminary development of a theoretical rate expression. In the catalytic cycle, there are three intermediates, $(SO_3)Co^{III}TSP(O_2^{-}\cdot)^{4-}$, $(SO_3)Co^{III}TSP(O_2^{-}\cdot)(SO_3)^{6-}$, and $(SO_3)Co^{II}TSP(O_2^{2-})^{6-}$. According to the method of King and Altman (*65*), $[(SO_3)Co^{II}TSP^{4-}]$, $[(SO_3)(Co^{III}TSP(O_2^{-}\cdot)^{4-}]$, $[(SO_3)Co^{III}TSP(O_2^{-}\cdot)(SO_3)^{6-}]$, and $[(SO_3)Co^{II}TSP(O_2^{2-})^{6-}]$ can be shown to be proportional to the sums of terms that are obtained from the reaction steps which either individually or sequentially lead to the formation of a particular species. Given these conditions, the concentrations of the various forms of the catalyst are expressed as follows:

$$[(SO_3)Co^{II}TSP^{4-}] \propto k_3k_4k_5[SO_3^{2-}] + k_{-2}k_{-3}k_5 + k_{-2}k_4k_5 \quad (9)$$

$$[(SO_3)Co^{III}TSP(O_2^{-}\cdot)^{4-}] \propto k_1k_4k_5[O_2] + k_2k_{-3}k_5[O_2] \quad (10)$$

$$[(SO_3)Co^{III}TSP(O_2^{-}\cdot)(SO_3)^{6-}] \propto k_2k_3k_5[O_2][SO_3^{2-}] \quad (11)$$

$$[(SO)_3Co^{II}TSP(O_2^{2-})^{6-}] \propto k_2k_3k_4[O_2][SO_3^{2-}] \quad (12)$$

where the proportionality constant for each equation is $[(SO_3)Co^{II}TSP]_{total}^{-1}$. The mass-balance condition for the total catalyst concentration is given by eq 13:

$$[(SO_3)Co^{II}TSP]_{total} = [(SO_3)Co^{II}TSP^{4-}] + [(SO_3)Co^{III}TSP(O_2^{-}\cdot)^{4-}] + [(SO_3)Co^{III}TSP(O_2^{-}\cdot)(SO_3)^{6-}] + [(SO_3)Co^{II}TSP(O_2^{2-})^{6-}] \quad (13)$$

From steady-state considerations

$$[(SO_3)Co^{III}TSP(O_2^{-}\cdot)(SO_3)^{6-}] = [k_2k_3k_5[(SO_3)Co^{II}TSP]_{total}[O_2] \times [SO_3^{2-}]]/[k_5(k_{-2}k_{-3} + k_{-2}k_4) + k_2k_5(k_{-3} + k_4)[O_2] + k_3k_4k_5[SO_3^{2-}] + k_2k_3(k_4 + k_5)[O_2][SO_3^{2-}]] \quad (14)$$

By use of this expression and the rate-limiting step of the reaction as defined by eq 6, the rate law for the production of sulfate can be written as

$$v = \frac{d[SO_4^{2-}]}{dt} = \frac{k'[(SO_3)Co^{II}TSP]_{total}[O_2][SO_3^{2-}]}{K_A + K_B[O_2] + K_C[SO_3^{2-}] + [O_2][SO_3^{2-}]} \quad (15)$$

where

$$k' = \frac{k_4k_5}{k_4 + k_5}$$

$$K_A = \frac{k_5(k_{-2}k_{-3} + k_{-2}k_4)}{k_2k_3(k_4 + k_5)}$$

$$K_B = \frac{k_5(k_{-3} + k_4)}{k_3(k_4 + k_5)}$$

and

$$K_C = \frac{k_4k_5}{k_2(k_4 + k_5)}$$

Equation 15 can be modified to account for the rapid equilibria preceding the catalytic cycle involving $(SO_3)Co^{II}TSP^{4-}$ as the reactive center. The concentration of the active center can be defined in terms of the dimer dissociation constant, K_d, and the formation constant, K_1, for the initial metal–sulfite complex:

$$K_d = \frac{[Co^{II}TSP^{2-}]^2}{[(Co^{II}TSP)_2^{4-}]} \quad (16)$$

$$K_1 = \frac{[(SO_3)Co^{II}TSP^{4-}]_{total}}{[Co^{II}TSP^{2-}][SO_3^{2-}]} \quad (17)$$

Equations 16 and 17 are combined to yield

$$[(SO_3)Co^{II}TSP^{4-}]_{total} = K_1K_d^{1/2}[(Co^{II}TSP)_2^{4-}]^{1/2}[SO_3^{2-}] \quad (18)$$

when $[SO_3^{2-}]_0 \gg [(Co^{II}TSP)_2^{4-}]_0$. This condition allows the approximation that the concentration of SO_3^{2-} in solution remains relatively constant with respect to the amount of substrate bound in the complex $(SO_3)Co^{II}TSP^{4-}$ to become valid such that

$$[(SO_3)Co^{II}TSP^{4-}]_{total} = K'[(Co^{II}TSP)_2^{4-}]^{1/2} \quad (19)$$

where $K' = K_1K_d^{1/2}[SO_3^{2-}]$ (i.e., K' is a conditional equilibrium constant). Substitution of eq 19 into eq15 gives an approximate form of the final rate law:

$$v = \frac{k'K'[(Co^{II}TSP)_2^{4-}]^{1/2}[O_2][SO_3^{2-}]}{K_A + K_B[O_2] + K_C[SO_3^{2-}] + [O_2][SO_3^{2-}]} \quad (20)$$

The theoretical rate expression can be simplified for the pseudo-order experimental conditions used in the current study. When $[O_2]_0 \gg [SO_3^{2-}]_0$ and $[SO_3^{2-}]_0$ is sufficiently low such that $K_B[O_2] \gg K_A$ and $K_C[SO_3^{2-}]$, eq 20 is reduced to the form

$$\nu \simeq \frac{k\mathcal{K}\mathcal{T}[(Co^{II}TSP)_2^{4-}]^{1/2}[SO_3^{2-}]}{K_B + [SO_3^{2-}]} \quad (21)$$

Two sets of limiting conditions for eq 21 can be considered. If $K_B \gg [SO_3^{2-}]$, then

$$\nu \simeq k\mathcal{K}_1K_d^{1/2}[(Co^{II}TSP)_2^{4-}]^{1/2}[SO_3^{2-}]^2/K_B \quad (22)$$

whereas if $[SO_3^{2-}] \gg K_B$, then

$$\nu \simeq k\mathcal{K}_1K_d^{1/2}[(Co^{II}TSP)_2^{4-}]^{1/2}[SO_3^{2-}] \quad (23)$$

Each limiting case can be compared with the experimentally determined rate laws for the autoxidation of S^{IV} at pH 6.7 and 9.2. According to eq 23, the rate of reaction is zero order in $[O_2]$ and approximately first order in $[SO_3^{2-}]$ which is in agreement with observation. Under neutral pH conditions, the catalytic reaction rate exhibited a fractional-order dependence of 0.3 on the concentration of total added catalyst. However, eq 23 predicts a half-order rate dependence on $[(Co^{II}TSP)_2^{4-}]$. Schelly and co-workers (*67*) have reported that phthalocyanine complexes of cobalt(II) and copper(II) tend to form higher order polymers in aqueous solution, especially at high ionic strength ($\mu > 0.01$ M). Consideration of the equilibria between aggregate species and $Co^{II}TSP^{2-}$ in the derivation of the theoretical rate law would further reduce the apparent kinetic order in catalyst concentration. Evaluation of k_{obsd} as a function of $[Co^{II}TSP]$ for reactions conducted in the presence of EDTA yielded a reaction order of approximately 0.5. Since the dimer and polymers of $Co^{II}TSP$ are the dominant catalyst species in water at pH 6.7, a nonintegral rate dependence on phthalocyanine is consistent with the conclusion that the monomer is the active form. Nonintegral reaction orders arise frequently in polar reactions when the principal reactive species is formed through the dissociation of a polymer (*54*). At pH 9.2, a first-order dependence in catalyst concentration is observed. This result would be consistent with the postulated kinetic formulation if $(Co^{II}TSP)_2^{4-}$ is no longer the dominant species in solution. Cookson et al. (*70*) obtained ESR spectra that were indicative of a shift in the monomer/dimer equilibrium toward the monomer as pH increased from 7 to 10. In this case eq 2 can be neglected, and the theoretical rate expression would show a first-order dependence on total catalyst concentration.

Equation 20 can be simplified in a similar fashion for the case in which the oxidation of sulfite proceeds under pseudo-order concentration conditions in oxidant. When $[SO_3^{2-}]_0 \gg [O_2]_0$ and $K_C[SO_3^{2-}] \gg K_A$ and K_B, the approximate rate equation

$$\nu \simeq \frac{k\mathcal{K}\mathcal{T}[(Co^{II}TSP)_2^{4-}]^{1/2}[O_2]}{K_C + [O_2]} \quad (24)$$

can be expressed in the simplified form

$$\nu \simeq k\mathcal{K}_1K_d^{1/2}[(Co^{II}TSP)_2^{4-}]^{1/2}[O_2][SO_3^{2-}]/K_C \quad (25)$$

if the value of $K_C \gg [O_2]$. For the opposite extreme, i.e., $[O_2] \gg K_C$, eq 24 will be reduced to yield eq 23. The limiting rate law given in eq 25 is consistent with the apparent first-order $[O_2]$ dependence observed in reactions carried out in the presence of excess S^{IV}.

A variant of the proposed mechanism occurs when sulfite ion reacts with the SO_3-bound cobalt(II)–dioxygen adduct without the formation of a ternary activated complex of sufficiently long life to be kinetically significant. This type of reaction pathway was originally suggested by Theorell and Chance (*72*). The resulting form of the theoretical rate expression is identical with eq 15, except that K_A, K_B, and K_C are specified by different combinations of individual rate constants:

$$K_A = \frac{k_{-2}k_4k_5}{k_2k_3(k_4 + k_5)}$$

$$K_B = \frac{k_4k_5}{k_3(k_4 + k_5)}$$

$$K_C = \frac{k_4k_5}{k_2(k_4 + k_5)}$$

in accordance with the assumption that $k_4 \gg k_{-3}$. Support for this mechanistic scheme was obtained through an assessment of the influence of ionic strength on the rate of sulfite autoxidation. If $k_4 \gg k_{-3}$, then the rate-determining step would be defined by reaction 5 in which two negatively charged ions, SO_3^{2-} and $(SO_3)Co^{III}TSP(O_2^{-}\cdot)^{4-}$, combine to form an intermediate complex bearing an overall negative charge. The primary salt effect predicts that a reaction between ions of similar charge would proceed at a faster rate upon an increase in the ionic strength of the solvent medium (*54*). Even though the experimental conditions ($\mu > 0.1$ M) exceed the upper boundary for strict applicability of the Debye–Hückel theory ($\mu = 0.01$ M), a positive slope was observed for plots of log k_{obsd} vs. $\mu^{1/2}$ at pH 6.7 ($m = 0.425$, $b = -3.42$, and $R^2 = 0.9972$) and pH 9.2 ($m = 1.47$, $b = -3.54$, and $R^2 = 0.9973$). In general, the reaction rate increases with increasing values of μ. Hoffmann and Lim (*47*) reported a positive ionic strength effect for the $Co^{II}TSP$-catalyzed autoxidation of HS^- in aqueous solution.

In order to verify the applicability of eq 20, the experimental data were analyzed in terms of double-reciprocal plots of $1/\nu_0$ vs. $1/[SO_3^{2-}]_0$ where ν_0 and $[SO_3^{2-}]_0$ are the initial reaction rate and initial substrate concentrations (*69*). Rearrangement of eq 20 yields

$$1/\nu_0 = [1 + K_A/([O_2][SO_3^{2-}]) + K_B/[SO_3^{2-}] + K_C/[O_2]]/V_0 \quad (26)$$

where $V_0 = k\mathcal{K}\mathcal{T}[(Co^{II}TSP)_2^{4-}]^{1/2}$. A plot of $1/\nu_0$ vs. $1/[SO_3^{2-}]_0$ at constant $[O_2]$ should be linear with a slope of

$$(K_A/[O_2] + K_B)/V_0 \quad (27)$$

and an intercept on the $1/\nu_0$ axis of

$$(1 + K_C/[O_2])/V_0 \quad (28)$$

Shown in Figure 5 are the double-reciprocal plots for pH 6.7 and 9.2. Linearity of these functions is consistent with the proposed bisubstrate ternary complex mechanism.

Direct spectrophotometric evidence for complexation of SO_3^{2-} and dioxygen by cobalt(II)–phthalocyanine as a prelude to electron transfer was obtained as shown in Figure 4. The absorption spectrum of $Co^{II}TSP$ (denoted by the solid line) in the 600–700-nm wavelength range has two characteristic bands which are attributed to an equilibrium mixture of the dimeric complex (λ_{max} 636 nm) and a combination of an oxygen-free monomer and a $Co^{III}TSP(O_2^{-}\cdot)$ adduct (λ_{max} 670 nm) (*66*, *67*, *73*, *74*). Addition of sulfite caused a rapid increase in A_{670} in proportion to a decrease in absorbance at 636 nm. This change corresponds to a shift in the equilibrium speciation of the catalyst due to the formation of intermediates such

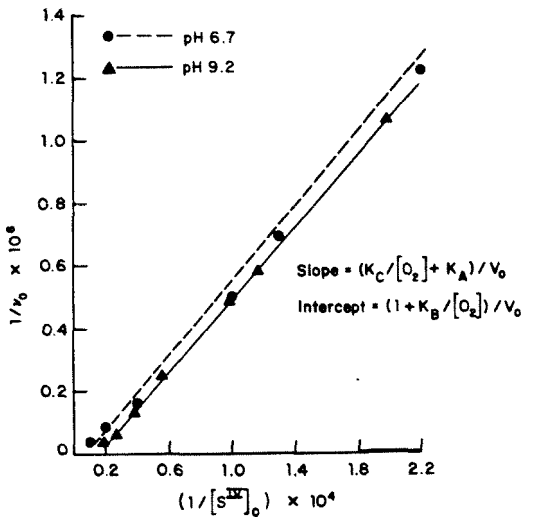

Figure 5. Lineweaver–Burk plots for the rate of the catalytic autoxidation of sulfite as a function of $[S^{IV}]_0$. $[S^{IV}]_0 = 2.5 \times 10^{-5}$–$1 \times 10^{-3}$ M, $[O_2]_0 = 2.5 \times 10^{-4}$ M, and $[Co^{II}TSP]_0 = 1 \times 10^{-6}$ M; μ = 0.4 M, T = 25 ± 0.1 °C.

as $(SO_3)Co^{II}TSP^{4-}$, $(SO_3)Co^{III}TSP(O_2^{-}\cdot)^{4-}$, and $(SO_3)Co^{III}TSP(O_2^{-}\cdot)(SO_3)^{6-}$. Preliminary stopped-flow experiments have shown that the equilibrium between $Co^{II}TSP^{2-}$ and $(SO_3)Co^{II}TSP^{4-}$ is attained rapidly (in the absence of O_2) in comparison to the rate of conversion of S^{IV} to sulfate. The value of A_{670} decreases with time as the oxidation of sulfite proceeds. At the conclusion of the reaction, the absorbance at 670 nm is approximately equivalent to the initial intensity of the 636-nm peak. Subsequent introduction of substrate results in the reemergence and decline in the 670-nm absorption maximum as a second catalytic cycle unfolds. In subsequent reactions the oscillation in peak height at 670 nm is repeated. These data confirm that $Co^{II}TSP$ participates in a closed-sequence catalytic cycle. There appears to be only a minor loss in catalytic activity upon successive additions of substrate as indicated by a net 25% decrease in k_{obsd} after five consecutive catalytic runs.

Results obtained from a series of experiments in which strong complexing reagents such as EDTA and cyanide were added to reaction solutions containing $Co^{II}TSP$ lend further support to the hypothesis that inner-sphere coordination of sulfite and molecular oxygen to cobalt(II) plays an important role in the catalytic autoxidation of S^{IV}. Addition of EDTA and CN^- reduced significantly the measured values of k_{obsd} at pH 9.2 as shown in Table III. The inhibitory effect of EDTA on reactions conducted under neutral pH conditions seems to be associated primarily with the complexation of background levels of trace-metal contaminants. For example, the half-life for the "uncatalyzed" oxidation of sulfite increased from 333 min to approximately 60 h upon the introduction of EDTA at 10^{-5} M. Cyanide did not inhibit the reaction of sulfur(IV) with O_2 at pH 6.7 because it exists almost entirely as HCN (pK_a = 9.2) which is a much weaker ligand than CN^- for the binding of transition-metal ions (*55*).

Under strongly alkaline conditions (pH ≥12), $Co^{II}TSP$ undergoes reversible oxygenation as shown in eq 29 and 30 to produce a dioxygen-bridged dicobalt complex which

$$(HO)Co^{II}TSP^{3-} + O_2 \rightleftharpoons (HO)Co^{III}TSP(O_2^{-}\cdot)^{3-} \quad (29)$$

$$(HO)Co^{III}TSP(O_2^{-}\cdot)^{3-} + (HO)Co^{II}TSP^{3-} \rightleftharpoons [(HO)CoTSP]_2O_2^{6-} \quad (30)$$

Table III. Effect of Inhibitors on k_{obsd}[a]

[inhibitor] × 10^6, M	k_{obsd} (s^{-1}) × 10^3 at pH 6.7	pH 9.2
none, 0	1.62	1.83
EDTA, 1	1.52	
EDTA, 2.5	1.45	
EDTA, 5.0	0.94	
EDTA, 10.0	0.78	0.33
mannitol, 10.0	1.25	0.85
NaCN, 10.0	1.61	0.29

[a] $[S^{IV}]_0 = 1 \times 10^{-4}$ M, $[O_2]_0 = 1.2 \times 10^{-3}$ M, and $[Co^{II}TSP]_0 = 1 \times 10^{-6}$ M; μ = 0.4 M, T = 25 ± 1 °C.

may also exhibit catalytic properties for the autoxidation of S^{IV}. The μ-superoxo dimer of $Co^{II}TSP$ may participate in either a one-electron-transfer or two-electron-transfer redox process as proposed by Davies et al. (*7*) for $(NH_3)_5Co^{III}$–O_2^-–$Co^{II}(NH_3)_5^{5+}$ and by Yatsimirskii et al. (*75*) for (L-histidine)$_2Co^{III}$–O_2^-–Co^{II}(L-histidine)$_2$. According to this hypothesis, the active catalytic center $[(HO)CoTSP]_2O_2^{6-}$ reacts with sulfite in one of the following ways as shown in either Scheme I or Scheme II.

Scheme I

$$[(HO)CoTSP]_2O_2^{6-} + SO_3^{2-} \xrightarrow[slow]{} SO_4^{2-} + (HO)Co^{II}TSP^{3-} + (HO)Co^{IV}TSP(O^{2-})^{3-} \quad (31)$$

$$(HO)Co^{IV}TSP(O^{2-})^{3-} + SO_3^{2-} \rightarrow SO_4^{2-} + (HO)Co^{II}TSP^{3-} \quad (32)$$

Scheme II

$$[(HO)CoTSP]_2O_2^{6-} + SO_3^{2-} \xrightarrow[slow]{} SO_3^{-}\cdot + (HO)Co^{III}TSP\text{–}O_2^-\text{–}Co^{II}TSP(OH)^{7-} \quad (33)$$

$$(HO)Co^{III}TSP\text{–}O_2^-\text{–}Co^{II}TSP(OH)^{7-} + SO_3^{-}\cdot \rightarrow SO_3 + (HO)Co^{II}TSP(O_2^{2-})^{5-} + (HO)Co^{II}TSP^{3-} \quad (34)$$

$$SO_3 + H_2O \rightarrow SO_4^{2-} + 2H^+ \quad (35)$$

$$(HO)Co^{II}TSP(O_2^{2-})^{5-} + 2H^+ \rightarrow (HO)Co^{II}TSP^{3-} + H_2O_2 \quad (36)$$

In Scheme I, production of sulfate through an O–O bond cleavage would be hindered by formation of a highly unstable cobalt(IV) oxide intermediate (*76*). While the second pathway is chemically viable, it seems to be less consistent with the reported kinetic data than is the proposed bisubstrate complexation pathway. For example, Scheme II predicts a second-order reaction rate dependence on the concentration of the $Co^{II}TSP$ monomer. This condition was not observed in the present study.

The relative efficiency of $Co^{II}TSP$, $Fe^{II}TSP$, and $Mn^{II}TSP$ as homogeneous catalysts for the autoxidation of SO_3^{2-} appears to be directly related to the stability of the corresponding 1:1 metal–dioxygen adduct of each complex in aqueous solution. In organic as well as water-based solvent systems, macrocyclic complexes of iron(II) and manganese(II) react with O_2 to yield oxygen-bridged dinuclear species of the general form M^{III}–O_2^{2-}–M^{III} (*59*). These products then decompose irreversibly to μ-oxo dimers as shown in eq 37 and 38. In contrast, the oxygenation of most cobalt(II) complexes is reversible under a majority of reaction conditions. Ochiai (*76*) has attributed this contrasting behavior to the rela-

$$M^{III}\text{–}O_2^{2-}\text{–}M^{III} \rightarrow 2M^{IV}(O^{2-}) \quad (37)$$

$$M^{IV}(O^{2-}) + M^{II} \rightarrow M^{III}\text{–}O\text{–}M^{III} \quad (38)$$

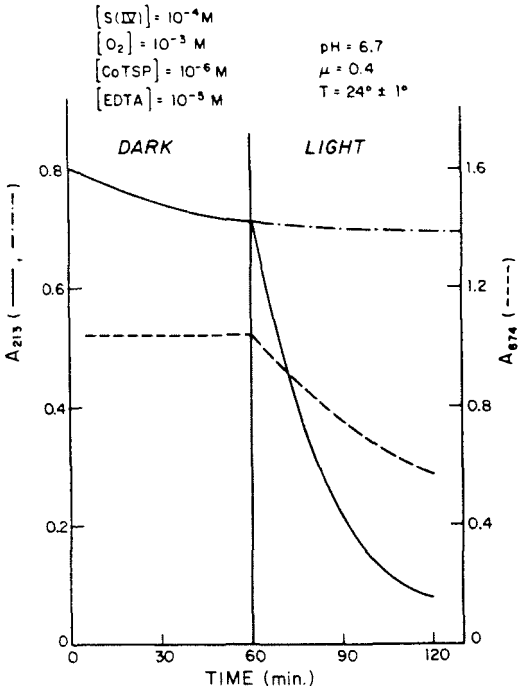

Figure 6. Effect of fluorescent room light on the catalytic autoxidation of sulfite. $[S^{IV}]_0 = 1 \times 10^{-4}$ M, $[O_2]_0 = 1.2 \times 10^{-3}$ M, and $[Co^{II}TSP]_0 = 1 \times 10^{-6}$ M, pH 6.7; $\mu = 0.4$ M, $T = 25 \pm 1$ °C.

tively high stability of the Fe^{IV}– and Mn^{IV}–oxides in comparison to $Co^{IV}(O^{2-})$. Both $Fe^{II}TSP$ and $Mn^{II}TSP$ have been shown to undergo irreversible oxidation upon dissolution in water of neutral or alkaline pH (*56*).

Photoassisted Catalysis. A noteworthy result of the current investigation involves the apparent photochemical reactivity of $Co^{II}TSP$ (Figure 6). Since a wide variety of transition metal–phthalocyanine complexes and structurally related metalloporphyrins are known to function as photosensitizers for the production of singlet oxygen ($^1O_2$) and/or superoxide ($O_2^{-}\cdot$), catalysis of the autoxidation of S^{IV} by $Co^{II}TSP$ may be light dependent (*77*, *78*). To test this hypothesis, a series of experiments was conducted in the presence and absence of conventional fluorescent room light. It should be noted that the kinetic measurements discussed in previous sections of this paper were obtained from reactions that occurred under background illumination. In the dark, the oxidation of SO_3^{2-} proceeded very slowly following rapid formation of the $Co^{II}TSP$–dioxygen complex as shown in Figure 6. However, the decline in the concentration of sulfite and the ternary intermediate was accelerated significantly upon exposure of the reaction solution to light. Addition of specific inhibitors for superoxide ion (superoxide dismutase) (*79*) and singlet molecular oxygen (1,4-diazabicyclo[2.2.2]octane) (*80*) did not have any perceptible effect on the rate of reaction. Reactions catalyzed by $Fe^{II}TSP$, $Mn^{II}TSP$, $Ni^{II}TSP$, $Cu^{II}TSP$, and $V^{IV}TSP$ were insensitive to irradiation.

Beelen and co-workers (*81*) observed that irradiation with visible light in the 600–700-nm wavelength range enhanced the catalytic activity of $Co^{II}TSP$ for the aqueous-phase autoxidation of 2-mercaptoethanol. These authors suggested that the increased rate of disulfide formation resulted from a light-induced shift in the $Co^{II}TSP$ dimer dissociation equilibrium (eq 2) in favor of the catalytically reactive monomer. In an earlier study, Ferraudi and Srisankar (*82*) demonstrated that $(Co^{II}TSP)_2^{4-}$ undergoes photochemical dissociation to form metastable Co^{I}– and Co^{III}–TSP ligand radical species upon ultraviolet photolysis under anoxic conditions. However, photochemical redox activity did not occur at excitation energies of less than 105 kcal/mol (i.e., $\lambda > 260$ nm).

An alternative explanation for the observed photocatalytic effect on the autoxidation of sulfite may involve the absorption of light by the ternary intermediate $(SO_3)Co^{II}TSP\ (O_2^{-}\cdot)(SO_3)^{6-}$ to form a cobalt(II)–singlet oxygen complex, $(SO_3)Co^{II}TSP(^1O_2)(SO_3)^{6-}$, in the excited state. This species would possess more favorable spin-state symmetry for two-electron transfer during the rate-limiting step (reaction 6). The electronic spectra of numerous μ-superoxo–dicobalt complexes have been shown to contain O_2 (π_v^*) → $Co^{II}(d\sigma^*)$ ligand-to-metal charge-transfer transitions ($\log \epsilon \simeq 3.3$–3.5) in the visible wavelength region at 300–400 nm (*83*). Electron transfer from SO_3^{2-} to the $Co^{II}TSP$–dioxygen system would be enhanced further by the potential delocalization of excess electron density from the metal center to the conjugated π-orbital system of the phthalocyanine ligand. Many porphyrin complexes of cobalt(II) undergo intramolecular redox transformations in solution (*84*). Further details concerning photoassisted catalysis by $Co^{II}TSP$ will be presented in a subsequent communication.

Conclusion

The heterolytic mechanism summarized in Figure 5 and eq 2–8 appears to explain the kinetic and spectral data for a broad range of experimental conditions. The simplified kinetic expressions of eq 22, 23, and 25 account for both the apparent shift in the reaction order of sulfite to values of greater than one as reported by some investigators and the observed zero-order rate dependence on $[O_2]$. The current results do not necessarily preclude a homolytic pathway; but if free-radical intermediates were significantly involved in the oxidation of S^{IV}, than a considerable yield of dithionate should be formed as a chain termination product. Since $S_2O_6^{2-}$ was not detected and sulfate was the only observed product, the contribution of a free-radical chain process to the overall reaction seems unlikely. Furthermore, the addition of free-radical scavengers such as mannitol did not inhibit the autoxidation of sulfite in the presence of $Co^{II}TSP$.

Summary

Cobalt(II)–4,4′,4″,4‴-tetrasulfophthalocyanine is an effective homogeneous catalyst for the quantitative conversion of sulfur(IV) to sulfate in aqueous solution. Addition of $Co^{II}TSP^{2-}$ at concentrations of 10^{-8}–10^{-6} M can result in dramatic increases in the rate of autoxidation. Other water-soluble phthalocyanine complexes are less effective.

The catalytic properties of $Co^{II}TSP$, $Fe^{II}TSP$, $Mn^{II}TSP$, $Ni^{II}TSP$, $Cu^{II}TSP$, and $V^{IV}TSP$ have been determined, and differences in activity have been evaluated in terms of the relative capacity of the square-planar complexes to reversibly bind molecular oxygen. The kinetics of the autoxidation of SO_3^{2-} in the presence of $Co^{II}TSP^{2-}$ have been interpreted in terms of a bisubstrate Michaelis–Menten rate expression. The empirical rate law and spectral data indicate that the reaction proceeds through the formation of an activated complex in which two sulfite ions and O_2 are reversibly bonded to $Co^{II}TSP^{2-}$, followed by hydrolysis under the influence of light to yield SO_4^{2-} and hydrogen peroxide. The pH dependence of the reaction rate has been attributed to the acid dissociation of HSO_3^{-} and the

deprotonation of a coordinated water molecule at high pH.

Registry No. $Fe^{II}TSP^{4-}$, 86508-34-1; $Mn^{II}TSP^{4-}$, 62792-11-4; $Co^{II}TSP^{4-}$, 29012-54-2; SO_2, 7446-09-5; EDTA, 60-00-4; NaCN, 143-33-9; mannitol, 69-65-8.

Literature Cited

(1) Aubuchon, C. Ph.D. Thesis, Johns Hopkins University, Baltimore, MD, 1976.
(2) Barron, C. H.; O'Hern, H. A. *Chem. Eng. Sci.* **1966**, *21*, 397–404.
(3) Bengtsson, S.; Bjerle, I. *Chem. Eng. Sci.* **1975**, *30*, 1429–1435.
(4) Brimblecombe, P.; Spedding, D. J. *Atmos. Environ.* **1974**, *8*, 937–345.
(5) Chen, I. H.; Barron, C. H. *Ind. Eng. Chem. Fundam.* **1972**, *11*, 466–470.
(6) Coughanowr, D. R.; Krause, F. E. *Ind. Eng. Chem. Fundam.* **1965**, *48* 61–66.
(7) Davies, R.; Hagopian, A. K. E.; Sykes, A. G. *J. Chem. Soc. A* **1969**, 623–629.
(8) Freiberg, J. *Environ. Sci. Technol.* **1974**, *8*, 731–734.
(9) Fuller, E. C.; Crist, R. H. *J. Am. Chem. Soc.* **1941**, *63*, 1644–1650.
(10) Fuzzi, S. *Atmos. Environ.* **1978**, *12*, 1439–1442.
(11) Ibusuki, T. *Atmos. Environ.*, in press.
(12) Kaplan, D. J.; Himmelblau, D. M.; Kanaoka, C. *Atmos. Environ.* **1981**, *15*, 763–773.
(13) Linek, V.; Mayrhoferova, J. *Chem. Eng. Sci.* **1970**, *25*, 787–800.
(14) Lunak, S.; El-Wakil, A.; Veprek-Siska, J. *Collect. Czech. Chem. Commun.* **1978**, *43*, 3306–3316.
(15) Martin, L. R. In "Acid Precipitation: SO_2, NO, NO_2 Oxidation Mechanisms: Atmospheric Considerations"; Calvert, J. G., Ed.; Ann Arbor Science Publishers: Ann Arbor, MI, 1982, in press.
(16) Matteson, J. J.; Stōber, W.; Luther, H. *Ind. Eng. Chem. Fundam.* **1969**, *8*, 677–684.
(17) Mishra, G. C.; Srivastava, R. D. *Chem. Eng. Sci.* **1975**, *30*, 1387–1390.
(18) Mishra, G. C.; Srivastava, R. D. *Chem. Eng. Sci.* **1976**, *31*, 969–971.
(19) Sawicki, J. E.; Barron, C. H. *Chem. Eng. J* **1973**, *5*, 153–159.
(20) Yagi, S.; Inoue, H. *Chem. Eng. Sci.* **1962**, *17*, 411–421.
(21) Hegg, D. A.; Hobbs, P. V. *Atmos. Environ.* **1978**, *12*, 241–253.
(22) Hoffmann, M. R.; Boyce, S. D. *Adv. Environ. Sci. Technol.* **1983**, *12*, 147–189.
(23) Hoffman, M. R. *Environ. Sci. Technol.* **1980**, *14*, 1061–1066.
(24) Beilke, S.; Gravenhorst, G. *Atmos. Environ.* **1978**, *12*, 231–239.
(25) Larson, T. V.; Horike, N. R.; Halstead, H. *Atmos. Environ.* **1978**, *12*, 1597–1611.
(26) Meyer, B. "Sulfur, Energy and the Environment"; Elsevier: Amsterdam, The Netherlands, 1977.
(27) Nriagu, J. O. Ed. "Sulfur in the Environment"; Wiley-Interscience: New York, 1978.
(28) Hoffmann, M. R.; Jacob, D. J. In "SO_2, NO, NO_2 Oxidation Mechanisms: Atmospheric Considerations"; Calvert, J. G., Ed.; Ann Arbor Science Publishers: Ann Arbor, MI, 1983, in press.
(29) Backstrōm, H. *Z. Phys. Chem., Abt. B* **1934**, *25B*, 122–138.
(30) Bassett, H.; Parker, W. G. *J. Chem. Soc.* **1951**, 1540–1560.
(31) Hayon, E.; Treinin, A.; Wilf, J. *J. Am. Chem. Soc.* **1972**, *94*, 47–57.
(32) Lunak, S.; Veprek-Siska, J. *Collect. Czech. Chem. Commun.* **1976**, *41*, 3495–3503.
(33) Lunak, S.; Veprek-Siska, J. *React. Kinet. Catal. Lett.* **1976**, *5*, 157–161.
(34) Veprek-Siska, J.; Lunak, S.; El-Wakil, A. *Z. Naturforsch. B: Anorg. Chem., Org. Chem.* **1974**, *29B*, 812–813.
(35) Dolansky, J.; Wagnerova, D. M.; Veprek-Siska, J. *Collect. Czech. Chem. Commun.* **1976**, *41*, 2326–2332.
(36) Kundo, N. N.; Keier, N. P. *Russ. J. Phys. Chem.*, (*Engl. Transl.*) **1968**, *42*, 707–711.
(37) Wagnerova, D. M.; Schwertnerova, E.; Veprek-Siska, J. *Collect. Czech. Chem. Commun.* **1973**, *38*, 756–768.
(38) Wagnerova, D. M.; Schwertnerova, E.; Veprek-Siska, J. *Collect. Czech. Chem. Commun.* **1974**, *39*, 3036–3047.
(39) Cook, A. H. *J. Chem. Soc.* **1938**, 1761–1768.
(40) Cook, A. H. *J. Chem. Soc.* **1938**, 1768–1774.
(41) Dufour, M. N.; Crumbliss, A. L.; Johnston, G.; Gaudemer, A. *J. Mol. Catal.* **1980**, *7*, 277–287.
(42) Dufour-Ricroch, M. N.; Gaudemer, A. *Tetrahedron Lett.* **1976**, 4079–4082.
(43) Uchida, K.; Soma, M.; Naito, S.; Oriski, T.; Tamaru, K. *Chem. Lett.* **1978**, 471–474.
(44) Waldmeier, P.; Prijs, B.; Sigel, H. *Z. Naturforsch., B: Anorg. Chem., Org. Chem., Biochem., Biophys., Biol.* **1972**, *27B*, 95–100.
(45) Waldmeier, P.; Sigel, H. *Inorg. Chim. Acta* **1971**, *5*, 659–666.
(46) Hajibrahim, S. K.; Tibbetts, P. J. C.; Watts, C. D.; Maxwell, J. R.; Eglington, C.; Colin, H.; Guiochon, G. *Anal. Chem.* **1978**, *50*, 549–553.
(47) Hoffmann, M. R.; Lim, B. C. *Environ. Sci. Technol.* **1979**, *13*, 1406–1413.
(48) Weber, J. H.; Busch, D. H. *Inorg. Chem.* **1965**, *48* 469–471.
(49) Huss, A., Jr.; Lim, P. K. Eckert, C. A. *J. Am. Chem. Soc.* **1978**, *100*, 6252–6253.
(50) "Standard Methods for the Examination of Water and Wastewater", 15th ed.; American Public Health Association: Washington, DC, 1981; pp 439–440.
(51) Perschke, H.; Broda, E. *Nature (London)* **1961**, *190*, 257–258.
(52) Higginson, W. C. E.; Marshall, J. W. *J. Chem. Soc.* **1957**, 447–458.
(53) Mancy, K. H.; Westgarth, W. C. *J. Water Pollut. Control Fed.* **1962**, *34*, 1037–1051.
(54) Frost, A. A.; Pearson, R. G. "Kinetics and Mechanism", 2nd ed.; Wiley-Interscience: New York, 1961.
(55) Smith, R. M.; Martell, A. E. "Critical Stability Constants Inorganic Complexes"; Plenum Press: New York, 1976; Vol. 4.
(56) Boucher, L. J. In "Coordination Chemistry of Macrocyclic Compounds"; Melson, G. A. Ed.; Plenum Press: New York, 1979; pp 461–516.
(57) Hoffmann, M. R.; Edwards, J. O. *J. Phys. Chem.* **1975**, *79*, 2096–2098.
(58) Collman, J. P.; Halpert, T. R.; Suslick, K. S. In "Metal Ion Activation of Dioxygen"; Spiro, T. G., Ed.; Wiley-Interscience: New York, 1980; pp 1–72.
(59) Jones, R. D.; Sommerivlle, D. A.; Basolo, F. *Chem. Rev.* **1979**, *79*, 139–179.
(60) Kropf, H.; Hoffmann, Hd. *Tetrahedron Lett.* **1967**, 659–663.
(61) Kropf, H.; Knaack, K. *Tetrahedron* **1972**, *28*, 1143–1151.
(62) Kothari, V. M.; Tazuma, J. J. *J. Catal.* **1976**, *41*, 180–189.
(63) Mahler, H. R.; Cordes, E. H. "Biological Chemistry"; Harper and Row: New York, 1966.
(64) Laidler, K. J.; Bunting, S. J. "The Chemical Kinetics of Enzyme Action"; Clarendon Press: Oxford, England, 1973.
(65) King, E. L.; Altman, C. *J. Phys. Chem.* **1956**, *60*, 1375–1378.
(66) Gruen, L. C.; Blagrove, R. J. *Aust. J. Chem.* **1973**, *26*, 319–323.
(67) Schelly, Z. A.; Farina, R. D.; Eyring, E. M. *J. Phys. Chem.* **1970**, *74*, 617–620.
(68) Carter, M. J.; Rillema, D. P.; Basolo, F. *J. Am. Chem. Soc.* **1974**, *96*, 392–400.
(69) Rollmann, L. D.; Chan, S. I. *Inorg. Chem.* **1971**, *10*, 1978–1982.
(70) Cookson, D. J.; Smith, T. D.; Boas, J. F.; Hicks, P. R.; Pilbrow, J. R. *J. Chem. Soc.* **1977**, 109–114.
(71) Przywarska-Boniecka, H.; Fried, K. *Pol. J. Chem.* **1976**, *50*, 43–52.
(72) Theorell, H.; Chance, B. *Acta Chem. Scand.* **1951**, *5*, 1127–1144.
(73) Bernauer, K.; Fallab, S. *Helv. Chim. Acta* **1961**, *44*, 1287–1292.
(74) Wagnerova, D. M.; Schwertnerova, E.; Veprek-Siska, J. *Collect. Czech. Chem. Commun.* **1974**, *39*, 1980–1988.
(75) Yatsimirskii, K. B.; Bratushko, I. Y.; Zatsny, I. L. *Zh. Neorg. Khim.* **1977**, *22*, 1611–1666.

(76) Ochiai, E. *Inorg. Nucl. Chem. Lett.* **1974**, *10*, 453–457.
(77) Cox, G. S.; Whitten, D. G.; Gianotti, G. *Chem. Phys. Lett.* **1979**, *67*, 511–515.
(78) Harbour, J. R.; Hair, M. L. *Photochem. Photobiol.* **1978**, *28*, 721–727.
(79) McCord J. M.; Fridovich, I. *J. Biol. Chem.* **1969**, *244*, 6056–6063.
(80) Wasserman, H. H.; Murray, R. W.; Eds. "Singlet Oxygen"; Academic Press: New York, 1979.
(81) Beelen, T. P. M.; de Costa Gomez, C. O.; Kuijer, M. *Recl. Trav. Chim. Pays-Bas* **1979**, *98*, 521–522.
(82) Ferraudi, G.; Srisanskar, E. V. *Inorg. Chem.* **1978**, *17*, 3164–3168.
(83) Lever, A. B. P.; Gray, H. B. *Acc. Chem. Res.* **1978**, *11*, 348–355.
(84) Berezin, B. D. "Coordination Compounds of Porphyrins and Phthalocyanines"; Wiley-Interscience: New York, 1981.

Received for review December 21, 1982. Accepted May 23, 1983. Financial support for this research was provided by the U.S. Environmental Protection Agency under Contract R808086-01.

Chapter 3

Catalytic Oxidation of Reduced Sulfur Compounds by Homogeneous and Hybrid Co(II) Phthalocyanine Complexes

Michael Hoffmann, Andrew Hong

Sci. Total Environ., 1987, 64, 99-115.

The Science of the Total Environment, 64 (1987) 99–115
Elsevier Science Publishers B.V., Amsterdam — Printed in The Netherlands

CATALYTIC OXIDATION OF REDUCED SULFUR COMPOUNDS BY HOMOGENEOUS AND HETEROGENEOUS Co(II) PHTHALOCYANINE COMPLEXES

MICHAEL R. HOFFMANN and ANDREW P.K. HONG

Environmental Engineering Science, W.M. Keck Laboratories, California Institute of Technology, Pasadena, CA 91125 (U.S.A.)

ABSTRACT

An overview of the kinetics and mechanisms of the reactions of reduced sulfur compounds and other reductants with molecular oxygen as catalyzed by homogeneous and heterogeneous metal phthalocyanine complexes is presented. Catalysis of the autoxidation of S(IV) by Co(II) tetrasulfophthalocyanine was characterized in terms of an ordered ternary-complex mechanism in which S(IV) and oxygen are simultaneously bound to the Co(II)/Co(III) metal center. Hydrogen peroxide was identified as an intermediate reduction product of bound dioxygen. The reaction was examined by spectrophotometric and EPR methods and was found to proceed via a sulfito–cobalt(III)–superoxide complex that subsequently combines with a second sulfite molecule to produce sulfate and a sulfito–cobalt(III)–peroxide. The catalytic cycle is closed by the regeneration of the cobalt(II) complex via the production of H_2O_2. Direct evidence for the active sulfito–cobalt(III)–superoxide intermediate was obtained.

INTRODUCTION

Oxidation by reagents such as molecular oxygen (O_2), chlorine (Cl_2), ozone (O_3), hydrogen peroxide (H_2O_2) and permanganate (MnO_4^-) is one of the primary modes by which pollutants are removed from industrial and domestic wastewaters. With the exception of O_2, chemical oxidants are commercially cost intensive in addition to being inherently hazardous under certain conditions. These factors invariably contribute to the cost of water treatment processes. In contrast to the highly reactive oxidizing agents, molecular oxygen usually requires the presence of a catalyst in order to insure complete and rapid reaction with reductants. For example, microorganisms are used as efficient catalysts in secondary wastewater treatment. However, in the absence of either biological or chemical catalysts, the autoxidation of most organic and inorganic substrates is kinetically slow.

The term autoxidation refers to the reaction of any oxidizable substance with molecular oxygen [1]. In general, the oxidation of reductants by O_2 proceeds slowly in the absence of catalysts because of unfavourable spin state symmetries that result from differences in the electronic configurations of the reactants. In the ground state of $O_2(^3\Sigma_g^-)$, the two degenerate π-antibonding molecular orbitals each contain one electron of the same spin. Conversely, the

0048-9697/87/$03.50

electronic configurations of most inorganic and virtually all organic compounds conform to ground-states with spin multiplicities of zero. Therefore, the electronic structure of either the reductant and/or O_2 must be altered in order to surmount the activation energy barrier imposed on the reaction by spin-state symmetry restrictions.

Autoxidation reactions of many inorganic and organic compounds are accelerated in the presence of first-row transition-metal ions and complexes, in which the metal center has access to more than one stable oxidation state [2]. Catalysis usually results from an initial rapid redox reaction of the metal with either the reductant or oxygen, thereby lowering the activation energy of the overall oxidation process. The ability of the transition metal to form coordination complexes with the reactants may also play an important role in catalysis. Through alternating reactions with the reductant and oxidant, the metal center is reduced and oxidized cyclically at a rapid rate with concomitant acceleration of an otherwise slow reaction.

A considerable amount of research has been directed toward determining the mechanisms of transition-metal catalysis in the reactions of O_2 with a wide variety of reduced sulfur compounds such as sulfur dioxide (SO_2), hydrogen sulfide (H_2S), and mercaptans (RSH) in aqueous solution (Eqns (1)–(3)):

$$H_2S + 2O_2 \longrightarrow 2H^+ + SO_4^{2-} \quad (1)$$

$$2SO_2 \cdot H_2O + O_2 \longrightarrow 4H^+ + 2SO_4^{2-} \quad (2)$$

$$2RSH + O_2 \longrightarrow R\text{–}SS\text{–}R + H_2O_2 \quad (3)$$

Sulfur-containing compounds are ubiquitous contaminants in wastewaters discharged from mining facilities, pulp and paper mills, tanneries, and oil refineries [3,4]. Furthermore, the catalytic oxidation of S(– II) and S(IV) in aquatic environments plays an important role in the natural sulfur cycle.

Metal ions, such as Fe(III), Co(III) and Cu(II), that undergo facile and reversible redox cycles between two oxidation states, are known to catalyze autoxidation. For example, Backstrom [5] proposed that the aqueous-phase autoxidation of S(IV) proceeds via a free-radical chain mechanism in which a metal ion, M^{n+}, initiates the reaction through outer-sphere electron-transfer.

Initiation: $$M^{n+} + SO_3^{2-} \longrightarrow M^{(n-1)+} + SO_3^{\cdot-} \quad (4)$$

Propagation: $$SO_3^{\cdot-} + O_2 \longrightarrow SO_5^{\cdot-} \quad (5)$$

$$SO_5^{\cdot-} + SO_3^{2-} \longrightarrow SO_5^{2-} + SO_3^{\cdot-} \quad (6)$$

Oxidation: $$SO_5^{2-} + SO_3^{2-} \longrightarrow 2SO_4^{2-} \quad (7)$$

Termination: $$2SO_3^{\cdot-} \longrightarrow S_2O_6^{2-} \quad (8)$$

$$SO_3^{\cdot-} + SO_5^{\cdot-} \longrightarrow S_2O_6^{2-} + O_2 \quad (9)$$

$$2SO_5^{\cdot-} \longrightarrow S_2O_8^{2-} + O_2 \quad (10)$$

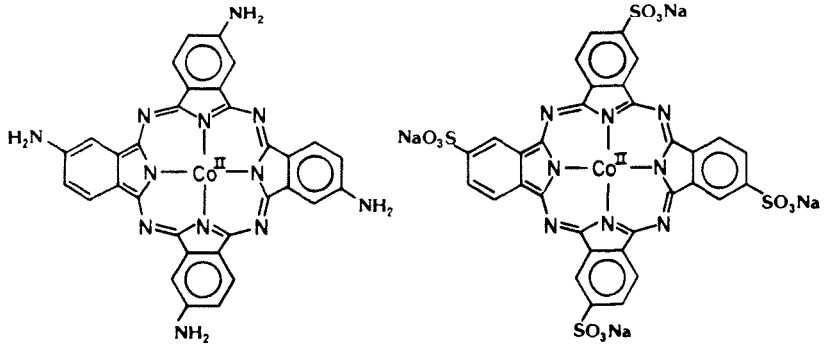

Fig. 1. The structures of Co(II) tetrasulfophthalocyanine and tetraaminophthalocyanine complexes.

Molecular oxygen participates only in the propagation steps which involve SO_3^-, SO_5^-, and SO_5^{2-} as intermediates. In this case, $M^{(n-1)-}$ is reoxidized by O_2 in order to complete the catalytic cycle. However, recent work in this laboratory has shown that the metal ion must first form a discrete inner sphere complex with S(IV) before electron transfer can take place. Analogous schemes have been proposed by Chen and Morris [4] and Wallace et al. [6] to describe the metal-catalyzed oxidations of H_2S and RSH by O_2. In each case, metal–substrate complexation may occur as a prelude to electron transfer.

An alternative mode of catalysis involves direct mediation by metals in the transfer of O_2 to the substrate. "Activation" of molecular oxygen results from formation of a discrete metal–dioxygen adduct. Coordination of dioxygen to a first-row transition metal ion in a low oxidation state, e.g. Fe(II), Mn(II), Co(II) and Cu(I), formally alters the electronic configuration of dioxygen to either a superoxide (O_2^-) or peroxide (O_2^{2-}) [7–16]. Thus, metal–dioxygen bonding overcomes the symmetry restrictions that are imposed on the reactivity of O_2 in its triplet ground state. Numerous metalloenzymes function in this manner. The properties of natural and synthetic oxygen carriers have been discussed previously by Akhrem et al. [7], Basolo et al. [8], Collmann [9], Jones et al. [10], Khan and Martell [11], Lever and Gray [12], McLendon and Martell [13], Ochiai [14], Savitskii and Nelyubrin [15], and Vaska [16].

In order to study the solution-phase autoxidations of hydrogen sulfide, sulfur dioxide and thiols in a well defined catalytic system, we have examined the catalytic properties of homogeneous and heterogeneous phthalocyanine complexes of Fe(II), Mn(II), Co(II), Ni(II) and Cu(II). Phthalocyanines are macrocyclic tetrapyrrole compounds that readily form square planar coordination complexes in which the metal atom is bonded to the four pyrrole nitrogen atoms, as shown in Fig. 1. Structurally related porphyrin and Schiff-bases form

analogous complexes with first-row transition-metals. The catalytic properties of divalent and trivalent metal-phthalocyanine, -porphyrin and -Schiff base derivatives have been compared with those of catalase, peroxidase, oxidase, and oxygenase enzymes [10, 11, 13, 17–23]. In addition, these compounds represent suitable models with which to study the catalytic effects of trace metals in the aquatic environment because of their similarities to the structure of naturally occurring pigments such as chlorophyll.

Hoffmann and Lim [24] studied the autoxidation of hydrogen sulfide in aqueous solution catalyzed by water soluble Co(II)-, Ni(II)- and Cu(II)-tetrasulfophthalocyanine [M(II)TSP]. Under alkaline pH conditions, the principal products of the reaction of O_2 with HS^- in the presence of Co(II)TSP were sulfate and colloidal sulfur. Lesser yields of SO_3^{2-}, dithionate ($S_2O_6^{2-}$), polysulfide (S_4^{2-} and S_5^{2-}), and tetrathionate ($S_4O_6^{2-}$) were also produced. The kinetics of the oxidation of HS^- to sulfate were interpreted in terms of a mechanism in which sulfide ion and dioxygen are reversibly bound to the catalytic center.

$$O_2 + Co(II)TSP^{2-} \rightleftharpoons Co(III)TSP(O_2^-)^{2-} \quad (11)$$

$$HS^- + Co(III)TSP(O_2^-)^{2-} \rightleftharpoons Co(III)TSP(O_2^-)(SH^-)^{3-} \quad (12)$$

$$Co(III)TSP(O_2^-)(SH^-)^{3-} \xrightarrow[k]{slow} Co(II)TSP^{2-} + HSO_2^- \quad (13)$$

$$HSO_2^- + O_2 \xrightarrow{fast} H^+ + SO_4^{2-} \quad (14)$$

This postulated mechanism is similar to a bisubstrate Michaelis–Menton scheme for enzymatic catalysis. The intrinsic rate constant, k, was calculated to be $1.0(\pm 0.2) \times 10^5 M^{-2} min^{-1}$, which corresponds to a catalytic turnover number of $> 100\,000\,min^{-1}$.

Boyce et al. [25] reported that metal phthalocyanines in the concentration range of 1 nM to 1 μM catalyze the rapid oxidation of S(IV) to SO_4^{2-} in aqueous solution. The relative catalytic activity of the M(II)TSP complexes [i.e. Co(II) $\gg$ Fe(II) > Mn(II) > Ni(II) ~ Cu(II)] follows a trend that reflects the relative capacities of the metal centers to reversibly bind dioxygen. The rate of S(IV) oxidation at pH 9.2 exhibited first-order dependences on the concentrations of substrate and catalyst, and a variable order (0–1) dependence on $[O_2]$. A fractional reaction order of 0.5 in $[Co(II)TSP]_{total}$ was observed for oxidations conducted under neutral pH conditions. The kinetic measurements, coupled with spectroscopic data, indicate that the reaction proceeds through the bisubstrate complexation pathway depicted in Fig. 2. The first step of the reaction involves formation of $Co(II)TSP^{2-}$ from the dimeric form of cobalt phthalocyanine ($K_2 = 4.88 \times 10^{-6} M$ at 58°C). Complexation of SO_3^{2-} by $Co(II)TSP^{2-}$ at an axial site facilitates coordination of O_2. Reaction of the cobalt(III)–superoxide adduct with an additional molecule of reductant yields sulfate and H_2O_2 following hydrolysis.

The ordered-ternary complex mechanism of Fig. 2 was postulated on the basis of observed kinetics and identification of intermediates. Derivation of the

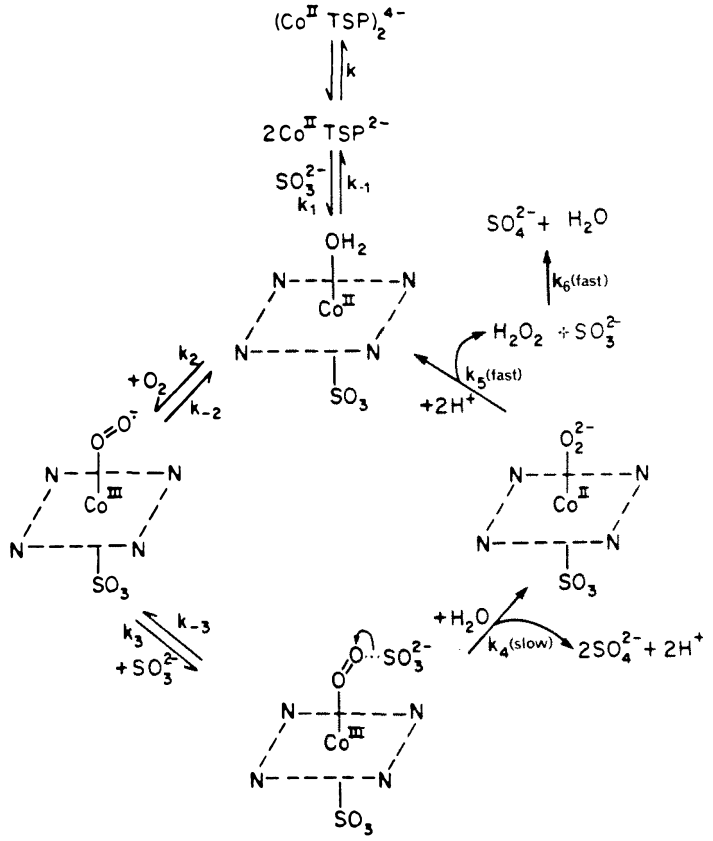

Fig. 2. A schematic diagram for the catalytic autoxidation of sulfite by Co(II)tetrasulfophthalocyanine via the formation of an ordered ternary complex.

resultant rate expression and a detailed discussion of the kinetic data that support this mechanism has been provided by Boyce et al. [25]. However, recent experiments in this laboratory, which were conducted at very low catalyst concentrations, show a pronounced induction period that was indicative of a free radical pathway. We have examined the catalytic reaction under these conditions in order to establish the validity of the mechanism of Boyce et al. [25] at low catalyst concentrations.

The catalyst autoxidation of SO_2 dissolved in atmospheric water droplets represents a viable pathway for the formation of acidic sulfates [26–28], whereas oxidation of reduced sulfur compounds in the aquatic environment plays a fundamental role in the natural sulfur cycle [29, 30]. Numerous attempts to characterize the kinetics and mechanisms of the metal-catalyzed autoxidation of sulfur dioxide in aqueous solution [26, 28] have led to large disagreements as to the rates, rate laws, and pH-dependences of the reactions.

104

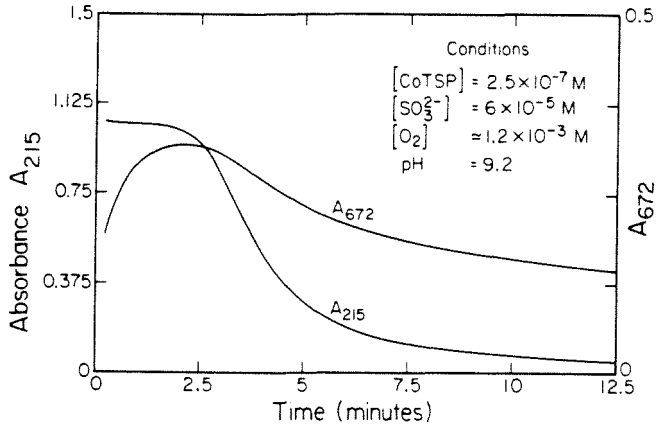

Fig. 3. Absorbance versus time profiles for SO_3^{2-} at λ = 215 nm and for the catalytically active intermediate complex at λ = 672 nm.

EXPERIMENTAL

The tetrasodium salt of cobalt(II)–4,4′, 4″,4‴-tetrasulfophthalocyanine dihydrate was synthesized according to the method of Weber and Busch [31]. Buffers (pH 9.2, μ = 0.1) were prepared with reagent-grade sodium borate (Mallinkrodt) and sodium perchlorate (G.F. Smith). Deionized water (18 MΩ-cm resistivity) obtained from a Milli RO-4/Milli Q purification system (Millipore) was used to prepare all solutions. Other experimental details are described elsewhere [25].

Reactions were carried out in either 10 cm or 1 cm quartz cells. The 1 cm cell was equipped with a ground-glass joint for vacuum line deoxygenation. UV/VIS measurements were made with a Hewlett-Packard Model 8450A diode-array spectrophotometer. EPR spectra were obtained with a Varian Model E-1 spectrometer with 100 kHz modulation and an X-band klystron at 77 K.

RESULTS

The catalytic autoxidation of sulfite in the presence of Co(II)tetrasulfophthalocyanine exhibited a pronounced induction period, which was followed by a rapid depletion of sulfite. Figure 3 shows a typical absorbance versus time profile at two different wavelengths during the course of the reaction at pH 9.2 with [Co(II)TSP] = 0.25 μM, [SO_3^{2-}] = 60 μM, and [O_2] = 1.2 mM at μ = 0.1 M. The two wavelengths λ = 215 and 672 nm correspond, respectively, to the absorbance of SO_3^{2-} and to the absorbance of an intermediate complex that forms during the initial stages of the reaction. This intermediate was observed only in the presence of SO_3^{2-} and O_2. These observations suggest that the intermediate is a ternary complex of monomeric Co(II)TSP with O_2 and SO_3^{2-} bound *trans* to one another to the two available axial coordination sites. We have previously assumed that this complex is of the form (SO_3)Co(III)-

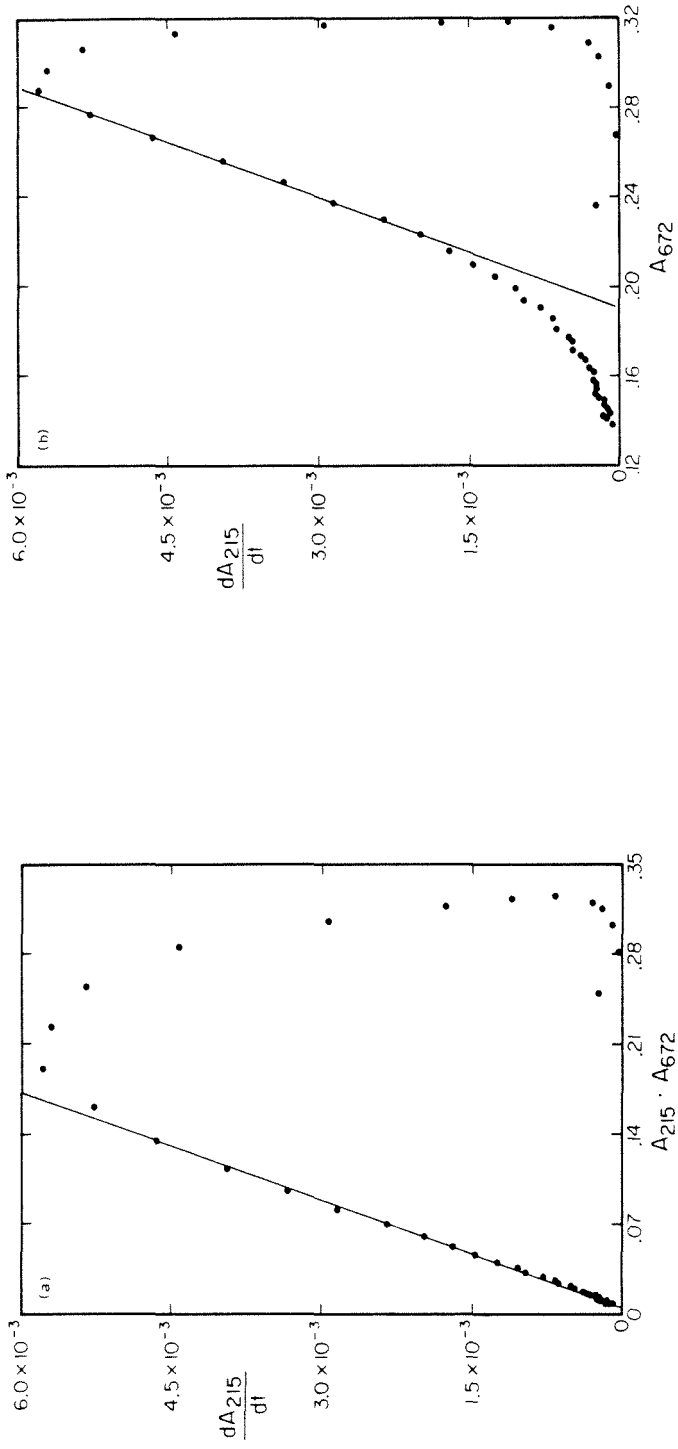

Fig. 4. (a) The rate of disappearance of S(IV), $-dA_{215}/dt$, plotted against the product of [S(IV)], A_{215}, times $[(SO_3)Co(III)TSP(O_2^{\cdot})^{4-}]$, A_{627}. Linear dependence of the observed reaction rate on the product $A_{215}A_{672}$ indicates that the slow step of the mechanism is the reaction of $(SO_3)Co(III)TSP(O_2^{\cdot})^{4-}$ and SO_3^{2-}. (b) $-dA_{215}/dt$ vs. A_{672}. The non-linear dependence of the reaction rate on A_{672} indicates that the slow step is unlikely to be the k_4 step of Fig. 2.

106

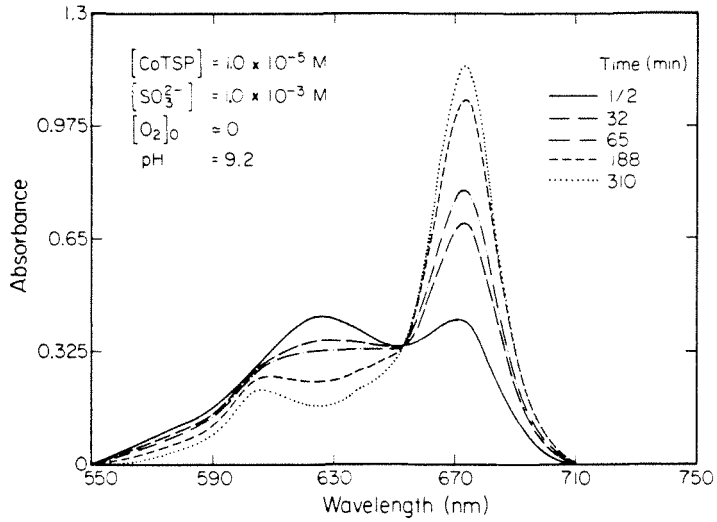

Fig. 5. Change in the visible spectrum of Co(II)TSP solutions of monomer and dimer in the presence of SO_3^{2-} and in the initial absence of O_2. The peak at λ = 672 nm rises slowly as O_2 diffuses into the sealed cuvette.

$TSP(O_2^-)^{4-}$. As shown in Fig. 2, the rate-determining step is thought to involve electron transfer from SO_3^{2-} to $(SO_3)Co(III)TSP(O_2^-)^{4-}$. The rate-limiting electron transfer is followed by hydrolysis of bound SO_3^{2-} to yield SO_4^{2-} and a Co(II)-TSP-peroxide intermediate. For this step we can write Eqn (15):

$$v = -\frac{d[SO_3^{2-}]}{dt} = k_4[(SO_3)Co(III)TSP(O_2^-)(SO_3^{2-})^{6-}] \quad (15)$$

Assuming a rapid pre-equilibrium step, Eqn (15) can be rewritten as Eqn (16):

$$v = \frac{k_3 k_4}{k_{-3} + k_4}[(SO_3)Co(III)TSP(O_2^-)^{4-}][SO_3^{2-}] \quad (16)$$

According to Eqn (16) a plot of $-(dA_{215})/dt$ versus $(A_{672} \cdot A_{215})$ should yield a straight line after a short induction period for the formation of $(SO_3)Co(III)$-$TSP(O_2^-)^{4-}$. The plot of Fig. 4a is consistent with this prediction. In this analysis, $-(dA_{215})/dt$ is assumed to correspond directly to the rate of reaction, $A_{215} \propto [SO_3^{2-}]$, and $A_{672} \propto [(SO_3)Co(III)TSP(O_2^-)]$. Furthermore, a plot of $-(dA^{215})/dt$ versus A_{672} is non-linear, as shown in Fig. 4b. These two relationships, when considered together, suggest that a second sulfite ion reacts with $(SO_3)Co(III)TSP(O_2^-)^{4-}$ without the formation of a ternary activated complex of sufficiently long life to be kinetically significant. The ionic strength dependence of the observed rate constant was found to be positive [25]. In this case, the primary salt effect predicts that a reaction between ions of similar charge [i.e. SO_3^{2-} and $(SO_3Co(III)TSP(O_2^-)^{4-}]$ should proceed at a faster rate at higher ionic strength.

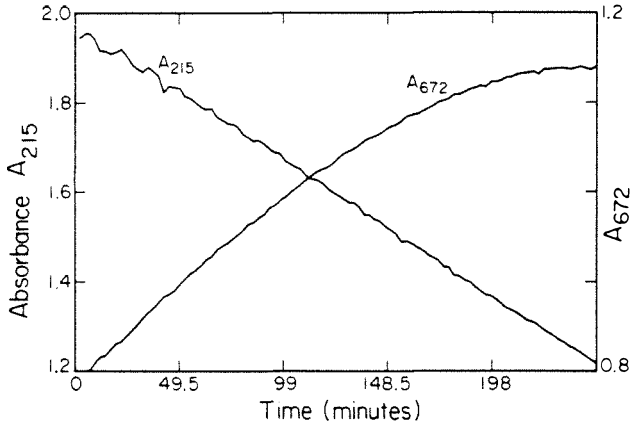

Fig. 6. Concentration versus time profiles for SO_3^{2-} at λ = 215 nm and for the catalytically active intermediate complex at λ = 672 nm for a system initially devoid of oxygen.

In the preceding analysis, we have attributed the absorbance peak at λ = 672 nm to the catalytically active center, $(SO_3)Co(III)TSP(O_2^-)^{4-}$. In order to verify this assumption, experiments were carried out in the absence of O_2. Figure 5 shows changes in the visible spectrum of $Co(II)TSP^{2-}$ as a function of time after SO_3^{2-} had been added in a molar ratio of 100:1 to a system devoid of O_2. The absorbance at λ = 672 increased as the absorbance at λ = 626 decreased. The peak at A_{672} reached a maximum in the time-frame of hours in the absence of O_2, whereas the characteristic time was reduced to minutes in the presence of O_2. During this time, SO_3^{2-} as measured by $-(dA_{215})/dt$ was oxidized slowly with apparent zero-order rate, as shown in Fig. 6. The rate of oxidation of S(IV) under these conditions appears to be controlled by diffusion of air into the sample. We conclude that the measured absorbance at λ = 672 is caused by

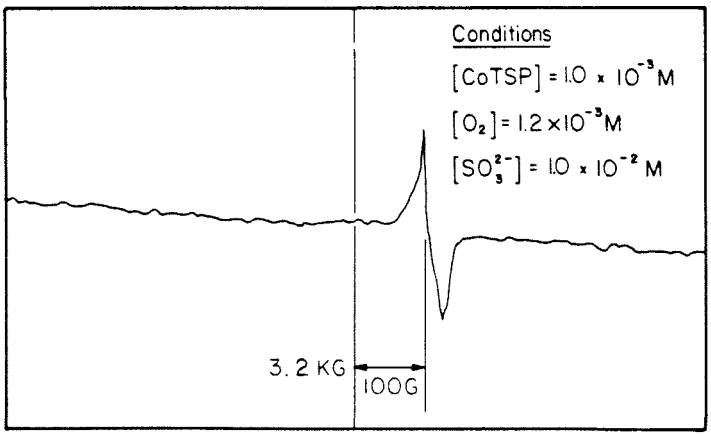

Fig. 7. EPR spectrum of a frozen 10% DMF/90% H_2O solution of $Co(II)TSP^{2-}$ (1 mM) saturated with ($[O_2]$ = 2.5 × 10^{-4} M).

108

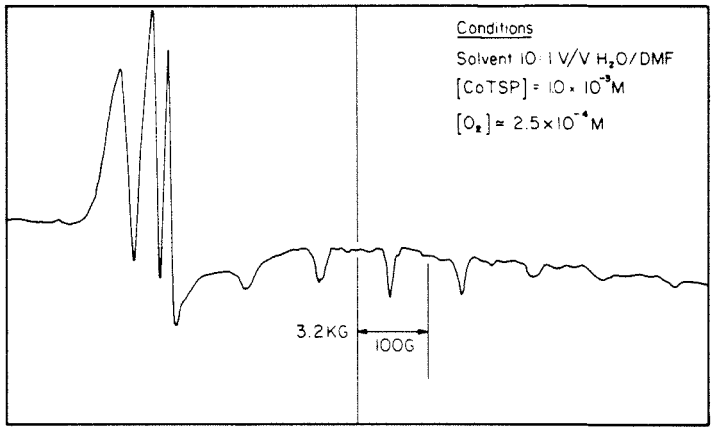

Fig. 8. EPR spectrum of a 10% DMF/90% H_2O solution of Co(II)TSP^{2-} (1 m*M*), O_2 (0.25 m*M*) and sulfite (1 m*M*).

various monomeric species of Co(II)TSP^{2-}. No change in the inherent Co(II) spectrum was observed upon bubbling oxygen through S(IV)-free Co(II)T-SP^{2-} solution for 1 h. This suggests that the formation of a ternary complex of SO_3^{2-}, Co(II)TSP^{2-}, and O_2 is essential for the initiation of the catalytic cycle.

To determine the oxidation state of cobalt and the nature of the bound O_2, EPR spectra were obtained under a variety of conditions. Figure 7 shows the EPR spectrum of 1 m*M* CO(II)TSP in 10% DMF aqueous solution at 77 K. In this case the DMF/H_2O solvent enhanced the concentration of the monomeric form of Co(II)TSP^{2-} relative to the dimeric form. When 1 m*M* of SO_3^{2-} as Na_2SO_3 was introduced into the solution, the resultant spectrum (Fig. 8) was almost identical to that reported previously by Cookson et al. [32] for (OH)Co(II)T-

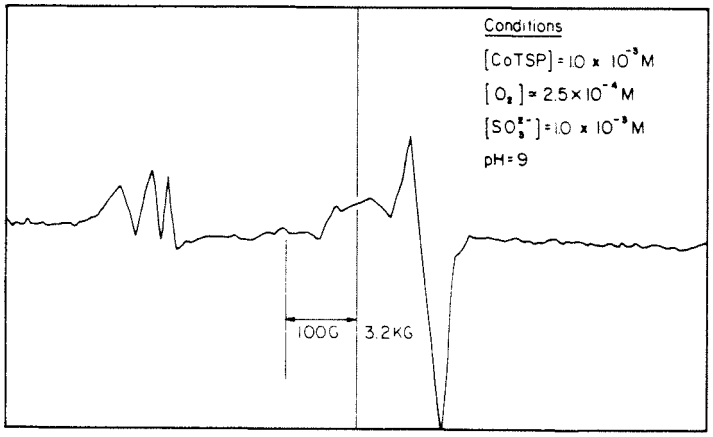

Fig. 9. EPR spectrum of a frozen 10% DMF/90% H_2O solution of Co(II)TSP^{2-} (1 m*M*) and O_2 (1.2 m*M*).

$SP(O_2^-)^{3-}$. This spectrum may be attributed to an oxygen adduct of the general form $(SO_3)Co(III)TSP(O_2^-)^{4-}$. The pH of the reaction mixture after addition of Na_2SO_3 was ~9. Because there is no observable signal due to $[(OH)Co(III)(O_2^-)]^{3-}$ at this pH, we believe the signal to come from a ternary complex involving SO_3^{2-}, O_2, and Co(II)TSP. The spectrum appears to result from a mixture of $(SO_3)Co(II)TSP^{4-}$ and $(SO_3)Co(II)TSP(O_2^-)^{4-}$, because O_2 at $2.5 \times 10^{-4} M$ is stoichiometrically limiting in this case. When a solution of $1\,mM$ $Co(II)TSP^{2-}$ and $10\,mM$ SO_3^{2-} was exposed to pure O_2 at 1 atm ($[O_2]_{aq} \sim 1.2 \times 10^{-3} M$), the signal due to Co(II) around 2800 G disappeared and only the cobalt(III) superoxide signal was observed (Fig. 9). These observations and the UV-VIS spectral changes are consistent with a reaction sequence that has $(SO_3)Co(III)TSP(O_2^-)^{4-}$ as the intermediate complex.

DISCUSSION

The catalytic autoxidation of sulfite proceeds in four distinct steps (Fig. 2). The first step involves the dissociation of the Co(II)TSP dimer [33, 34] into monomers. In the second step sulfite binds to the complex to form $(SO_3)Co(II)TSP^{4-}$. The observed initial increase of the product of A_{215} and A_{672} corresponds to these first two steps (Fig. 4a). In the third step the catalytically active species, $(SO_3)Co(III)TSP(O_2^-)^{4-}$, is formed by binding of dioxygen to the vacant apical coordination site of monomeric $(SO_3)Co(III)TSP^{4-}$. This step increases the apparent oxidation rate, $-(dA_{215})/dt$ and decreases the product $[(SO_3)Co(III)TSP(O_2^-)^{4-}][SO_3^{2-}]$ (i.e. $A_{215} \cdot A_{672}$) slightly due to loss of SO_3^{2-}. These three steps correspond to the induction period shown in Fig. 4a. The fourth step involves the rate-limiting reaction of the active catalytic center, $(SO_3)Co(III)TSP(O_2^-)^{4-}$, with a second sulfite molecule to produce sulfate. The straight line region of Fig. 4a accurately correlates the observed reaction rate with the concentration of the reactants in the rate-limiting step.

Substitution of sulfite into an axial coordination site of $Co(II)TSP^{2-}$ enhances the subsequent uptake of molecular oxygen to form the active catalytic center. In a study of reversible binding of dioxygen to Co(II) complexes of the general formula Co(II)(L)(B) (L = a quadridentate Schiff base or porphyrin ligand; B = an axial base), Carter et al. [35] have shown that the electron density on the cobalt atom increases with increasing π-electron donating ability of B. High electron density on cobalt strengthens the "π-backbonding" interaction between Co and O_2. Rollman and Chan [36] reported that the imidazole complex of Co(II)TSP reacts rapidly with O_2, whereas the corresponding pyridine derivative was unreactive. Electronic properties of axial ligands have been shown to affect both the thermodynamics and kinetics of reversible O_2 transfer [8].

The apparent decrease in the absorbance of $(SO_3)Co(III)(O_2^-)^{4-}$ may be due to irreversible oxidation to $Co(III)TSP^-$ by the intermediate reaction product, H_2O_2. Cookson et al. [32] observed irreversible oxidation of $Co(II)TSP^{2-}$ to $Co(III)TSP^-$ upon prolonged standing of the complex in air.

110

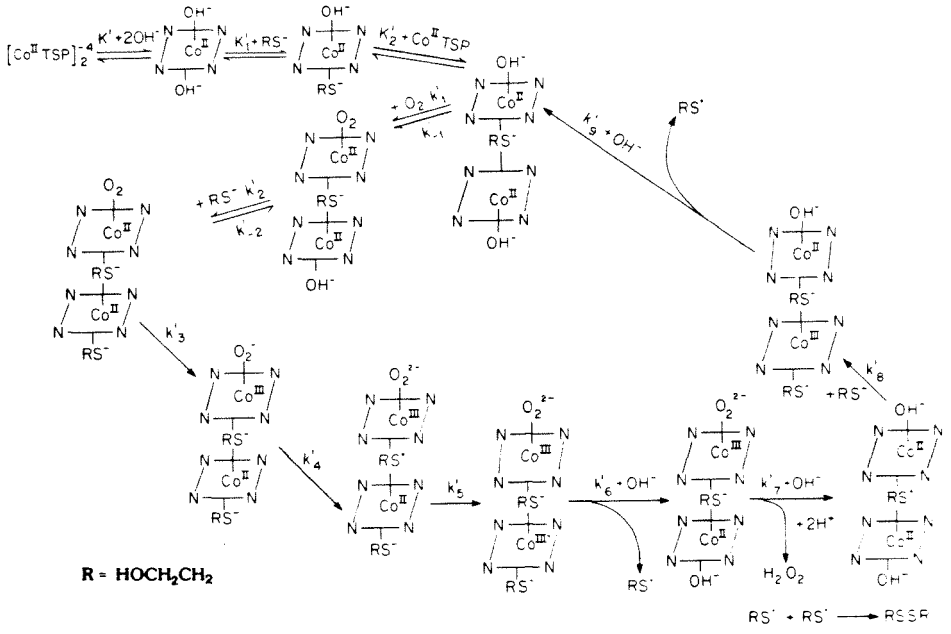

Fig. 10. Postulated reaction mechanism for the autoxidation of 2-mercaptoethanol catalyzed by Co(II)TSP^{2-} at pH 11.

The catalyzed autoxidation of 2-mercaptoethanol also appears to follow an ordered ternary-complex mechanism [37]. Analysis of the rate data and the observed rate law suggest that the oxidation of RS^- to RSSR involves reversible coordination of the substrate and dioxygen by Co(II)TSP^{2-} to form an active catalytic center, which is dimeric (Fig. 10). Successive electron-transfers from each of the two substrate molecules precedes thiyl radical dimerization. It is especially interesting to note that rapid oxidation of 2-mercaptoethanol in the presence of Co(II)TSP^{2-} does not require photochemical sensitization, in contrast to results obtained by Beelen and co-workers [38].

APPLICATIONS

A major disadvantage associated with the application of homogeneous catalysis to water pollution control involves the problem of separating the catalyst and oxidation products at the end of the reaction. This drawback may be overcome through attachment of a reactive transition-metal complex to the surface of an inert solid matrix. In this case, a hybrid/heterogeneous complex is substituted for the water-soluble metal–organic complex, thereby facilitating recovery of the catalyst [39, 40]. Hybrid complexes may be utilized conveniently either in batch or continuous-flow reactors where the catalyst is removed by coarse filtration [40].

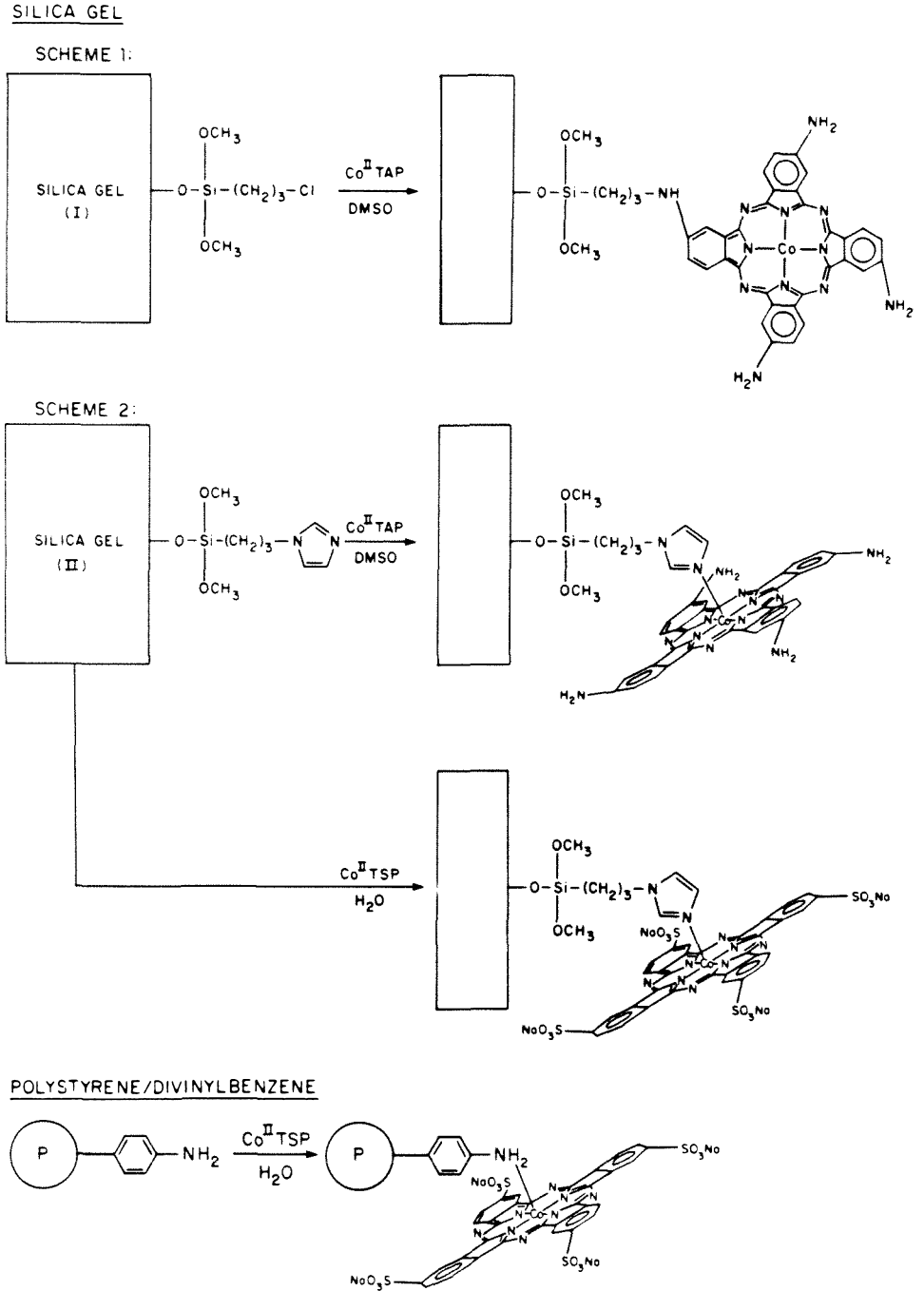

Fig. 11. Syntheses and structures of solid-supported cobalt(II)–phthalocyanine complexes. Reprinted with permission from ref. [46].

112

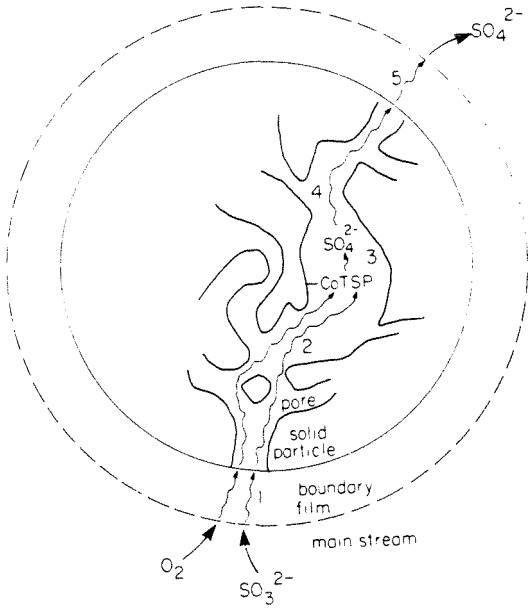

Fig. 12. Schematic diagram illustrating the diffusion of reactants and products to and away from reactive sites within a porous catalyst bead.

Maas and co-workers [41] and Schutten et al. [42, 43], reported that the rate of the aqueous-phase conversion of thiosalts to disulfides (RSSR) was enhanced upon addition of cobalt(II)-phthalocyanines attached to polyacrylamide, polyvinylamine, or a cross-linked sytrene/divinylbenzene copolymer. Experiments performed in this laboratory have shown that the hybrid Co(II)TSP^{2-} and Co(II)-4, 4′,4″,4‴-tetraminophthalocyanine, Co(II)TAP^{2+} complexes depicted in Fig. 11, are efficient catalysts for the autoxidation of S(−II), S(IV), RSH and N_2H_4 [44]. Attachment to a solid-support may make the macrocyclic complex catalytically more active than its water-soluble analog by inhibiting formation of a catalytically inactive μ-peroxo-bridged cobalt(III) dimer (Eqns (17) and (18)).

$$\text{Co(II)PC} + O_2 \rightleftharpoons \text{Co(III)PC}(O_2^-) \tag{17}$$

$$\text{Co(III)PC}(O_2^-) + \text{Co(II)PC} \rightleftharpoons \text{PC[Co(III)}\text{–}O_2^{2-}\text{–Co(III)]PC} \tag{18}$$

PC = phthalocyanine

Zwart and van Wolput [45] obtained electron spin resonance data indicative of the formation of a 1:1 Co(III)–superoxide adduct upon exposure of solid-supported cobalt(II) complexes to oxygen. These results suggest that hybrid metal complexes may provide a convenient and economical method of water pollution control.

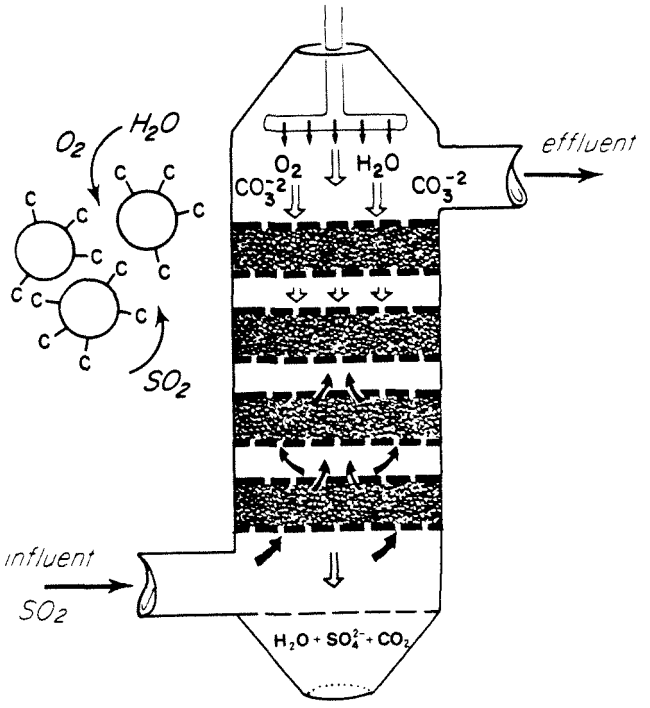

Fig. 13. An application of hybrid catalysts for SO_2 stack-gas scrubbing. The active catalyst C is anchored on particle beads that are placed in a countercurrent-flow reactor. Reprinted with permission from ref. [46].

Kinetic analysis of the heterogeneous reaction systems suggests that the mechanism of oxidation involves "activation" of molecular oxygen and complexation of the substrate by the metal center at the solid surface in a manner analogous to that observed for homogeneous catalysis [44]. In general, reactions on solid matrices occur more slowly because access of the reactants to the active site may be influenced by mass-transfer effects such as pore diffusion, as illustrated in Figure 12. Further experimentation is required to quantify the effects of mass-transport properties on the catalytic reactions of O_2 with water-soluble reductants in binary-phase catalytic systems. The hybrid phthalocyanine complexes can serve as simple models for adsorbed metal in natural waters and may potentially be used for pollution control, for instance for SO_2 stack-gas scrubbing, post-Klaus plant scrubbing of H_2S and SO_2, sweetening of sour oil refining wastewaters, elimination of excess rocket fuel wastes, and odor control in conventional wastewater treatment facilities. With a growing likelihood of emission control requirements for SO_2 from power plants, alternatives to limestone slurry scrubbers will be needed. In this laboratory, countercurrent reactors with fixed beds of solid-supported catalysts are being examined for SO_2 scrubbing efficiency (Fig. 13). In this case, H_2SO_4 can be recovered as a potentially useful by-product.

114

REFERENCES

1 R.A. Sheldon and J.K. Kochi, Metal-catalyzed Oxidation of Organic Compounds, Academic Press, New York, 1981.
2 M.R. Hoffmann, Trace metal catalysis in aquatic environments, Environ. Sci. Technol., 14 (1980) 1061–1066.
3 J.O. Niragu (Ed.), Sulfur in the Environment, Wiley-Interscience, New York, 1978, p. 38.
4 K.Y. Chen and J.C. Morris, Kinetics of oxidation of aqueous sulfide by O_2, Environ. Sci. Technol., 6 (1972) 529–537.
5 H. Backstrom, Der Kettenmechanismus bei der Autoxydation von Natriumsulfitlösungen, Z. Phys. Chem., 52B (1934) 122–138.
6 T.J. Wallace, A. Schriesheim, H. Humvitz and M.B. Glaser, Base-catalyzed oxidation of mercaptans in the presence of inorganic transition metal complexes, Ind. Eng. Chem. Proc. Des. Develop., 3 (1964) 237–241.
7 A.A. Akhren, D.I. Metelista and M.R. Skurko, Mono-oxygenase enzymes and their simulation, Russ. Chem. Rev., 44 (1975) 398–412.
8 F. Basolo, B.M. Hoffmann and J.A. Ibers, Synthetic oxygen carriers of biological interest, Acc. Chem. Res., 8 (1975) 384–392.
9 J.P. Collman, Synthetic models for the oxygen-binding hemoproteins, Acc. Chem. Res., 10 (1975) 265–272.
10 R.C. Jones, D.A. Summerville and F. Basolo, Synthetic oxygen carriers related to biological systems, Chem. Rev., 79 (1979) 139–179.
11 M.M. Khan and A.E. Martell, Homogeneous Catalysis by Metal Complexes, Academic Press, New York, 1974, pp. 79–180.
12 A.B.P. Lever and H.B. Gray, Electronic spectra of metal–dioxygen complexes, Acc. Chem. Res., 11 (1978) 348–355.
13 G. McLendon and A.E. Martell, Inorganic oxygen carriers as models for biological systems, Coord. Chem. Rev., 19 (1976) 1–39.
14 E. Ochiai, Bioinorganic chemistry of oxygen, J. Inorg. Nucl. Chem., 37 (1974) 1503–1509.
15 A.V. Savitskii and V.I. Nelyubin, Activation of molecular oxygen on interaction with transition metal complexes, Russ. Chem. Rev., 44 (1975) 214–235.
16 L. Vaska, Dioxygen metal complexes: Toward a unified view, Acc. Chem. Res., 9 (1975) 175–183.
17 L.J. Boucher, Metal complexes of phthalocyanines, in G.A. Melson (Ed.), Coordination Chemistry of Macrocyclic Compounds, Plenum Press, New York, 1979, pp. 461–516.
18 A.H. Cook, Catalytic properties of the phthalocyanines. Part I. Catalase properties, J. Chem. Soc., (1938) 1761–1768.
19 A.H. Cook, Catalytic properties of the phthalocyanines. Part II. Oxidase properties, J. Chem. Soc., (1938) 1768–1774.
20 J. Dolansky, D.M. Wagnerova and J. Veprek-Siska, Autoxidation of cystein catalyzed by cobalt(II) tetrasulphophthalocyanine. Models of oxidases V, Collect. Czech. Chem. Commun., 41 (1976) 2326–2332.
21 A. Nishinaga and H. Tomita, Model catalytic oxygenations with Co(II)-Schiff base complexes and the role of cobalt–oxygen complexes in the oxygenation process, J. Molec. Catal., 7 (1980) 179–199.
22 K. Uchida, H. Soma and S. Nato, Manganese phthalocyanine as a model of tryptophan-2,3-dioxygenase, Chem. Lett., (1978) 471–474.
23 D.M. Wagnerova, E. Schwertnerova and J. Veprek-Siska, Autoxidation of hydoxylamine catalysed by cobalt(II)-tetrasulphophthalocyanine. Models of oxidases, Collect. Czech. Chem. Commun., 39 (1974) 1980–1988.
24 M.R. Hoffmann and B.C.H. Lim, Kinetics and mechanism of the oxidation of sulfide by oxygen: Catalysis by homogeneous metal–phthalocyanine complexes, Environ. Sci. Technol., 13 (1979) 1406–1413.
25 S.D. Boyce, M.R. Hoffmann, P.A. Hong and L.M. Moberly, Catalysis of the autoxidation of aquated sulfur dioxide by homogeneous metal–phthalocyanine complexes, Environ. Sci. Technol., 17 (1983) 602–611.

26 M.R. Hoffmann and S.D. Boyce, Theoretical and experimental considerations of the catalytic autoxidation of aqueous sulfur dioxide in relationship to atmospheric systems, Adv. Environ. Sci. Technol., 12 (1983) 149–189.

27 M.R. Hoffmann and D.J. Jacob, Kinetics and mechanism of the catalytic oxidation of dissolved SO_2 in aqueous solution: Application to nightime fog water chemistry, in J.G. Calvert (Ed.), SO_2, NO and No_2 Oxidation Mechanisms: Atmospheric Considerations; Acid Precipitation Series, Vol. 3, Butterworth, Stoneham, MA, 1984, pp. 101–172.

28 D.J. Jacob and M.R. Hoffmann, A dynamic model for the production of H^+, NO_3^- and SO_4^{2-} in urban fog, J. Geophys. Res., 88 (1983) 6611–6621.

29 B. Meyer, Sulfur, Energy and the Environment, Elsevier Scientific Publishing Co., Amsterdam, The Netherlands, 1977.

30 J.O. Nriagu (Ed.), Sulfur in the Environment, Wiley-Interscience, New York, 1978, p. 25.

31 J.H. Weber and D.H. Busch, Complexes derived from strong field ligands. XIX. Magnetic properties of transition metal derivatives of 4,4′,4″,4‴-tetrasulfophthalocyanine, Inorg. Chem., 4 (1965) 469–471.

32 D.J. Cookson, T.D. Smith, J.F. Boas, P.R. Hicks and J.R. Pilbrow, Electron spin resonance study of the autoxidation of hydrazine, hydroxylamine, and cysteine catalysed by the Co(II) chelate complex of 3,10,17,24-tetrasulfophthalocyanine, J. Chem. Soc., Dalton Trans., (1977) 109–114.

33 L.C. Gruen and R.J. Blagrove, The aggregation and reaction with oxygen of the tetrasodium salt of cobalt phthalocyanine – 4,4′,4″,4‴-tetrasulphonic Acid, Aust. J. Chem., 26 (1973) 319–323.

34 N.N. Kundo and N.P. Keier, Mechanisms of the catalytic action of cobalt tetrasulfophthalocyanine, Russ. J. Phys. Chem., 42 (1968) 707–711.

35 M.J. Carter, D.P. Rillema and F. Basolo, Oxygen carrier and redox properties of some neutral cobalt chelates. Axial and in-plane ligand effects, J. Am. Chem. Soc., 96 (1974) 392–400.

36 L.D. Rollmann and S.I. Chan, Electron spin resonance studies of low spin cobalt(II) complexes. Base adducts of cobalt phthalocyanine, Inorg. Chem., 10 (1971) 1978–1982.

37 P.S.K. Leung and M.R. Hoffmann, Oxidation of 2-mercaptoethanol by molecular oxygen: Catalysis by cobalt(II)-4,4′,4″,4‴-tetrasulfophthalocyanine, J. Phys. Chem., (1987) submitted.

38 T.P.M. Beelen, C.O. de Costa Gomez and M. Kuijer, The enhancement by visible light of the catalytic activity of Co(II)-tetrasulphophthalocyanine of the oxidation of mercaptoethanol, Recl. Trav. Chim. Pay-Bas, 98 (1979) 521–522.

39 R.H. Grubbs, Hybrid-phase catalysts, Chemtech., 7 (1977) 512–518.

40 F.R. Hartley and P.N. Vezey, Supported transition metal complexes as catalysts, Adv. Organomet. Chem., 15 (1977) 189–234.

41 T.A.M.M. Maas, M. Kuijer and J. Zwart, Activation of cobalt-phthalocyanine catalyst by polymer attachment, J. Chem. Soc., Chem. Commun., (1976) 86–88.

42 J.H. Schutten and T.P.M. Beelen, The role of hydrogen peroxide during the autoxidation of thiols promoted by bifunctional polymer bound cobalt phthalocyanine catalysts, J. Molec. Catal., 10 (1981) 85–97.

43 J.H. Schutten and J. Zwart, Autoxidation of mercaptans promoted by a bifunctional catalyst prepared by polymer attachment of cobalt-phthalocyanine, J. Molec. Catal., 5 (1979) 109–123.

44 P.A. Hong, L.M. Moberly, M.R. Hoffmann and S.D. Boyce, Catalytic autoxidation of chemical contaminants by hybrid metal-phthalocyanine complexes, Environ. Sci. Technol., submitted.

45 J. Zwart and J.H.M.C. van Wolput, An ESR study of the reaction of cobalt phthalocyanine with ammonia and dioxygen, J. Molec. Catal., 5 (1979) 235–239.

46 S.D. Boyce, M.R. Hoffmann, P. Andrew Hong and L.M. Moberly, Catalysis of the autoxidation of aquated sulfur dioxide by homogeneous and heterogeneous transition metal complexes, in C.M. Bhumralkar (Ed.), Meteorological Aspects of Acid Rain; Acid Precipitation Series, Vol. 1, Butterworth, Stoneham, MA, 1984, pp. 163–211.

Chapter 4

Catalysis of the Autoxidation of Aquated Sulfur Dioxide by Homogeneous and Heterogeneous Transition Metal Complexes

Scott Boyce, Michael Hoffmann, Andrew Hong, Lorraine Moberly

Acid Precipitation, J. Teasley, ed., Ann Arbor Science,
Ann Arbor, MI 1984, Chapter 11.

Catalysis of the Autoxidation of Aquated Sulfur Dioxide by Homogeneous and Heterogeneous Transition Metal Complexes

Scott D. Boyce
Michael R. Hoffman
P. Andrew Hong
Lorraine M. Moberly

GENERAL CONSIDERATIONS

The relationship between acid precipitation and the fate of sulfur dioxide (SO_2) and nitrogen oxides (NO_x) in the atmosphere has become the subject of intensive study in recent years. Fundamental questions about the multifarious pathways for the chemical transformation of SO_2 and NO_x to oxyacids remain to be answered before a complete description of this complex reaction network can be provided.

SO_2 and NO_x can be oxidized to acidic sulfate and nitrate aerosols either homogeneously in the gas phase or heterogeneously in atmospheric microdroplets [1–3]. Field studies indicate that the relative importance of homogeneous and heterogeneous processes depends on a variety of climatological factors such as relative humidity and the intensity of incident solar radiation [4–9].

Until recently, most literature discussions of the oxidation of SO_2 have focused on homogeneous gas-phase reactions involving hydroxyl ($HO\cdot$) and hydroperoxyl ($HO_2\cdot$) radicals. However, recent measurements have indicated that the rates of oxidation of SO_2 by $HO_2\cdot$ and organic peroxides are slower than previously thought [1]. Furthermore, the apparent oxidation rate of sulfur dioxide by $HO\cdot$ also does not appear to be sufficiently fast to account for observed sulfate formation rates in the atmosphere [2,3]. This is especially true in cases where rapid conversion of SO_2 has been observed under conditions of high humidity or at night in the

absence of photolytically generated radical species [4]. For these reasons, it is now believed that condensed-phase (i.e., aqueous solution) homogeneous and heterogeneous pathways contribute significantly to the production of sulfuric acid (H_2SO_4) in the atmospheric microdroplets. As a result, considerable experimental and theoretical work has been directed toward an evaluation of the potential role of ozone (O_3), hydrogen peroxide (H_2O_2) and nitrous acid (HNO_2) as liquid-phase oxidants. The reactions of SO_2 with these species in aqueous solution are discussed by Schwartz [10] and Martin [11].

Catalytic autoxidation of sulfur dioxide dissolved in aqueous microdroplets has been suggested as a nonphotolytic pathway for the rapid accumulation of sulfuric acid in humid atmospheres [12–20]. In general, reactions of the triplet ground electronic state of molecular oxygen (O_2) (Figure 1) with singlet state reductants such as SO_2 proceed slowly because they involve changes in spin multiplicity and a large degree of bond deformation or alteration in the formation of products. In many cases, autoxidation reactions can be initiated photolytically through irradiation of the reactant species. For example, ultraviolet light exerts a strong catalytic effect on the solution-phase autoxidation of SO_2 [21]. Alternatively, the reactions of O_2 with a variety of organic and inorganic substrates can be accelerated in the presence of transition metal ions, such as Co(II), Co(III), Cu(II), Fe(II), Fe(III), Mn(II) and Ni(II) [22,23].

Oxidation of sulfur dioxide by molecular oxygen proceeds according to the following stoichiometry:

$$S(IV) + \frac{1}{2} O_2 \longrightarrow H_2SO_4 \qquad (1)$$

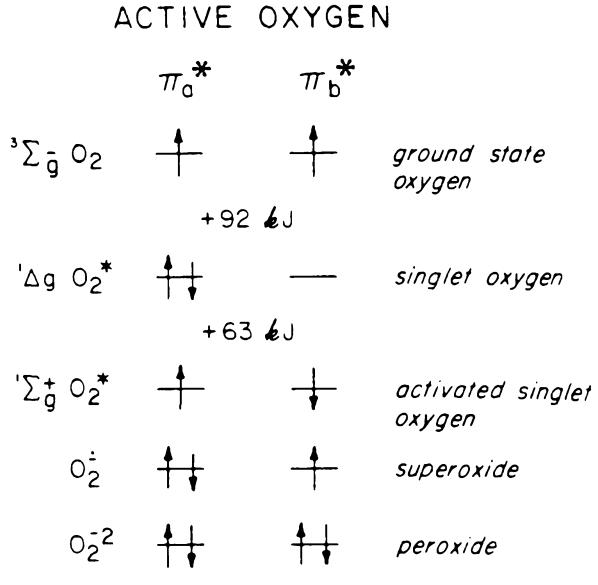

Figure 1. Electronic distributions into pi-antibonding orbitals of dioxygen according to molecular orbital theory and associated energies shown with corresponding spin states.

S(IV) denotes the overall speciation of SO_2 in aqueous solution including aquated sulfur dioxide ($SO_2 \cdot H_2O$), bisulfite ion (HSO_3^-) and sulfite ion (SO_3^{2-}) such that $[S(IV)] \simeq [SO_2 \cdot H_2O] + [HSO_3^-] + [SO_3^{2-}]$. This reaction is particularly sensitive to catalysis by metal ions at trace concentrations. Numerous investigators have examined the kinetics of this redox process under a wide range of experimental conditions [16,24–35]. Unfortunately, the results of these studies (Table I) show a considerable degree of disagreement as to the quantitative effects of catalyst (metal ion) concentration, pH and light on the rate of autoxidation.

A review of the available literature [36] revealed that three general categories of mechanistic pathways have been proposed to explain observed kinetic data. The postulated mechanisms include:

1. Thermally initiated free-radical chain processes involving a sequence of one-electron transfer steps such as [37]:

$$\text{initiation:} \quad M^{n+} + SO_3^{2-} \longrightarrow M^{(n-1)+} + SO_3^- \tag{2}$$

$$\text{propagation:} \quad SO_3^- + O_2 \longrightarrow SO_5^- \tag{3}$$

$$SO_5^- + SO_3^{2-} \longrightarrow SO_5^{2-} + SO_3^- \tag{4}$$

$$\text{oxidation:} \quad SO_5^{2-} + SO_3^{2-} \longrightarrow 2SO_4^{2-} \tag{5}$$

$$\text{termination:} \quad 2SO_3^- \longrightarrow S_2O_6^{2-} \tag{6}$$

$$SO_3^- + SO_5^- \longrightarrow S_2O_6^{2-} + O_2 \tag{7}$$

$$2SO_5^- \longrightarrow S_2O_6^{2-} + 2O_2 \tag{8}$$

Table I. Empirical Rate Laws Reported for Metal-Catalyzed Autoxidation of SO_2^a

M^{n+}				*Reference*
Fe^{3+}	1	1–2	?	16
	1	1	0	26,28
Cu^{2+}	0.5	1.5	0	24
	1	1	0	31
Co^{2+}	0.5	1.5	0	25
	2	1	1	29
	0.5	?	1	32
	1	1	1	35
Co^{3+}	0.5	1.5	0	27
	0.5	?	2	34
Mn^{2+}	2	0	0	28
	≤ 1	≤ 1	0	33

2. Nonradical, polar mechanisms in which formation of an inner-sphere metal sulfite coordination complex precedes two-electron transfer from the substrate to oxygen [30,38]:

$$M^{n+} + SO_3^{2-} \rightleftharpoons MSO_3^{(n-2)+} \tag{9}$$

$$MSO_3^{(n-2)+} + SO_3^{2-} \rightleftharpoons M(SO_3)_2^{(n-4)+} \tag{10}$$

$$M(SO_3)_2^{(n-4)+} + O_2 \rightleftharpoons M(SO_3)_2\ O_2^{(n-4)+} \tag{11}$$

$$M(SO_3)_2 \cdot O_2^{(n-4)+} \xrightarrow[\text{slow}]{} M^{n+} + 2SO_4^{2-} \tag{12}$$

3. Photoassisted pathways in which the reaction is initiated through absorption of light ($h\nu$) by sulfite, the metal ion or a metal-sulfite complex [39]:

Of the three alternatives, free-radical mechanisms are most frequently cited in attempts to achieve an adequate interpretation of experimental measurements. Several modifications to the scheme originally suggested by Backström [37] (Equations 2–8) have also been reported in which species such as the sulfate radical ($SO_4^{\cdot-}$), $HO_2\cdot$ and $HO\cdot$ are thought to act as chain carriers [21,40]. From an analysis of kinetic expressions corresponding to the various hypothetical mechanisms, it became apparent that the kinetics of the autoxidation of sulfite conform to a complex multiterm rate law.

The basic hypothesis that governs the research being conducted in the authors' laboratory is that the autoxidation of aquated SO_2 and other water-soluble reductants and the nonphotolytic production of H_2O_2, $HO_2\cdot$ and $HO\cdot$ as liquid-phase oxidants may represent interrelated phenomena. According to this scheme, hydrogen peroxide would form as a two-electron reduction product of O_2 from a catalyzed reaction pathway in which molecular oxygen is "activated" via coordination to a transition metal center. Complexation of dioxygen reduces the activation energy barrier for direct reaction of O_2 with a substrate. It is well understood that numerous metalloenzyme redox systems function in this manner [41]. Subsequently, H_2O_2 may either decompose in the presence of metal ions such as iron to form hydroxyl and hydroperoxyl radical intermediates as in the classic "Fenton's reagent" cycle [42]:

$$Fe^{2+} + H_2O_2 \longrightarrow Fe(OH)^{2+} + HO\cdot \tag{13}$$

$$Fe^{3+} + H_2O_2 \longrightarrow Fe^{2+} + H^+ + HO_2\cdot \tag{14}$$

$$Fe^{3+} + HO_2\cdot \longrightarrow Fe^{2+} + H^+ + O_2 \tag{15}$$

$$HO\cdot + H_2O_2 \longrightarrow H_2O + HO_2\cdot \tag{16}$$

$$HO_2\cdot + H_2O_2 \longrightarrow O_2 + H_2O + HO\cdot \qquad (17)$$

or participate directly in the oxidation of additional dissolved sulfur dioxide.

EXPERIMENTAL OBJECTIVES

To investigate further some of the fundamental aspects of the solution-phase oxidation of sulfur dioxide, a study of the reaction of dissolved SO_2 with molecular oxygen in a well defined catalytic system was undertaken. In natural systems, transition-metal ions are frequently associated with organic and inorganic ligands. Lunde et al. [43] have identified a broad range of organic micropollutants, including several aliphatic and aromatic carboxylic acids in precipitation samples collected over Norway. Many of these compounds could readily form stable coordination complexes with trace metal species dissolved in atmospheric microdroplets. Unfortunately, only a very few studies of the catalytic properties of organometallic complexes have been carried out using aqueous solutions.

One type of organometallic complex that has been the subject of detailed examination is the phthalocyanine series. Phthalocyanines are tetrapyrrole derivatives that form square planar complexes in which a divalent metal ion, M(II) is coordinated to the four pyrrole nitrogen atoms of the macrocyclic structure as depicted in Figure 2. Metal-phthalocyanines have been shown to be effective homo-

$$2SO_3^{2-} + O_2 \xrightarrow{\text{catalyst}} 2SO_4^{2-}$$

catalyst = M−4,4′,4′,4‴−tetrasulfophthalocyanine

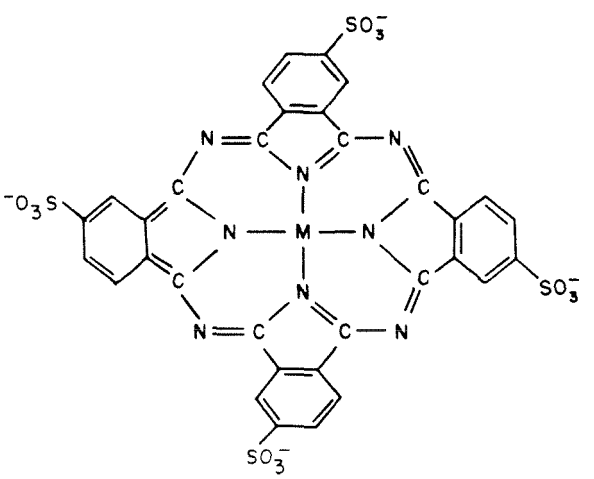

M ≡ Fe^{II}, Mn^{II}, Co^{II}, Ni^{II}, Cu^{II}, V^{IV}

Figure 2. Stoichiometric relationship between sulfite and sulfate in metal-catalyzed reactions where the stoichiometric coefficient for oxygen is 0.5 and the catalyst is Co(II).

geneous and heterogeneous catalysts for the autoxidation of many types of substrates, including aldehydes [44,45], phenols [46,47], mercaptans [48], hydrazine [49], and hydroxylamine [50].

Hoffmann and Lim [51] have studied the catalyzed autoxidation of hydrogen sulfide (HS^-) in aqueous solution over the pH range 5–12. The catalytic properties of water-soluble Co(II)-, Cu(II)- and Ni(II)-4,4′,4″,4′″-tetrasulfophthalocyanines (M(II)-TSP) were evaluated in terms of the generalized rate equation:

$$\nu = \frac{-d[HS^-]}{dt} = \frac{k[M(II)TSP][O_2][HS^-]}{K_C + K_B + K_A[HS^-] + [O_2][HS^-]} \tag{18}$$

which simplifies to a rate law with an apparent zero-order dependence on $[O_2]$ and first-order dependence on $[HS^-]$ when $[O_2] >> [HS^-] > K_C$ and $K_B > [HS^-]$.

$$\nu = k'[M(II)TSP][HS^-] \tag{19}$$

Mechanistically, the kinetic expression of Equation 18 combined with spectrophotometric data indicate that the reaction proceeds via the formation of a ternary activated complex in which O_2 and HS^- are reversibly bound to the metal center as shown below for Co(II)-TSP:

$$Co(II)TSP + O_2 \overset{\beta_1}{\rightleftharpoons} Co(III)TSP\text{-}O_2\cdot \tag{20}$$

$$Co(III)TSP\cdot O_2 + HS^{2-} \overset{\beta_2}{\rightleftharpoons} Co(III)TSP\text{-}O_2\cdot SH^- \tag{21}$$

$$Co(III)TSP\text{-}O_2\cdot SH^- \xrightarrow[\text{slow}]{k} Co(II)TSP + HSO_2^- \tag{22}$$

$$HSO_2^- + O_2 \rightleftharpoons HSO_4^- \tag{23}$$

$$Co(III)TSP\text{-}O_2\cdot SH^- \rightleftharpoons Co(II)TSP\text{-}O_2H^- + S^o \tag{24}$$

$$Co(II)TSP\text{-}O_2H^- + H^+ \rightleftharpoons Co(II)TSP + H_2O_2 \tag{25}$$

$$H_2O_2 + S^o \longrightarrow H_2SO_2 \xrightarrow{O_2} H_2SO_4 \tag{26}$$

The terms K_A, K_B and K_C in the overall kinetic expression for this process (Equation 18) correspond to collections of the forward and reverse rate constants for the individual complexation reactions (Equations 20 and 21) that precede the rate-controlling step. Redox processes that are sensitive to homogeneous trace metal catalysis often exhibit rate laws that are first order with respect to the concentration of reductant and zero order in oxidant. Experimental results suggested that the autoxidation of dissolved SO_2 also falls into this general category of redox reactions.

This chapter describes the synthesis of both water-soluble metal phthalocyanine derivatives and their solid-supported analogs, which were formed by attachment of the macrocyclic complex to an inert silica gel surface. These compounds were subsequently used as active homogeneous and heterogeneous catalysts for the autoxidation of aquated SO_2 due to their well defined geometry and chemical behavior in aqueous media. Certain metal-phthalocyanines such as Co(II)-TSP are known to actively bind dioxygen and serve as O_2 carriers in solution [52].

Preliminary kinetic measurements and mechanistic results are described in this chapter. Particular emphasis is focused on the following features of the catalytic process:

1. Alternatives of one- or two-electron transfer steps;
2. Binding of molecular oxygen by an active catalytic center;
3. Inner-sphere complexation of the substrate as a prelude to electron transfer;
4. The possible role of photoassisted metal catalysis, and
5. Changes in catalytic behavior when the metal complex is anchored to a solid surface.

EXPERIMENTAL PROCEDURE

Synthesis of Co(II)-Phthalocyanine Complexes

Co(II)-4,4′,4″,4‴-tetraminophalocyanine [Co(II)-TAP] was prepared according to a procedure derived from the method of Weber and Busch [53]. A mixture of 4-aminophthalic acid, ammonium molybdate, ammonium chloride and Co(II) sulfate-7-hydrate was heated under reflux in nitrobenzene for 6 h. The crude product was washed with methanol and subsequently heated to boiling in 0.5 *M* HCl. After filtration, dissolution in dimethylsulfoxide (DMSO) at 70 C removed the insoluble impurities. The product crystallized on addition of (500 mL) H_2O and was isolated by centrifugation. Further purification involved repetitive washings of the solid in boiling H_2O and centrifugation. After initial treatment with absolute ethanol, pure Co(II)-TAP was obtained by heating the solid in absolute ethanol under reflux for 5 h. The tetrasodium salt of Co(II)-4,4′,4″,4‴-tetrasulfophothalocyanine was synthesized in an analogous manner. The structure of each complex was confirmed by elemental analysis (Table II), ultraviolet/visible (UV/VIS) and ^{1}H nuclear magnetic resonance (NMR) spectrophotometry.

Preparation of the Heterogeneous Catalyst Support

Preparation of the catalyst supported involved the treatment of silica gel with an appropriate silylation reagent as illustrated in Figure 3 [54,55]. In preparation I, a suspension of 22 g of silica gel (Fisher Scientific, specific area 330 $m^2 \cdot g^{-1}$) and

Table II. Elemental Analyses of Co(II)-Phthalocyanine Complexes[a]

	Co(II)-TSPc		*Co(II)-TAPc*	
	Calculated	*Found*	*Calculated*	*Found*
% C	37.82	36.95	57.48	49.83
% H	1.59	2.03	3.40	3.88
% N	11.04	10.73	25.19	23.07
% S	12.63	12.12		

[a] Elemental analyses performed by Galbraith Laboratories, Inc., Knoxville, Tennessee.

7.5 g of 3-chloropropyltrimethoxysilane in 150 mL xylene was heated under reflux for 8 h. Addition of 3.5 g of imidazole enabled the formation of product II. After filtration, the modified gel was washed with acetone and allowed to dry in the atmosphere overnight. Gel II contained 1.71×10^{-3} mol-g^{-1} of nitrogen as determined by elemental analysis.

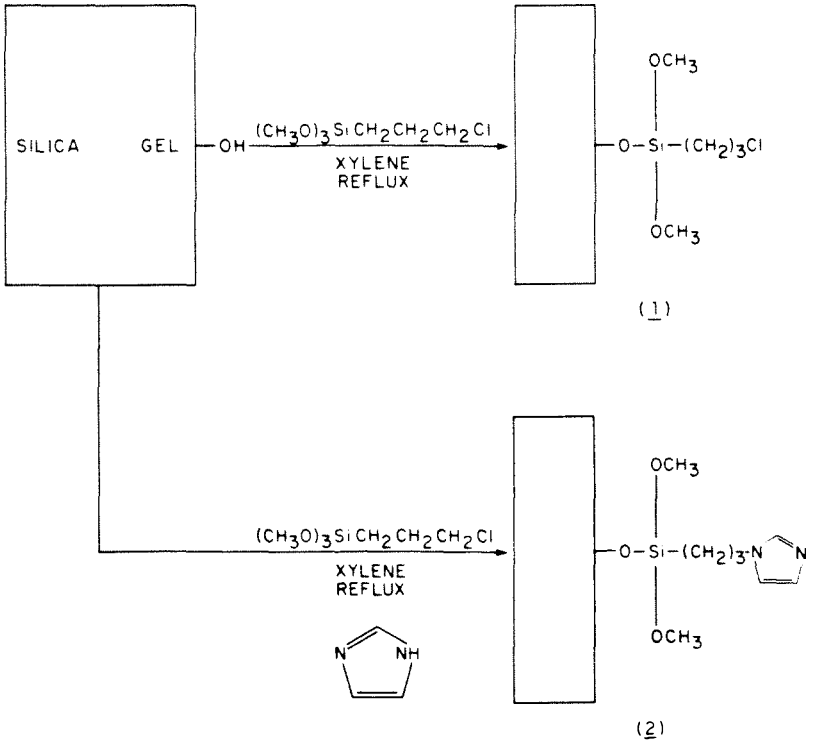

Figure 3. Flow diagram for the preparation of a modified silica gel system for Co(II)-TAP and Co(II)-TSP catalysts using 3-chloropropyltrimethoxysilane and imidazole as reagents.

Attachment of Co(II) Phthalocyanine Complexes to the Solid Support

Two methods were used to anchor the Co(II) phthalocyanine complexes to the modified silica gel. In scheme 1 (Figure 4), attachment was achieved through covalent bonding of the surface ligand to the amino side chain of Co(II)-TAP. The second procedure (scheme 2) involved direct complexation of the modified silica gel surface to the central metal atom of the phthalocyanine complexes.

Scheme 1

A stirred mixture of the modified silica gel and 6.7 g Co(II)-TAP in 30 mL DMSO was heated at 80 C for 4 h. The hybrid catalyst was isolated by filtration and washed successively with warm DMSO and 0.1 *M* NaOH to remove any residual chloride. Final purification was attained by extraction of the product with H_2O in a Soxhlet apparatus for 5 h. The supported Co(II)-TAP III was dried in an oven at 80 C. Elemental analysis revealed 2.7×10^{-5} mol-g^{-1} of Co (0.16%).

Scheme 2

In this procedure, a 2.5-cm-diameter column was packed with modified gel. A 150-mL volume of a 7.8×10^{-5} *M* aqueous Co(II)-TSP solution was poured into the column and eluted dropwise. DMSO was used as a solvent for Co(II)-TAP. The hybrid products IV and V were washed several times with the appropriate solvent and collected by filtration. Analysis of the eluent from the column by UV/VIS spectrophotometry indicated the following Co(II) content for each supported catalyst:

- Co(II)-TSP: 1.09×10^{-6} moles of Co per gram of solid, and
- Co(II)-TAP: 1.19×10^{-6} moles of Co per gram of solid.

Kinetic Measurements

Reagents

Sulfite solutions were prepared from reagent-grade Na_2SO_3 (Mallinkrodt). The following reagent-grade chemicals were used to prepare the pH buffer solutions:

- tris-(hydroxymethyl) aminomethane (TRIS), Sigma;
- tris-(hydroxymethyl) aminomethane hydrochloride (TRIS-HCl), Sigma;
- N-tris-(hydroxymethyl) methyl-2-aminomethane sulfonic acid (TES), Sigma;
- sodium phosphate—monobasic, Mallinkrodt;
- sodium phosphate—dibasic, Mallinkrodt;
- sodium phosphate—tribasic, Mallinkrodt;
- sodium borate, Mallinkrodt;

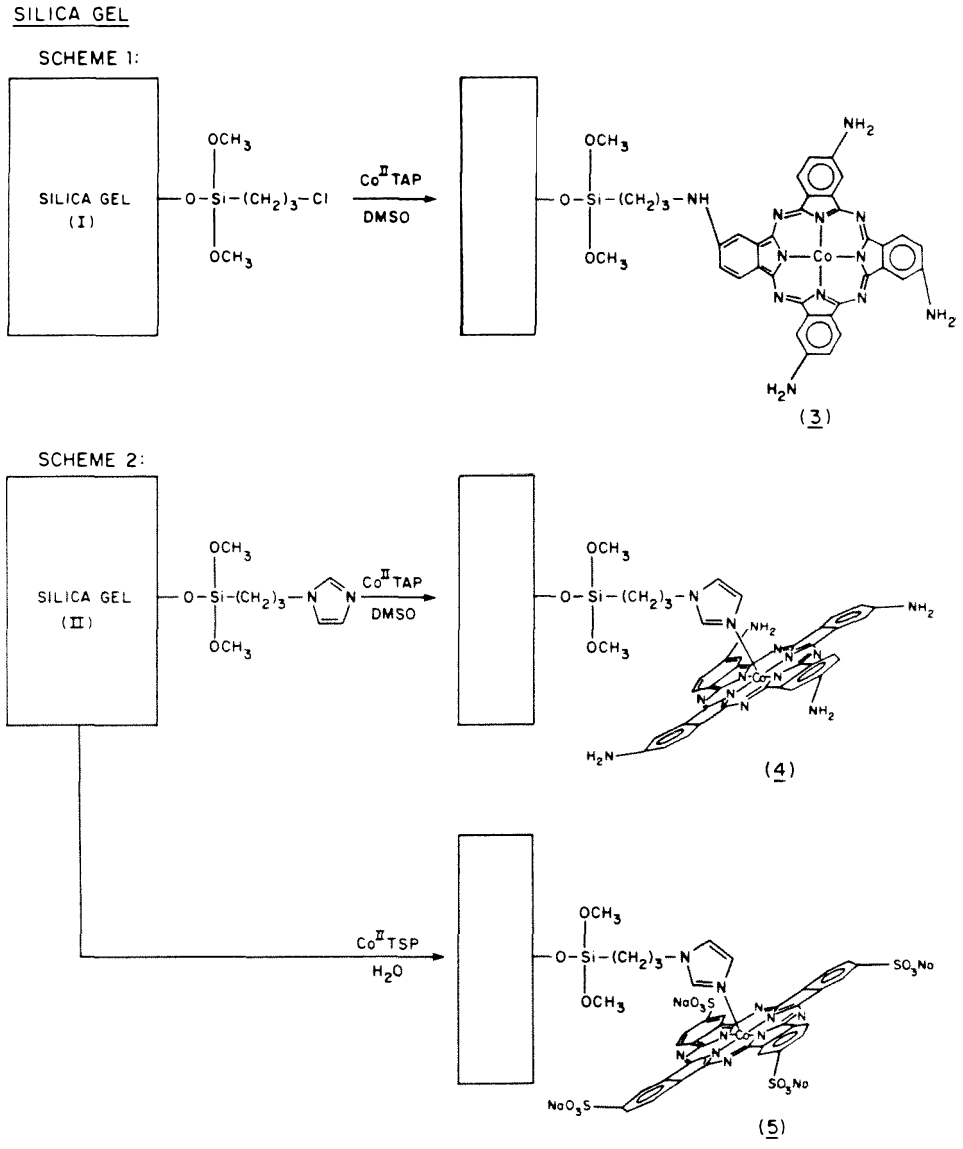

Figure 4. Modes of attachment of cobalt phthalocyanine complexes to silica gel support systems I and II. Attachment was achieved by indirect linkage through a ring amino group (III) and by direct coordination through the central metal of the complex (IV and V).

- sodium chloride, Mallinkrodt; and
- sodium hydroxide, Mallinkrodt.

Sodium perchlorate (G. F. Smith) was used to maintain the ionic strength constant at $\mu = 0.4$ *M*. Deionized water (18 MΩ-cm resistivity) obtained from a Milli RO-4/Milli Q purification system (Millipore) was used in the preparation of all reagent solutions. The water was deoxygenated by purging with N_2 before preparation of the Na_2SO_3 solutions.

Kinetic Data

Kinetic data were obtained from two series of experiments. In the initial set of experiments with the homogeneous Co(II)-TSP catalyst, sulfite concentration [S(IV)] was determined by monitoring the UV absorption spectrum ($\lambda_{max} = 212$ nm) of the reaction solution as a function of time. Optical absorption data were collected with a Hewlett-Packard Model 8450A UV/VIS spectrophotometer. The instrument was equipped with a reversed-optic diode detector, which permitted simultaneous detection over 200–800 nm in 1 s. As a result, changes in the absorption spectrum of Co(II)-TSP were also recorded during the reaction. The reactions were performed at 24 ± 1 C directly in Teflon-stoppered quartz spectrophotometer cells (2 or 10 cm pathlength).

In a second set of experiments, the reactions were followed by continuous measurement of O_2 concentration as a function of time. Dissolved oxygen was determined using an Orion Model 97–08–00 O_2 electrode coupled to an Orion Model 901 Ionanalyzer/Model 951 digital printer system. The pH of the reaction mixture was monitored simultaneously via an Orion combination pH electrode. The O_2 and pH electrodes were interfaced to the Ionanalyzer through an Orion Model 605 Electrode Switch.

These reactions were conducted in a water-jacketed glass and Teflon reactor with a total volume of 2.0 L. The design and operation of the batch reactor has been described previously [51]. To minimize the potential catalytic effect of trace metal contaminants, all glassware was washed with phosphate-free detergent (Alconox), soaked in 5.2 *M* HNO_3, and rinsed several times with deionized water.

In a typical experiment, a 2.0-L volume of a buffer solution and the appropriate catalyst were transferred to the reactor system. Air (Matheson), oxygen (Matheson) or a controlled N_2/O_2 mixture was purged through the solution with constant stirring for 30 min. After saturation, the reactor was sealed from the atmosphere. A constant temperature of 25 ± 0.1 C was maintained using a Haake Model FK-2 water circulation system and temperature controller.

To initiate a reaction, a known volume of a stock sulfite solution was added to the buffer-catalyst mixture. [S(IV)] ranged from 5×10^{-5} to 5×10^{-3} *M*. Dissolved oxygen varied from 2.5×10^{-4} to 1.2×10^{-3} *M*. Addition of ethylenediaminetetracetic acid (EDTA) disodium salt (Sigma) reduced the catalytic effect of residual trace metal contaminants in control reactions [58]. Mannitol, sodium cyanide (NaCN) and EDTA were used selectively as free radical scavengers [37] and trace metal complexation inhibitors [57].

RESULTS AND DISCUSSION

Homogeneous Catalysis by Co(II)-, Fe(II)-, Mn(II)-, Ni(II)-, Cu(II)- and V(IV)-4,4',4'',4'''-Tetrasulfophthalocyanine Complexes

Reaction Rate as a Function of Total Sulfite Concentration

The catalytic rate for the oxidation of S(IV) by oxygen was followed spectrophotometrically as described in the experimental section. Reactions were conducted under pseudo-first-order conditions in sulfite at constant pH and ionic strength (i.e., $[O_2]_o >> [S(IV)]_o$ where $[S(IV)] \simeq [HSO_3^-] + [SO_3^{2-}]$ at pH > 3.0). The observed rate constants (k_{obs}) for the reactions were calculated from plots of absorbance ($ln A_t/A_o$) vs time.

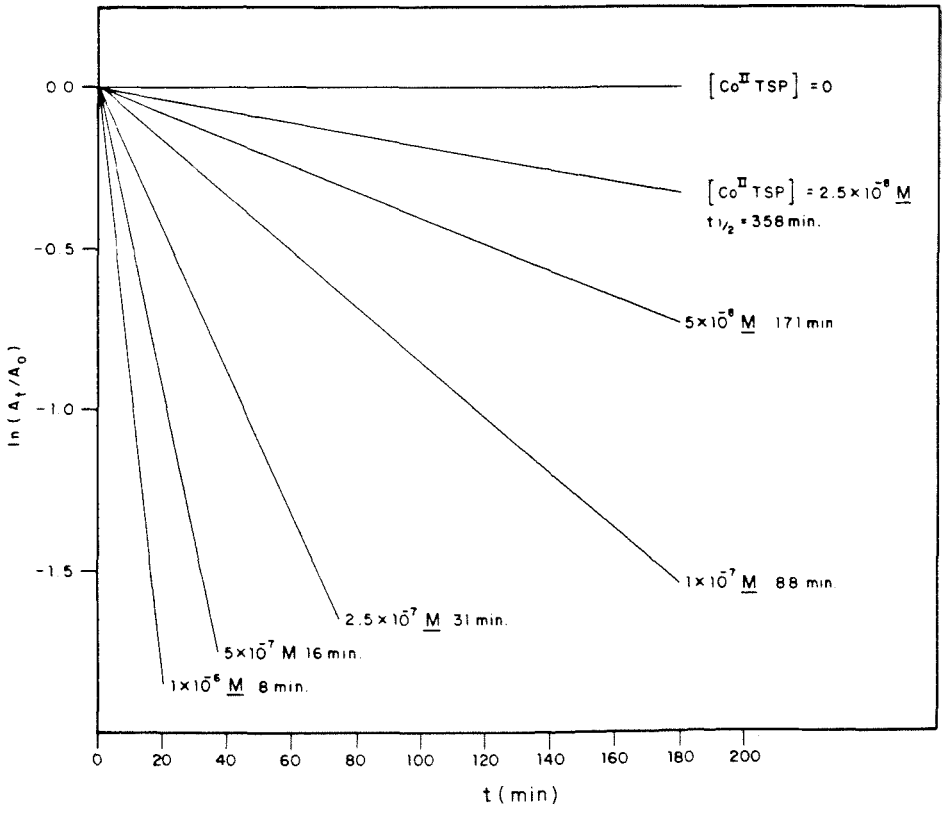

Figure 5. Pseudo-first-order plots of $ln(A_t/A_o)$ for the reaction of S(IV) with O_2 at pH 9.2 in a borate buffer system with $\mu = 0.4$.

Kinetic data obtained from a typical series of experiments are summarized in Figure 5. At the principal wavelength for light absorption due to SO_3^{2-} (λ_{max} = 212 nm), Beer's law ($A = \epsilon lc$) was valid over a broad range of [S(IV)] as reported previously [21]. Under the reaction conditions outlined in Figure 5, the observed pseudo-first-order rate constants ranged from 3.35×10^{-5} s^{-1} at $[Co(II)\text{-}TSP]_o = 2.5 \times 10^{-8}$ *M* to 5.21×10^{-3} s^{-1} at $[Co(II)\text{-}TSP]_o = 2.5 \times 10^{-6}$ *M* ($0.985 < R^2 < 0.999$) under alkaline conditions (pH 9.2). No measurable decrease in [S(IV)] was detected after 12 h in the absence of Co(II)-TSP.

Similar first-order behavior in total sulfite was observed in neutral solution (pH 6.7) and over the entire pH range under study. The linearity of plots of *ln* A_t/A_o as a function of time can be accepted as conclusive evidence that the reaction order in [S(IV)] is unity. Further support for this conclusion is provided by the kinetic results collected from the measurement of changes in the concentration of dissolved oxygen during the course of the reaction. The amperometric response of the oxygen electrode is a linear function of the aqueous-phase O_2 concentration ($i_\infty \alpha [O_2]$). A plot of electrode response vs time was linear from t = O for experiments conducted under initial reaction conditions in which $[O_2]_o >> [S(IV)]_o$.

Application of the van't Hoff method of initial rates to the results determined from $[O_2]$ vs time functions enabled us to calculate the reaction order in total sulfite over a wide range in [S(IV)]. Shown in Figure 6 are *ln-ln* plots of the initial rate of oxygen depletion ($\nu_o = -d[O_2]_o/dt$) as a function of $[S(IV)]_o$ for a series of reactions performed at pH 6.7 and 9.2. The slopes of these linear functions (1.18 at pH 6.7 and 1.25 at pH 9.2) confirm that the reaction order in [S(IV)] is approximately one. A moderate degree of uncertainty in the experimental measurements accounts for the empirical values of slightly greater than unity. This observation suggests that one source of variability in reaction orders previously reported for the metal-catalyzed autoxidation of dissolved SO_2 (Table I) may be due to selective fitting of experimental results over a narrow concentration range and/or a moderate degree of scatter in data points.

Reaction Rate as a Function of Total Oxygen Concentration

The dissolved oxygen vs time profiles exhibited zero-order behavior throughout most of the reactant concentration ranges employed in the kinetic evaluations. However, deviations from linearity were observed when the initial concentration conditions were designed such that $[S(IV)]_o >> [O_2]_o$. Under these circumstances, an apparent exponential decay in the concentration of oxygen as a function of time was detected. The latter result signifies either the attainment of a "saturation effect" as would be predicted for enzymatic catalysis or a shift in the reaction mechanism with a change in relative reactant concentrations.

Additional evidence for a rate law bearing a zero-order dependence in $[O_2]$ was obtained through the determination of k_{obs} at different initial concentrations of dissolved oxygen. The observed first order kinetic constants that were measured over a range of $[O_2]_o$ from 2.5×10^{-4} to 1.2×10^{-3} *M* remained constant within

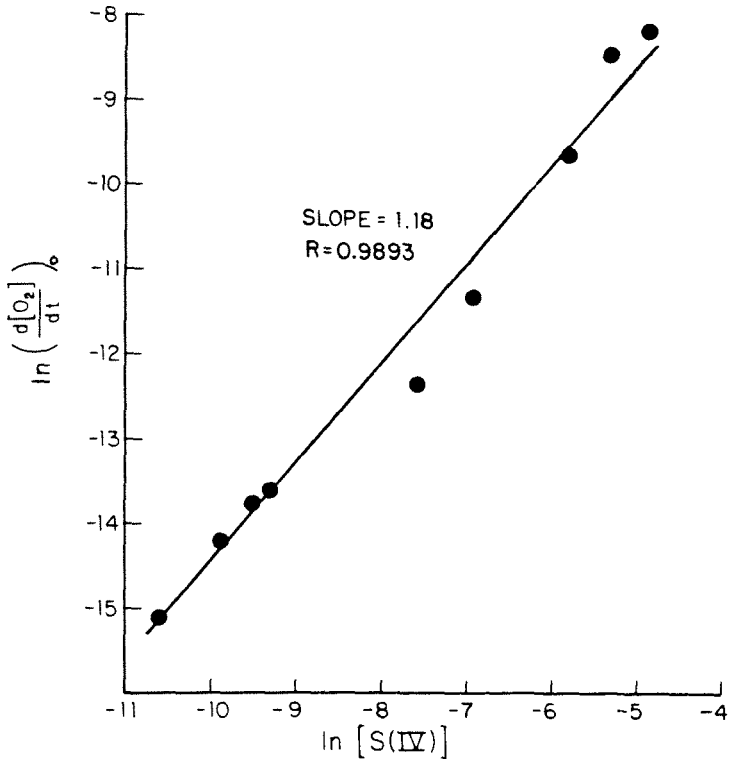

Figure 6. Determination of the S(IV) reaction order by the van't Hoff method of initial rates where $d[O_2]/dt$ is obtained from the slope of $[O_2]$ vs time response function at $t = 0$.

the limits of experimental error (±5%) under both neutral and alkaline pH conditions.

Reaction Rate as a Function of Total Catalyst Concentration

The experimental data presented in Figure 5 were examined to determine the influence of catalyst concentration as the observed rate of sulfite oxidation. A plot of *ln* k_{obs} vs *ln* $[Co(II)TSP]_o$ indicates that the reaction order with respect to cobalt-phthalocyanine is approximately 1.0 at pH 9.2 (Figure 7a). However, a comparable analysis of kinetic measurements recorded from reactions conducted in neutral solution yields a nonintegral concentration dependence of 0.3 (Figure 7b). This variability in reaction order implies that a change in the catalyzed autoxidation mechanism may accompany a change in the pH of the reaction solution. Alternatively, an increase in pH could affect the speciation of active forms of

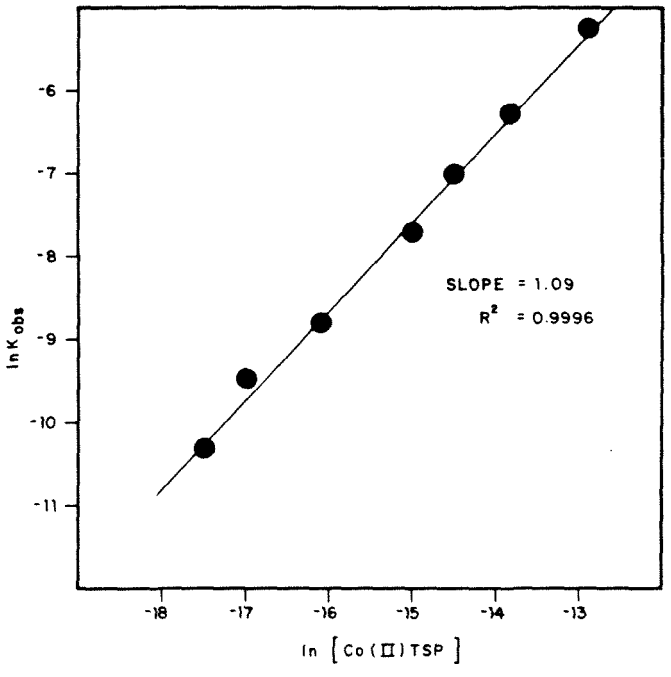

(a)

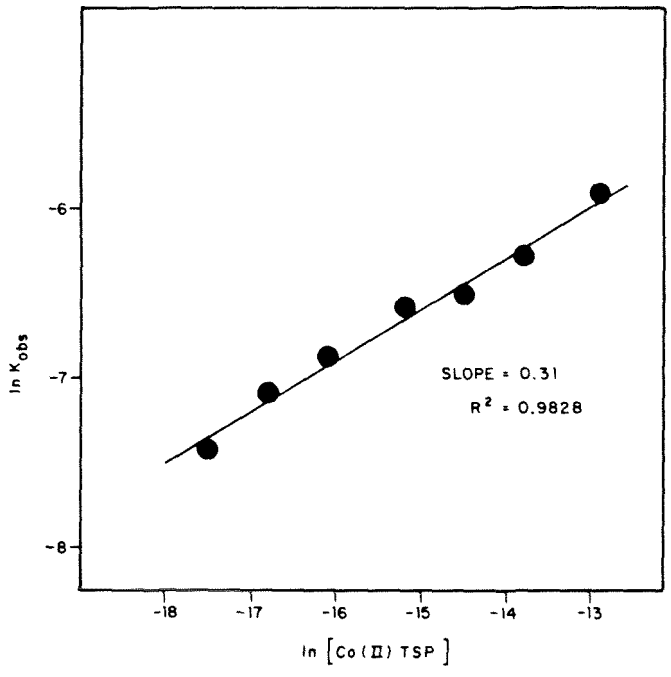

(b)

Figure 7. Determination of the reaction order with respect to the total concentration at pH 9.2 (a) and pH 6.7 (b).

the catalyst through a shift in the equilibria between monomeric and polymeric structures of the Co(II)-TSP complex.

Ancillary Observations: Effects of pH, Complexation, Inhibitors, Light and Central Metal Atom on Reaction Rate

Since this report constitutes a preliminary communication, exhaustive parametric results will not be presented; however, sufficient information is available at this stage to formulate tentative conclusions about many of the primary and secondary factors affecting the autoxidation rate of aquated sulfur dioxide.

The pH-dependence of the oxidation of sulfite by molecular oxygen is unusually complicated as shown in Table III. The sharp increase in the catalyzed reaction rate between pH 4.1 and 6.7 may be attributed to the acid dissociation of bisulfite to give sulfite ion:

$$HSO_3^- \underset{K_a}{\rightleftharpoons} H^+ + SO_3^{2-} \tag{27}$$

$K_a = 1.62 \times 10^{-7}$ *M* ($pK_a = 6.79$) at a temperature of 20 C and ionic strength $\mu = 0.1$ *M* [56]. As the fraction of [S(IV)] present at SO_3^{2-} increases, the rate of autoxidation also increases. This behavior clearly shows that sulfite is the principal reactive S(IV) species in aqueous solution.

As suggested previously [30,33,38], the rate-controlling step in the catalyzed autoxidation of dissolved SO_2 is preceded by rapid formation of discrete inner-sphere complexes between the active metal center and sulfite. While numerous investigators have successfully characterized the structure of crystalline metal-sulfite salts [58–64] few stability constants and rate constants have been reported for the formation of these species in solution due to the instability of SO_3^{2-} toward oxidation. However, it is interesting to note that the thermodynamic constants which have been reported are significantly larger than corresponding β values for metal-sulfate derivatives (Table IV).

Table III. Effect of pH on v_o: Results of pH Dependence Study[a]

pH	*Buffer System*	v_o (10^3 *M*-*min*$^{-1}$)
4.4	0.1 *M* NaH_2PO_4; 0.3 *M* $NaClO_4$	No reaction
6.9	0.1 *M* NaH_2PO_4; 0.1 *M* Na_2HPO_4	-7.6856×10^{-7}
7.7	0.2 *M* TES; 0.1 *M* NaOH; 0.3 *M* $NaClO_4$	-9.675×10^{-8}
8.4	0.1 *M* TRIS; 0.1 *M* TRIS-HCl; 0.3 *M* $NaClO_4$	-1.355×10^{-7}
9.4	0.1 *M* NaB_4O_7; 0.1 *M* $NaClO_4$	-1.581×10^{-6}
10.1	0.1 *M* Na_2CO_3; 0.1 *M* $NaHCO_3$	-1.041×10^{-6}
11.5	0.044 *M* Na_2HPO_4; 0.444 *M* Na_3PO_4	-1.256×10^{-6}
12.7	0.1 *M* NaCl; 0.1 *M* NaOH; 0.2 *M* $NaClO_4$	-2.1053×10^{-6}

Table IV. Comparison of Stability Constants[a] for Metal-Sulfito and -Sulfato Complexes at 25.0 C

Metal	μ	*log* β, SO_3^{2-}	μ	*log* β, SO_4^{2-}
Ag^+	0	$AgSO_3^+$, 5.6	0	$AgSO_4^+$, 1.3
Cd^{2+}	1.0	$Cd(SO_3)_2^{2-}$, 4.2	1.0	$Cd(SO_4)_2^{2-}$, 1.6
Hg^{2+}	1.0	$Hg(SO_3)_2^{2-}$, 24.1	0.5	$Hg(SO_4)_2^{2-}$, 2.4
Ce^{3+}	0	$CdSO_3^+$, 8.0	0	$CdSO_4^+$, 3.6
Fe^{3+}	0.1	$FeSO_3^+$, 18.1[b]	0	$FeSO_4^+$, 4.0
Fe^{2+}			0	$FeSO_4^0$, 2.2

[a] All constants reported in this table were taken from Smith and Martell [57], except that for $FeSO_3^+$.
[b] Hansen et al. [65].

$$Fe^{3+} + H_2O \cdot SO_2 \rightleftharpoons FeSO_3^+ + 2H^+ \qquad \log K = 9.7$$
$$H^+ + HSO_3^- \rightleftharpoons H_2O \cdot SO_2 \qquad \log K = 1.6$$
$$H^+ + SO_3^{2-} \rightleftharpoons HSO_3^- \qquad \log K = 6.8$$
$$Fe^{3+} + SO_3^{2-} \rightleftharpoons FeSO_3^+ \qquad \log K = 18.1$$

Carlyle [66] has reported that evidence for inner-sphere complexation of Fe(III) and subsequent reduction by coordinated sulfite can be observed visually: "iron(III) solutions became brown-red upon addition of sulfite and then slowly fade." Similar changes in color have also been described by Hoffmann et al. [66] for the oxidation of vanadyl cation (VO^{2+}) by peroxydiphosphate ($H_2P_2O_8^{2-}$). For this redox system, kinetic measurements showed that formation of an inner-sphere complex of finite stability ($\log \beta \simeq 4.0$) occurred before electron transfer, which took place on a slower time scale.

Preliminary experimental evidence that sulfite and/or dioxygen coordination play an important role in the phthalocyanine-catalyzed reactions was obtained through the introduction of competitive complexing reagents. Addition of EDTA and cyanide to reaction solutions containing Co(II)-TSP resulted in a significant reduction in k_{obs} at pH 9.2, whereas only EDTA exerted a negative influence on the reaction rate at pH 6.7 (Table V). Under neutral pH conditions, the inhibitory effect of EDTA appears to be associated primarily with the complexation of background levels of trace-metal contaminants. For example, the half-life for the uncatalyzed oxidation of sulfite in the absence of EDTA increased from 333 to ~1800 min at an EDTA concentration of 10^{-5} *M*. In neutral solution, cyanide failed to inhibit the reaction because it exists almost completely as HCN ($pK_a = 9.2$), which is a much weaker ligand than CN^- for the binding of transition metal ions [57]. However, the oxidation of sulfite ceased completely at pH 11.5 on addition of sodium cyanide at 10^{-5} *M* concentrations. In contrast, reactions conducted in the presence of an equivalent concentration of an effective free-radical inhibitor (d-mannitol at 10^{-5} *M*) were retarded only to a slight degree.

Direct spectrophotometric evidence for the complexation of sulfite and O_2

Table V. Effect of Inhibitors on k_{obs} at pH 6.7 and 9.2[a]

Inhibitor	*Inhibitor Concentration* (10^6 *M*)	k_{obs} (10^3 s^{-1})	
		pH 6.7	*pH 9.4*
None	0	1.62	1.83
EDTA	1	1.52	
	2.5	1.45	
	5.0	0.94	
	10.0	0.78	0.33
Mannitol	10.0	1.25	0.85
NaCN	10.0	1.61	0.29

[a] Initial conditions: $[S(IV)]_o = 10^{-4}$ *M*; $[O_2]_o = 10^{-3}$ *M*; $[Co(II)\text{-}TSP]_o = 10^{-6}$ *M*; $\mu = 0.4$; T = 26.0 C.

by cobalt-phthalocyanine has been obtained as shown in Figure 8. The visible spectrum of Co(II)-TSP, denoted by the solid line in Figure 8, has two characteristic absorption bands, which have been attributed to an oxygen-free monomer complex (λ_{max} = 636 nm) and to a monomeric dioxygen adduct (λ_{max} = 670 nm) [68,69]. Other researchers [70–72] have interpreted these spectral characteristics in terms of a simple monomer/dimer equilibrium, in which the electronic transition at higher energy is associated with the dimeric phthalocyanine complex. Hoffmann and Lim [51] observed that the absorbance of the peak at 670 nm increased on dissolution of Co(II)-TSP in progressively more alkaline solutions containing O_2. Over the pH range 9–12, this behavior was accompanied by a decrease in the value of A_{636}.

At the beginning of a typical autoxidation reaction, the spectrum of the catalyst changes dramatically on addition of sulfite, as indicated by the dotted line in Figure 8. Introduction of sulfite causes a rapid growth of the absorption maximum at 670 nm in relative proportion to the peak at 636 nm. The value of A_{670} decreases slowly with time as the oxidation reaction proceeds. At the conclusion of the reaction, the absorbance at 670 nm is comparable to the initial intensity of the 636-nm peak as represented by the dashed-line spectrum. Further addition of sulfite results in the reemergence and subsequent decline of the peak at λ_{max} = 670 nm as the second catalytic cycle unfolds. This spectroscopic behavior can be reproduced a number of times with slight changes in catalytic activity as indicated by the tabulation of observed rate constants for successive catalytic cycles given in Table VI.

The data presented in Table VI also indicate that the cobalt(II)-phthalocyanine complex is participating in a closed catalytic sequence of reaction steps in which the active catalytic center is regenerated in situ. There appears to be a minor loss of catalytic activity on successive addition and oxidation of S(IV). The reduction in the catalytic efficiency of Co(II)-TSP may be attributed to irreversi-

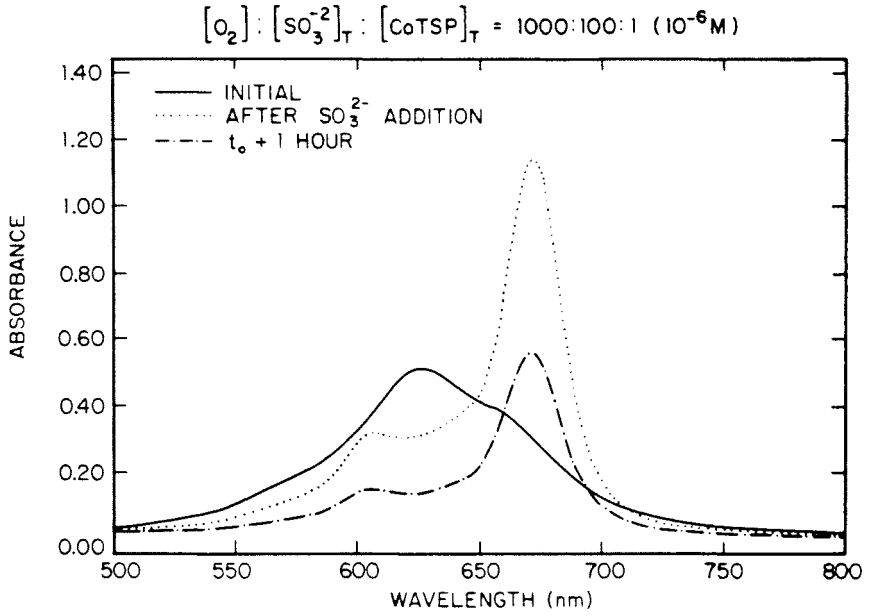

Figure 8. Visible absorption spectra for Co(II)-TSP before, during and after addition of sulfite at pH 6.7. Growth of the absorption maximum at 670 nm occurs after sulfite addition. Before addition, λ_{max} = 636 nm.

ble decomposition of the macrocylic ligand structure, which is susceptible to oxidative degradation [71].

Since metal-phthalocyanine complexes are common dye molecules and potential sensitizers for the photolytic activation of dioxygen, catalysis of autoxidation reactions by Co(II)-TSP may be light-dependent. To test this hypothesis, experi-

Table VI. Tests of Catalytic Activity with Successive Additions of Sulfite at pH 6.7[a]

Catalytic Cycle	k_{obs} ($10^4\ s^{-1}$)
1	7.46
2	7.43
3	6.85
4	6.35
5	5.60

[a] $[Co(II)\text{-}TSP]_o = 10^{-6}$ *M*; $[SO_3^{2-}]_o = 10^{-4}$ *M*; $[O_2]_o = 10^{-3}$ *M*; μ = 0.4 with 10^{-6} *M* EDTA.

ments were conducted in the presence and absence of conventional fluorescent room light. The kinetic results described in the previous sections of this paper were derived from reactions carried out under background illumination. In the absence of an external light source, autoxidation of sulfite proceeded very slowly after rapid formation of an intermediate Co(II)-TSP/SO_3^{2-}/O_2 complex. The solid and dashed lines in Figure 9, A_{213} and A_{670}, correspond to the absorbance due to sulfite and the intermediate species, respectively. The decline in the concentration of S(IV) and the cobalt-sulfite-dioxygen adduct was accelerated dramatically on exposure of the reactant solution to room light. Reactions catalyzed by Fe(II)-TSP and Mn(II)-TSP seemed to be insensitive to the effects of irradiation. The origin of this apparent "photoassisted" catalysis is being investigated in greater detail.

Variation of the central metal atom in the structure of the phthalocyanine complex produced noticeable changes in the rate of oxidation of sulfite as shown in Table VII. Co(II)-TSP exerted the most pronounced catalytic effect on the

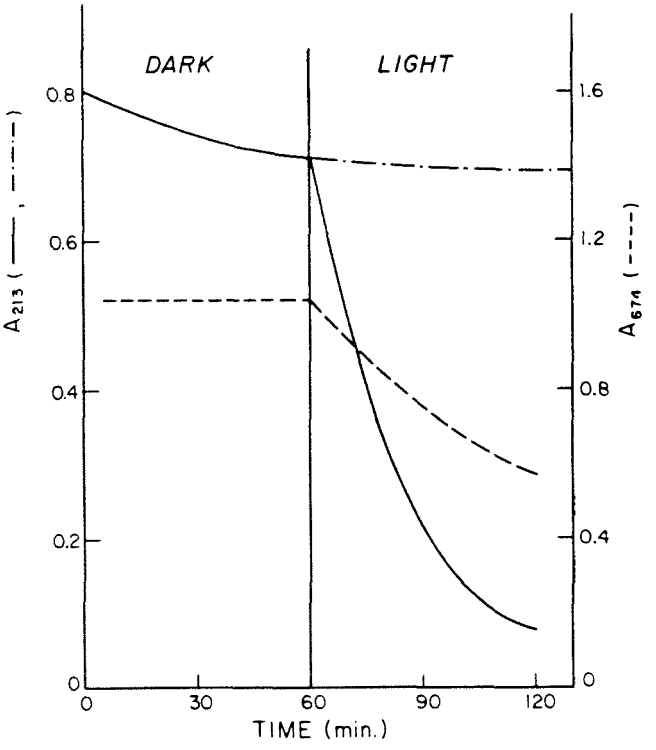

Figure 9. Relative effect of fluorescent room light on the catalytic autoxidation of sulfite. The solid line refers to absorbance of SO_3^{2-} and the dashed line refers to the absorbance of all monomeric Co(II) complexes.

Table VII. Effect of a Variation in the Central Metal on Rate of Autoxidation of S(IV) at pH 9.2[a]

Metal	k_{obs} ($10^4\ s^{-1}$)
Co(II)	18.30
Fe(II)	2.23
Mn(II)	0.24
Cu(II)	$\simeq 0$
Ni(II)	$\simeq 0$
V(IV)	$\simeq 0$

[a] $[S(IV)]_0 = 10^{-4}\ M$; $[O_2]_0 = 10^{-3}\ M$; $\mu = 0.4\ M$.

autoxidation process. Similar trends in catalytic activity have been reported by Hoffman and Lim [51] for the reaction of hydrogen sulfide with molecular oxygen in aqueous solution and by Kropf [74] and Kropf and Hoffman [75] for the liquid-phase autoxidation of hydrocarbons.

Presumably, the differences in the catalytic properties of the various metal-phthalocyanines can be explained in terms of the relative capacities of the complexes to bind molecular oxygen. Many square planar Co(II) complexes undergo solution-phase reactions with Lewis bases to yield five-coordinate derivatives of the type Co(II)(L)(B):

$$\text{Co(II) L} + \text{B} \rightleftharpoons \text{Co(II)(L)(B)} \tag{28}$$

$$\text{Co(II)(L)(B)} + \text{O}_2 \rightleftharpoons \text{Co(II)(L)(B)} - \text{O}_2 \tag{29}$$

where L = tetradentate phthalocyanine, porphyrin or Schiff-base ligand
B = electron-donor attached to an axial coordination site

Coordination of an axial base promotes the reversible formation of mononuclear dioxygen adducts (Equation 29) in which the bonding of O_2 to the metal center is represented nominally either as a superoxide ion (O_2^-) coordinated to Co(III) or as a singlet oxygen bound to Co(II) [76,77]. Electron spin resoncance spectroscopic measurements and theoretical calculations suggest that the structure of metal-dioxygen is correctly assigned as cobalt(III)-superoxide [77]. A qualitative molecular orbital (MO) description predicts that bonding of oxygen to cobalt(II) occurs in a bent end-on configuration involving overlap of the singly occuped d_{π}^2 orbital on Co(II) with an antibonding π-orbital (π^*) of O_2 as depicted in Figure 10. According to this simplified model, there is only a minor cobalt d_{π}-oxygen p_{π}

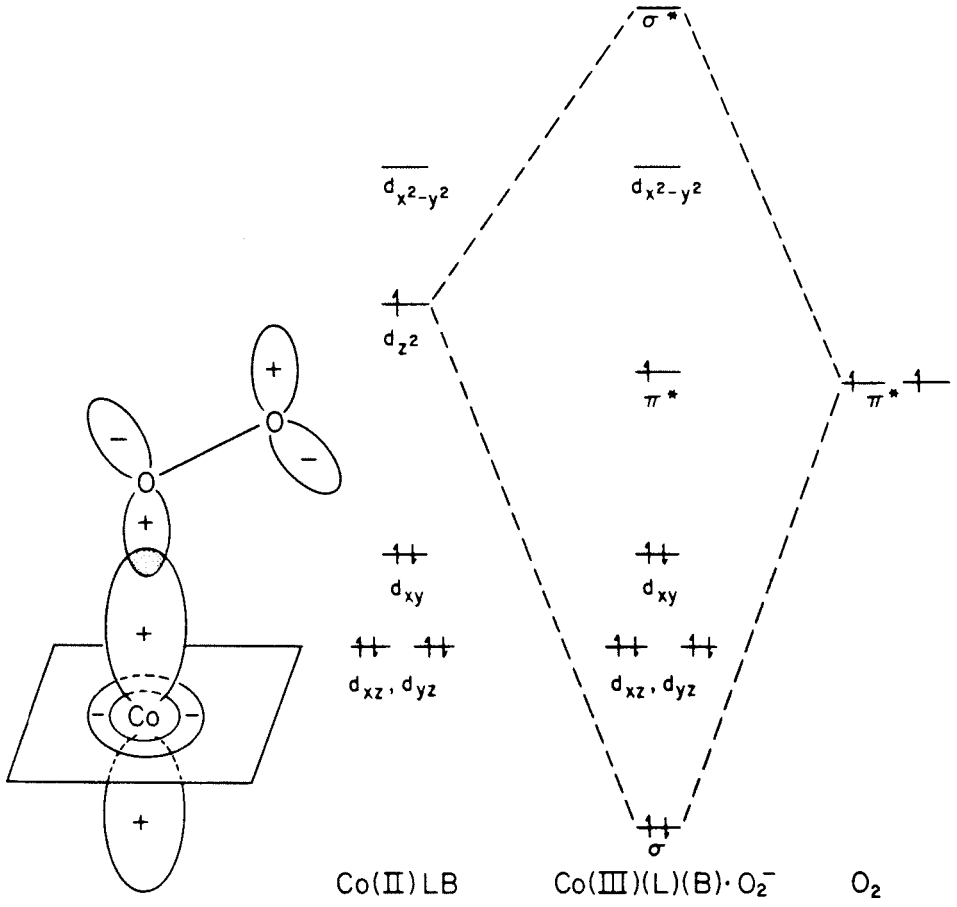

Figure 10. Qualitative molecular orbital description of the bonding between Co(II)(L)(B) complex and dioxygen. Sigma bond formation results from overlap of electron density between the singly occupied d_{z2} orbital on Co and the π^* MO of O_2. L denotes a planar tetradentate ligand, and B denotes an axial base.

interaction and the unpaired electron resides primarily in the remaining π^* MO on O_2.

Studies of the catalytic properties of cobalt-substituted model hemesystems have demonstrated that the stability and reversibility of formation of metal-dioxygen adducts are affected by the nature of the ligand B coordinated in the axial position trans to O_2 [77]. For example, thermodynamic data for this reaction suggest that the oxygen affinity of metal complexes is associated with the σ-donor, π-donor and π-acceptor electronic properties of B [78]. These correlations follow the general notion that increased electron density at the metal atom due to axial coordination

of B enhances the bonding interaction with oxygen, thereby promoting an "intramolecular redox reaction" of Co(II)-O_2 to give CO(III)-O_2^-. Complexes of Fe(II) and, to a much lesser extent, Mn(II) may bind dioxygen in a similar fashion. The electron configurations of VO^{2+}, Cu(II) and Ni(II) do not favor coordination of axial ligands. Consequently, synthetic dioxygen adducts of V(IV), Ni(II) and Cu(II) complexes are virtually unknown [79].

In aqueous solution, Fe(II)- and Co(II)-TSP undergo reversible oxygenation to form dimeric oxygen adducts in which the product is formulated as the μ-peroxo species M(III)-O_2^{2-}-M(III) [52]. Oxygenation of Fe(II)-TSP proceeds spontaneously at neutral pH (6.5) via the following sequence of reactions:

$$\text{Fe-(TSP)}(H_2O)_2^{4-} + O_2 \underset{K_1}{\rightleftharpoons} \text{Fe-(TSP)}(H_2O)O_2^{4-} + H_2O \quad (30)$$

$$\text{Fe-(TSP)}(H_2O)O_2^{4-} + \text{Fe-(TSP)}(H_2O)_2 \underset{K_2}{\rightleftharpoons} [\text{Fe-(TSP)}(H_2O)]_2O_2 + H_2O \quad (31)$$

The values of the equilibrium constants K_1 and K_2 are 2×10^4 and 4×10^7 M^{-1}, respectively [80,81]. Formation of the corresponding 2:1 cobalt complex occurs only under strongly alkaline conditions (pH $\geq$ 12). Analysis of the kinetic data supported the assertion mechanism involves two discrete stages:

$$\text{Co-(TSP)}(H_2O)(OH)^{5-} + O_2 \rightleftharpoons \text{Co-(TSP)}(OH)O_2^{5-} + H_2O \quad (32)$$

$$\text{Co-(TSP)}(H_2O)(OH)^{5-} + \text{Co-(TSP)}(OH)O_2^{5-} \rightleftharpoons [\text{Co-(TSP)}(OH)]_2O_2^{10-} + H_2O \quad (33)$$

in which the initial oxygenation step constitutes the rate-limiting process with a second-order rate constant of 3.24 M^{-1}-s^{-1} at pH 13 [82].

The relative efficiencies of Co(II)- and Fe(II)-TSP as catalysts for the autoxidation of SO_3^{2-} seem to be related to the stability of the monomeric dioxygen adducts in aqueous solution. Hoffmann and Lim [51] proposed that a 1:1 Co(II)-TSP-O_2 addition product was the active catalytic center in the oxidation of HS^-. Mass et al. [48] also concluded that in polymer-supported Co(II)-TSP systems the reactive species for the autoxidation of thiols was a monomeric adduct. Increased catalytic activity in the heterogeneous phthalocyanine system relative to the homogeneous Co(II)-TSP complex may reflect constraints imposed on the dimerization reaction by the surface structure of the solid support. Spectral changes observed during the current study of the autoxidation of sulfite are consistent with the hypothesis that coordination of SO_3^{2-} in an axial position of Co(II)-TSP is a necessary prelude to the formation of a six-coordinate 1:1 cobalt-dioxygen adduct at pH 6.7 and 9.2. Complexation of sulfite and O_2 by Co(II)-TSP leads ultimately to a more rapid autoxidation step. Production of a peroxo-dimer Co(III)-TSP-O_2^{2-}Co(III) would occur only at high concentrations of hydroxide.

Mechanistic Interpretation of Kinetic Observations

Based on the experimental observations and kinetic data obtained to date, two alternative mechanisms can be proposed to describe the detailed molecular processes involved in the catalytic autoxidation of sulfite. They include a two-electron transfer, bisubstrate complexation pathway, and a one-electron transfer, chain reaction sequence. Each of these mechanistic possibilities will be presented and examined for consistency with experimental measurements.

Two-Electron Transfer, Bisubstrate Complexation Pathway

The catalytic activity of metal-phthalocyanines in aqueous solution was documented initially by Cook [83–85] for the decomposition of H_2O_2 and the oxidation of HI and later by Wagnerova and co-workers for the autoxidation of hydrazine [49], hydroxylamine [50] and cysteine [86]. As mentioned in the introduction to this chapter, these investigators compared the catalytic behavior of cobalt-, iron- and manganese-phthalocyanine complexes to the features of oxidase enzymes and peroxidase. A well known characteristic of the kinetics of enzymatic reactions is the variability of reaction orders for catalyst and substrate. Under certain conditions, the reaction order in substrate can vary between zero and one; but most likely a nonintegral value will be observed [87].

To interpret the observed kinetic behavior for the autoxidation of sulfite in terms of an enzymatic framework, a bisubstrate model for the catalytic activity of homogeneous metal-phthalocyanine complexes was developed. A rate law for this scheme was derived using the method of King and Altman [88], which is based on a standard determinant procedure used for solving a system of inhomogeneous linear equations obtained through steady-state considerations. The mechanism postulated to account for the observed kinetic behavior is the ordered-ternary complex pathway depicted symbolically in Figure 11 and given below.

$$(\text{Co(II)-TSP})_2^{4-} \overset{K_d}{\rightleftharpoons} 2\ \text{Co(II)-TSP}^{2-} \tag{34}$$

$$\text{Co(II)-TSP}^{2-} + SO_3^{2-} \underset{k_{-o}}{\overset{k_o}{\rightleftharpoons}} SO_3\text{Co(II)-TSP}^{4-} \tag{35}$$

$$SO_3\text{Co(II)-TSP}^{4-} + O_2 \underset{k_{-1}}{\overset{k_1}{\rightleftharpoons}} SO_3\text{Co(III)-TSPO}_2\cdot^{4-} \tag{36}$$

$$SO_3^{2-} + SO_3\text{Co(III)-TSPO}_2^{4-} \underset{k_{-2}}{\overset{k_2}{\rightleftharpoons}} SO_3\text{Co(III)-TSPO}_2\cdot SO_3^{6-} \tag{37}$$

$$H_2O + SO_3\text{Co(III)-TSPO}_2\cdot SO_3^{6-} \underset{h\nu}{\overset{k_3}{\rightleftharpoons}} SO_3\text{Co(II)-TSPO}_2^{6-} + H_2SO_4 \tag{38}$$

ORDERED TERNARY-COMPLEX MECHANISM

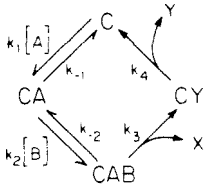

$$v = \frac{\{k_3k_4/(k_3+k_4)\}[C]_o[A][B]}{\frac{k_4(k_{-1}k_{-2}+k_{-1}k_{-3})}{k_1k_2(k_3+k_4)} + \frac{k_4(k_{-2}+k_3)}{k_2(k_3+k_4)}[A] + \frac{k_3k_4}{k_1(k_3+k_4)}[B] + [A][B]}$$

$C \equiv {}^{2-}(SO_3)Co(II)TSP$

$A \equiv O_2$

$B \equiv SO_3^{=}$

$X \equiv HSO_4^-$

$Y \equiv H_2O_2$

Figure 11. Theoretical rate expression obtained from the steady-state solution to the closed catalytic sequence above using the vector method of King and Altman [88].

$$SO_3Co(II)\text{-}TSPO_2^{6-} + 2H^+ \xrightarrow{k_4} SO_3Co(II)\text{-}TSP^{4-} + H_2O_2 \qquad (39)$$

$$H_2O_2 + SO_3^{2-} \xrightarrow{k_5} SO_4^{2-} + H_2O \qquad (40)$$

Equation 34 represents the formation of the reactive monomeric catalyst center (designated by C in Figure 11) from the predominant dimeric form of cobalt(II)-phthalocyanine in aqueous solution. This sequence of events is consistent with the spectral changes shown in Figure 8 that indicate a shift in the monomer-dimer equilibrium on addition of sulfite to the catalyst solution. Complexation of SO_3^{2-} by Co(II)-TSP in an axial position enhances coordination of molecular oxygen as written in Equation 36. The resulting intermediate is considered to be a mixed ligand Co(III) complex with a superoxide ion and sulfite bound at sites trans to one another about the metal center. In the proposed mechanism, this dioxygen adduct then reacts with an additional substrate ion to produce the ternary complex given in Equation 37. An intramolecular rate-limiting two-electron transfer followed by hydrolysis yields H_2SO_4 and a sulfito-cobalt(III)-peroxide derivative. After protonation, the coordinated O_2^{2-} is released as H_2O_2. Subsequently, hydrogen peroxide may be consumed via reaction with an additional molecule of substrate.

Evidence of a direct two-electron transfer redox step was reported recently by Schutten and Beelen [89], who observed the accumulation of H_2O_2 as an intermediate reduction product during the Co(II)-TSP–catalyzed autoxidation of 2-mercaptoethanol in water. Davies et al. [29] employed ^{18}O-tracer experiments to determine the source of the oxygen atoms in sulfate produced from the reaction of sulfite with O_2. The authors found that approximately one-half of the oxygen transferred to SO_3^{2-} originated from a dimeric superoxo- complex, $(NH_3)_5Co(III)\text{-}O_2^-\text{-}Co(III)(NH_3)_5$. Holt et al. [90] have shown that the ^{18}O content of the product sulfate in metal-catalyzed reaction systems varies as a linear function of the ^{18}O content of water and that at least three of the four O atoms in SO_4^{2-} are isotopically controlled by the solvent (the remaining oxygen atom originating from O_2). Finally, Yatsimirskii et al. [91] have obtained strong evidence that complexation of sulfite by a $[Co(II)\text{-}l\text{histidine}_2]_2O_2$ adduct occurs before electron transfer from S(IV) to O_2. In total, these results are compatible with the reaction mechanism outlined in Equations 34–40.

The observed photocatalytic effect (Figure 9) suggests that absorption of light by a reactive intermediate such as $SO_3Co(III)\text{-}TSPO_2\cdot SO_3^{6-}$ may play a key role in the mechanism for the oxidation of sulfite. Beelen et al. [92] attributed the influence of visible light in the 600 to 700-nm wavelength range on the phthalocyanine-catalyzed autoxidation of mercaptoethanol to a shift in the equilibrium composition of the Co(II)-TSP solution in favor of the catalytically active monomeric species. An alternative explanation that is consistent with the experimental data recorded in the current study is that the reactive ternary complex may absorb radiation to generate a bound singlet oxygen species of the form $SO_3Co(II)\text{-}TSP\cdot{}^1O_2\cdot SO_3^{6-}$. This intermediate would possess more favorable spin symmetry for facile electron transfer. Cox et al. [93] have shown that metalloporphyrins give rise to singlet-excited state O_2 on irradiation at appropriate wavelengths.

In the proposed reaction mechanism, the active catalytic center is the complex $SO_3Co(II)TSP^{4-}$. The catalytic reaction cycle begins and ends with this complex. Steps leading to formation of the active center are assumed to be in rapid equilibrium and may be ignored in the initial derivation of a rate expression. In the catalytic cycle, there are three intermediates, $SO_3Co(III)\text{-}TSPO_2\cdot{}^{4-}$, $SO_3Co(III)\text{-}TSPO_2\cdot SO_3^{6-}$ and $SO_3Co(III)\text{-}TSP\cdot O_2^{6-}$, and three steady-state equations for each species. Using the method of King and Altman [88], the concentration of reactive intermediate forms of the catalyst can be expressed as:

$$[SO_3Co(II)\text{-}TSP^{4-}] \propto k_{-1}k_{-2}K_{-4} + k_{-1}k_3k_4 + k_2k_3k_4[SO_3^{2-}] \tag{41}$$

$$[SO_3Co(III)\text{-}TSPO_2\cdot{}^{4-}] \propto k_1k_{-2}k_4[O_2] + k_1k_3k_4[O_2] \tag{42}$$

$$[SO_3Co(III)\text{-}TSPO_2\cdot SO_3^{6-}] \propto k_1k_2k_4[O_2][SO_3^{2-}] \tag{43}$$

$$[SO_3Co(II)\text{-}TSPO_2^{6-}] \propto k_1k_2k_3[O_2][SO_3^{2-}] \tag{44}$$

The mass balance for the total catalyst concentration is given by:

$$[SO_3Co(II)\text{-}TSP^{4-}]_T = [SO_3Co(II)\text{-}TSP^{4-}] + [SO_3Co(III)\text{-}TSPO_2\cdot^{4-}] + [SO_3Co(III)\text{-}TSPO_2\cdot SO_3^{6-}] + [SO_3Co(III)\text{-}TSPO_2^{6-}] \quad (45)$$

Since the rate of overall reaction is defined by the rate of the slow step in the closed cycle, the rate can be written as:

$$\nu = \frac{-d[SO_4^{2-}]}{dt} = k_3[SO_3Co(III)\text{-}TSPO_2\cdot SO_3^{6-}] \quad (46)$$

where, from steady-state considerations and from Equation 44:

$$[SO_3Co(III)TSP\text{-}O_2\cdot SO_3^{6-}] = \frac{k_1k_2k_4[SO_3Co(II)\text{-}TSP^{4-}]_T[O_2][SO_3^{2-}]}{D} \quad (47)$$

for which

$$D' = k_4(k_{-1}k_{-2} + k_{-1}k_3 + k_2k_3[SO_3^{2-}]) + k_1k_4(k_{-2} + k_3)[O_2] + k_1k_2(k_3 + k_4)[O_2][SO_3^{2-}] \quad (48)$$

Substitution of Equation 47 into Equation 46 gives the following theoretical rate expression for the formation of sulfate (Figure 12):

$$\nu = \frac{[k_3k_4\ /(k_3 + k_4)][SO_3Co(II)\text{-}TSP^{4-}]_T[SO_3^{2-}][O_2]}{D'} \quad (49)$$

where

$$D' = \frac{k_4(k_{-1}k_2 + k_{-1}k_3)}{k_1k_2(k_3 + k_4)} + \frac{k_4(k_{-2} + k_3)}{k_2(k_3 + k_4)}[O_2] + \frac{k_3k_4}{k_1(k_3 + k_4)}[SO_3^{2-}] + [O_2][SO_3^{2-}] \quad (50)$$

Equation 48 can be reduced to the form:

$$\nu = \frac{k'[SO_3Co(II)\text{-}TSP^{4-}]_T[SO_3^{2-}][O_2]}{K_A + K_B[O_2] + K_C[SO_3^{2-}] + [O_2][SO_3^{2-}]} \quad (51)$$

The constants K_A, K_B and K_C each represent the coefficients of the terms in the denominator of the rate expression as defined by Equation 50. The kinetic expression given by Equation 51 must be modified to account for the rapid equilibria that precede the catalytic cycle involving $SO_3Co(II)\text{-}TSP^{4-}$ as the active center. Concentration of the active species can be expressed in terms of the dimer dissociation constant K_d and the formation constant for the initial sulfito complex:

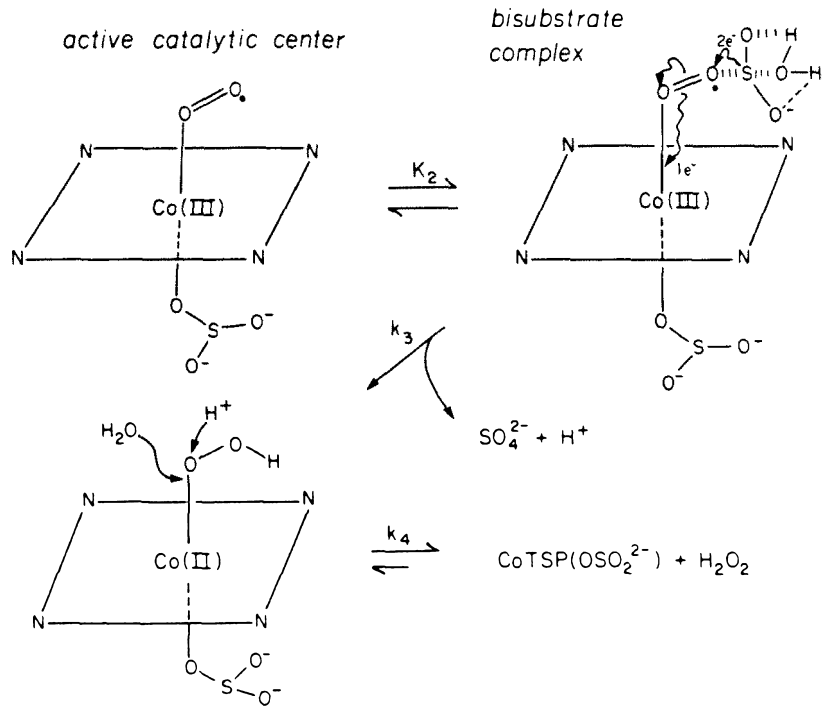

Figure 12. Schematic representation of the proposed catalytic reaction mechanism starting with the Co(II)-TSP sulfito complex as the active catalytic center. Reaction proceeds via the formation of a ternary dioxygen adduct and results in the formation of hydrogen peroxide as an intermediate reduction production of oxygen.

$$K_d = [\text{Co(II)-TSP}]^2/[(\text{Co(II)-TSP})_2^{4-}]^2 \quad (52)$$

$$\beta = [SO_3\text{Co(II)-TSP}^{4-}]/[\text{Co(II)-TSP}][SO_3^{2-}] \quad (53)$$

Equations 52 and 53 can be combined to yield:

$$[SO_3\text{Co(II)-TSP}^{4-}] = \beta K_d^{1/2}[(\text{Co(II)-TSP})_2^{4-}]^{1/2}[SO_3^{2-}] \quad (54)$$

Further simplification of Equation 54 is possible because $[SO_3^{2-}]_o >> [(\text{Co(II)-TSP})_2]_o$. This condition allows the approximation that the concentration of sulfite in solution is relatively constant with respect to the amount coordinated in the active complex, $SO_3\text{Co(II)-TSP}^{4-}$, such that:

$$[SO_3\text{Co(II)-TSP}^{4-}]_T \simeq K'[(\text{Co(II)-TSP})_2^{4-}]^{1/2} \quad (55)$$

where $K' = \beta K_d^{1/2}[SO_3^{2-}]$ (i.e., K' is a pseudo-equilibrium constant). Substitution of Equation 55 into Equation 51 gives an approximate overall rate expression:

$$\nu = \frac{k'K'[(Co(II)\text{-}TSP)_4^{2-}]^{1/2}[SO_3^{2-}][O_2]}{K_A + K_B + K_C\,[SO_3^{2-}] + [O_2][SO_3^{2-}]} \tag{56}$$

The final rate law (Equation 56) can be simplified for the experimental pseudo-order reaction conditions, $[O_2] >> [SO_3^{2-}]$ such that $K_B[O_2] >> K_A$, $K_C[SO_3^{2-}]$ to obtain:

$$\nu = \frac{k'K'[(Co(II)\text{-}TSP)_2^{4-}]^{1/2}[SO_3^{2-}]}{K_B + [SO_3^{2-}]} \tag{57}$$

Two extremes can be considered for the reduced form of the theoretical rate law. If $K_B >> [SO_3^{2-}]$, Equation 57 becomes

$$\nu \simeq k'_\beta K_d^{1/2}[(Co(II)\text{-}TSP)_2^{4-}]^{1/2}[SO_3^{2-}]^2 \tag{58}$$

Similarly, when $[SO_3^{2-}] >> K_B$

$$\nu \simeq k'_\beta K_d^{1/2}[(Co(II)\text{-}TSP)_2^{4-}]^{1/2}[SO_3^{2-}] \tag{59}$$

The kinetic expressions for these limiting cases can be compared with the experimentally observed rate laws measured at pH 6.7

$$\nu_{obs} = k_{obs}[Co(II)\text{-}TSP]^{0.3}[SO_3^{2-}] \tag{60}$$

and pH 9.2

$$\nu_{obs} = k_{obs}[Co(II)\text{-}TSP][SO_3^{2-}] \tag{61}$$

In neutral solution, a fractional-order dependence of 0.3 in catalyst concentration is observed, whereas Equation 58 predicts a one-half order dependence on the dimeric form of Co(II)-TSP. Nonintegral reaction orders arise frequently in polar reactions when the principal reactive species is derived from the dissociation of a dimer [94]. Reevaluation of k_{obs} as a function of [Co(II)-TSP] in the presence of EDTA yielded a reaction order of approximately 0.5. Schelly et al. [72] also reported that divalent metal phthalocyanines tend to form higher-order oligomers in aqueous solution at high ionic strength. Consideration of the equilibria between higher-order aggregate species in the development of a theoretical rate expression would further reduce the apparent order in Co(II)-TSP. Since dimeric and polymeric phthalocyanine species are the dominant forms of the complex in solution at pH 6.7, a nonintegral dependence on total added Co(II)-TSP seems consistent with the assumption that the monomer is actually the active form of the catalyst.

At pH 9.2, a first-order dependence on the catalyst concentration is observed. This result is consistent with the kinetic formulation described in the preceding paragraphs if the dimeric form of Co(II)-TSP is no longer assumed to be the dominant species. Cookson et al. [95] presented evidence for a shift in the monomer-dimer equilibrium toward the monomer with an increase in pH. Under alkaline conditions, the remaining solvent molecules in the coordination sphere of Co(II)-TSP^{2-} are replaced by hydroxide groups (OH^-), resulting in increased stability of monomeric complexes such as (HO)Co(II)-TSP^{3-}, $(HO)_2$Co(II)-TSP^{4-} and HOCo(III)-$TSPO_2{\cdot}^{3-}$. In this situation, the prior equilibrium designated by Equation 34 could be neglected. Consequently, the theoretical rate expression would show a first-order dependence in catalyst, as indicated in Equation 61.

The postulated mechanism appears to explain the kinetic and spectral data for a broad range of reaction conditions. The extremes described by Equations 56 to 58 account for the slight shifts in the reaction order of S(IV) to values greater than unity, and the apparent zero-order dependence on $[O_2]$. A schematic representation of the two-electron transfer complexation pathway is presented in Figure 12 for the pH range in which sulfite (SO_3^{2-}) is the principal reactive S(IV) species in solution.

A variant of the proposed mechanism occurs when SO_3^{2-} reacts with SO_3Co(III)-$TSPO_2{\cdot}^{4-}$ without formation of a ternary complex of sufficiently long lifetime to be kinetically significant. This type of mechanism was originally suggested by Theorell and Chance [96]. The theoretical rate expression for this second alternative is identical in form to that given by Equation 50, except that the constant terms K_A, K_B and K_C are defined by different combinations of rate constants.

To verify the applicability of Equation 55 to the experimental measurements, a double-reciprocal analysis of the initial rate data was performed. Rearrangement of Equation 55 gives

$$1/\nu_o = (1 + K_A/[O_2][SO_3^{2-}] + K_B[SO_3^{2-}] + K_C/[O_2])/\nu_o \tag{61}$$

where $\nu_o = (k_3k_4/k_3 + k_4)\beta K_d^{1/2}[SO_3^{2-}][Co(II)TSP)_2^{4-}]^{1/2}$

$K_A = k_4(k_{-1}k_2 + k_{-1}k_3)/k_1k_2(k_3 + k_4)$

$K_B = k_4(k_{-2} + k_3)/k_2(k_3 + k_4)$

$K_C = k_3k_4/k_3 + k_4)$

A plot of $1/\nu_o$ vs $1/[SO_3^{2-}]_o$ at constant $[O_2]_o$ should be linear with a slope of:

$$(K_A/[O_2] + K_B^1)/\nu_o \tag{63}$$

and an intercept on the $1/\nu_o$ axis of:

$$(1 + K_C/[O_2])/\nu_o \tag{64}$$

Figure 13 shows the Lineweaver-Burk plots for the catalyzed autoxidation of sulfite at pH 6.7 and 9.2 [87]. The linearity of these functions lends strong support for the postulated ternary-complex mechanism.

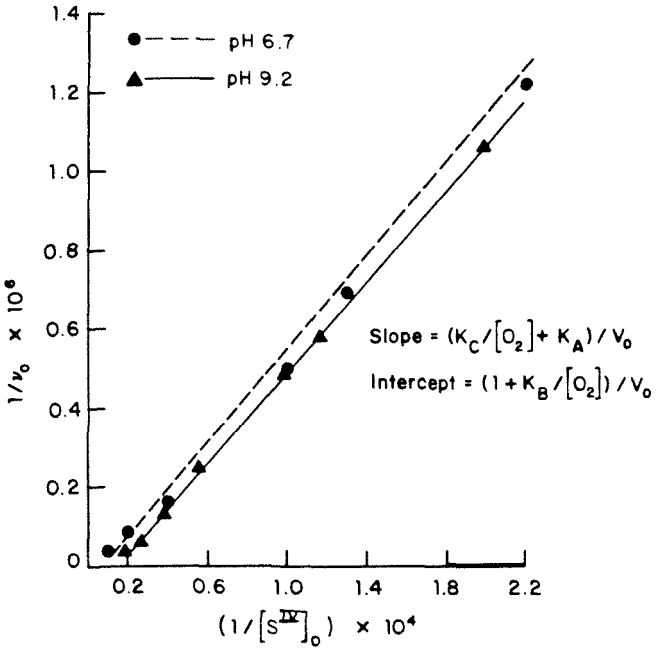

Figure 13. Lineweaver-Burk plots for the initial rate of oxygen depletion v_o, as a function of $[S(IV)]_o$ at pH 6.7 (A) and pH 9.2 (B). Reaction conditions: $[O_2]_o = 2.5 \times 10^{-4}$ *M*, $[Co(II)\text{-}TSP]_o = 1 \times 10^{-6}$ *M*, T = 25.0 C, and $\mu = 0.4$ *M*.

Analysis of the variation in reaction rate as a function of ionic strength (μ) provides evidence in support of the Theorell–Chance scheme. If $k_3 >> k_{-2}$, then the rate-limiting step is defined by Equation 36, in which two negatively charged ions (SO_3^{2-} and $SO_3Co(III)\text{-}TSPO_2^{\cdot 4-}$) react to form an intermediate species bearing an overall net negative charge. The "primary salt effect" states that ionic reactions between ions of the same charge (i.e., both reactants are either positively or negatively charged) will proceed at a faster rate upon an increase in the ionic strength of the medium. From the Debye–Hückel theory, it can be shown that:

$$\log k = \log k_o + 1.02\, Z_a Z_b \mu^{1/2} \tag{65}$$

in which $Z_a(SO_3^{2-}) = -2$ and $Z_b(SO_3Co(III)\text{-}TSPO_2^{\cdot 4-}) = -4$. Even though the experimental conditions ($\mu > 0.1$) exceed the upper boundary for strict applicability of the Debye–Hückel theory ($\mu < 0.01$), a positive slope for a plot of $-\log k_{obs}$ vs $\mu^{1/2}$ (m = 1.47, $R^2 = 0.9973$) was obtained at pH 9.2. In general, the reaction rate increases with increasing ionic strength.

One-Electron Transfer Chain Reaction

An alternative mechanism for the catalytic action of Co(II)TSP on the autoxidation of sulfur dioxide is outlined in Figure 14. In this sequence of steps, the ternary

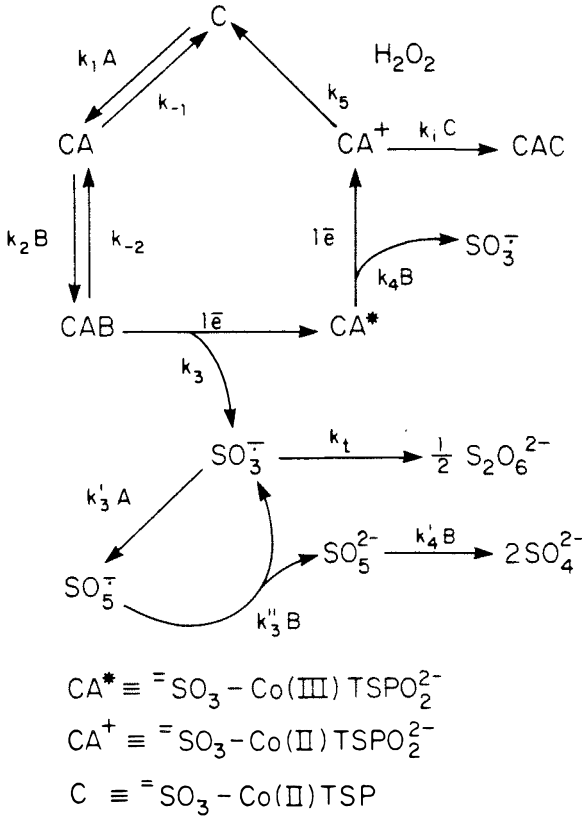

Figure 14. Alternative reaction mechanism for the Co(II)-TSP–catalyzed autoxidation of sulfite involving a one-electron transfer radical pathway in which the complex $SO_3Co(III)$-$TSPO_2^{\cdot 4-}$ acts as the primary chain-reaction initiator.

dioxygen-sulfito complex initiates the catalytic cycle via a chain reaction process identical to that described by Backström [37] and several other investigators. An additional one-electron transfer to the reduced form of the ternary complex would yield H_2O_2 as an intermediate reduction product. If the complexation equilibria are attained rapidly relative to initiation of the free-radical chain process, then the theoretical kinetic expression would be of the form:

$$\nu = k'[M^{n+}]^{0.5}[SO_3^{2-}]^{1.5} \tag{66}$$

where $[M^{n+}] = [SO_3Co(III)\text{-}TSPO_2^{\cdot 4-}]$ and $[SO_3Co(III)\text{-}TSPO_2^{\cdot 4-}] \simeq \beta K_d^{1/2}$ $[Co(II)\text{-}TSP)_2^{4-}]^{1/2}[SO_3^{2-}][O_2]$. Substitution of these relationships into Equation 66 gives a rate law that is second-order in sulfite and first-order in oxygen. These concentration dependencies are not observed under the experimental conditions employed in the current study; therefore, the one-electron transfer mechanism is an unlikely candidate.

Alternative one-electron transfer or two-electron pathways involving the μ-superoxo complex of Co(II)-TSP can be considered as suggested by Davies

et al. [29] for $(NH_3)_5Co(III)O_2Co(II)(NH_3)_5^{5+}$ and by Yatsimirskii et al. [91] for (L-histidine)$_2$ Co(III)O_2Co(II)(L-histidine)$_2$. In this mechanism, the μ-superoxo complex, $(CoTSP)_2O_2^{4-}$, is the active catalytic center and it reacts as follows:

$$(Co\text{-}TSP)_2O_2^{4-} + SO_3^{2-} \xrightarrow{slow} SO_4^{2-} + Co(II)\text{-}TSP + Co(IV)\text{-}TSPO \quad (67)$$

$$Co(IV)\text{-}TSPO + SO_3^{2-} \longrightarrow SO_4^{2-} + Co(II)\text{-}TSP \quad (68)$$

or

$$(Co\text{-}TSP)_2O_2^{4-} + SO_3^{2-} \xrightarrow{slow} Co(III)\text{-}TSPO_2Co(II)\text{-}TSP^{5-} + SO_3^{-} \quad (69)$$

$$Co(III)\text{-}TSPO_2Co(II)\text{-}TSP^{5-} + SO_3^{-} \longrightarrow Co(II)\text{-}TSPO_2^{4-} + SO_3 + Co(II)\text{-}TSP^{2-} \quad (70)$$

$$SO_3 + H_2O \longrightarrow H_2SO_4 \quad (71)$$

$$Co(II)\text{-}TSPO_2^{4-} + 2H^+ \longrightarrow Co(II)\text{-}TSP^{2-} + H_2O_2 \quad (72)$$

The alternative mechanistic pathways, summarized by Equations 67–72 seem to be less feasible chemically than the proposed bisubstrate complexation scheme. For example, the electron configuration of cobalt does not readily permit formation of the nominally Co(IV) oxide intermediate as defined by Reaction 66. These mechanisms also predict a second-order rate dependence on the concentration of the Co(II)-TSP monomer (or first-order as the dimeric complex) as well as a first-order dependence on $[O_2]$. Such conditions are clearly at odds with the experimental observations.

Research in these areas is continuing with an examination of the catalytic role of simple hexaaquo metal ions and transition-metal complexes using stopped-flow/temperature-jump relaxation techniques to determine the kinetic details of the complexation and electron transfer steps. The nature of the innersphere intermediates is being elucidated further by ESR and resonance Raman spectroscopic measurements.

Effect of Metal-Catalyzed Autoxidation on the Formation of Sulfate Aerosols

The central theme of the current research explores the contribution of condensed-phase chemical processes to the transformation of sulfur dioxide to sulfuric acid in the atmosphere. The hypothesis set forth in the introduction to this chapter postulates that metal-complexation reactions are key steps in the mechanistic pathway for the catalyzed autoxidation of SO_2 dissolved in aqueous microdroplets. Kinetic data obtained under carefully controlled experimental conditions demon-

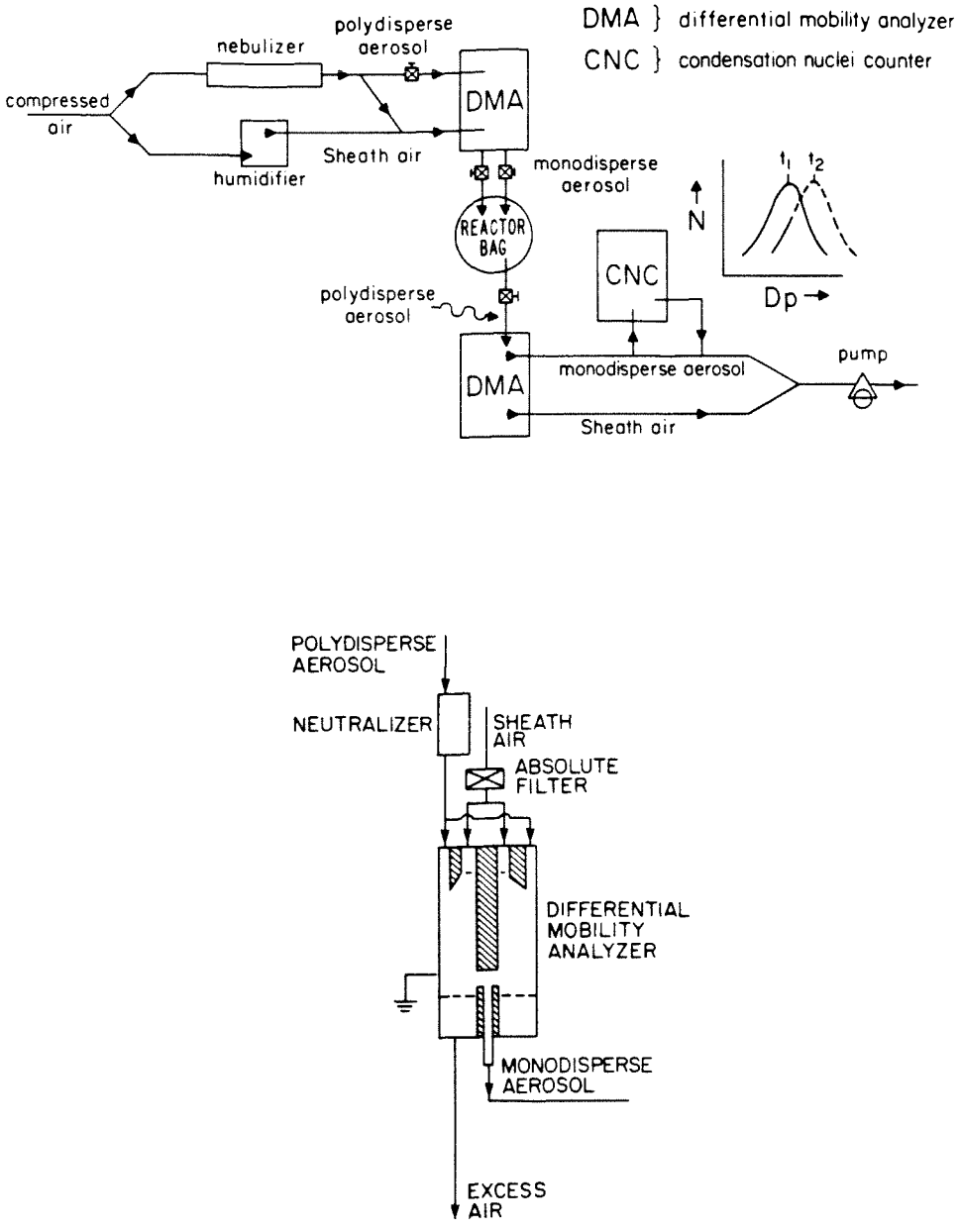

Figure 15. Schematic diagram of the experimental apparatus used to measure aerosol particle growth rates. Details of the design of the DMA are also shown.

strate that transition metal species capable of reversibly binding molecular oxygen function as effective catalysts for the oxidation of sulfite by O_2 in bulk aqueous solution. To evaluate the efficiency of the pathway under droplet-phase conditions, a series of experiments was conducted to measure the influence of the model phthalocyanine catalysts on the growth of sulfate aerosol particles.

A schematic diagram of the experimental system employed in this study is shown in Figure 15. A differential mobility analyzer (DMA) was used to initially generate an aerosol of known size and composition and then for the measurement of changes in particle diameter following the condensed-phase oxidation of SO_2. Particles are charged at the DMA inlet to achieve a Boltzmann equilibrium charge distribution on the aerosol. For the particle size range under investigation (<0.2 μm), virtually all of the particles have either 0 or ±1 unit of electrical charge. Particles are classified according to electrical mobility as the aerosol flows through the cylindrical condensor assembly of the DMA as shown in Figure 16. The voltage between the collecting rod of the condensor and the outer cylinder is varied until particles are detected by the condensation nuclei counter (CNC). At the appropriate voltage, particles have the correct electrical mobility to penetrate the slit to the

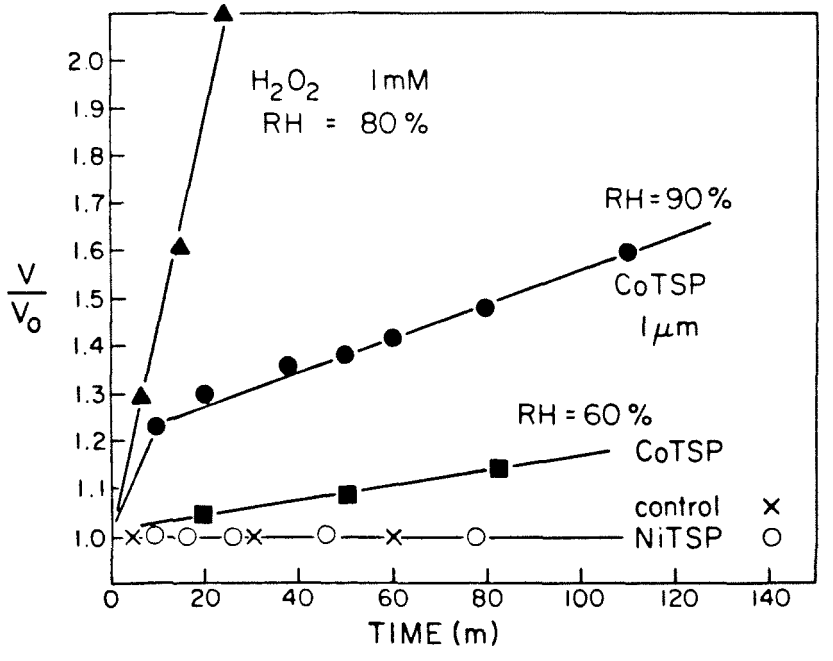

Figure 16. Preliminary experimental data showing the increase in the volume of monodisperse aerosol particles as a function of time. Particle growth rate was caused by catalytic Co(II)-TSP autoxidation of SO_2 or by reaction of SO_2 with H_2O_2. Initial particle diameters were nominally 0.06 μm in all experiments, and the SO_2 concentrations were approximately 45 ppm.

collection rod. Because the particles are singly charged there is a unique relationship between electrical mobility and size. Liu and co-workers [97,98] have used this approach to study the growth of monodisperse aerosols on humidification and for an examination of the reactions between H_2SO_4 particles and gaseous ammonia (NH_3).

In a typical experiment, a polydisperse aerosol was generated by atomizing a 10^{-4} *M* aqueous sulfuric acid solution containing the appropriate catalyst or oxidant through a nebulizer. Diversion of the flow of vapor through the DMA permitted the selection of a monodisperse droplet phase (nominally 0.06 μm in diameter) before initiation of the oxidation reaction. Sulfur dioxide was injected directly into the opaque plastic reactor bag and the growth of the aerosol particles was monitored as a function of time using a second DMA and CNC. The experiments were conducted in the dark at constant temperature and relative humidity.

Some of the SO_2 gas introduced to the reaction chamber will dissolve in the aqueous droplets according to Henry's law. Calculations by Schwartz and Freiberg [99,100] suggest that dissolution of SO_2 is instantaneous with respect to the solution-phase reaction time for droplet diameters of <1.0 μm. When a molecule of sulfur dioxide is oxidized to sulfate, another molecule plus additional water will dissolve, to maintain phase equilibrium. Addition of SO_2 and H_2O to the droplet causes an increase in the volume of the aerosol particle. The volume growth rate of the particle is directly related to the reaction rate of SO_2 oxidation within the droplet phase by:

$$\frac{dV}{dt} = \frac{1}{\rho a}(M_{SO_2} + \gamma M_{H_2O})\frac{d}{dt}([SO_2]v) \tag{73}$$

where
V = particle volume
ρ_a = aerosol density
M_{SO_2}, M_{H_2O} = molecular weights of SO_2 and H_2O
γ = mole ratio of H_2O to sulfate in the aerosol droplet as determined by the relative humidity
$[SO_2]$ = molar concentration of dissolved sulfur dioxide

Preliminary kinetic data obtained from the aerosol experiments are summarized in Figure 16, which shows a plot of the increase in particle size (normalized with respect to the initial monodisperse droplet volume) as a function of reaction time. Droplets containing hydrogen peroxide at an initial solution concentration of 10^{-3} *M* were observed to double in volume after approximately 20 min. The aerosol containing Co(II)-TSP also grew, but at a significantly lower rate. In a control experiment, an aerosol containing a mixture of sulfuric acid and ammonium sulfate failed to exhibit any increase in particle size on exposure to SO_2 in the absence of catalyst or oxidant. These results support the assertion that H_2O_2 acts as a highly efficient liquid-phase oxidant for nonphotolytic atmospheric conversion of aquated SO_2 to H_2SO_4.

In the model experiments with metal-phthalocyanine complexes, oxidation

of SO_2 in the presence of Co(II)-TSP at 10^{-6} *M* resulted in a 10–50% increase in particle volume over the course of 2 h. The rate of particle growth was enhanced dramatically on an increase in relative humidity from 60 to 90%, which indicates that liquid-phase reaction processes are primarily responsible for the formation of sulfate aerosol in the experimental system. In this context, it is especially interesting to note that addition of Ni(II)-TSP failed to cause an increase in particle size. The catalytic response of the rates of solution-phase reactions and aerosol growth to the presence of homogeneous transition metal complexes such as Co(II)-TSP suggests that complexation of sulfite and coordination of molecular oxygen is a feasible mechanism for the autoxidation of aquated SO_2 in atmospheric microdroplets. Further experimentation is in progress to determine the effect of light, dew point, SO_2 concentration, catalyst speciation and concentration, initial droplet pH, and solution composition on the rate of aerosol formation.

Heterogeneous Catalysis by Co(II)-TSP and Co(II)-TAP Complexes Supported on Silica Gel

Metal-catalyzed autoxidation reactions offer attractive possibilities for the development of pollution control methodologies. In commercial systems, transition metal ions are frequently associated with organic ligands as an organometallic complex, which is soluble in the solvent of interest. One major disadvantage associated with the application of homogeneous catalysis centers around the problem of separating the catalyst and products after termination of the reaction. This drawback may be overcome through attachment of the reactive complex to a solid surface. In this case a hybrid heterogeneous system is substituted for the soluble organometallic complex, thereby facilitating recovery of the catalytic species. Schutten and co-workers [101–103] have observed that the autoxidation of thio salts is accelerated in the presence of cobalt(II)-phthalocyanines bound to polyvinylamine and cross-linked styrene divinylbenzene. Catalytic autoxidation of reduced sulfur compounds in Klaus plants or sulfur dioxide in flue gas using supported metal-phthalocyanines represent two potential applications of this method.

Application of catalytic autoxidation to the formulation of an alternative technique for sulfur dioxide pollution control requires a detailed understanding of the dynamic behavior of the reaction system. The solid-supported analogs of Co(II)-TAP and Co(II)-TSP were synthesized as described in the experimental section and tested in the same batch reactor system used for the characterization of their homogeneous counterparts. The catalysts of interest are depicted schematically in Figure 17. Each of two different modes of attachment of the phthalocyanine complexes to the solid silica gel surface are illustrated in Figure 4. In one case, Co(II)-TAP is anchored to the solid support through covalent bonding of the surface ligand to the peripheral group of the macrocyclic ring, and in the second case through direct coordination of a surface imidazole functionality to the central metal atom of the phthalocyanine complex.

Kinetic data in the heterogeneous reaction systems were obtained exclusively

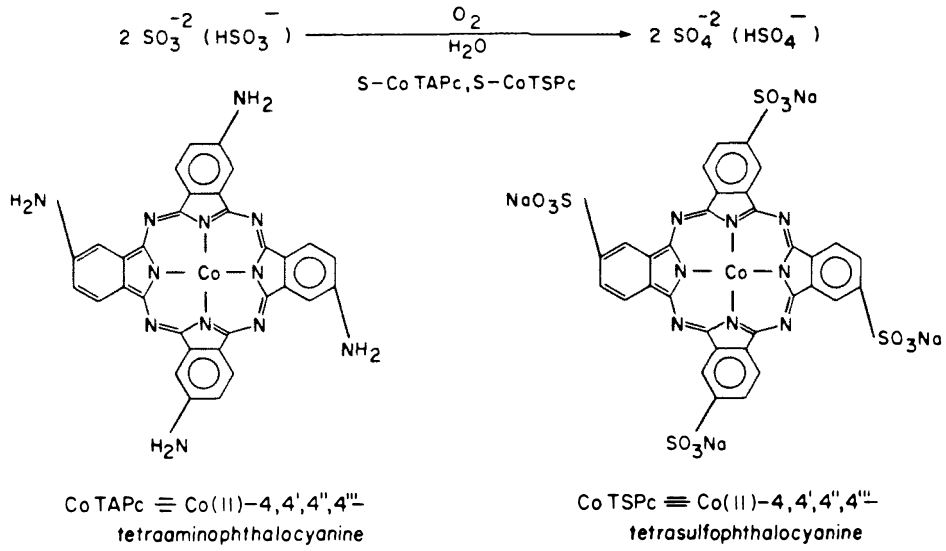

Figure 17. Stoichiometric representation of the reaction of S(IV) with oxygen in a heterogeneous suspension of cobalt phthalocyanine complexes supported on silica gel particles with a surface area of 300 m^2-g^{-1}.

by monitoring dissolved oxygen concentration with respect to time. As opposed to the concentration conditions employed in the homogeneous reactions, the heterogeneous processes were studied under pseudo-first- or zero-order concentration conditions in oxygen (i.e., $[S(IV)]_o > [O_2]_o$) such that an initial stoichiometric excess of sulfite was present in solution.

Results of the preliminary experiments in which the depletion of oxygen was measured as a function of time are summarized in Figure 18 and Table VIII. At first glance, the most effective solid-supported or "hybrid" catalyst appears to be Co(II)-TAP complex III, covalently linked to the silica gel surface through the peripheral amino group of the phthalocyanine structure. Attachment achieved via direct complexation of the surface-bound imidazole to the Co(II) center results in lower catalytic activity, and apparent deactivation of imidazole-Co(II)-TAP system IV occurs after one half-life or less of the autoxidation reaction. However, when the effect of imidazole-bonded Co(II)-TSP V is normalized with respect to the surface concentration of covalently linked Co(II)-TAP, there appear to be no differences in net catalytic activity. In this context, it should be mentioned that some of the activity exhibited by the former system under alkaline conditions may be due to dissociation of the hybrid complex from the surface to give active Co(II)-TSP in solution.

Since DMSO was used as a solvent in the preparation of Co(II)-TAP, and since McCord and Fridovich [104] have reported that DMSO is an effective catalyst for the autoxidation of sulfite, a series of control experiments was performed to

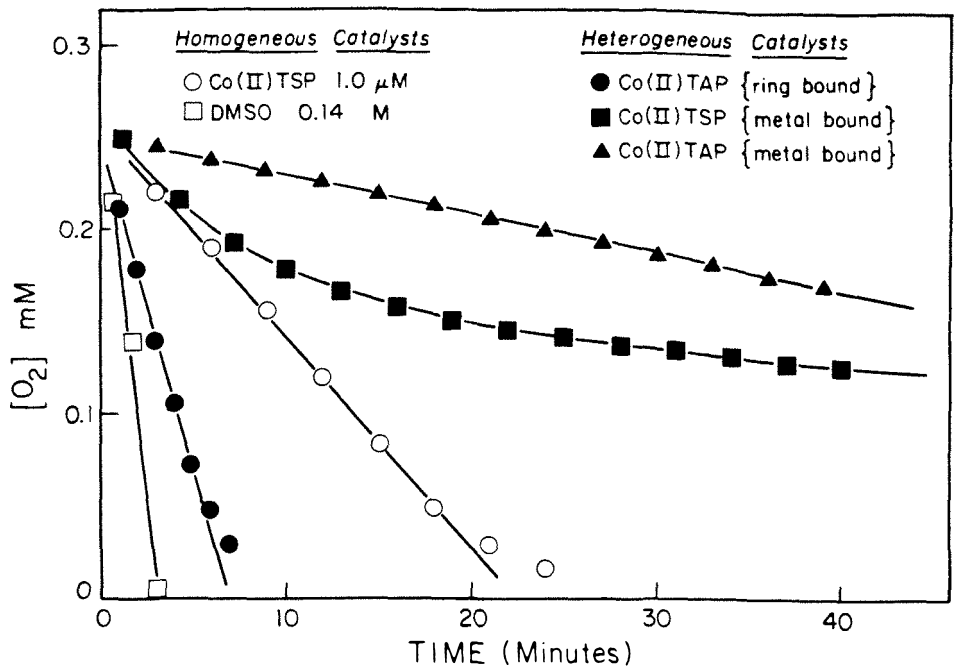

Figure 18. Comparison of the catalytic activity of various solid-supported cobalt phthalocyanine complexes toward the autoxidation of sulfite at pH 6.7 where $S(IV)_0 = 1.0$ m*M* and $O_{2_0} = 0.25$ m*M*. Additional information is provided in Table VIII.

Table VIII. Summary of Kinetic Results for Autoxidation of Sulfite at pH 6.7 in the Presence of Heterogeneous (Hybrid) Co(II)-Phthalocyanine Complexes[a]

Catalyst	$[CAT]$ (μM)	$[O_2]_o$ (mM)	$[O_2]_f$ (mM)	t_∞ (min)	τ (min)
Co(II)-TSP					
Soluble	1.0	0.260	0.003	34	11
Imidazole Hybrid	0.82[b]	0.251	0.106	120	78
Co(II)-TAP					
Soluble	1.0	0.253	0.003	3.1	1.5
Imidazole Hybrid	0.89[b]	0.253	Inactivated		43
Covalent Hybrid	20.32[b]	0.251	0.003	13	3.3
DMSO	1.4×10^5	0.260	0.003	3.9	1.8

[a] $[O_2]_o = 2.6 \times 10^{-4}$ *M*; $[S(IV)]_o = 1.0 \times 10^{-3}$ *M*; $[EDTA]_o = 1 \times 10^{-5}$ *M*; T = 25.0 C; μ = 0.4 *M*.

evaluate the catalytic properties of the solvent. As shown by the data in Table VIII, the reaction half-life (τ) at $[DMSO]_o = 0.14\ M$ is comparable to the value of τ for the homogeneous system containing Co(II)-TAP at $10^{-6}\ M$. However, the concentration of DMSO necessary to attain the observed reaction rate is much greater than that required for Co(II)-TAP. As a result, it seems unlikely that residual solvent from the synthetic procedure could account for the measure catalytic effects of the tetraaminophthalovyanine complexes.

Another factor complicates the analysis of liquid phase–reaction/solid phase–catalyst systems: the potential contribution of homogeneous processes promoted by dissolution of the active species from the surface of the solid support during the reaction. For example, Cohen et al. [105] have attributed the catalytic autoxidation of S(IV) in aqueous fly ash scrubbers to the presence of dissolved iron leached from the particulate matter. Unfortunately, equilibria and solution-phase species are frequently neglected in the study of heterogeneous catalysis.

In the current study, the potential role of homogeneous catalysis was examined by exposing each of the hybrid Co(II)-TAP and Co(II)-TSP complexes to the aqueous solution before initiation of the oxidation reaction. The solid-supported phthalocyanine complexes were removed by filtration before addition of sulfite. In each case, the reaction of S(IV) with O_2 was accelerated to a significant extent. Analysis by atomic absorption spectrophotometry detected trace concentrations of cobalt in the aqueous filtrate. Under alkaline conditions, dissolved cobalt exists principally as Co^{3+}. Barron and co-workers [24,34] have demonstrated that Co(III) is an effective catalyst for autoxidation of aquated SO_2. We are conducting further experiments to quantify the contribution of homogeneous processes.

Preliminary results for the heterogeneous system show that the initial rate of oxygen depletion depends on the amount of hybrid cobalt phthalocyanine initially suspended in solution. The surface coverage of Co(II)-TSP and Co(II)-TAP was determined analytically (see experimental section) to facilitate the kinetic analysis. The initial reaction rate is directly proportional to the amount of covalently bound Co(II)-TAP added to the system, as shown in Figure 19. Application of the van't Hoff method to these data suggests that the oxidation rate of sulfite exhibits a reaction order of 0.5 in effective catalyst concentration (expressed as [Co(II)]). However, because of the high porosity and surface area ($\sim 300\ m^{-2}\text{-}g^{-1}$) of the silica gel, this apparent reaction order may be influenced by mass transfer effects such as pore diffusion. The effect of diffusion on the observed reaction kinetics remains to be determined.

In general, the rates of reactions catalyzed by hybrid catalysts tend to be slower than those catalyzed by the corresponding homogeneous form of the catalyst. However, there are reports of improved catalytic activity and longer catalyst lifetimes when homogeneous species are anchored to solid surfaces. In such a heterogeneous system, the reaction is constrained to take place on the surface of the catalyst; but in the case of catalyst molecules attached to pore-wall surfaces, substrate accessibility to the active site may limit reactivity. Therefore, homogeneous catalysis is potentially more efficient in terms of the absolute amount of catalyst necessary to promote a reaction to a given extent, because all of the catalyst molecules are

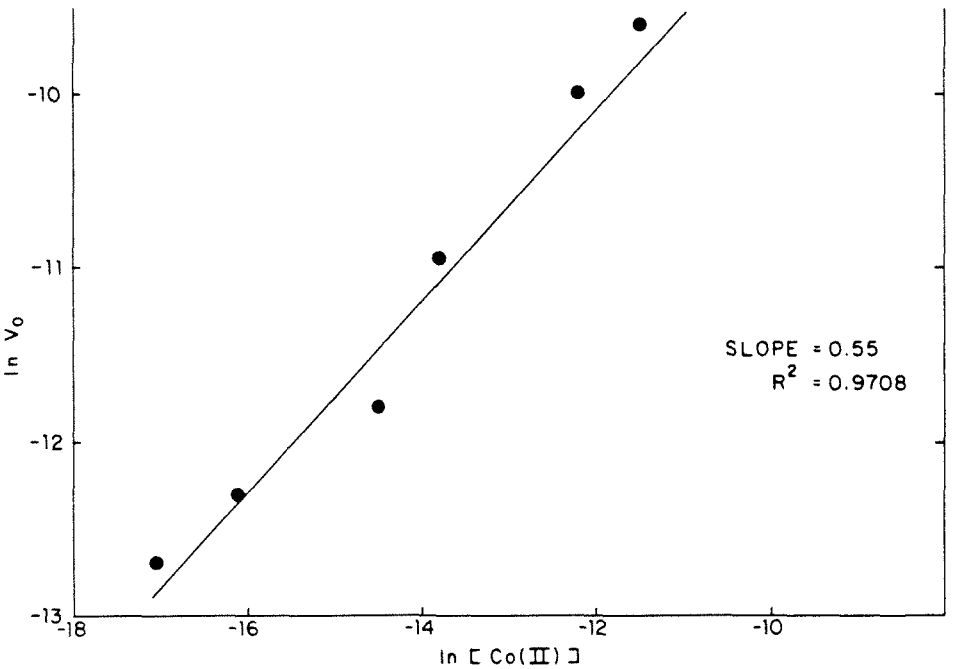

Figure 19. A van't Hoff plot of the initial oxygen depletion rate vs the initial concentration of suspended hybrid catalyst, Co(II)-TAP, attached to modified silica gel particles.

available as active centers. For a hybrid system, the catalytic properties will depend on the solid phase characteristics such as surface area, porosity and the degree of cross-linking in polymeric supports.

CONCLUDING REMARKS

As suggested previously [30,33,38], and observed in this study, certain metal-catalyzed autoxidations of sulfite proceed via the formation of discrete inner-sphere complexes between the reductant, SO_3^{2-}, and the catalyst as a prelude to electron transfer. Additional experimental evidence presented in this study, suggests that the binding and subsequent activation of dioxygen plays a significant role in the catalytic cycle. From this perspective, the most effective catalysts should involve complexes of Fe(II)/Fe(III), Mn(II)/Mn(III), Co(II)/Co(III) and V(III)/V(IV) in which the central metal is reversibly oxidized and reduced on complexation by oxygen and/or sulfite. Inhibition of catalytic activity by strong chelating and complexing agents supports this conclusion.

Certain metal-catalyzed reactions of sulfite may be enhanced by a photoassisted pathway as shown in this study for Co(II) and reported previously [39]

for Fe(III). This apparent coupling of photolytic and metal-catalyzed processes may help to explain relative differences between night- and daytime SO_2 conversion rates. More work is needed in this area to extend and apply this concept to aerosol systems.

In liquid aerosol systems, important factors to consider are the nature and roles of dissolved organic molecules that can act as competitive complexing agents for metals. For example, liquid-phase autoxidation of benzaldehyde produces benzoic acid, which can act as a suitable complexing agent (e.g., $pK_{a1} = 3.97$, $\log\beta_{11} = 1.51$ for $Cu(C_7H_6O_2)^+$) and a similar oxidation of 2-hydroxybenzaldehyde to 2-hydroxybenzoic acid produces even a stronger potential ligand (e.g., $pK_{a1} =$

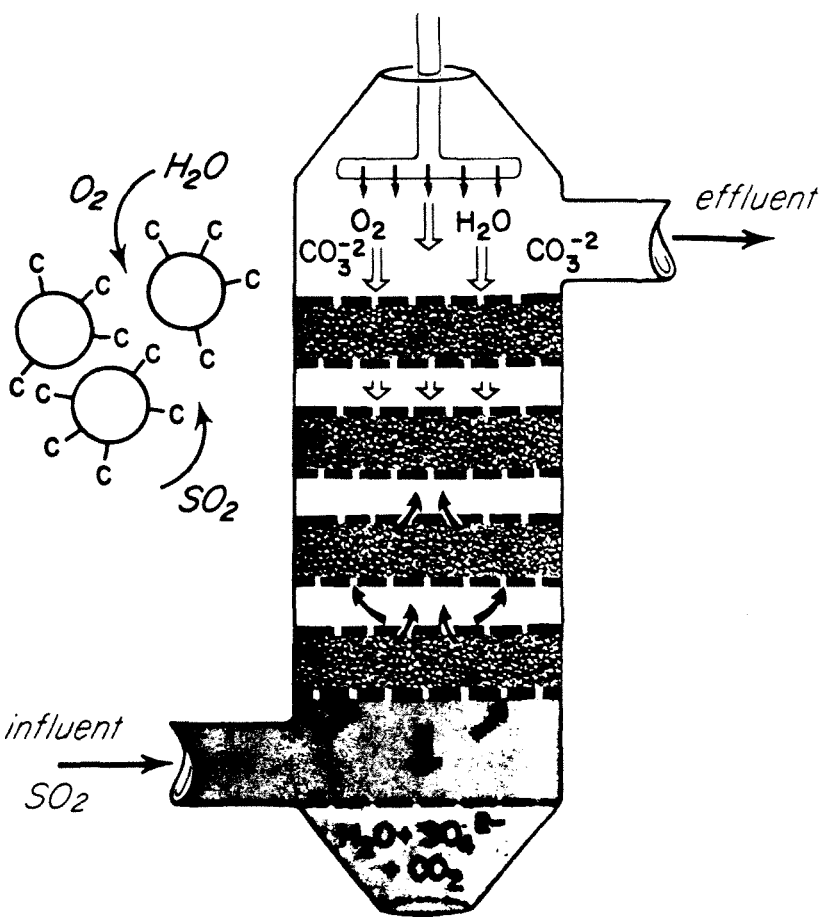

Figure 20. A potential application of polymer-supported organometallic catalysts for sulfur dioxide stack gas scrubbing is illustrated above. The active catalyst C is supported on appropriate solid supports and placed in fixed beds in a countercurrent-flow reactor.

2.78, $-\log\beta_{11} = 10.13$ for $Cu(C_7H_6O_3)^+$). The presence of complexing agents of this type will accelerate the dissolution of Fe_2O_3 and MnO_2, which are the likely sources of soluble iron and manganese in aerosol systems. As shown by Cohen et al. [105], the catalytic activity of soot-derived aerosols correlates well with the total iron released to the liquid phase.

Results of this study, along with the work of others, indicate that H_2O_2 is a major intermediate reduction product of the catalyzed oxidation of various sulfur compounds and oxidizable organic molecules. As such, metal-catalyzed autoxidation reactions in liquid aerosols may be a significant source of atmospheric peroxide [106,107]. However, accumulation of H_2O_2 would not occur to an appreciable extent in liquid aerosols that contain or are exposed to high concentrations of SO_2.

Preliminary research on hybrid organometallic catalysts has shown that attachment of homogeneous catalysts to solid surfaces results in a negligible loss of catalytic activity for the autoxidation of dissolved S(IV). Improved catalytic ability, elimination of recovery problems and longer catalyst lifetimes may be achieved with supported organometallic catalysts. Mass et al. [48] and Schutten and co-workers [89,101] have reported an enhanced catalytic autoxidation of mercaptoethanol by Co(II)-TAP attached to cross-linked polyacrylamide and polyvinylamine, respectively. Figure 20 illustrates a hypothetical countercurrent reactor with fixed beds of solid supported catalyst that could be used for SO_2 scrubbing with the production of H_2SO_4 as an alternative to limestone slurry scrubbers, which produce an unusable solid reaction product. Similarly, a fixed-bed reactor of mixed solid-supported catalysts with variable reactivity and specificity may be employed for tertiary wastewater treatment of refractory organics remaining after biological oxidation of industrial or domestic wastes. Research along these lines is being pursued presently in this laboratory.

ACKNOWLEDGMENTS

The authors acknowledge gratefully the financial support of the U.S. Environmental Protection Agency (grant R808086-01) and President's Fund/Sloan Foundation Grant administered by the California Institute of Technology. They are also indebted to their colleagues in the air pollution field, P. McMurry, G. Cass, R. Flagan, G. McRae and J. Seinfeld, for their informative discussions on the subject of aerosol chemistry. The aerosol experiments were conducted under the direction of Peter W. McMurry in the Particle Technology Laboratory, Department of Mechanical Engineering, University of Minnesota.

REFERENCES

1. Calvert, J.G., F. Su, J.W. Bottenheim and O.P. Strausz. "Mechanisms of Homogeneous Oxidation of Sulfur Dioxide in the Troposphere," *Atmos. Environ.* 12:197–226 (1978).

2. Middleton, P., C.S. Kiang and V.A. Mohnen. "Theoretical Estimates of the Relative Importance of Various Urban Sulfate Aerosol Production Mechanisms," *Atmos. Environ.* 14:463–472 (1980).
3. Möller, D. "Kinetic Model of Atmospheric Oxidation Based on Published Data," *Atmos. Environ.* 14:1067–1076 (1980).
4. Cass, G.R., and F.H. Shair. "Transport of Sulfur Oxides Within the Los Angeles Sea Breeze/Land Breeze Circulation System," in *Proceedings of the Second Joint Conference on Applications of Air Pollution Meteorology* (American Meteorological Society, 1980), pp. 320–327.
5. Cass, G.R. "Methods for Sulfate Air Quality Management with Applications to Los Angeles," PhD Thesis, California Institute of Technology, Pasadena, CA (1977).
6. Cox, R.A. "Particle Formation from Homogeneous Reactions of Sulfur Dioxide and Nitrogen Dioxide," *Tellus* 26:235–240 (1974).
7. McMurry, P.H., D.J. Rader and J.L. Smith. "Studies of Aerosol Formation in Power Plant Plumes. I. Parametrization of Conversion Rate for Dry, Moderately Polluted Ambient Conditions," *Atmos. Environ.* 15:2315–2329 (1981).
8. Smith, F.B. and G.H. Jeffrey. "Airborne Transport of Sulphur Dioxide from the U.K.," *Atmos. Environ.* 9:643–659 (1975).
9. Wilson, J.C., and P.H. McMurry. "Studies of Aerosol Formation in Power Plant Plumes. II. Secondary Aerosol Formation in the Navajo Generating Station Plume," *Atmos. Environ.* 15:2329–2339 (1981).
10. Schwartz, S.E. "Gas-Aqueous Reactions of Sulfur and Nitrogen Oxides in Liquid-Water Clouds," in *Acid Rain, Vol. 3, SO_2, NO and NO_2 Oxidation Mechanisms: Atmospheric Considerations*, J.G. Calvert, Ed. (Ann Arbor, MI: Ann Arbor Science Publishers, 1983).
11. Martin, L.R. "Kinetic Studies of Sulfite Oxidation in Aqueous Solution," in *Acid Rain, Vol. 3, SO_2, NO, and NO_2 Oxidation Mechanisms: Atmospheric Considerations*, J.G. Calvert, Ed. (Ann Arbor, MI: Ann Arbor Science Publishers, 1983).
12. Cheng, R.T., M. Corn and J.O. Frohliger. "Contributions to the Reaction Kinetics of Water-Solubles and SO_2 in Air at ppm Concentrations," *Atmos. Environ.* 5:987–1008 (1971).
13. Beilke, S., and G. Gravenhorst. "Heterogeneous SO_2-Oxidation in the Droplet Phase," *Atmos. Environ.* 12:231–239 (1978).
14. Dasgupta, P.K., P.A. Mitchell and P.W. West. "Study of Transition Metal-S(IV) Systems," *Atmos. Environ.* 13:775–782 (1979).
15. Freiberg, J. "Effects of Relative Humidity and Temperature on Iron-Catalyzed Oxidation of SO_2 in Atmospheric Aerosols," *Environ. Sci. Technol.* 8:731–734 (1974).
16. Fuzzi, S. "Study of Iron(III) Catalyzed Sulphur Dioxide Oxidation in Aqueous Solution over a Wide Range of pH," *Atmos. Environ.* 12:1439–1442 (1978).
17. Hegg, D.A., and P.V. Hobbs. "Oxidation of Sulfur Dioxide in Aqueous Systems with Particular Reference to the Atmosphere," *Atmos. Environ.* 12:241–253 (1978).
18. Kaplan, D.J., D.M. Himmelblau and C. Kanaoka. "Oxidation of Sulfur Dioxide in Aqueous Ammonium Sulfate Aerosols Containing Manganese as a Catalyst," *Atmos. Environ.* 15:763–773 (1981).
19. Larson, T.V., N.R. Horike and H. Halstead. "Oxidation of Sulfur Dioxide by Oxygen and Ozone in Aqueous Solution: A Kinetic Study with Significance to Atmospheric Processes," *Atmos. Environ.* 12:1597–1611 (1978).
20. Penkett, S.A., B.M.R. Jones and A.E.J. Eggleton. "A Study of SO_2 Oxidation in Stored Rainwater Samples," *Atmos. Environ.* 13:139–147 (1979).

21. Hayon, E., A. Treinin and J. Wilf. "Electronic Spectra, Photochemistry, and Autoxidation Mechanism of the Sulfite–Bisulfite–Pyrosulfite Systems. The SO_2^-, SO_3^-, and SO_5^- Radicals," *J. Am. Chem. Soc.* 94:47–57 (1972).
22. Sheldon, R.A., and J.K. Kochi. *Metal-Catalyzed Oxidations of Organic Compounds* (New York: Academic Press, Inc., 1981).
23. Hoffmann, M.R. "Trace Metal Catalysis in Aquatic Environments," *Environ. Sci. Technol.* 14:1061–1066 (1980).
24. Barron, C.H., and H.A. O'Hern. "Reaction Kinetics of Sodium Sulfite by the Rapid-Mixing Method," *Chem. Eng. Sci.* 21:397–404 (1966).
25. Bengtsson, S., and I. Bjerle. "Catalytic Oxidation of Sulphite in Dilute Aqueous Solutions," *Chem. Eng. Sci.* 30:1429–1435 (1975).
26. Brimblecombe, P., and D.J. Spedding. "The Catalytic Oxidation of Micromolar Aqueous Sulphur Dioxide," *Atmos. Environ.* 8:937–945 (1974).
27. Chen, T.I., and C.H. Barron. "Some Aspects of the Homogeneous Kinetics of Sulfite Oxidation," *Ind. Eng. Chem. Fundam.* 11:466–470 (1972).
28. Coughanowr, D.R., and F.E. Krause. "The Reaction of SO_2 and O_2 in Aqueous Solutions of $MnSO_4$," *Ind. Eng. Chem. Fundam.* 4:61–66 (1965).
29. Davies, R., A.K.E. Hagopian and A.G. Sykes. "Kinetics and Oxygen-18 Tracer Studies of Sulphite with the Superoxo Complex $(NH_3)_5Co{\cdot}O_2{\cdot}Co(NH_3)_5^{5+}$ in Aqueous Media," *J. Chem. Soc.* (A):623–629 (1969).
30. Freiberg, J. "The Mechanism of Iron Catalyzed Oxidation of SO_2 in Oxygenated Solutions," *Atmos. Environ.* 9:661–672 (1975).
31. Fuller, E.C., and R.H. Crist. "The Rate of Oxidation of Sulfite Ions by Oxygen," *J. Am. Chem. Soc.* 63:1644–1650 (1941).
32. Linek, V., and J. Mayrhoferova. "The Kinetics of Oxidation of Aqueous Sodium Sulfite Solution," *Chem. Eng. Sci.* 25:787–800 (1970).
33. Matteson, J.J., W. Stöber and H. Luther. "Kinetics of the Oxidation of Sulfur Dioxide by Aerosols of Manganese Sulfate," *Ind. Eng. Chem. Fundam.* 8:677–684 (1969).
34. Sawicki, J.E., and C.H. Barron. "On the Kinetics of Sulfite Oxidation in Heterogeneous Systems," *Chem. Eng. J.* 5:153–159 (1973).
35. Yagi, S., and H. Inoue. "The Adsorption of Oxygen into Sodium Sulfite Solution," *Chem. Eng. Sci.* 17:411–421 (1962).
36. Hoffmann, M.R., and S.D. Boyce. "Theoretical and Experimental Considerations of the Catalytic Autoxidation of Aqueous Sulfur Dioxide in Relationship to Atmospheric Systems," in *Advances in Environmental Science and Technology, Vol. 12*, S.E. Schwartz, Ed. (New York: John Wiley & Sons, Inc., 1982).
37. Backström, H. "Der Kettenmechanisms bei der Autoxydation von Naturimsulfirlösungen," *Z. Phys. Chem.* 25B:122–138 (1934).
38. Bassett, H., and W.G. Parker. "The Oxidation of Sulphurous Acid," *J. Chem. Soc.* (1951), pp. 1540–1560.
39. Lunak, S., and J. Veprek-Siska. "Photochemical Autooxidation of Sulphite Catalyzed by Iron(III) Ions," *Collect. Czech. Chem. Commun.* 41:3495–3503 (1976).
40. Schmittkunz, H. "Chemilumineszenzder Sulfitooxidation," Dissertation, Naturwissenschaftliche Fakultät der Universität Frankfurt, Frankfurt, Germany (1963).
41. Spiro, T. G., Ed. *Metal Ion Activation of Dioxygen* (New York: John Wiley & Sons, Inc., 1980).
42. Walling, C. "Fenton's Reagent Revisited," *Accts. Chem. Res.* 12:125–131 (1975).
43. Lunde, G., J. Gether, N. Gjos and M.S. Lande. "Organic Micropollutants in Precipitation over Norway," *Atmos. Environ.* 11:1007–1014 (1977).

44. Inoue, H., Y. Kida, and E. Imoto. "Organic Catalysts. V. Specific Catalytic Properties of Copper-Iron-Phthalocyanine in the Oxidation of Aldehydes," *Bull. Chem. Soc. Japan* 41:692–696 (1968).
45. Ohkatsu, Y., O. Sekiguchi and T. Osa. "The Liquid-Phase Oxidation of Aldehydes with Fe, Cu-Polyphthalocyanine and Cobalt Tetra-p-tolyporphyrin," *Bull. Chem. Soc. Japan* 50:701–705 (1977).
46. Kothari, V.M., and J.J. Tazuma. "Selective Autoxidation of Some Phenols Using Salcomines and Metal Phthalocyanines," *J. Catal.* 41:180–189 (1976).
47. Tada, M., and T. Katsu. "The Autoxidation of Phenols Catalyzed by Phthalocyanine-Fe(II) and Salcomine-pyridine," *Bull. Chem. Soc. Japan* 45:2558–2559 (1972).
48. Mass, T.A.M.M., M. Kuijer and J. Zwart. "Activation of Cobalt-Phthalocyanine Catalyst by Polymer Attachment," *Chem. Commun.* (1976), pp. 86–88.
49. Wagnerova, D.M., E. Schwertnerova and J. Veprek-Siska. "Autoxidation of Hydrazine Catalyzed by Tetrasulphophthalocyanines," *Collect. Czech. Chem. Commun.* 38:756–764 (1973).
50. Wagnerova, D.M., E. Schwertnerova and J. Veprek-Siska. "Autoxidation of Hydroxylamine Catalyzed by Cobalt(II) Tetrasulphophthalocyanine Models of Oxidases," *Collect. Czech. Chem. Commun.* 39:3036–3047 (1974).
51. Hoffmann, M.R., and B.C. Lim. "Kinetics and Mechanisms of the Oxidation of Sulfite by Oxygen: Catalysis by Homogeneous Metal-Phthalocyanine Complexes," *Environ. Sci. Technol.* 13:1406–1414 (1979).
52. Boucher, L.J. "Metal Complexes of Phthalocyanines," in *Coordination Chemistry of Macrocyclic Compounds*, G.A. Melson, Ed. (New York: Plenum Press, 1979), pp. 461–516.
53. Weber, J.H., and D.H. Busch. "Complexes Derived from Strong Field Ligands. XIX. Magnetic Properties of Transition Metal Derivatives of 4,4,',4",4' "-Tetrasulfophthalocyanine," *Inorg. Chem.* 4:469–470 (1965).
54. Allum, K.G., R.D. Hancock, I.V. Howell, S. McKenzie, R.C. Pitkethly and P.J. Robinson. "Supported Transition Metal Complexes," *J. Organomet. Chem.* 87:203–216 (1975).
55. Leal, O., D.L. Anderson, R.G. Bowman, F. Basolo and R.L. Burwell, Jr. "Reversible Adsorption of Oxygen on Silica Gel Modified by Imidazole-Attached Iron Tetraphenylporphyrin," *J. Am. Chem. Soc.* 97:5125–5129 (1975).
56. Huss, A., Jr., P.K. Lim and C.A. Eckert. "On the Uncatalyzed Oxidation of Sulfur(IV) in Aqueous Solution," *J. Am. Chem. Soc.* 100:6252–6253 (1978).
57. Smith, R.M., and A.E. Martell. *Critical Stability Constants, Vol. 4, Inorganic Complexes* (New York: Plenum Press, 1976).
58. Baldwin, M.E. "Sulphitobis(ethylenediamine) Cobalt(III) Complexes," *J. Chem. Soc.* (1961), pp. 3123–3128.
59. Elder, R.C., M.J. Heeg, M.D. Payne, M. Tikula and E. Deutsch. "Trans Effect in Octahedral Complexes. 3. Comparison of Kinetic and Trans Effects Induced by Coordinated Sulfur in Sulfito- and Sulfinapentamine Cobalt(III) Complexes," *Inorg. Chem.* 17:431–440 (1978).
60. Johansson, L. G., and O. Lindqvist. "Manganese(II) Sulfite Trihydrate," *Acta Crystallog.* B36:2739–2741 (1980).
61. Johansson, L.G., and E. Ljundstrom. "Structure of Iron(II) Sulfite 2.5 Hydrate," *Acta Crystallog.* B36:1184–1186 (1980).
62. Magnusson, A., L.G. Johannson and O. Lindqvist. "The Structure of Manganese(II) Sulfite," *Acta Crystallog.* B37:1108–1110 (1981).

63. Newman, G., and D.B. Powell. "The Infra-red Spectra and Structures of Metal-Sulfite Compounds," *Spectrochim. Acta* 19:213–224 (1963).
64. Raston, C.L., A.H. White and J.K. Yandell. "Structural and Kinetic Effects in Cobalt(III) Complexes with Cobalt-Sulfur Bonds. The Crystal Structure of trans-Bis (Ethylenediamine)-imidazolesulfito-Cobalt(III) Perchlorate Dihydrate," *Aust. J. Chem.* 31:993–998 (1978).
65. Hansen, L.D., L. Whiting, D.J. Eatough, T.E. Jensen and R.M. Izatt. "Determination of Sulfur(IV) and Sulfate in Aerosols by Thermometric Methods," *Anal. Chem.* 48:634–638 (1976).
66. Carlyle, D. "A Kinetic Study of the Aquation of Sulfitoiron(III) Ion," *Inorg. Chem.* 10:761–764 (1974).
67. Hoffmann, M.R., R.A. Stern, P.H. Rieger and J.O. Edwards. "A Kinetic Study of Pyrophosphate and Peroxodiphosphate Complexation of Oxovanadium(IV) Ion," *Inorg. Chim. Acta* 19:181–187 (1976).
68. Abel, E.W., J.M. Pratt and R. Whelan. "Formation of a 1:1 Oxygen Adduct with Cobalt(II)-tetrasulphophthalocyanine," *Chem. Commun.* (1971), pp. 449–450.
69. Veprek-Siska, J., E. Schwertnerova and D.M. Wagnerova. "Reversible Reaction of Cobalt(II) Tetrasulfophthalocyanine with Molecular Oxygen," *Chimia* 26:75–76 (1972).
70. Bernauer, K., and S. Fallab. "Phthalocyanine in wässeriger Lösung I," *Helv. Chim. Acta* 44:1287–1292 (1961).
71. Gruen, L.C., and R.J. Blagrove. "The Aggregation and Reaction of the Tetrasodium Salt of Cobalt Phthalocyanine-4,4′,4″,4‴-Tetrasulphonic Acid," *Aust. J. Chem.* 26:319–323 (1973).
72. Schelly, Z.A., R.D. Farina and E.M. Eyring. "A Concentration-Jump Relaxation Method Study on the Kinetics of the Dimerization of the Tetrasodium Salt of Aqueous Cobalt(II)-4,4′,4″,4‴-Tetrasulfophthalocyanine," *J. Phys. Chem.* 74:617–620 (1970).
73. Rollman, L.D., and R.T. Iwamoto. "Electrochemistry, Electron Paramagnetic Resonance and Visible Spectra of Cobalt, Nickel, Copper and Metal-Free Phthalocyanines in Dimethyl Sulfoxide," *J. Am. Chem. Soc.* 90:1455–1463 (1968).
74. Kropf, H. "Catalysis by Phthalocyanine Complexes," *Angnew. Chem. Int. Ed.* 11:239–240 (1972).
75. Kropf, H., and H.D. Hoffmann. "Autoxidation von Cumol in Gegenwart von Substituierten Kupfer-Phthalocyaninen und Verwandten Kupfer-Komiplexen," *Tetrahedron Lett.* (1967), pp. 659–663.
76. Basolo, F., B.M. Hoffmann and J.A. Ibers. "Synthetic Oxygen Carriers of Biological Interest," *Accts. Chem. Res.* 8:384–392 (1975).
77. Jones, R.D., D.A. Summerville and F. Basolo. "Synthetic Oxygen Carriers Related to Biological Systems," *Chem. Rev.* 79:139–179 (1979).
78. Collmann, J.P., T.R. Halbert and K.S. Suslick. "O_2 Binding to Hemes and Their Synthetic Analogs," in *Metal Ion Activation of Dioxygen*, T.G. Spiro, Ed. (New York: John Wiley & Sons, Inc., 1980), pp. 1–72.
79. McLendon, G., and A.E. Martell. "Inorganic Oxygen Carriers as Models for Biological Systems," *Coord. Chem. Rev.* 19:1–39 (1976).
80. Sigel, H., P. Waldmeier and B. Prijs. "The Dimerization, Polymerization, and Hydrolysis of Fe^{III}-4,4′,4″,4‴-Tetrasulfophthalocyanine," *Inorg. Nucl. Chem. Lett.* 7:161–169 (1971).
81. Vonderschmitt, D., K. Bernauer and S. Fallab. "Reaktivat von Koordinationverbin-

dungen XIV [1]. Reversible O_2-Bindung an Eisen(II)-Phthalocyanintetrasulfonsäure," *Helv. Chim. Acta* 48:951–954 (1964).

82. Wagnerova, D.M., E. Schwertnerova and J. Veprek-Siska. "Kinetics of the Reaction of Cobalt(II) Tetrasulphophthalocyanine with Molecular Oxygen," *Collect. Czech. Chem. Commun.* 39:1980–1988 (1974).
83. Cook, A.H. "Catalytic Properties of the Phthalocyanines. Part I. Catalase Properties," *J. Chem. Soc.* (1938), pp. 1761–1768.
84. Cook, A.H. "Catalytic Properties of the Phthalocyanines. Part II. Oxidase Properties," *J. Chem. Soc.* (1938), pp. 1768–1774.
85. Cook, A.H. "Catalytic Properties of the Phthalocyanines. Part III," *J. Chem. Soc.* (1938), pp. 1774–1780.
86. Dolansky, J., D.M. Wagnerova and J. Veprek-Siska. "Autoxidation of Cysteine Catalyzed by Cobalt(II) Tetrasulphophthalocyanine. Models of Oxidases V," *Collect. Czech. Chem. Commun.* 41:2326–2332 (1976).
87. Laidler, K., and P.S. Bunting. *The Chemical Kinetics of Enzyme Action* (Oxford: Clarendon Press, 1973).
88. King, E.L., and C. Altman. "A Schematic Method of Deriving the Rate Laws for Enzyme Catalyzed Reactions," *J. Phys. Chem.* 60:1375–1378 (1956).
89. Schutten, J.H., and T.P.M. Beelen. "The Role of Hydrogen Peroxide During the Autoxidation of Thiols Promoted by Bifunctional Polymer-Bonded Cobalt Phthalocyanine Catalysts," *J. Molec. Catal.* 10:85–97 (1981).
90. Holt, B.D., R. Kumar and P.T. Cunningham. "Oxygen-18 Study of the Aqueous Phase Oxidation of Sulfur Dioxide," *Atmos. Environ.* 15:557–566 (1981).
91. Yatsimirskii, K., B. Bratushko, I. Yu and I.L. Zatsny. "Kinetics and Mechanism of the Reduction of Molecular Oxygen Coordinated in the Complex Co_2(L-histidine)$_4O_2$ by Sodium Sulphite in Aqueous Solution," *Zh. Neorgh. Khimii* 22:1611–1616 (1977).
92. Beelen, T.P.M., C.O. de Costa Gomez and M. Kuijer. "The Enhancement by Visible Light of the Catalytic Activity of Co(II)-Tetrasulphophthalocyanine on the Oxidation of Mercapto-Ethanol," *Recl. Trav. Chim. Pays-Bas.* 98:521–522 (1979).
93. Cox, G.S., D.G. Whitten and C. Giannotti. "Interaction of Porphyrin and Metalloporphyrin Excited States with Molecular Oxygen. Energy-Transfer Quenching Mechanisms in Photo Oxidations," *Chem. Phys. Lett.* 67:511–515 (1979).
94. Frost, A.A., and R.G. Pearson. *Kinetics and Mechanism* (New York: John Wiley & Sons, Inc., 1961).
95. Cookson, D.J., T.D. Smith, J.F. Boas, P.R. Hicks and J.R. Pilbrow. "Electron Spin Resonance Study of the Autoxidation of Hydrazine, Hydroxylamine and Cysteine Catalyzed by the Cobalt(II) Chelate Complex of 3,10,17,24-Tetrasulphophthalocyanine," *J. Chem. Soc.* (1977), pp. 109–114.
96. Theorell, H., and B. Chance. "Studies on Liver Alcohol Dehydrogenase. II. The Kinetics of the Compound of Horse Liver Alcohol Dehydrogenase and Reduced Diphosphopyridine Nucleotide," *Acta Chem. Scand.* 5:1127–1144 (1951).
97. Liu, B.Y.H., D.Y.H. Pui, K.T. Whitby and D.B. Kittelson. "The Aerosol Mobility Chromatograph: A New Detector for Sulfuric Acid Aerosols," *J. Aerosol Sci.* 6:433–451 (1978).
98. McMurry, P.H., and B.Y.H. Liu. "The Tandem Differential Mobility Analyzer Applied to Studies on Particle Growth and Gas Phase Titration," DOE Report EY-76-S-02-1248 (1978).
99. Schwartz, S.E. and J.E. Freiberg. "Mass-Transport Limitation to the Rate of Reaction

of Gases in Liquid Droplets: Application to Oxidation of SO_2 in Aqueous Solutions," *Atmos. Environ.* 15:1129–1144 (1981).

100. Freiberg, J.E., and S.E. Schwartz. "Oxidation of SO_2 in Aqueous Droplets: Mass-Transport Limitation in Laboratory Studies and the Ambient Atmosphere," *Atmos. Environ.* 15:1145–1154 (1981).
101. Schutten, J.H., P. Piet and A.L. German. "Some Observations on Complexes of a Cobalt Phthalocyanine with Poly(vinylamine) and Their Catalytic Activity in the Autoxidation of Thiols," *Makromol. Chem.* 180:2341–2350 (1979).
102. Schutten, J.H., and J. Zwart. "Autoxidation of Mercaptans Promoted by a Bifunctional Catalyst Prepared by Polymer Attachment of Cobalt-Phthalocyanine," *J. Mol. Catal.* 5:109–123 (1979).
103. Schutten, J.H., C.H. van Hastenberg, P. Piet and A.L. German. "Marcroporous Styrene Divinylbenzene Copolymers for Poly(vinylamine)–Cobaltphthalocyanine Oxidation Catalysts," *Angew. Makromol. Chem.* 89:201–219 (1980).
104. McCord, J.M., and I. Fridovich. "The Utility of Superoxide Dismutase in Studying Free Radical Reactions," *J. Biol. Chem.* 244:6056–6063 (1969).
105. Cohen, S.H., S.G. Chang, S.S. Markowitz and T. Novakov. "Role of Fly Ash in Catalytic Oxidation of S(IV) Slurries," *Environ. Sci. Technol.* 15:1498–1502 (1981).
106. Kok, G.L. "Measurements of Hydrogen Peroxide in Rainwater," *Atmos. Environ.* 14:653–656 (1980).
107. Kok, G.L. "Measurements of Hydrogen Peroxide in Rainwater," *EOS Trans. Am. Geophys. Union* 45:884 (1981).

Chapter 5

Catalytic Autoxidation of Chemical Contaminants by Hybrid Complexes of Cobalt(II) Phthalocyanine

Andrew Hong, Scott Boyce, Michael Hoffmann

Environ. Sci. Tech. 1987, submitted.

ABSTRACT

Cobalt(II)-4,4',4'',4'''-tetraminophthalocyanine ($Co^{II}TAP$) and cobalt(II)-4,4',4'',4'''-tetrasulfophthalocyanine ($Co^{II}TSP$) were linked to the surfaces of a chemically modified silica gel support and a macroporous cross-linked styrene/divinylbenzene copolymer. These hybrid organometallic complexes have been shown to be effective catalysts for the aqueous-phase autoxidation of hydrazine, hydrogen sulfide, sulfur dioxide, and thiols under neutral and alkaline conditions. The hybrid catalysts exhibited longer catalytic lifetimes than their homogeneous analogs for the autoxidation of reductants. However, the attachment of the reactive complexes to solid supports resulted in reduced catalytic activity. This was attributed to diffusion limitations within internal pores. The relative efficiency of the various catalysts, which are linked to the surface either through direct complexation of the metal center or through covalent bonding of a peripheral group on the macrocyclic ligand, follows a trend that reflects the relative capacity of the hybrid complexes to activate molecular oxygen; this ability depends on the nature of the complexing ligand located trans to dioxygen. Heterogeneous transition-metal catalysis may offer a potential method for tertiary pollution control.

INTRODUCTION

Metal-catalyzed autoxidation may provide an efficient and economical method for pollution control. Autoxidation in this context is defined as the oxidation of a reductant by molecular oxygen (1). In general, reactions of the triplet ground electronic state of O_2 with singlet spin-state reductants proceed very slowly because they involve changes in spin multiplicity and a considerable degree of bond alteration or deformation in the formation of products. The oxidation of many inorganic and organic substrates by oxygen is often accelerated dramatically in the presence of multivalent first-row transition-metal cations, M^{n+}, such as Mn^{2+}, Fe^{2+}/Fe^{3+}, Co^{2+}/Co^{3+}, Ni^{2+}, and Cu^{2+}(1,2). Catalysis usually results from a rapid initial reaction between M^{n+} and the reductant and/or oxidant (e.g., complexation or redox transformation), which functions to overcome spin-state symmetry restrictions.

In commercial systems, M^{n+} is frequently complexed by organic ligands. One type of metal-organic complex that has been the subject of extensive research is the metal-phthalocyanine {M(PC)} series. Phthalocyanines are aromatic tetrapyrrole compounds that readily form square planar chelates in which the metal center is coordinated to the four pyrrole nitrogen-atoms of the macrocyclic structure as depicted in Figure 1. Various M(PC) derivatives have been shown to be effective homogeneous catalysts for the autoxidation of aldehydes (3-5), aromatic hydrocarbons (6), ascorbic acid (7), hydrazine (8), hydroxylamine (9), hydrogen sulfide (10), mercaptans (11,12), phenols (13), and sulfur

dioxide (14) in organic solvents and in water. Catalytic activity of different metal phthalocyanines generally follows a trend ($Co^{II} > Fe^{II} > Mn^{II} > Cu^{II} \simeq Ni^{II}$) that reflects the relative capacity of each complex to bind molecular oxygen reversibly (15). Complexation of dioxygen lowers the activation energy for the direct reaction of O_2 with the substrate. In this context, the reactivity of cobalt(II)-4,4',4'',4'''-tetrasulfophthalocyanine ($Co^{II}TSP$) in aqueous solution has been compared to the catalytic properties of heme-containing oxidase and catalase enzymes (3,8,16,17).

A major disadvantage associated with the application of homogeneous catalysis for either commercial syntheses or pollution control involves the problem of separating the catalyst and products following termination of the reaction. This drawback may be overcome through attachment of the reactive transition-metal complex to the surface of an inert solid. In this case, a hybrid/heterogeneous complex is substituted for the soluble metal-organic chelate complex, thereby facilitating recovery of the catalytic species. Maas and co-workers (18) and Schutten et al. (19) reported that the rate of the aqueous-phase conversion of thiosalts to disulfides was enhanced upon addition of substituted-Co^{II}(PC) complexes bound to polyacrylamide, polyvinylamine, and a cross-linked styrene/divinylbenzene copolymer. The catalytic autoxidation of SO_2 in flue gas and reduced sulfur compounds in Klaus plant effluents represents two potential applications of this methodology.

The current paper describes the syntheses of two cobalt(II)-phthalocyanines and their hybrid analogs that are obtained upon

attachment of the macrocyclic complexes to the surface of a chemically modified silica gel support and an amino-substituted polystyrene/divinylbenzene copolymer. These compounds, because of their well-defined geometry and chemical behavior, were utilized as active homogeneous and heterogeneous catalysts for the autoxidation of sulfur dioxide, hydrogen sulfide, cysteine, 2-mercaptoethanol, and hydrazine in aqueous media. Kinetic measurements and mechanistic interpretations are presented. Particular emphasis is directed toward an evaluation of catalytic activity and the development of a complex model that results from mass-transport limited kinetics.

Experimental

All chemicals used for substrates, buffer solutions, and synthetic precursors were of reagent grade. Sodium phosphate, borate, perchlorate, hydroxide salts were employed to maintain pH and a constant ionic strength (μ) of 0.4 M in all experiments. The water used in all procedures was de-ionized water (18 MΩ-cm resistivity) obtained from a Milli RO-4/Milli Q purification system (Millipore). The water was deoxygenated by purging with N_2 prior to the preparation of substrate stock solutions

The progress of each reaction was followed by continuous measurement of changes in O_2 concentration as a function of time. Dissolved oxygen was determined using an Orion Model 951 digital printer system. The pH of the reaction mixture was monitored simultaneously with an Orion Model 91-62 combination pH electrode. The O_2 and pH

electrodes were interfaced to the Ionanalyzer through an Orion Model 605 Electrode Switch.

The reactions were conducted in a water-jacketed, glass and Teflon batch reactor with a total volume of 2.0 L. The design and operation of the batch reactor system have been described previously by Hoffmann and Lim (10) and Boyce et al. (14). A constant temperature of 25 ± 0.1°C was maintained during the course of the reaction using a Haake Model FK-2 water circulation system and temperature controller.

To initiate a reaction, the prescribed volume of a substrate stock solution was added to the buffer/catalyst mixture, which was oxygenated to a desired concentration by prior purging of an O_2/N_2 gas mixture. EDTA was used to reduce the catalytic effect of homogeneous trace-metal contaminants (20). Mannitol and sodium cyanide were utilized selectively as free-radical scavengers and complexation inhibitors.

During the course of desorption experiments to evaluate the diffusivity of SO_3^{2-} in the support pores, bulk SO_3^{2-} concentrations were followed by periodically withdrawing aliquots and removing the solids by filtration; the resulting solution was measured for SO_3^{2-} spectrophotometrically.

Results and Discussion

Synthesis of Cobalt(II)-Phthalocyanine Complexes

The tetrasodium salt of Cobalt(II)-4,4',4'',4'''-tetrasulfophthalocyanine ($Co^{II}TSP$) was synthesized from sodium 4-sulfophthalate according to the method of

Weber and Busch (21). Cobalt(II)-4,4',4'',4'''-tetraminophthalocyanine ($Co^{II}TAP$) was prepared according to the following modified procedure. A mixture of sodium 4-aminophthalate (19 mmoles) (ICN Pharmaceuticals), ammonium chloride (12 mmoles), ammonium molybdate (6.6 mmoles), urea (0.13 moles), and cobalt(II) sulfate-7-hydrate (6.6 mmoles) was ground until homogeneous and the mixture heated under reflux at 170°C in nitrobenzene (20 ml) for 6 hours. The crude product was washed with methanol and then heated to boiling in 0.5 N HCl (400 ml). After filtration, the solid was dissolved in hot (70°C) dimethylsulfoxide (DMSO) (250 ml) to remove insoluble impurities. The product precipitated upon addition of H_2O (500 ml) and was collected by centrifugation. Further purification involved repetitive washings with boiling H_2O and centrifugation. Following initial treatment with absolute ethanol, pure $Co^{II}TAP$ was obtained by heating the solid in ethanol under reflux for 5 hours. The structure of each complex was verified by elemental analysis and through a comparison of UV/VIS and ^1H NMR spectra with published reference data (21,22).

Analyses

Microanalyses were performed by Galbraith Laboratories (Knoxville, TN). Absorption spectra were measured on a Hewlett-Packard Model 8450A UV/VIS spectrophotometer. ^1H nuclear magnetic resonance data were recorded using a Varian Model EM390 NMR spectrometer.

Preparation of the Modified Silica Gel Catalyst Support

The synthesis of the catalyst support involved treatment of silica gel with an appropriate silylation reagent as illustrated in Figure 2 (23,24). In the preparation of 1, a suspension of silica gel (22 g) (Fisher, specific area = 330 m^2/g) and 3-chloropropyltrimethoxysilane (7.5 g) (Aldrich, redistilled) in xylene (150 ml) was heated under reflux for 8 hours. Addition of imidazole (3.9 g) enabled the formation of 2. After filtration, each modified gel was washed thoroughly with acetone and dried under vacuum. Gel 2 contained 1.7×10^{-3} moles N/g as determined by elemental analysis.

Attachment of $Co^{II}TAP$ and $Co^{II}TSP$ to the Modified Silica Gel Supports

Two methods were utilized to anchor the Co^{II}-phthalocyanine complexes to the modified silica gels (Figure 3).

Scheme 1: Attachment was achieved through covalent bonding of the surface ligand to the amino group of $Co^{II}TAP$. A stirred mixture of the modified silica gel 1 (10 g) and $Co^{II}TAP$ (6.7 g) in DMSO (30 ml) was heated at $80^{o}C$ for 4 hours. The hybrid cobalt-phthalocyanine complex 3 was isolated by filtration and washed successively with warm DMSO and 0.1 N NaOH in order to remove excess $Co^{II}TAP$ and hydrochloride. Further purification of the reaction product was accomplished through the extraction of impurities with H_2O using a Soxhlet apparatus. The solid was dried in an oven at $100^{o}C$. The hybrid $Co^{II}TAP$ catalyst 3 contained 2.7×10^{-5} moles of Co/gram as determined by elemental analysis. It can be calculated that there are 150 $Co^{II}TAP$ molecules per μm^2, or that

0.06 % of the support's surface is covered with the complex, assuming an area of 400 $\mathring{A}^2$ for the complex.

Scheme 2: Attachment involved direct coordination of the surface imidazole functionality to the metal center of each phthalocyanine complex. A column of 2.5 cm in diameter was packed with the imidazole substituted silica gel 2. An aqueous solution of $Co^{II}TSP$ (7.8×10^{-5} M) was introduced onto the column and eluted dropwise. Dimethylsulfoxide was utilized as a solvent for $Co^{II}TAP$. The hybrid reaction products, 4 and 5, were washed several times with DMSO and H_2O, respectively, followed by an acetone wash, and then collected by filtration. Analysis of the eluents by UV/VIS spectrophotometry yielded cobalt concentration of 1.1×10^{-6} moles Co/g for both catalysts 4 and 5, respectively. It can be calculated that in each hybrid catalyst there are 6 molecules of the complex per μm^2, or that 0.0024 % of the support's surface is covered with the complex.

Attachment of $Co^{II}TSP$ to Polystyrene/Divinylbenzene

$Co^{II}TSP$ was also coupled to a macroporous, amino-substituted polystyrene/divinylbenzene matrix. The organometallic complex was linked to the polymer surface through direct complexation of the NH_2-functionality to the metal center.

The preparation of 6 involved the addition of Amberlite IRA-93 resin (10 g) (Rohm and Haas, specific area = 35 m^2/g) to 500 ml of an aqueous $Co^{II}TSP$ solution (2.5×10^{-5} M). The reaction mixture was agitated continuously for 1 hour at room temperature. Stirring was accomplished using a rotary evaporator in order to prevent mechanical

damage to the particle structure. The product was isolated by filtration and the solid was washed several times with de-ionized water. Spectrophotometric analysis of the filtrate showed an effective cobalt concentration of 4.8×10^{-5} moles Co/g in the hybrid catalyst. It can be calculated that 9 % of the resin's surface is covered with the complex.

Theoretical Considerations

In heterogeneous systems where reactions take place in the presence of catalyst molecules attached to the wall of porous support, the observed reaction kinetics are often influenced by mass transfer processes such as the diffusion of substrates through pores. In this section, we will formulate a heterogeneous kinetic model that will account for both the reactions and diffusion processes. A method for obtaining individual rate constants in various reaction steps will also be outlined.

As depicted in Figure 4, the physicochemical mechanism of the autoxidation reaction, using sulfite oxidation as an example, in a heterogeneous system can be considered to involve the following processes:

1. Transport of reactants, O_2 and SO_3^{2-}, from bulk solution to the solid particle surface.
2. Transport of reactants into active catalyst centers, i.e., CoTSP sites, through pores of the solid.
3. Chemical reactions at the catalytic centers.

4. Transport of product, SO_4^{2-}, back to surface through pores.

5. Transport of product away from the surface to the bulk solution. Consequently, the heterogeneous autoxidation leads to an overall process in which chemical reactions are coupled with the physical diffusion. Because of the complex nature of the entire process, it is desirable first to investigate the kinetics of the homogeneous reaction and thereby obtain the basis for further heterogeneous modelling; perturbation of kinetics due to diffusion can be included and verified experimentally.

The homogeneous catalytic autoxidation of S^{IV} in aqueous solution has been studied in detail and found to proceed according to the following stoichiometry;

$$2\ S^{IV} + O_2 \longrightarrow 2\ S^{VI} \qquad (1)$$

where $[S^{IV}] = [SO_2 \bullet H_2O] + [HSO_3^-] + [SO_3^{2-}]$ and $[S^{VI}] = [H_2SO_4] + [HSO_4^-] + [SO_4^{2-}]$. Boyce et al. (14) have proposed an ordered-ternary complex pathway for the oxidation of S^{IV} as follows:

$$(Co^{II}TSP_2^{4-}) \overset{k_d}{\rightleftharpoons} 2Co^{II}TSP^{2-} \qquad (2)$$

$$Co^{II}TSP^{2-} + SO_3^{2-} \overset{K_1}{\rightleftharpoons} (SO_3)Co^{II}TSP^{4-} \qquad (3)$$

$$(SO_3)Co^{II}TSP^{4-} + O_2 \underset{k_{-2}}{\overset{k_2}{\rightleftharpoons}} (SO_3)Co^{III}TSP(O_2^{\cdot-})^{4-} \qquad (4)$$

$$(SO_3)Co^{III}TSP(O_2^{\cdot-})^{4-} + SO_3^{2-} \underset{k_{-3}}{\overset{k_3}{\rightleftharpoons}} (SO_3)Co^{III}TSP(O_2^{\cdot-})(SO_3)^{6-} \quad (5)$$

$$(SO_3)Co^{III}TSP(O_2^{\cdot-})(SO_3)^{6-} + H_2O \xrightarrow[\text{slow}]{k_4} (SO_3)Co^{II}TSP(O_2^{2-})^{6-} + SO_4^{2-} + 2H^+ \quad (6)$$

$$(SO_3)Co^{II}TSP(O_2^{2-})^{6-} + 2H^+ \xrightarrow[\text{rapid}]{k_5} (SO_3)Co^{II}TSP^{4-} + H_2O_2 \quad (7)$$

$$H_2O_2 + SO_3^{2-} \xrightarrow[\text{rapid}]{k_6} SO_4^{2-} + H_2O \quad (8)$$

Assuming k_4 to be rate determining in this mechanism, a resulting rate expression has been shown to be as follows:

$$v = \frac{d[SO_4^{2-}]}{dt} = \frac{k'[(SO_3)Co^{II}TSP]_{total}\,[O_2][SO_3^{2-}]}{K_A + K_B[O_2] + K_C[SO_3^{2-}] + [O_2][SO_3^{2-}]} \quad (9)$$

where $k' = \dfrac{k_4k_5}{k_4+k_5}$

$$K_A = \frac{k_5(k_{-2}k_{-3}+k_{-2}k_4)}{k_2k_3(k_4+k_5)}$$

$$K_B = \frac{k_5(k_{-3}+k_4)}{k_3(k_4+k_5)}$$

$$K_C = \frac{k_4k_5}{k_2(k_4+k_5)}$$

The rate expression (Eq. 9), which can be modified to account for the initial dimer dissociation and SO_3^{2-} complexation steps (i.e., rxns 2 & 3), has been shown to be in close agreement with kinetic data under various conditions (14). The homogeneous mechanism for the oxidation of sulfite in which the reaction proceeds via a 2-electron transfer from sulfite to a preformed octahedral cobalt(III)-sulfito-superoxide complex (rxns 5 & 6) has further been verified by spectroscopic and ESR studies (25).

A mechanism, which is based on the the homogeneous case, for the heterogeneous systems is proposed as shown in Figure 5. The CoTSP complex in this hybrid catalyst is bound to the solid surface by the coordination of a surface functional group with the metal center through one of its apical coordination sites, e.g., catalysts 4, 5, and 6. Hence, assuming that k_4 remains rate-determining, the rate expression for the heterogeneous autoxidation can be written as:

$$v = \frac{k'[(solid)Co^{II}TSP]_{total}\ [O_2][SO_3^{2-}]}{K_A + K_B[O_2] + K_C[SO_3^{2-}] + [O_2][SO_3^{2-}]} \qquad (9')$$

To incorporate the effect of the physical diffusion, Fick's law is used to describe the transport of chemical species through pores;

$$N_j = -D_{e,j}\ \frac{dC_j}{dr} \qquad (10)$$

where N_j denotes the molar flux of species j per unit area, C_j the molar

concentration of species j, and $D_{e,j}$ the effective diffusivity of species j. Numerous factors such as the bulk diffusivity of the species, pore diameter, tortuosity and porosity of the solid particle, and electrostatic interaction between charged surface and ionic species can influence diffusion kinetics. These factors are lumped together as an effective diffusivity, D_e.

Considering the reaction in the pores to be isothermal (calculated ΔH° for S^{IV} to S^{VI} under the observed rate does not cause any significant perturbation in temperature), we can write the continuity equations in spherical geometry for O_2 and SO_3^{2-} as:

$$D_{e,O_2}\left[\frac{\partial^2[O_2]}{\partial r^2} + \frac{2}{r}\frac{\partial[O_2]}{\partial r}\right] + R_{O_2} = \epsilon_p \frac{\partial[O_2]}{\partial t} \qquad (11)$$

where the boundary conditions are:

$$[O_2] = [O_2]_{bulk} \qquad \text{at } r = a$$

$$\frac{\partial[O_2]}{\partial r} = 0 \qquad \text{at } r = 0$$

and the initial condition is:

$$[O_2] = [O_2]_{o,bulk} \qquad \text{at } t = 0$$

$[O_2]$ denotes the concentration of O_2 in pore, R_{O_2} the formation rate of O_2. ϵ_p and a are the porosity and the radius of the solid,

respectively. The first boundary condition implies that the external diffusional resistance is eliminated by stirring, and the second boundary condition arises from symmetry of the particle. The initial condition corresponds to a well-oxygenated medium effected by purging with an O_2/N_2 mixture. Similarly, a mass balance is written for SO_3^{2-} as:

$$D_{e,SO_3^{2-}}\left[\frac{\partial^2[SO_3^{2-}]}{\partial r^2} + \frac{2}{r}\frac{\partial[SO_3^{2-}]}{\partial r}\right] + R_{SO_3^{2-}} = \epsilon_p \frac{\partial[SO_3^{2-}]}{\partial t} \qquad (12)$$

where the boundary conditions are:

$$[SO_3^{2-}] = [SO_3^{2-}]_{bulk} \qquad \text{at } r = a$$

$$\frac{\partial[SO_3^{2-}]}{\partial r} = 0 \qquad \text{at } r = 0$$

and the initial condition are:

$$[SO_3^{2-}] = 0 \qquad \text{at } t = 0,\ r < a$$

$$[SO_3^{2-}] = [SO_3^{2-}]_{o,bulk} \qquad \text{at } t = 0,\ r = a$$

The same boundary conditions apply as in Equation (11). The initial conditions correspond to the start of reaction by the addition of the substrate SO_3^{2-} to the oxygenated suspension. The result of this analysis yields two coupled partial differential equations, which

describe the concentration profiles of reactants and can be solved simultaneously by numerical methods.

The solution method can be greatly simplified by assuming a steady-state condition. The steady-state approximation is warranted because continuous flow reactors (where the hybrid catalysts are expected to find practical applications) are normally operated over prolonged periods; hence, a steady state can be reached. Under the steady-state assumption, the species continuity equation becomes:

$$D_j\left[\frac{\partial^2 C_j}{\partial r^2} + \frac{2}{r}\frac{\partial C_j}{\partial r}\right] + R_j = 0 \qquad (13)$$

Measurement of Effective Diffusivity D_e

In order to justify the simplification, i.e., the steady-state assumption, and to interpret the kinetic data in the appropriate time domain, the time required to reach steady state needs to be determined. This requires the measurement of D_e. The effective diffusivity, D_e, for SO_3^{2-} in pores of untreated IRA-93 polymer bead was measured. This experiment was performed by allowing the void volume of the particles to equilibrate with a 0.2 M SO_3^{2-} solution; the particles, the pores of which were filled with the SO_3^{2-} solution, were recovered by filtration and subsequently added into fresh water. The desorption of SO_3^{2-} from pores to bulk solution was monitored and the resulting concentration vs. time profile was used to evaluate for D_e. The mass balance equations for the desorption experiment can be written as:

$$\epsilon_p \frac{\partial C_r}{\partial t} = D_e \left[\frac{\partial^2 C_r}{\partial r^2} + \frac{2}{r} \frac{\partial C_r}{\partial r} \right] \qquad (14)$$

$$V \frac{dC}{dt} = - D_e A \left[\frac{\partial C_r}{\partial r} \right]_{r = a} \qquad (15)$$

at t=0: $C_r = C_o$ for $0 \leq r \leq a$

$C = 0$

$t > 0$: $\frac{\partial C_r}{\partial r} = 0$ at $r = 0$

$C = C_r$ at $r = a$

where C = conc. of SO_3^{2-} in bulk solution

C_r = conc. of SO_3^{2-} in pore

C_o = initial conc. of SO_3^{2-} in pore = 0.2 M

V = volume of bulk solution

A = total external surface area of the particles

ϵ_p = porosity of the particle

The solution to these equations has been given by Crank (26), and adapted by Komiyama et al. (27) in solving a similar mass transport problem as follows:

$$\frac{M_t}{M_\infty} = 1 - \sum_n \frac{6\varphi(\varphi+1)\exp[-(D_a t/a^2)\lambda_n^2]}{9 + 9\varphi + \lambda_n^2 \varphi^2} \qquad (16)$$

where M_t, M_∞ = amount of SO_3^{2-} in bulk solution at time t, and at very long time, respectively

$$\varphi = \frac{\epsilon_p V}{v}$$

v = total volume of the particles

$$D_a = D_e \frac{v}{V} \frac{C_o - C_\infty}{C_\infty}$$

λ_n are the non-zero roots of $\tan \lambda_n = \frac{3\lambda_n}{3+\varphi\lambda_n^2}$

The result of the desorption experiment plotted in $\frac{M_t}{M_\infty}$ vs. $t^{1/2}/a$ (for one batch of particles with $0.589 \leq a \leq 0.701$ mm) is shown in Figure 6. Using $\langle a \rangle$ = 0.032 cm, the apparent diffusivity D_a is found to be 5.5×10^{-6} cm^2/s, and hence D_e is determined to be 2.6×10^{-6} cm^2/s. It can be calculated from Figure 6 that 0.75 min will be required to reach 95% of steady state (i.e., $\frac{M_t}{M_\infty} = 0.95$). It should be noted that the untreated polymer bead did not catalyze the oxidation of S(IV). In a case where diffusion of a species is coupled with its depletion reaction, the steady state is expected to be reached sooner; therefore, 0.75 min represents an upper limit of the time required to reach such a state; i.e., the steady-state assumption (Eq. 13) is valid within the first min of reaction. D_e for a different batch of IRA-93 particles with $0.70 \leq a \leq 0.83$ mm was found to be 2.5×10^{-6} cm^2/s (D_e is independent of particle size as expected).

Development of the Effectiveness Factor, η

With the effective diffusivity measured and the steady-state approximation justified, Eq. 13 can be used to derive an effectiveness factor, η. In accordance with pseudo-order experimental conditions established in actual experiments, we consider the case $[O_2] >> [SO_3^{2-}]_o$ for which Eq. 9' can be written as:

$$R_{SO_3^{2-}} = - \frac{K_E[SO_3^{2-}]}{K_F + K_G[SO_3^{2-}]} \tag{17}$$

where $K_E = k'[(solid)Co^{II}TSP]_{total}[O_2]$

$$K_F = K_A + K_B[O_2]$$

$$K_G = K_C + [O_2]$$

K_E, K_F, and K_G are constants if one assumes that a small neutral molecule such as O_2 diffuses through the porous material faster the SO_3^{2-}. The continuity equation for SO_3^{2-} is now written as:

$$D_e\left[\frac{\partial^2 C_r}{\partial r^2} + \frac{2}{r}\frac{\partial C_r}{\partial r}\right] = \frac{K_E C_r}{K_F + K_G C_r} \tag{18}$$

$$C_r = C \quad \text{at } r = a$$

$$\frac{\partial C_r}{\partial r} = 0 \quad \text{at } r = 0$$

where $C_r = [SO_3^{2-}]_{pore}$ and $C = [SO_3^{2-}]_{bulk}$. It should be noted that the first boundary condition is valid if one neglects the film resistance around the particles. An effectiveness factor, η, can be defined as the ratio of the observed rate to the rate taking place under external surface conditions:

$$\eta = \frac{\text{reaction rate with pore diffusion resistance}}{\text{reaction rate with surface condition}}$$

$$= \frac{\int r(C_r)dV_p}{V_p r(C)} \qquad (19)$$

where V_p = volume of particles. In general, the effectiveness factor can be derived by first solving the continuity equation (Eq. 18) to obtain a concentration profile of reactants in the particle; this profile is then used in the rate expression (Eq. 17), and the latter integrated over the particle volume to yield the actual rate of reaction. The actual rate can be used in Eq. 19 to evaluate η. The value of η is useful as an indicator of the extent of the diffusion limitation and for expressing the observed actual rate in terms of measurable bulk concentrations (as will be shown later).

η for a first-order reaction (r = kC) in a slab geometry of width 2L is found to be:(28)

$$\eta = \frac{\tanh \varphi}{\varphi} \qquad (20)$$

where φ = Thiele modulus = $L(k/D_e)^{1/2}$. The simple form of η can be

extended to arbitrary pellet geometries by modifying the Thiele modulus (29) as:

$$\varphi = \frac{V_p}{S_x} (k/D_e)^{1/2}$$

$$\text{e.g. } \varphi = (k/D_e)^{1/2} a/3 \text{ for a sphere} \qquad (21)$$

where S_x = external surface area of pellet. The φ can be further modified such that η given in Eq. 20 can be used to describe a general rate expression and arbitrary pellet geometry as follows:(28)

$$\varphi = \frac{V_p r(C)}{S_x (2D_e)^{1/2}} \left[\int_0^C r(C_r') dC_r' \right]^{-1/2} \qquad (22)$$

In our proposed model for the heterogeneous autoxidation of SO_2 in a spherical catalyst particle with the rate expression given by Eq. 17, the Thiele modulus can be shown to be:

$$\varphi = \frac{a K_E^{1/2} C}{3(2D_e)^{1/2}(K_F + K_G C)} \left[\frac{C}{K_G} - \frac{K_F}{K_G^2} \ln\left[\frac{K_G C}{K_F} + 1 \right] \right]^{-1/2} \qquad (23)$$

Since η is readily determined, once φ is evaluated, one may express the actual rate of reaction by:

$$r_{actual} = \eta r(C) = \frac{\tanh \varphi}{\varphi} \frac{K_E C}{K_F + K_G C} \qquad (24)$$

Eq. 24 can be used to compare with experimental observations. In order to do this, however, values of K_E, K_F, and K_G are needed. To obtain intrinsic rate constants, the hybrid catalyst can be prepared with metal complex loading far below saturation. In such cases, the active catalytic centers are distributed primarily on the outer surface of the particle such that pore diffusion may be neglected. Laidler et al. (30) have treated the case of a supported enzyme, in which the enzyme is very inactive or in low concentration, as in free solution. In light of this assumption, the rate expression of S(IV) oxidation (Eq. 9') can be rearranged as:

$$\frac{[(\text{solid})Co^{II}TSP]_{total}}{v} = \frac{K_A}{k'}\frac{1}{[O_2][SO_3^{2-}]} + \frac{K_B}{k'}\frac{1}{[SO_3^{2-}]} + \frac{K_C}{k'}\frac{1}{[O_2]} + \frac{1}{k'} \tag{25}$$

$$= \left(\frac{1}{k'} + \frac{K_B}{k'}\frac{1}{[SO_3^{2-}]}\right) + \left(\frac{K_A}{k'}\frac{1}{[SO_3^{2-}]} + \frac{K_C}{k'}\right)\frac{1}{[O_2]} \tag{26}$$

$$\text{or} \quad = \left(\frac{1}{k'} + \frac{K_C}{k'}\frac{1}{[O_2]}\right) + \left(\frac{K_B}{k'} + \frac{K_A}{k'[O_2]}\right)\frac{1}{[SO_3^{2-}]} \tag{27}$$

Two series of experiments can be done under the conditions $[SO_3^{2-}] >> [O_2]_o$, and $[O_2] >> [SO_3^{2-}]_o$, respectively; initial reaction rates can be obtained for various $[O_2]_o$ and $[SO_3^{2-}]_o$. For example, in the case of $[SO_3^{2-}] >> [O_2]_o$, a double reciprocal plot of $[(\text{solid})Co^{II}TSP]_{total}/v_o$ vs. $1/[O_2]_o$ gives the slope and intercept that are related to the lumped rate constants of individual steps in the catalytic cycle, as given by

Eq. 26. Similar analysis can be done for $[O_2] >> [SO_3^{2-}]_o$ and more kinetic information extracted with the aid of Eq. 27. The 4 constants k', K_A, K_B, and K_C can be calculated from the 2 slopes and 2 intercepts in Eqs. 26 and 27; hence, K_E, K_F, and K_G are determined.

To obtain some estimates for the rate parameters k', K_A, K_B, and K_C, one can do the following analysis. By assuming k_4 to be significantly smaller than the other rate constants, k', K_A, K_B, and K_C can be simplified as follows:

$$k' = \frac{k_4 k_5}{k_4 + K_5} = k_4 \tag{28}$$

$$K_A = \frac{k_5(k_{-2}k_{-3} + k_{-2}k_4)}{k_2 k_3(k_4 + k_5)} = \frac{k_{-2}k_{-3}}{k_2 k_3} \tag{29}$$

$$K_B = \frac{k_5(k_{-3} + k_4)}{k_3(k_4 + k_5)} = \frac{k_{-3}}{k_3} \tag{30}$$

$$K_C = \frac{k_4 k_5}{k_2(k_4 + k_5)} = \frac{k_4}{k_2} \tag{31}$$

The rate constant of the slowest step k_4 is readily given by the value of k'. Extracting intrinsic rate constants of elementary step via this scheme appears promising.

Kinetics

Typical $[O_2]$ vs. time profiles for initially air-saturated reaction mixtures containing 1 mM S(IV) and 0.17 μM CoTSP solution or an equivalent amount (in CoTSP content) of various suspensions of supported catalyst (3 - 6) at pH 6.7 are shown in Figure 7. Each supported catalyst is observed to be catalytically active toward the oxidation of S(IV). It should be noted that 1 to 10 μM EDTA were used in these and subsequent reaction mixtures to ensure that no significant ($\leq$ 3 % of $[S(IV)]_o$) background oxidation occurs (because of homogeneous trace-metal catalysis) within the first 30 min when initial reaction rates v_o are determined.

The hybrid catalysts, 3 - 6, were further tested for activity in the autoxidation of various organic and inorganic substrates such as hydrogen sulfide, 2-mercaptoethanol, cysteine, and hydrazine by measuring the rate of O_2 consumption (Eqs. 32 - 35);

$$HS^- + 2O_2 \longrightarrow H^+ + SO_4^{2-} \qquad (32)$$

$$2SO_3^{2-} + O_2 \longrightarrow 2SO_4^{2-} \qquad (33)$$

$$2RSH + O_2 \longrightarrow RSSR + H_2O_2 \qquad (34)$$

$$N_2H_4 + O_2 \longrightarrow N_2 + 2H_2O \qquad (35)$$

The results of these experiments are shown in Table I. In general, reactivity of the metal phthalocyanine complex was lower when supported

on a solid substrate. This suggests that reaction taking place at the catalytic centers that are attached to the internal pore surfaces is hindered by the physical diffusion of the substrate through pores.

The higher activity of the hybrid catalyst (6) compared to (5) may be attributed to the natures of the two different supports. The support for (6), IRA-93, has a typical pore dimension of 1000 Å, whereas the support for (5), silica gel, has much smaller pore size. The interaction of charged species such as SO_3^{2-} with the surface hydroxyl group of silica gel is also expected to exert a retention effect. Furthermore, the electronic properties of the complexing ligands (imidazole for 5 or amine for 6) that occupies one of the apical sites of the CoTSP have been shown to alter the catalyst's ability to activate coordinated dioxygen in the opposite apical site (31, 32).

The higher reaction rate of (4) compared to (3) confirms our previous finding (25) that a basic ligand at one of the open apical sites of the metal complex is required to activate the bound dioxygen. The presence of this ligand promotes an electron transfer from the metal center to O_2, resulting in the formation of an active complex $Co^{III}-O_2^{\cdot-}$, which is capable of accepting 2 electrons from a S(IV) molecule.

The catalytic lifetime of the complex is prolonged by its attachment to a solid support. Table II shows the reaction rate during successive runs with SO_3^{2-}. Some deactivation of the hybrid catalyst was observed during the successive runs. However, when compared to the homogeneous complex, the hybrid catalyst was found to retain 88 % of its initial activity after 4 successive kinetic runs in which 4 mM S(IV) was oxidized while the homogeneous complex retained 75 % of its initial

activity after the same number of runs in which only 0.4 mM of S(IV) was oxidized.

Conclusions

We have reported the syntheses of hybrid catalysts in which cobalt phthalocyanines have been supported on solid surfaces. We have considered the physicochemical processes of heterogeneous catalysis, which can influence the kinetics of such a system, and we integrated these elements to build an analytical model. A series of experiments were performed to evaluate the activity of the hybrid catalysts. The results show that the hybrid catalysts are effective in catalyzing the oxidation of a variety of pollutants. The hybrid metal complexes showed lower catalytic activity than their homogeneous analogs; this was attributed to diffusion limitations and ligand effects. Attachment of the active metal complexes to solids of small particle size may reduce the diffusion limitations; selecting appropriate donor ligands may also enhance the activation of molecular O_2 by the metal center and subsequently enhance catalytic activity. Hybrid catalysts can be recovered by coarse filtration. In addition, the hybrid catalysts have been shown to retain their catalytic activity for longer periods of time.

Acknowledgements:

We gratefully acknowledge the financial support of the U.S. Environmental Protection Agency (R811612-01-0). In addition, we want to thank Dr. Donald Carey for his encouragement and support.

Literature Cited

1. Sheldon, R. A.; Kochi, J. K., *Metal-Catalyzed Oxidations of Organic Compounds*, Academic Press: New York, 1981.

2. Hoffmann, M. R. *Environ. Sci. Technol.* **1980**, *14*, 1061-1066.

3. Cook, A. H. *J. Chem. Soc.* **1938**, 1774-1780.

4. Ohkatsu, Y.; Hara, T.; Osa, T. *Bull. Chem. Soc. Jap.* **1977**, 50, 696-700.

5. Ohkatsu, Y.; Sekiguchi, O.; Osa, T. *Bull. Chem. Soc. Jap.* **1977**, 50, 701-705.

6. Hara, T.; Ohkatsu, Y.; Osa, T. *Bull. Chem. Soc. Jap.* **1975**, 48, 85-89.

7. Wagnerova, D. M.; Blanck, J.; Smettan, G.; Veprek-Siska, J. *Collect. Czech. Chem. Commun.* **1978**, 43, 2105-2110.

8. Wagnerova, D. M.; Schwertnerova, E.; Veprek-Siska, J. *Collect. Czech. Chem. Commun.* **1973**, 38, 756-764.

9. Wagnerova, D. M.; Schwertnerova, E.; Veprek-Siska, J. *Collect. Czech. Chem. Commun.* **1974**, 39, 3036-3047.

10. Hoffmann, M. R.; Lim, B. C., *Environ. Sci. Technol.* **1979**, 13, 1406-1414.

11. Dolansky, J.; Wagnerova, D. M.; Veprek-Siska, J. *Collect. Czech. Chem. Commun.* **1976**, 41, 2326-2332.

12. Beelen, T. P. M.; de Costa Gomez, C. O.; Kuijer, M. *Rec. Trav. Chim.* **1979**, 98, 521-522.

13. Tada, M.; Katsu, T. *Bull. Chem. Soc. Jap.* **1972**, 45, 2558-2559.

14. Boyce, S. D.; Hoffmann, M. R.; Hong, A. P.; Moberly, L. M. *Environ. Sci. Technol.* **1983**, *17*, 602-611.

15. Boucher, L. J. *Coordination Chemistry of Macrocyclic Compounds*, Melson, G. A., Ed., Plenum Press, New York, 1979; pp. 461-516.

16. Cook, A. H. *J. Chem. Soc.* **1938**, 1761-1768.

17. Waldmeier, P.; Prijs, B.; Sigel, H., Z. *Naturforsch.* 1972, 27b, 95-100.

18. Maas, T. A. M. M.; Kuijer, M.; Zwart, J. *Chem. Commun.* **1976**, 86-88.

19. Schutten, J. H.; Beelen, T. P. M. *J. Molec. Catal.* **1981**, *10*, 85-97.

20. Huss, A.; Lim, P. K.; Eckert, C. A. *J. Am Chem. Soc.* 1978, 100, 6252-6253.

21. Weber, J. H.; Busch, D. H. *Inorg. Chem.* **1965**, *4*, 469-470.

22. Lever, A. B. P. *Advances in Inorganic Chemistry and Radiochemistry*, Vol. 7; Emeleus, H. J., Sharpe, A. G., Eds.; Academic Press: New York, 1963; pp. 27-114.

23. Leal, O.; Anderson, D. L.; Bowman, R. G.; Basolo, F.; Burwell, R. *J. Am. Chem. Soc.* **1975**, 97, 5125-5129.

24. Allum, K. G.; Hancock, R. D.; Howell, I. V.; McKenzie, S.; Pitkethly, R. C.; Robinson, P. J. *J. Organomet. Chem.* 1975, 87, 203-216.

25. Hoffmann, M. R.; Hong, A. P. *Sci. Total Environ.* **1987**, 64, 99-115.

26. Crank, J. *The Mathematics of Diffusion*; Clarendon Press: Oxford, 1956.

27. Komiyama, H.; Smith, J. A. *I. Ch. E. J.* **1974**, 20, 728-734.

28. Froment, G. F.; Bischoff, K. B. *Chemical Reactor Analysis and Design*; John Wiley & Sons: New York, 1979.

29. Aris, R. *Chem. Eng. Sci.* **1957**, 6, 262.

30. Laidler, K. J.; Bunting, S. J. *The Chemical Kinetics of Enzyme Action*; Clarendon Press: Oxford, England, 1973.

31. Jones, R. D.; Summerville, D. A.; Basolo, F. *Chem. Rev.* **1979**, 79, 139-179.

32. Collmann, J. P.; Halbert, T. R.; Suslick, K. S. *Metal Ion Activation of Dioxygen*; Spiro, T. G., Ed.; John Wiley and Sons: New York, 1980, pp 1-72.

Table I. Summary of Kinetic Results for the Autoxidation of Chemical Contaminants in the Presence of Homogeneous ($Co^{II}TSP$) and Heterogeneous (Hybrid) Cobalt(II)-Phthalocyanine Complexes.[a]

			v_o(M/min) x 10^6			
Substrate	pH	$Co^{II}TSP$	3	4	5	6
Sulfur(IV)	6.7	16.6	20.3	91.6	3.8	4.50
Sulfur(IV)	9.2	19.5	2.50	4.05[b]	0.11	0.89
Sulfide	9.2	14.4	0.41	1.26[b]	0.10	0.79
2-Mercaptoethanol	9.2	10.8	1.00	1.62[b]	0.18	0.44
Cysteine	9.2	3.00	0.18	0.73[b]	0.06	0.11
Hydrazine	12.9	58.7	0.76	3.08[b]	1.48	2.83

[a] $[Substrate]_o$ = 1.0 mM; $[Co^{II}]_o$ = 0.17 μM; $[O_2]_o$ = 0.25 mM, T = 25 ± 0.1°C; μ = 0.4 M

[b] These rates were obtained after normalizing to 0.17 μM assuming a first order dependence of catalyst; catalyst conc. used was 0.042 μM.

Table II. Comparison of the Activity of Hybrid Catalyst 3 with Homogeneous Co(II)TSP After Successive Reactions.[a]

	3[b]	$Co^{II}TSP$[c]
Run #	v_o (M/min) x 10^5	v_o (M/min) x 10^6
1	1.62	4.48
2	1.68	4.46
3	1.60	4.11
4	1.59	3.81
5	1.43	3.36
6	1.33	

[a] The kinetic rate of each run was obtained by measuring the initial O_2 depletion rate, followed by the purging of O_2/N_2 gas mixture until the S(IV) was completely depleted and the O_2 content resumed its original value; after this an addition of the substrate began the subsequent run.

[b] Conditions were: $[S(IV)]_o$ = 1.0 mM; $[Co^{II}]_o$ = 0.17 μM; $[O_2]_o$ = 0.25 mM; pH = 9.2; μ = 0.4 M; T = 25 ± 0.1°C.

[c] Conditions were: $[S(IV)]_o$ = 0.1 mM; $[Co^{II}]_o$ = 1 μM; $[O_2]_o$ = 1 mM; pH = 6.7; μ = 0.4 M; T = 25 ± 0.1°C.

Figure Captions

Figure 1. Molecular structures of cobalt(II)-4,4',4'',4'''-tetraamino-phthalocyanine (Co(II)TAP) and cobalt(II)-4,4',4'',4'''-tetrasulfophthalocyanine (Co(II)TSP).

Figure 2. Schematic diagram for the preparation of modified silica gel support systems 1 and 2 using 3-chloropropyltrimethoxysilane and imidazole as reagents.

Figure 3. Schematic diagram for various modes of attaching Cobalt(II)-phthalocyanine complexes to silica gel supports 1 and 2 and cross-linked polystyrene/divinylbenzene copolymer.

Figure 4. Overview of the physicochemical process for the heterogeneous autoxidation of S(IV).

Figure 5. The heterogeneous autoxidation of sulfite, which is analogous to the homogeneous CoTSP, as catalyzed by the surface bound CoTSP (e.g., 6).

Figure 6. Desorption kinetics of SO_3^{2-} from polymer bead IRA-93 and mathematical fits according to Eq. 16. Conditions were: V = 300 ml, v = 2.3 ml, ϵ_p = 0.48, a = 0.032 cm, [Co] = 0.2 M, pH = 9.6.

Figure 7. Comparison of the catalytic activity of various solid supported cobalt(II)-phthalocyanine complexes toward the autoxidation of sulfite at pH 6.7: [S(IV)] = 1.0 mM, $[O_2]_o$ = 0.25 mM, $[Co]_o$ = 0.17 μM, μ = 0.4 M.

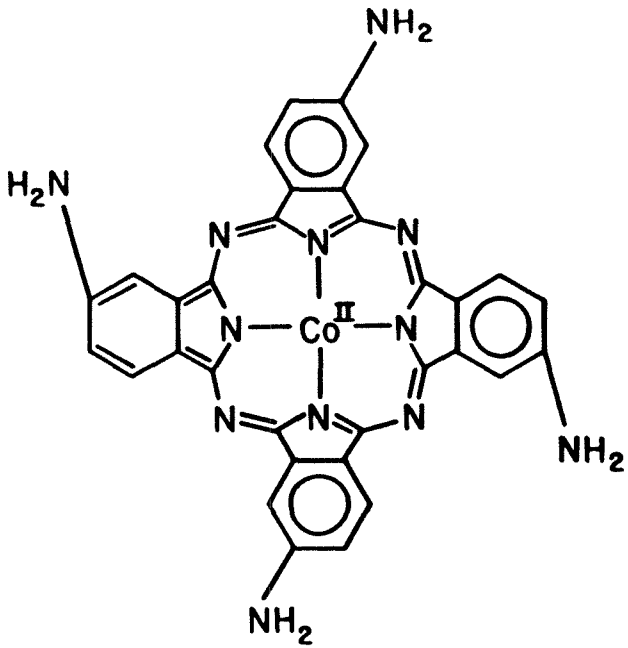

Co^{II}TAP ≡ Co^{II} —4,4′,4″,4‴—
tetraaminophthalocyanine

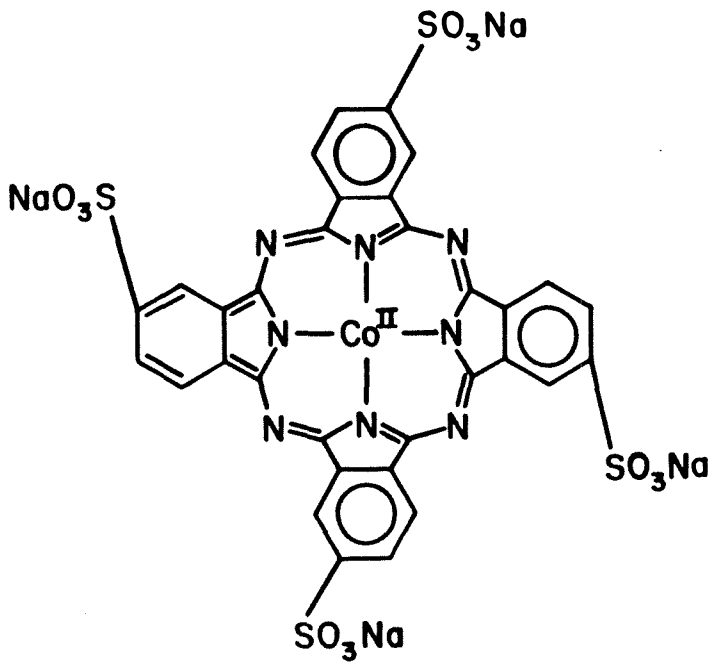

Co^{II}TSP ≡ Co^{II} —4,4′,4″,4‴—
tetrasulfophthalocyanine

Figure 1

PREPARATION OF MODIFIED SILICA GEL SUPPORT

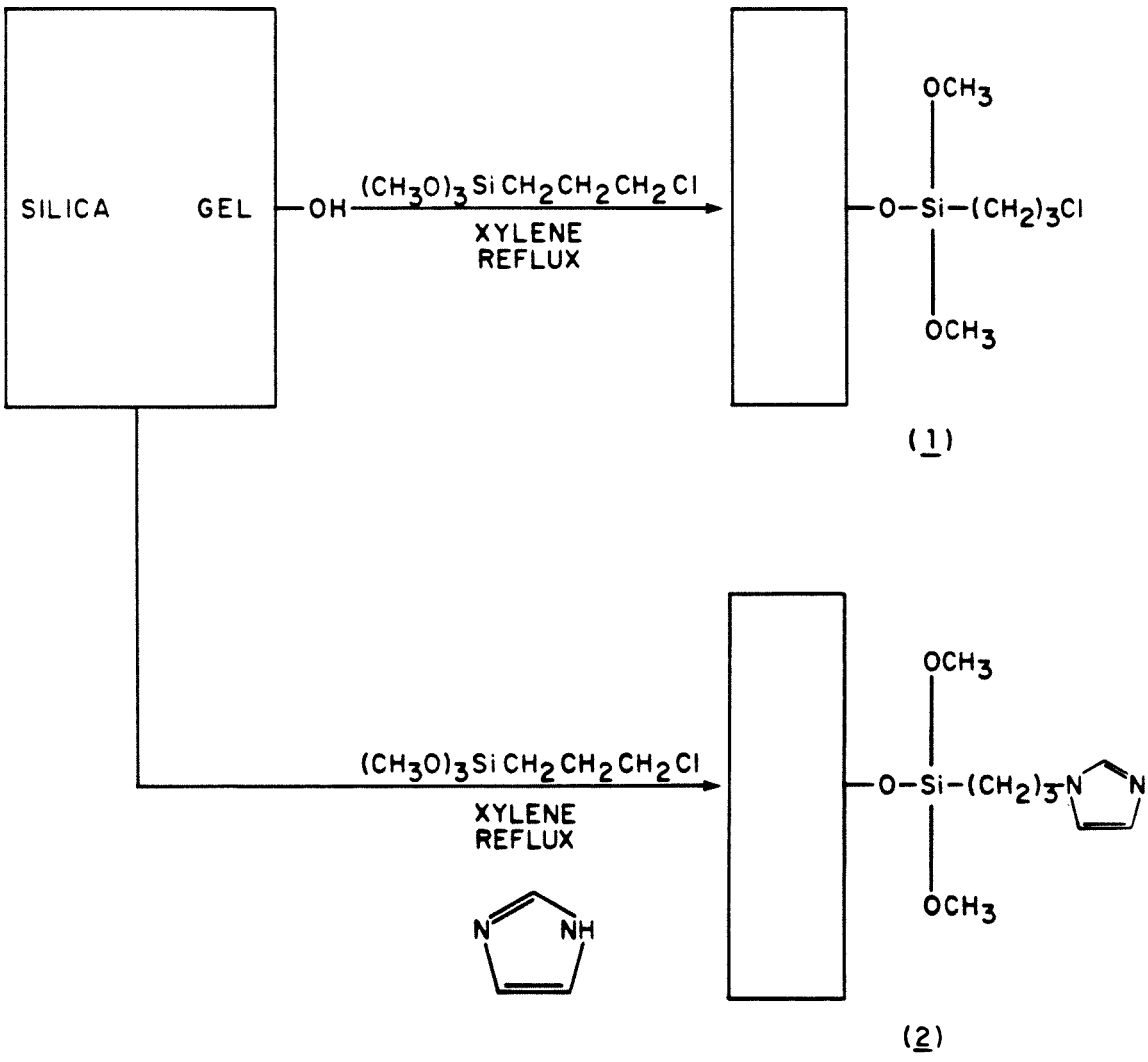

Figure 2

ATTACHMENT OF COBALT(II)-PHTHALOCYANINE COMPLEXES TO SOLID SUPPORTS

SILICA GEL

SCHEME 1:

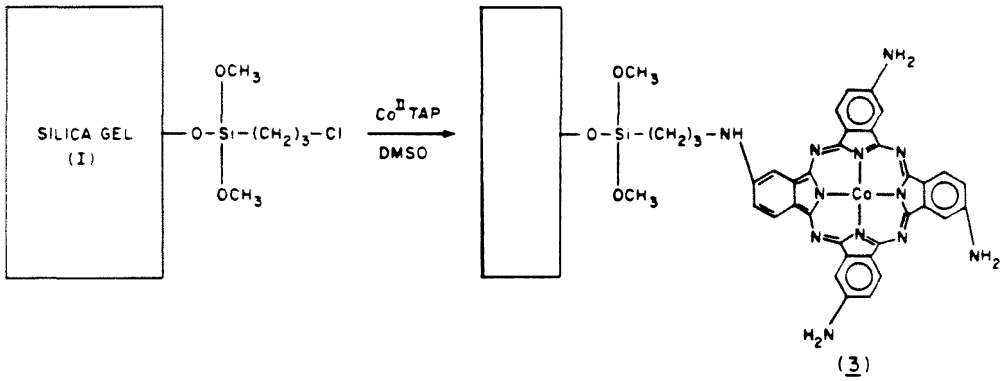

SCHEME 2:

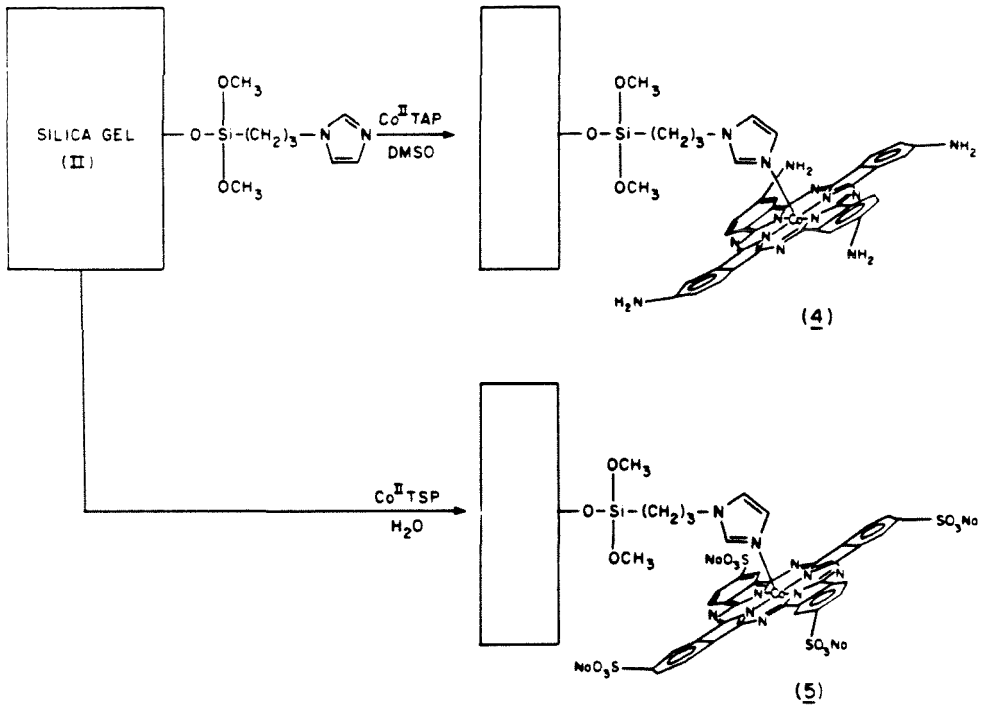

POLYSTYRENE/DIVINYLBENZENE

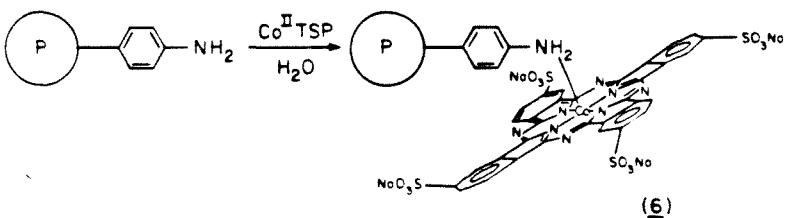

Figure 3

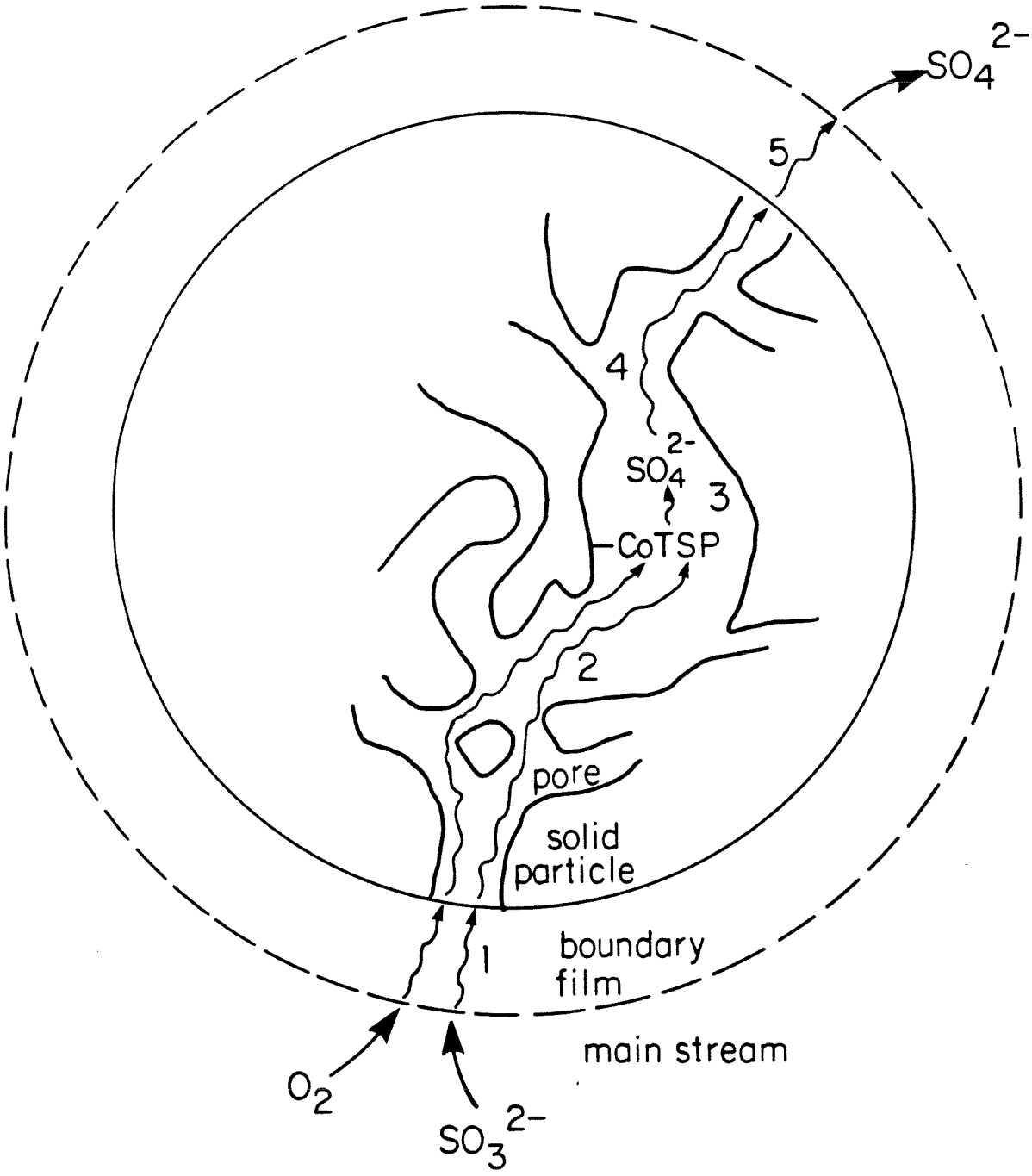
SO_4^{2-}
5
4
SO_4^{2-}
3
CoTSP
2
pore
solid particle
1
boundary film
main stream
O_2
SO_3^{2-}

Figure 4

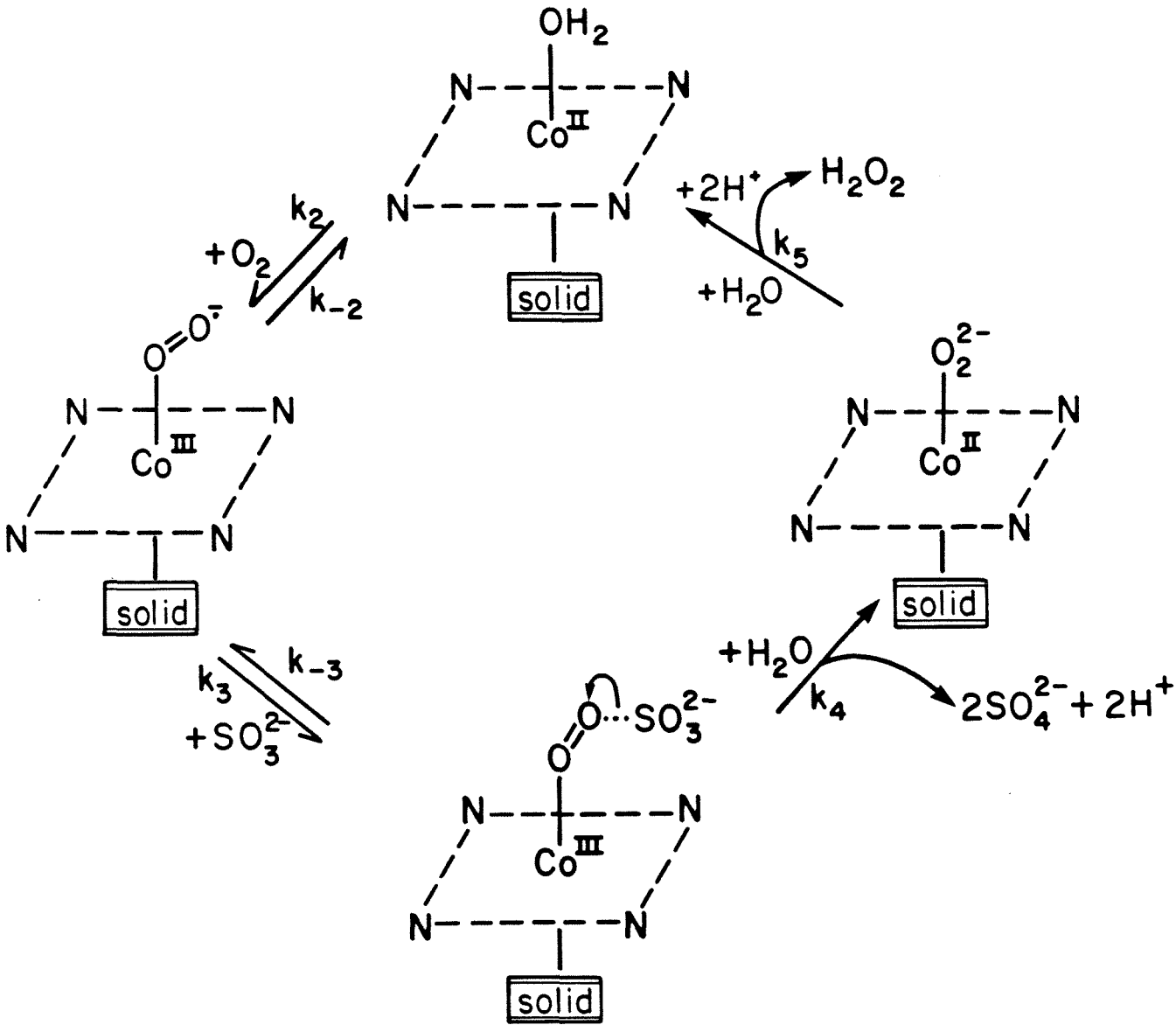
OH2
N
Co II
solid
+2H+
H2O2
k5
+H2O
k2
+O2
k-2
O=O-
Co III
k3
k-3
+SO3 2-
O2 2-
Co II
+H2O
k4
2SO4 2- + 2H+
O...SO3 2-
Co III

Figure 5

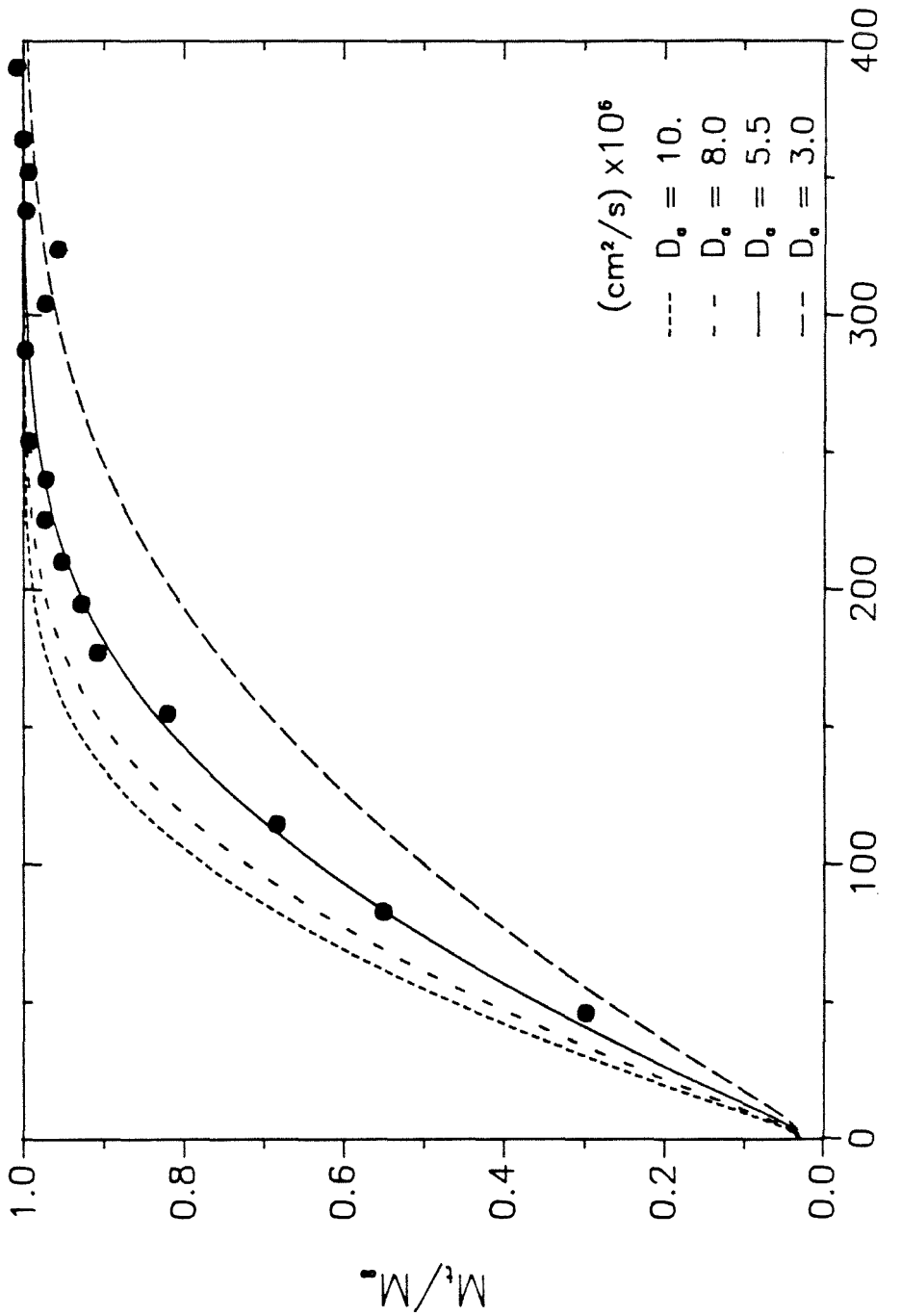
M_t/M_∞
1.0
0.8
0.6
0.4
0.2
0.0
0
100
200
300
400
$t^{0.5}/a$ $(sec^{0.5}/cm)$
$(cm^2/s) \times 10^6$
$D_o = 10.$
$D_o = 8.0$
$D_o = 5.5$
$D_o = 3.0$

Figure 6

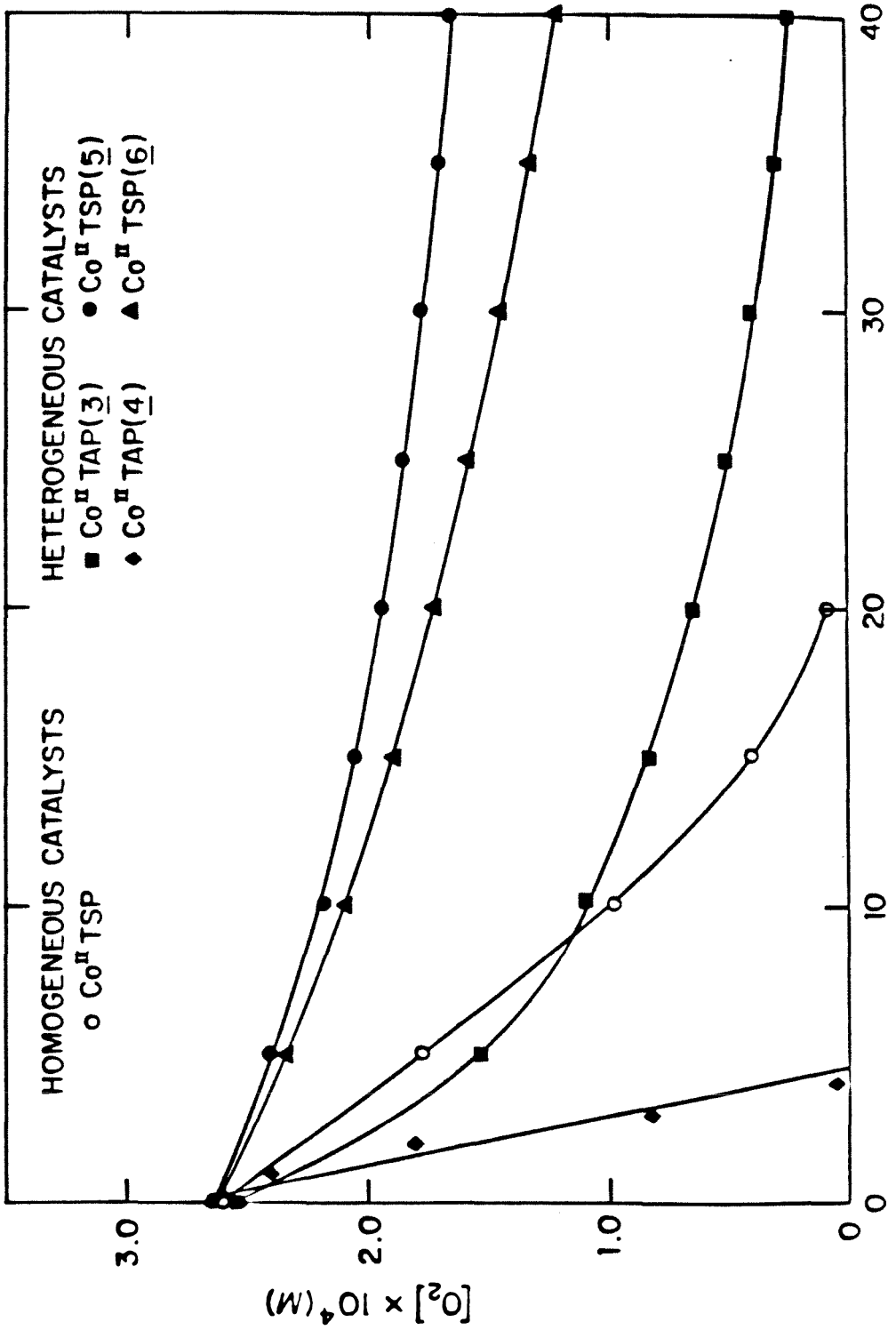
HOMOGENEOUS CATALYSTS
o Co^{II} TSP
HETEROGENEOUS CATALYSTS
■ Co^{II} TAP(3)
● Co^{II} TSP(5)
◆ Co^{II} TAP(4)
▲ Co^{II} TSP(6)
[O$_2$] x 10^4(M)
3.0
2.0
1.0
0
0
10
20
30
40
TIME (Minutes)

Figure 7

Chapter 6

Co(II) Tetrasulfophthalocyanine on Titanium Dioxide: A New Efficient Electron Relay for the Photocatalytic Formation and Depletion of Hydrogen Peroxide in Aqueous Suspensions

Andrew Hong, Detlef Bahnemann, Michael Hoffmann

J. of Phys. Chem., 1987, 91, 2109-2117.

Reprinted from The Journal of Physical Chemistry, 1987, 91, 2109.

Cobalt(II) Tetrasulfophthalocyanine on Titanium Dioxide: A New Efficient Electron Relay for the Photocatalytic Formation and Depletion of Hydrogen Peroxide in Aqueous Suspensions

Andrew P. Hong, Detlef W. Bahnemann,† and Michael R. Hoffmann*

W. M. Keck Laboratories, California Institute of Technology, Pasadena, California 91125
(Received: November 6, 1986)

A novel synthesis for the covalent linkage of cobalt(II) tetrasulfophthalocyanine ($Co^{II}TSP$) to the surface of titanium dioxide (TiO_2) particles ($d \leq 0.5$ μm) is described. Upon irradiation with light that exceeds the bandgap energy (E_g) of TiO_2 (i.e., $\lambda \leq 380$ nm), $Co^{II}TSP$ is reduced to $Co^{I}TSP$ under anoxic conditions both as a dry powder and in aqueous suspension. The photochemical reduction is shown to be fully reversible in the presence of molecular oxygen (O_2). Hydrogen peroxide (H_2O_2) is produced upon irradiation of an aerated aqueous suspension of the "hybrid" catalyst, TiO_2–$Co^{II}TSP$. Formation kinetics are followed in situ with a polarographic detector (detection limit $\simeq 10^{-7}$ M H_2O_2); quantum yields, $\phi_{H_2O_2}$, between 0.16 and 0.49 have been determined. The reactive photocatalytic center appears to be generated by the attachment of molecular oxygen in the open apical coordination site of the hybrid $Co^{II}TSP$ complex. Formation of $Co^{III}TSP$–$O_2^{\bullet-}$ is enhanced by the binding of TiO^- surface groups in the opposite apical position. Hydrogen peroxide is produced in a two-step electron transfer from the conduction band via the Co(III) center. The involvement of free radical intermediates in this mechanism appears to be highly unlikely. On the basis of its observed chemical and photochemical stability and the high quantum yields for O_2 reduction, the newly developed hybrid material is proposed to be applicable as a potent and stable oxidation catalyst.

Introduction

Electron-transfer reactions following the light-induced charge separation in submicron semiconductor particles have been studied in great detail during the past decade. The original interest in these systems stems from reports that they facilitate the simultaneous formation of dihydrogen and dioxygen from water.[1] Since the overall reaction of two conduction band electrons, e^-_{CB}, and four valence band holes, h^+_{VB}, is required to achieve this direct storage of solar energy in the form of chemical energy (reactions 1 and 2),[2] laboratory studies have shown that appropriate electron

$$2H_2O + 2e^-_{CB} \rightarrow H_2(\uparrow) + 2OH^-_{aq} \quad (1)$$

$$2H_2O + 4h^+_{VB} \rightarrow O_2(\uparrow) + 4H^+_{aq} \quad (2)$$

relays are necessary to compete with the e^-/h^+ recombination and thus achieve reasonable but still rather small quantum yields.[3-7] While suitable metal deposits (e.g., Pt) due to their ability to store electrons and/or adsorbed hydrogen atoms[8] are good catalysts for reaction 1,[4-7] metallic oxides (e.g., RuO_2, Rh_2O_3) seem to catalyze the four-hole water oxidation.[3-7]

Photodeposition[6,7] usually yields highly dispersed metal clusters on the semiconductor's surface. An ohmic contact between these metal islands and various n-type semiconductors has been proposed[9] to account for a potential gradient which drives the e^-_{CB} to the metal and repells the h^+_{VB} from this part of the interface,[10] thus resulting in the necessary e^-/h^+ separation. The major drawback of these catalytic systems is the efficient thermal catalysis of undesirable back-reactions by the Pt deposit.[10] In this paper we establish the effectiveness of cobalt(II) tetrasulfophthalocyanine ($Co^{II}TSP$) as an electron relay, which is chemically bound to the surface of titanium dioxide (TiO_2).

† Permanent address: Hahn-Meitner Institut GmbH, Bereich Strahlenchemie, Glienicker Strasse 100, D1000 Berlin 39, Federal Republic of Germany.
* To whom correspondence should be addressed.

(1) Recent reviews on this subject include: (a) Bockris, J. O'M.; Dandapani, B.; Cooke, D.; Ghoroghchian, J. *Int. J. Hydrogen Energy* **1985**, *10*, 179. (b) Fendler, J. H. *J. Phys. Chem.* **1985**, *89*, 2730. (c) Somorjai, G. A.; Hendewerk, M.; Turner, J. E. *Catal. Rev.—Sci. Eng.* **1984**, *26*, 683.
(2) Vanden Kerchove, F.; Praet, A.; Gomes, W. P. *J. Electrochem. Soc.* **1985**, *132*, 2357.
(3) Sobczynski, A.; White, J. M. *J. Mol. Catal.* **1985**, *29*, 379.
(4) Magliozzo, R. S.; Krasna, A. I. *Photochem. Photobiol.* **1983**, *38*, 15.
(5) (a) Blondeel, G.; Harriman, A.; Williams, D. *Sol. Energy Mater.* **1983**, *9*, 217. (b) Blondeel, G.; Harriman, A.; Porter, G.; Urwin, D.; Kiwi, J. *J. Phys. Chem.* **1983**, *87*, 2629.
(6) (a) Lehn, J.-M.; Sauvage, J.-P.; Ziessel, R. *Nouv. J. Chim.* **1979**, *3*, 423. (b) Lehn, J.-M.; Sauvage, J.-P.; Ziessel, R. *Nouv. J. Chim.* **1980**, *4*, 355. (c) Lehn, J.-M. In *Proceedings of the 3rd International Conference on Photochemical Conversion and Storage of Solar Energy, 1980*; Connolly, J. S., Ed.; Academic: New York, 1981; p 161.
(7) (a) Duonghong, D.; Borgarello, E.; Grätzel, M. *J. Am. Chem. Soc.* **1981**, *103*, 4685. (b) Yesodharan, E.; Grätzel, M. *Helv. Chim. Acta* **1983**, *66*, 2145.
(8) Henglein, A.; Lindig, B.; Westerhausen, J. *J. Phys. Chem.* **1981**, *85*, 1627.
(9) Aspnes, D. E.; Heller, A. *J. Phys. Chem.* **1983**, *87*, 4919.
(10) Gerischer, H. *J. Phys. Chem.* **1984**, *88*, 6096.

0022-3654/87/2091-2109$01.50/0

The idea of metal complexes as electron relays has very recently been introduced by Grätzel et al.[11] who chemisorbed cobaltocenium dicarboxylate on colloidal TiO_2 and observed its high efficiency for electron-transfer reactions by a kinetic laser flash photolysis study of the reduction of methylviologen (MV^{2+}) to the radical cation $MV^{\bullet+}$. Modification of semiconductor surfaces by newly established chemical bonds has so far only been used to increase the material's stability[12] or to attach sensitizer molecules in order to extend the photocatalytic activity of the catalyst into the visible part of the spectrum.[13-15] Similar properties have been reported by Bard et al.[16] and Loufty and Hor[17] when they deposited thin films of phthalocyanines (metal-free and metal-containing) on bulk semiconductor electrodes. While these authors reported very low quantum yields for this spectral sensitization ($0.01\% < \phi < 0.1\%$), they did not observe electron relay properties of these phthalocyanines under ultrabandgap irradiation.

A study of the photocatalytic formation and destruction of hydrogen peroxide (H_2O_2) was chosen as an initial test for the activity of the newly synthesized hybrid catalyst TiO_2–$Co^{II}TSP$. H_2O_2 can be formed by either the reduction of dioxygen (reaction 3) or the oxidation of water (reaction 4). Reaction 3 has been

$$O_2 + 2e^-_{CB} + 2H^+_{aq} \rightarrow H_2O_2 \quad (3)$$

$$2H_2O + 2h^+_{VB} \rightarrow H_2O_2 + 2H^+_{aq} \quad (4)$$

studied in great detail,[18-27] and it has been shown that appreciable yields of hydrogen peroxide are only detected when appropriate electron donors, D, are added prior to illumination. This indicates that it is this compound D which is adsorbed on the catalyst's surface and hence sacrificed via the reaction

$$D + h^+_{VB} \rightarrow D^{\bullet+} \quad (5)$$

to successfully interfere with the e^-/h^+ recombination and leave e^-_{CB} behind which then reacts with dioxygen via (3). The oxidation of water via reaction 4 has not been demonstrated unambiguously. Even though Rao et al.[28] reported the formation of H_2O_2 in water-splitting experiments on ZnO and TiO_2, Salvador and Decker[29] were unable to verify this observation. The intermediate production of H_2O_2 as the first molecular step of the four-hole process (reaction 2) has been predicted,[29,30] and a variety of free radical intermediates have already been detected.[31-33] When the oxidation of H_2O has been found to proceed with high yields, there has been no indication of hydrogen peroxide formation.[1-7,34-36] With the aid of a polarographic technique for the kinetic analysis of low hydrogen peroxide concentrations ($[H_2O_2] \geq 0.1\ \mu M$), we have gained further insight into the photocatalytic formation and destruction of H_2O_2 on TiO_2 surfaces.

Experimental Section

All chemicals were of reagent grade. The water used in all preparations and kinetic studies was purified by a Milli-Q/RO system (Millipore) resulting in a resistivity, ρ, of >18 MΩ cm.

Reflectance spectra of powder samples with $BaSO_4$ as a reference were taken with a Shimadzu UV-260 spectrophotometer equipped with an integrating sphere. The irradiation apparatus consisted of an Osram XBO 450-W xenon lamp in a PRA ALH220 lamp housing and a PRA B102 monochromator together with the appropriate UV and IR filters, as described by Faust.[37] Kinetic experiments were performed in a water-jacketed 360-mL cylindrical reactor with optical Pyrex glass windows at both ends. Actinometry at 366 nm was performed in the same vessel with (*E*)-2-(2,5-dimethyl-3-furylethylidene)(isopropylidene)succinic anhydride in toluene according to the method of Heller.[38] The UV–vis absorbance change of the photochromic system was measured with a HP 8451A spectrophotometer. The radiant flux at 366 nm entering the photoreactor was determined weekly and was found to vary between 1.0×10^{16} and 0.4×10^{16} photons/s.

The H_2O_2 concentration was measured continuously with a YSI-Clark 2510 Oxidase Probe connected to a YSI Model 25 Oxidase Meter. The surface of the electrode was covered with a dialysis membrane (molecular weight cutoff 12000–14000) to prevent any interference caused by the catalyst particles. Equilibration times between 30 and 60 min were allowed to ensure a stable signal once the electrode was immersed into the reaction solution. Following equilibration, changes in H_2O_2 content were monitored at a sensitivity at 10^{-7} M and a time constant of 1 s. The electrode was calibrated following each kinetic experiment by using a standard addition method; linear response was obtained between 10^{-7} and 2×10^{-5} M H_2O_2. Since this polarographic method is sensitive to any species with a redox potential of 700 mV, a different method was used to verify the formation of hydrogen peroxide. Following the illumination an aliquot of the solution was taken and titrated with iodide in the presence of a catalyst[39,40] to form the I_3^- anion which was quantitatively measured by spectrophotometry ($\epsilon_{352\ nm} = 26\,400\ M^{-1}\ cm^{-1}$).[41] An IBM PC/AT computer and associated software was used to analyze the kinetic data obtained from the oxidase meter after amplification and A/D conversion.

Gas chromatographic analyses were performed on an HP5880 GC equipped with a Supelco 80/120 Carbopack, 3% SP-1500 column, and a FID to detect traces of organics in aqueous solution, or on a Shimadzu GC8A with Molecular Sieve 5 Å 80/100

(11) Kölle, U.; Moser, J.; Grätzel, M. *Inorg. Chem.* **1985**, *24*, 2253.
(12) Fox, M. A.; Hohman, J. R.; Kamat, P. V. *Can. J. Chem.* **1983**, *61*, 888.
(13) (a) Anderson, S.; Constable, E. C.; Dare-Edwards, M. P.; Goodenough, J. B.; Hamnett, A.; Seddon, K. R.; Wright, R. D. *Nature (London)* **1979**, *280*, 571. (b) Dare-Edwards, M. P.; Goodenough, J. B.; Hamnett, A.; Seddon, K. R.; Wright, R. D. *Faraday Discuss. Chem. Soc.* **1980**, *70*, 285.
(14) (a) Ghosh, P. K.; Spiro, T. G. *J. Am. Chem. Soc.* **1980**, *102*, 5543. (b) Ghosh, P. K.; Spiro, T. G. *J. Electrochem. Soc.* **1981**, *128*, 1281.
(15) Duonghong, D.; Serpone, N.; Grätzel, M. *Helv. Chim. Acta* **1984**, *67*, 1012.
(16) (a) Jaeger, C. D.; Fan, F. F.; Bard, A. J. *J. Am. Chem. Soc.* **1980**, *102*, 2592. (b) Giraudeau, A.; Fan, F. F.; Bard, A. J. *J. Am. Chem. Soc.* **1980**, *102*, 5137.
(17) Loufty, R. O.; Hor, A. In *Photochemistry and Photobiology*; Zewail, A. H., Ed.; Harwood Academic: London, 1983; Vol. 2, p 759.
(18) (a) Baur, E.; Neuweiler, C. *Helv. Chim. Acta* **1927**, *10*, 901. (b) Böhi, J. *Helv. Chim. Acta* **1929**, *12*, 121.
(19) (a) Chari, C. N.; Qureshi, M. *J. Indian Chem. Soc.* **1944**, *21*, 97. (b) Chari, C. N.; Qureshi, M. *J. Indian Chem. Soc.* **1944**, *21*, 297.
(20) Markham, M. C.; Laidler, K. J. *J. Phys. Chem.* **1953**, *57*, 363.
(21) (a) Rubin, T. R.; Calvert, J. G.; Rankin, G. T.; MacNevin, W. M. *J. Am. Chem. Soc.* **1953**, *75*, 2850. (b) Calvert, J. G.; Theurer, K.; Rankin, G. T.; MacNevin, W. M. *J. Am. Chem. Soc.* **1954**, *76*, 2575.
(22) Stephens, R. E.; Ke, B.; Trivich, D. *J. Phys. Chem.* **1955**, *59*, 966.
(23) (a) Kuriacose, J. C.; Markham, M. C. *J. Catal.* **1962**, *1*, 498. (b) Morrison, S. R.; Freund, T. *J. Chem. Phys.* **1967**, *47*, 1543.
(24) (a) Harbour, J. R.; Hair, M. L. *J. Phys. Chem.* **1977**, *81*, 1791. (b) Harbour, J. R.; Hair, M. L. *J. Phys. Chem.* **1979**, *83*, 652. (c) Hair, M. L.; Harbour, J. R. *Adv. Chem. Ser.* **1980**, *No. 184*, 173.
(25) Pappas, S. P.; Fischer, R. M. *J. Paint Technol.* **1974**, *46*, 65.
(26) Cundall, R. B.; Rudham, R.; Salim, M. S. *J. Chem. Soc., Faraday Trans. 1* **1976**, *72*, 1642.
(27) (a) Harbour, J. R.; Hair, M. L. In *Magnetic Resonance in Colloid and Interface Science*; Fraissard, J. P., Resing, H. A., Eds.; Reidel: Dordrecht, 1980; p 431. (b) Harbour, J. R.; Tromp, J.; Hair, M. L. *Can. J. Chem.* **1985**, *63*, 204.
(28) Rao, M. V.; Rajeshwar, K.; Pal Verneker, V. R.; DuBow, J. *J. Phys. Chem.* **1980**, *84*, 1987.
(29) Salvador, P.; Decker, F. *J. Phys. Chem.* **1984**, *88*, 6116.
(30) Rives-Arnau, V. *J. Electroanal. Chem.* **1985**, *190*, 279.
(31) Jaeger, C. D.; Bard, A. J. *J. Phys. Chem.* **1979**, *83*, 3146.
(32) Anpo, M.; Shima, T.; Kubokawa, Y. *Chem. Lett.* **1985**, 1799.
(33) Serwicka, E. *Colloids Surf.* **1985**, *13*, 287.
(34) (a) Baur, E.; Perret, A. *Helv. Chim. Acta* **1924**, *7*, 910. (b) Perret, A. *J. Chim. Phys. Phys.-Chim. Biol.* **1926**, *23*, 97.
(35) Hada, H.; Yonezawa, Y.; Saikawa, M. *Bull. Chem. Soc. Jpn.* **1982**, *55*, 2010.
(36) Nishimoto, S.-I.; Ohtani, B.; Kajiwara, H.; Kagiya, T. *J. Chem. Soc., Faraday Trans. 1* **1983**, *79*, 2685.
(37) Faust, B. C. Report No. AC-1-85; California Institute of Technology: Pasadena, CA, 1985; pp 33–38.
(38) Heller, H. G.; Langan, J. R. *J. Chem. Soc., Perkin Trans. 2* **1981**, 341.
(39) Patrick, W. A.; Wagner, H. B. *Anal. Chem.* **1949**, *21*, 1279.
(40) Savage, D. J. *Analyst (London)* **1951**, *76*, 224.
(41) Mönig, J. Diplomathesis, Technical University Berlin, Germany, 1980, pp 38–40.

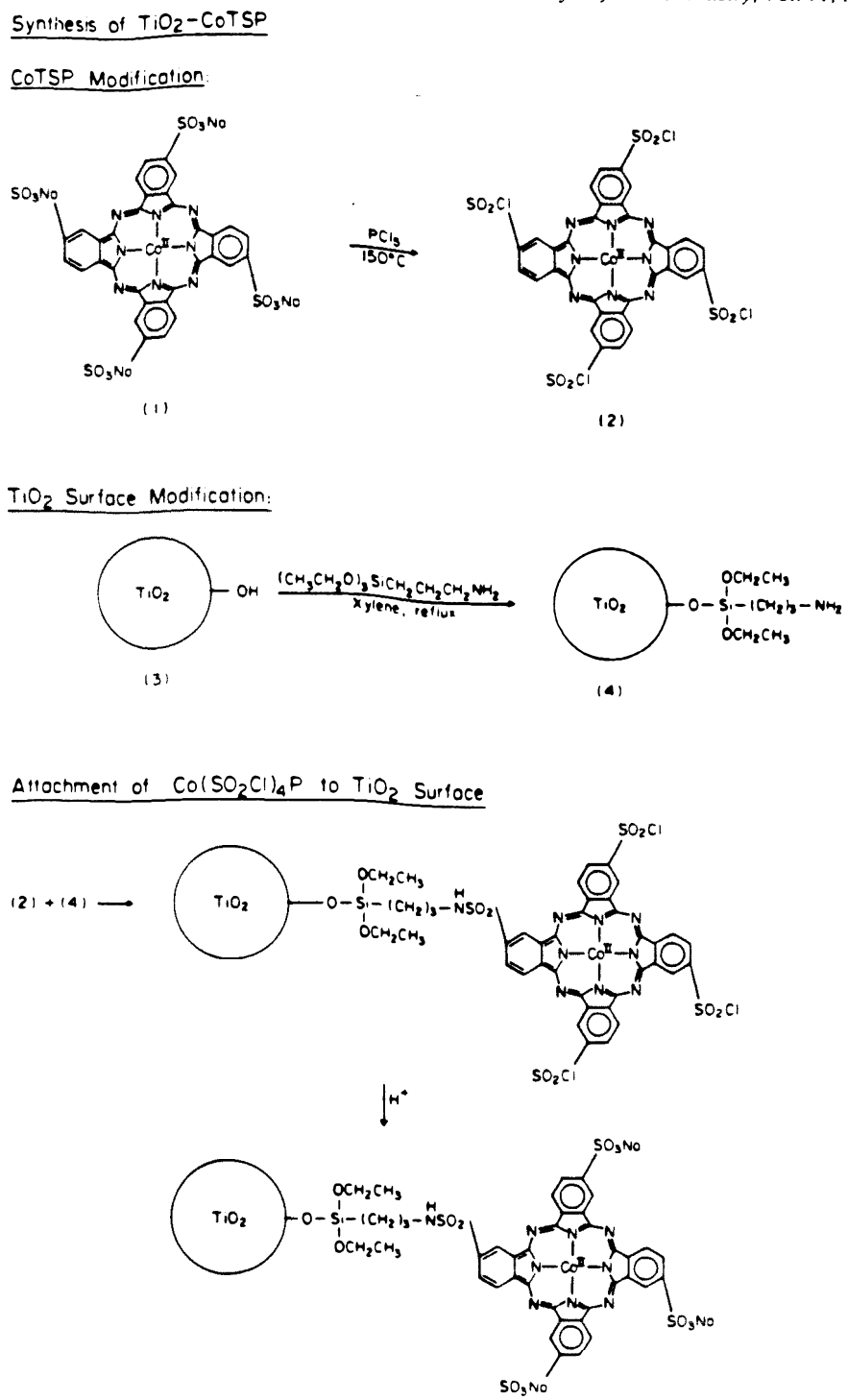

Figure 1. Schematic diagram summarizing various steps in the synthesis of cobalt(II) tetrasulfophthalocyanine chemically bound to the titanium dioxide surface (TiO_2–$Co^{II}TSP$).

columns and a TCD to monitor inorganic gases.

The synthesis of the TiO_2–$Co^{II}TSP$ hybrid catalyst is summarized in Figure 1 and described in detail below.

Synthesis of $Co^{II}TSP$ and $Co^{II}(SO_2Cl)_4P$. Blue cobalt(II) tetrasulfophthalocyanine ($Co^{II}TSP$) was synthesized according to Boyce et al.[42] Green cobalt(II) tetrasulfonylphthalocyanine ($Co^{II}(SO_2Cl)_4P$) was obtained by treatment of $Co^{II}TSP$ with PCl_5 as follows:

$$Co^{II}(SO_3Na)_4P + 4PCl_5 \rightarrow Co^{II}(SO_2Cl)_4P + 4POCl_3 + 4NaCl$$

$Co^{II}TSP$ and PCl_5 powders (molar ratio of 1:25) were ground together and allowed to react for 20 h at 150 °C (oil bath) in a round-bottom flask equipped with a condenser and a $CaCl_2$ drying tube. Excess reagent was removed by aspiration at the end of

(42) Boyce, S. D.; Hoffmann, M. R.; Hong, A. P.; Moberly, L. M. *Environ. Sci. Technol.* **1983**, *17*, 602 and references cited therein.

the reaction. The crude solid product was ground to a fine powder and stirred briefly in water to remove any remaining by-products and unreacted $Co^{II}TSP$. The solid was collected by filtration through a 0.2-μm membrane and dried under vacuum for 8 h. The reaction was quantitative.

Synthesis of TiO_2 and Surface-Modified TiO_2 Powders. In the early preparations titanium dioxide powder was synthesized by the hydrolysis of freshly distilled $TiCl_4$ at pH 7 and 0 °C. The resulting colloidal suspension contains TiO_2 particles; the crystal structure of these particles indicated that they were a mixture of amorphous and anatase phases.[43] The colloidal suspensions were allowed to coagulate for several days. Solvent evaporation and a subsequent heat treatment at 100 °C yielded the white metal oxide powder which was hence used for the preparation of the catalyst. Particle diameters varied between 50 and 500 nm as determined by scanning electron microscopy (SEM). Commercially available TiO_2 powder (P25 anatase from Degussa) was used as received for the later preparations of the hybrid catalyst. It has an average primary particle size of 30 nm and a surface area of 50 ± 15 m^2/g (BET, source Degussa Technical Bulletin Pigments No. 56).

The surface-derivatized TiO_2 powder was obtained by treatment of the TiO_2 powder with a silane reagent. In a typical preparation, 190 mmol of dry TiO_2 (115 °C for 12 h) and 43 mmol of (3-aminopropyl)triethoxysilane (freshly distilled) were stirred in 30 mL of xylene and refluxed for 12 h. At the end of the reaction, the solid was filtered and washed with benzene and acetone followed by drying under vacuum.

Linkage of the $Co^{II}(SO_2Cl)_4P$ to the Modified TiO_2 Surface. A sulfonamide linkage between $Co^{II}(SO_2Cl)_4P$ and the silane groups on the TiO_2 surface established the desired chemical bond. In preparation of the hybrid catalysts used in this paper, 0.023 g of $Co^{II}(SO_2Cl)_4P$ was dissolved in 20 mL of pyridine. The solution was added dropwise to 3 g of the modified TiO_2 suspended in 10 mL of pyridine. The mixture was stirred for 2 h at room temperature although colorization of the solid appeared very quickly. A quantitative reaction of $Co^{II}(SO_2Cl)_4P$ with the modified P25 powder was observed after stirring for only 30 min as indicated by the complete decolorization of the liquid. This showed a much higher coupling tendency toward $Co^{II}(SO_2Cl)_4P$ when compared with the powder derived from $TiCl_4$ which left most of the phthalocyanine in solution. The powder was then filtered and washed consecutively with pyridine, water, and acetone. As a final step, the blue hybrid catalyst was dried under vacuum. Centrifugation was employed for the collection of fine solids when, as in the case of P25, large batches of catalyst (50 g) were produced. Gas chromatographic analysis revealed that powders prepared and washed in the above-described way still contained traces of organic impurities on their surfaces which leached into the solvent phase after suspension. Further treatment involving overnight stirring in 2.5 M H_2SO_4 and several wash cycles with distilled H_2O followed by high vacuum (0.1 Torr) solvent evaporation at 120 °C was therefore applied, and this resulted in impurity levels below the detection limit of the GC.

Results and Discussion

(a) Characterization of the Surface-Attached Complex. Elementary analysis showed that the hybrid catalyst particles prepared from the $TiCl_4$ batch contained 39 ppm cobalt, which is equivalent to a molar ratio of 5.3×10^{-5}:1. Since particle diameters varied between 0.05 and 0.5 μm (as determined by SEM), the $Co^{II}TSP$ content ranged from 10^2 to 10^5 molecules per TiO_2 particle, respectively. The surface coverage was calculated to be 5% in the case of 0.05-μm particles and 50% for 0.5-μm particles, assuming a spherical geometry of the catalyst and a space of 400 $Å^2$ used by $Co^{II}TSP$ lying parallel to the surface (i.e., the arrangement with the highest required area). P25-TiO_2 quantitatively bound all $Co^{II}(SO_2Cl)_4P$ and hence contained 370 ppm cobalt (molar ratio 6.4×10^{-4}:1), leading to a surface coverage of 30% based on a total surface area of 50 m^2/g of this material. These calculations show that even though the $Co^{II}TSP$ content of each particle of these hybrid catalysts is very high, the resulting surface coverage remains well below a monolayer. In the following paragraphs the two differently prepared hybrid catalysts will be abbreviated as $TiO_2(TiCl_4)$–CoTSP and TiO_2(P25)–CoTSP, respectively.

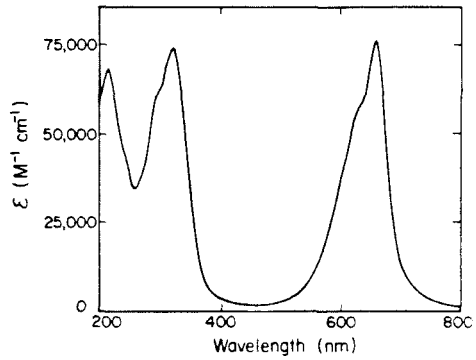

Figure 2. UV–vis absorption spectrum of $Co^{II}TSP$. Experimental conditions: 2×10^{-6} M $Co^{II}TSP$, pH 4.6, d = 10 cm.

A characterization of the mode of chemical linkage between $Co^{II}TSP$ and the TiO_2 surface is inevitable. We therefore prepared a different $Co^{II}TSP$-coated powder. A pale blue coloration of TiO_2(P25) is obtained when an aqueous suspension of this powder (20 g/L) is treated for 3 days with 1.2×10^{-5} M $Co^{II}TSP$ at pH 1.9 or 6; no coloration is observed at pH 12. The particles remain colored upon separation from the solvent, indicating an electrostatic interaction similar to that observed by Grätzel et al. for TiO_2 and a Ru(II) complex.[44] Once the blue powders from the treatment at pH 1.9 and 6 are resuspended in water at pH 12, they instantaneously lose the color yielding a blue supernatant, evincing that the mixing resulted merely in the adsorption of the metal complex to the semiconductor's surface. However, no color change of the hybrid catalyst is observed when it is suspended in strongly acidic (2.5 M H_2SO_4) or alkaline (0.1 M NaOH) media and stirred for 72 h. The photocatalytic activity of the powders (which will be discussed below) is not diminished after this treatment. These results clearly demonstrate that $Co^{II}TSP$ is bound to the surface of TiO_2 as suggested in Figure 1. Adsorption represents a much weaker interaction that is completely reversible at alkaline pH where electrostatic forces lead to a repulsion of the negatively charged $Co^{II}TSP$ from the TiO_2 surface. The coupling within the hybrid catalyst involves the silanation of surface hydroxyl groups of the oxide support as a first step followed by a condensation reaction with the sulfonyl derivative of $Co^{II}TSP$. The bond thus established is a silane linkage between a surface oxygen of TiO_2 and a side chain of the aromatic part of the phthalocyanine ring and therefore appears to be extremely stable. This paper focuses on the light-induced reduction of molecular oxygen to demonstrate the unique properties of TiO_2–$Co^{II}TSP$ as a photocatalyst and to elucidate its mode of action.

(b) Photochemical Processes Involving TiO_2–CoTSP. Prior to any photochemical experiment the nature of the light-absorbing species has to be ascertained. The absorption spectrum of an aqueous solution of cobalt(II) tetrasulfophthalocyanine (pH 4.6) is therefore shown in Figure 2. The two characteristic absorption bands in the visible part of this spectrum have been assigned to the monomeric (660 nm) and the dimeric (620 nm) form of $Co^{II}TSP$[45] which under the given experimental conditions are present as 70% and 30% of the reaction mixture, respectively.[46]

(43) (a) Duonghong, D.; Ramsden, J.; Grätzel, M. *J. Am. Chem. Soc.* **1982**, *104*, 2977. (b) Moser, J.; Grätzel, M. *J. Am. Chem. Soc.* **1983**, *105*, 6547.

(44) Desilvestro, J.; Grätzel, M.; Kavan, L.; Moser, J.; Augustynski, J. *J. Am. Chem. Soc.* **1985**, *107*, 2988.

(45) Gruen, L. C.; Blagrove, R. J. *Aust. J. Chem.* **1973**, *26*, 319.

(46) (a) Sigel, H.; Waldmeier, P.; Prijs, B. *Inorg. Nucl. Chem. Lett.* **1971**, *7*, 161. (b) Waldmeier, P.; Prijs, B.; Sigel, H. *Z. Naturforsch., B* **1972**, *27*, 95.

TABLE I: Quantum Yields ϕ_0 (Computed from the Initial Slope) and H_2O_2 Decomposition Rate k_2^{ss} (Calculated from the Steady-State Concentration) for the Photocatalyzed Formation of H_2O_2 under Various Conditions[a]

type of catalyst	C_{O_2}, %	pH	ϕ_0	k_2^{ss}, 10^{-3} s^{-1}
TiO_2(P25)–CoTSP	100	2.0	0	[b]
TiO_2(P25)–CoTSP	100	4.9	0.16	0.8
TiO_2(P25)–CoTSP	100	8.3	0.31	0.7
TiO_2(P25)–CoTSP	100	12.0	(0.24 ± 0.05)	(0.9 ± 0.2)
TiO_2(P25)–CoTSP	59	12.0	0.27	1.3
TiO_2(P25)–CoTSP	20	12.0	0.18	1.7
TiO_2(P25)–CoTSP	0	12.0	0	[b]
$TiO_2(TiCl_4)$–CoTSP	100	7.7	0.49	0.9
$TiO_2(TiCl_4)$–CoTSP	100	7.0	0.48	2.4[c]
$TiO_2(TiCl_4)$	100	7.0	0	[b]
P25–TiO_2	100	12.0	0	[b]
$Co^{II}TSP$	100	8.6	0	[b]
$Co^{II}TSP$	100	12.0	0	[b]

[a] Concentrations used were 0.3 g/L for P25–TiO_2 and TiO_2(P25)–CoTSP, 0.42 g/L for $TiO_2(TiCl_4)$ and $TiO_2(TiCl_4)$–CoTSP, and 1.7×10^{-6} M for $Co^{II}TSP$. [b] No H_2O_2 formation observed. [c] Incident photon flux 1×10^{16} photons/s (4×10^{15} to 5×10^{15} photons/s in all other cases).

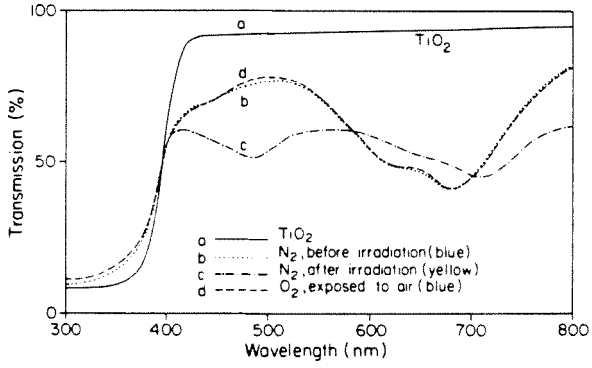

Figure 3. Reflectance spectra of dry TiO_2 and TiO_2–CoTSP powders: (a) plain $TiO_2(TiCl_4)$; (b) $TiO_2(TiCl_4)$–CoTSP under N_2; (c) $TiO_2(TiCl_4)$–CoTSP after illumination (≃2 min, λ_{ex} = 366 nm), N_2 purged; (d) like (c), but aerated after illumination.

The near-UV part of the absorption spectrum of $Co^{II}TSP$ has not been described in detail before. It should be noted that the first absorption band occurs at 320 nm; at 366 nm the primary wavelength for irradiation light absorption due to the cobalt complex is rather insignificant. From the extinction coefficient ($\epsilon_{366\ nm}(Co^{II}TSP)$ = 12 500 M^{-1} cm^{-1}) one calculates that even with the highest surface loading of 370 ppm less than 11% of the incident photons are absorbed by $Co^{II}TSP$ under typical experimental conditions, i.e., suspensions containing 0.3 g/L of the hybrid catalyst. No photocatalytic hydrogen peroxide formation is observed when oxygenated aqueous solutions containing 1.7 μM $Co^{II}TSP$ (the equivalent is present on the hybrid catalyst in typical irradiations) are irradiated at 366 nm in the absence of titanium dioxide (last entries in Table I). All quantum yields reported in this paper have been corrected to account for the partial light absorption due to the surface-bound complex.

Figure 3 shows the reflectance spectra measured for the untreated TiO_2 powder (curve a) and the $Co^{II}TSP$-bound hybrid catalyst (curve b). Pure TiO_2 is transparent to visible light. Absorption by TiO_2 begins below 380 nm, which is in good correlation with the bandgap energy of anatase (E_g = 3.2 eV).[47] The $Co^{II}TSP$-coated powder shows the same absorption features in the UV but has additional absorption bands in the visible region with two maxima at 620 and 680 nm that are similar to those seen in Figure 2 for the aqueous solution of $Co^{II}TSP$. A shift of the monomeric absorption band by 20 nm to longer wavelengths is apparent. A similar shift has been observed in an oxygenated $Co^{II}TSP$ solution at high pH.[45] It has been attributed to the formation of a $Co^{III}TSP$–$O_2^{\bullet-}$ complex facilitated by the σ-donating properties of an OH^- ligand in one of the apical positions (reactions 6 and 7). In case of the hybrid catalyst, the absence

$$Co^{II}TSP + OH^- \leftrightarrow (HO^-)Co^{II}TSP \quad (6)$$

$$(HO^-)Co^{II}TSP + O_2 \leftrightarrow (HO^-)Co^{III}TSP(O_2^{\bullet-}) \quad (7)$$

or presence of dioxygen has no influence on the observed spectral characteristics (compare curves b and d in Figure 3). This is apparently due to the fact that dioxygen cannot be removed completely even under reduced pressure (10^{-5} Torr) provided that it is chemisorbed in the superoxide form[48] as proposed in reaction 7. Upon illumination with near-UV light ($\lambda_{ex} \leq$ 380 nm) in the absence of O_2 the original blue color of the powder disappears and turns yellow with two new absorption bands at 480 and 720 nm (curve c in Figure 3). A similar spectrum has been reported by Kundo et al. for an aqueous solution of $Co^{I}TSP$.[49] This color change is completely reversible in the presence of dioxygen, and the reversible cycle has been successfully repeated a number of times with no apparent loss in activity. Furthermore, the spectral characteristics of the catalyst remain unchanged after prolonged irradiation with visible light (i.e., $\lambda_{ex} > 400$ nm or $h\nu_{ex} < E_g$) whether or not O_2 is present. Analogous spectral changes are observed for the irradiation of aqueous suspensions of TiO_2–$Co^{II}TSP$ above pH 4, i.e., when the particle's surface is negatively charged ($pH_{zpc}(TiO_2) \simeq 4.7$).[50] A slight color change, which is apparent after UV irradiation of an O_2-free aqueous suspension of the catalyst at pH 0, decays quickly once the sample is stirred.

The above observations are consistent with the transfer of conduction band electrons, e^-_{CB}, generated by bandgap irradiation of the TiO_2 support, to the surface-bound $Co^{II}TSP$. The effect of dioxygen upon the observed spectral changes suggests its involvement in this electron transfer and the possibility of hydrogen peroxide formation (reaction 3). To test this hypothesis, the oxidase probe was used to measure H_2O_2 in aqueous suspensions of the hybrid catalyst. Figure 4 shows a typical trace of the formation of H_2O_2 that is observed when an aqueous suspension of the hybrid catalyst (0.42 g/L $TiO_2(TiCl_4)$–CoTSP) is illuminated (λ_{ex} = 366 nm) in the presence of O_2. The initial steep slope of this curve indicates a high rate of hydrogen peroxide formation; however, H_2O_2 production slows down with attainment of a steady state after 30 min of irradiation. No further change in $[H_2O_2]$ can be detected even after prolonged irradiation. The H_2O_2 content of the reaction mixture remains constant when the

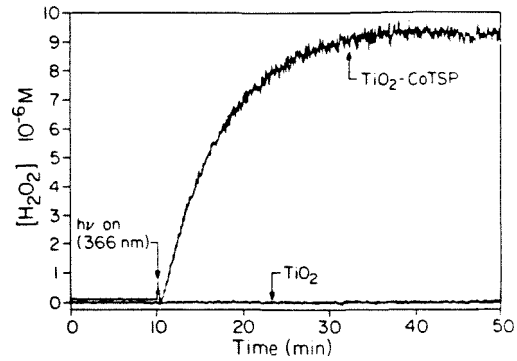

Figure 4. Formation of H_2O_2 on illumination (λ_{ex} = 366 nm) of O_2-saturated aqueous suspensions of $TiO_2(TiCl_4)$–CoTSP (upper curve) and $TiO_2(TiCl_4)$ (lower curve) [0.42 g/L catalyst, pH 7].

(47) Gerischer, H. *Top. Appl. Chem.* **1979**, *31*, 115.

(48) Many, A. *CRC Crit. Rev. Solid State Sci.* **1974**, 515.

(49) Kundo, N. N.; Keier, N. P. *Russ. J. Phys. Chem. (Engl. Transl.)* **1968**, *42*, 707.

(50) Johansen, P. G.; Buchanan, A. S. *Aust. J. Chem.* **1957**, *10*, 392.

(51) Brown, G. T.; Darwent, J. R. *J. Phys. Chem.* **1984**, *88*, 4955.

(52) Rollmann, L. D.; Chan, S. I. *Inorg. Chem.* **1971**, *10*, 1978.

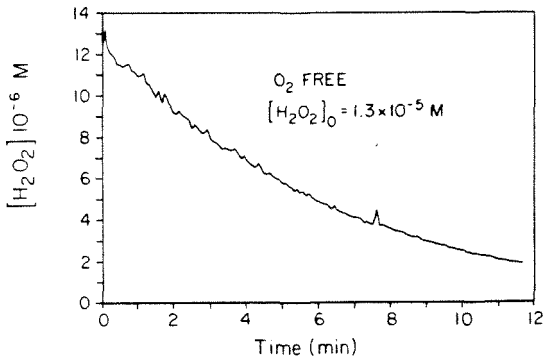

Figure 5. Decay of H_2O_2 on illumination (λ_{ex} = 366 nm) of an N_2-purged aqueous suspension of 0.42 g/L $TiO_2(TiCl_4)$–CoTSP ($[H_2O_2]_0$ = 1.3 × 10^{-5} M, pH 7).

TABLE II: *Quantum* Yields ϕ_0 and H_2O_2 Decomposition Rate k_2[d] (Both Computed from the Kinetic Decay Curve) for the Photocatalyzed Destruction of H_2O_2 under Various Conditions[a]

type of catalyst	pH	ϕ_0	k_2^d, 10^{-3} s^{-1}
TiO_2(P25)–CoTSP	2.1	0.16	0.3
TiO_2(P25)–CoTSP	8.2	0.27	0.5
TiO_2(P25)–CoTSP	12.1	0.47	0.9
$TiO_2(TiCl_4)$–CoTSP	7.0	0.78	2.8[b]
P25–TiO_2	12.0	0.70	1.4

[a] Concentrations used were 0.3 g/L for P25–TiO_2 and TiO_2(P25)–CoTSP and 0.42 g/L for $TiO_2(TiCl_4)$–CoTSP; N_2-purged; $C_{H_2O_2}$ (initial) = 1 × 10^{-5} M for P25–TiO_2 and TiO_2(P25)–CoTSP and 1.3 × 10^{-5} M for $TiO_2(TiCl_4)$–CoTSP. [b] Incident photon flux 1 × 10^{16} photons/s (4 × 10^{15} to 5 × 10^{15} photons/s in all other cases).

light is turned off. In contrast, homogeneous solutions of Co^{II}TSP are known to act as catalysts for the disproportionation of H_2O_2.[46b] No hydrogen peroxide production is observed when an aqueous suspension of uncoated TiO_2 powder (0.46 g/L) is irradiated in the absence of any additional electron donor (lower curve in Figure 4 and Table I). The formation of H_2O_2 on the hybrid catalyst was verified both qualitatively and quantitatively by titration with KI in the presence of a molybdenum catalyst.[39,40] A quantum yield of ϕ = 0.48 is calculated from the initial slope of the upper curve in Figure 4 by assuming that all incident photons are absorbed by the suspended catalyst powder and correcting for the Co^{II}TSP absorption as described above.

The formation of a steady-state concentration of H_2O_2 indicates that photocatalytic decomposition might be occurring. In order to test this hypothesis, irradiations are performed using anoxic (i.e., 1 h of N_2 purging before and during irradiation) aqueous suspensions of the hybrid catalyst (0.42 g/L $TiO_2(TiCl_4)$–CoTSP) in the presence of added hydrogen peroxide (1.3 × 10^{-5} M). Figure 5 shows the rapid depletion of H_2O_2. A quantum yield of ϕ = 0.78 is calculated from the initial slope of this plot (Table II). All H_2O_2 is depleted under these conditions. While no photochemical production of H_2O_2 is observed with untreated TiO_2 (Table I), the photocatalytic activity of pure P25 powder is obvious from the high yield of hydrogen peroxide depletion (ϕ = 0.7, Table II) which is observed when an aqueous suspension containing 0.3 g/L P25–TiO_2 and 1 × 10^{-5} M H_2O_2 is irradiated at pH 12 (λ_{ex} = 366 nm). This result is in good agreement with a recent report from Brown and Darwent,[51] who observed the efficient photocatalytic oxidation of H_2O_2 on colloidal TiO_2. Comparison of the activity of bare TiO_2 with the hybrid catalyst suggests that Co^{II}TSP is an efficient electron relay for O_2 reduction.

Formation and decay of hydrogen peroxide have been studied under a variety of different conditions with TiO_2(P25)–CoTSP as a catalyst (see Tables I and II). The formation of a true steady

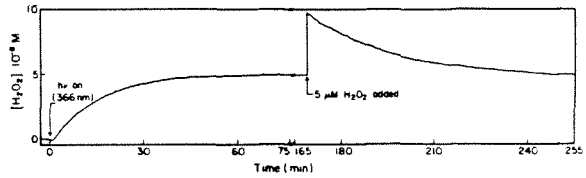

Figure 6. Formation and depletion of H_2O_2 upon irradiation (λ_{ex} = 366 nm) of an oxygenated aqueous suspension of 0.3 g/L TiO_2(P25)–CoTSP at pH 12.

state of $C_{H_2O_2}$ is shown in Figure 6 where nearly 5 μM of H_2O_2 is formed over a period of 45 min upon irradiation of an oxygenated suspension of 0.3 g/L TiO_2(P25)–CoTSP with no H_2O_2 present initially. No further change in $C_{H_2O_2}$ is recorded as the irradiation continued for another 2 h. A decrease of the amount of hydrogen peroxide in solution is observed after the sudden addition of 5 μM H_2O_2 under prolonged irradiation, again leading to the same steady-state concentration. Comparing the efficiencies for photocatalytic hydrogen peroxide formation (Table I) and destruction (Table II), it is obvious that TiO_2(P25)–CoTSP is less active than $TiO_2(TiCl_4)$–CoTSP as a catalyst. This lower activity may be explained by differences in the preparation of the titanium dioxide support which can greatly influence its photocatalytic properties. However, it should be noted that the observed quantum yields between 16% and 47% are certainly much higher than those reported in most related studies.

The observed pH dependency again shows that negative surface charges on the TiO_2 support are a prerequisite for the activity of Co^{II}TSP as an electron relay: no H_2O_2 formation is detected below pH_{zpc}. The photocatalytic depletion of H_2O_2, on the other hand, proceeds at pH 2.1 with a lower quantum yield.

Further insight into the reaction mechanism comes from the observation of a vigorous formation of gas bubbles as an evacuated cuvette containing an aqueous suspension of the hybrid catalyst and 0.05 M H_2O_2 is irradiated with near-UV light. No color change is apparent during the course of this reaction while all hydrogen peroxide is consumed. Gas chromatographic analysis performed before and during this H_2O_2 depletion qualitatively confirmed the formation of O_2 during the irradiation. O_2 is also detected under identical experimental conditions during the photolytic H_2O_2 depletion on naked P25 powder.

Figure 7 presents a mechanism which accounts for these observations. TiO^- groups present on the surface of TiO_2 over a wide pH range (pH ≥4) are thought to act as σ donors toward the metal center of the surface-bound complex, thus facilitating the binding of O_2 as a ligand into the opposite apical position of the octahedral complex yielding the structure denoted "blue". The observation of a bathochromic shift of 20 nm in the absorption spectrum of the hybrid catalyst (cf. Figure 3) supports this suggestion since it resembles the spectral features of a similar octahedral complex found in homogeneous solution, i.e., reaction 7. There is considerable ESR evidence that O_2 is bound to the Co center as a superoxide radical anion,[52,53] leading to the effective oxidation of the former to Co(III). We envision the arrangement TiO^-–Co^{III}TSP–$O_2^{\bullet-}$ to be the blue powder present in all our studies. Dioxygen bound in this way cannot be removed by high vacuum or N_2 purging,[48] resulting in identical spectral characteristics of oxic and anoxic samples (Figure 3). Absorption of a photon with sufficient energy produces an e^-_{CB}/h^+_{VB} pair via the reaction[47]

$$TiO_2 \xrightarrow{h\nu} e^-_{CB} + h^+_{VB} \qquad (8)$$

The e^-_{CB} leads to the further reduction of $O_2^{\bullet-}$, yielding H_2O_2 (Figure 7) which in turn scavenges h^+_{VB}. The absorption of a second photon results in the formation of the original Co(II) complex (e^-_{CB} reaction) and the release of O_2 (h^+_{VB} reaction). This part of the overall reaction sequence constitutes a special type of photodesorption of molecular oxygen. The concentration of O_2 released cannot exceed that of the TiO^-–Co^{III}TSP–$O_2^{\bullet-}$ initially present. An upper limit of 0.1 μL of O_2 formed upon irradiation of 3 mL of deoxygenated solution containing 0.3 g/L TiO_2-

(53) Zwart, J.; Van Wolput, J. H. M. C. *J. Mol. Catal.* **1979**, *5*, 235.
(54) Fenton, H. J. H. *J. Chem. Soc.* **1894**, *65*, 899.

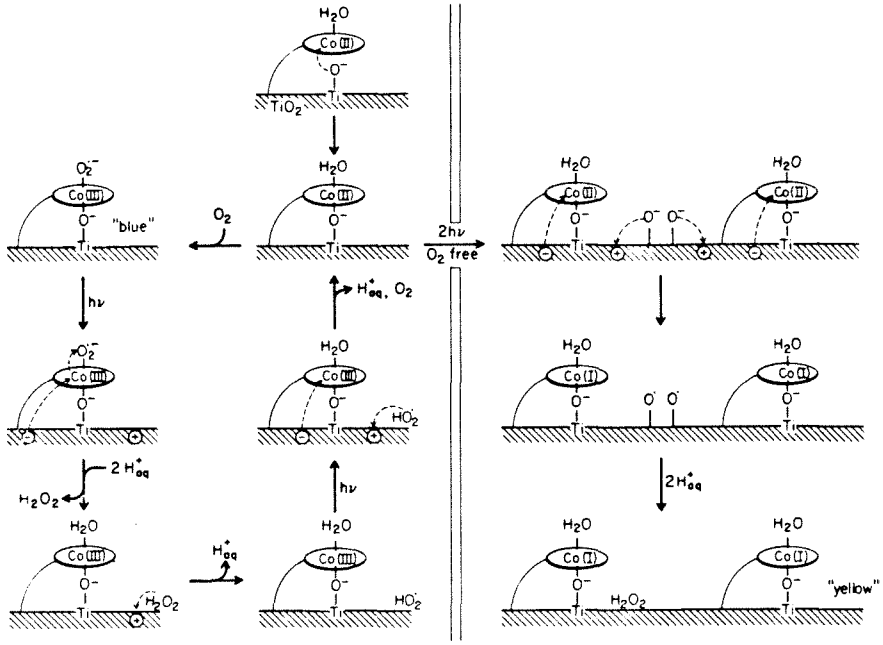

Figure 7. Schematic diagram of the proposed reaction mechanism involving formation and illumination of an octahedral TiO^-–$Co^{III}TSP$–$O_2^{\bullet-}$ complex.

(P25)–CoTSP is calculated, which is far below the detection limit of the analytical procedure for O_2 analysis. The concentration of photodesorbed O_2 is also too low to again drive the cycle shown on the left side of Figure 7 to any considerable extent. Further absorption of photons by the O_2-free preparations of the dry powder of the aqueous suspension of the catalyst should then lead into the right-hand part of Figure 7, resulting in the observed formation of yellow Co(I). We envisage the production of hydrogen peroxide from the reaction of the valence band holes which, however, under the given experimental conditions will be formed in concentrations below the detection limit of the polarographic detector. When air is introduced to the system, the blue color of the powder reappears and the cycle can be repeated.

The pronounced pH effect on the photocatalytic activity of the hybrid catalyst again indicates the importance of the TiO^-–$Co^{III}TSP$–$O_2^{\bullet-}$ complex. While no H_2O_2 formation is observed at pH 2 where this complex should be unstable (Table I), the quantum yield of hydrogen peroxide destruction also decreases significantly at low pH (Table II).

A fast buildup of a steady-state concentration of hydrogen peroxide is detected when oxygenated aqueous suspensions of the hybrid catalyst are irradiated with near-UV light—in clear contrast to the observations in the anoxic case. According to the reaction mechanism presented in Figure 7 the presence of O_2 should lead to a new start of the photolytic cycle without the production of H_2O_2. We therefore envoke a competition between reactions 9 and 4 to explain the net formation of hydrogen peroxide.

$$2H_2O + 2h^+_{VB} \rightarrow H_2O_2 + 2H^+_{aq} \qquad (4)$$

$$H_2O_2 + 2h^+_{VB} \rightarrow O_2 + 2H^+_{aq} \qquad (9)$$

The occurrence of reaction 4 has been strongly debated over the recent years;[28-33] our observations that a steady-state concentration of H_2O_2 is formed while no signs of "long-lived" holes are apparent might be regarded as an indirect evidence for water oxidation on TiO_2. The fact that rather low steady-state concentrations of H_2O_2 (5–10 μM) have been measured demonstrates, on the other hand, the high efficiency of reaction 9. The gas chromatographic detection of O_2 upon the photodecomposition of high concentrations of H_2O_2 is taken as further evidence for this reaction.

A word of caution should be added at this point. Our study was intended to synthesize and employ a new relay compound for e^-_{CB} photogenerated in titanium dioxide. A complete study of the h^+_{VB} reactions including isotopic labeling experiments and other sophisticated methods would be necessary to obtain positive proof for the occurrence of reaction 4. However, TiO_2–$Co^{II}TSP$ is a priori not a suitable catalyst for a light-induced water-splitting experiment as its high affinity toward molecular oxygen predetermines the material to transfer electrons to O_2 and thus to "short-circuit" water splitting. As pointed out earlier (see Experimental Section), analysis of the aqueous phase from a suspension of the hybrid catalyst revealed traces of organic material (remainders of the synthesis) which apparently leached off the particles' surfaces. Reaction 10 therefore has to be discussed as an alternative channel for h^+_{VB}

$$2h^+_{VB} + D \rightarrow D(-2H) + 2H^+_{aq} \qquad (10)$$

where D represents any organic electron donor molecule. Photolysis experiments with the thoroughly washed powder (where traces of surface contaminants were no longer detectable) showed, however, that H_2O_2 was still produced with comparable quantum yields and even higher steady-state concentrations ($\cong$25 μM). Hence, water oxidation by valence band holes still presents an attractive and possible pathway but has not been positively proven by this study.

No loss of the catalyst is observed in any of the experiments described above. $Co^{II}TSP$, which is chemically bound to the surface of TiO_2, proved to be resistant to H_2O_2 in concentrations up to 0.05 M for several days over almost the whole pH range. An experiment at pH 0 (HCl) and 1 M H_2O_2 indicates a slow destruction of the catalyst over 72 h by a bleaching of its color. A homogeneous aqueous solution of $Co^{II}TSP$ is extremely sensitive to the presence of high concentrations of H_2O_2.[46] Figure 8 shows the depletion of 2 μM $Co^{II}TSP$ at pH 4.6 (as monitored by its absorbance at 670 nm) after 0.037 M H_2O_2 has been added to its solution. An aqueous solution of the copper analogue, $Cu^{II}TSP$, seems to be more resistant toward H_2O_2 in that no absorption change is observed over a period of 2 h under otherwise identical conditions (dashed line in Figure 8). The pH dependence of the observed rate of decomposition by H_2O_2 is indicated in Table III. While the number of data points is not sufficient to decide whether there is a maximum in rate around pH 4.6, there is strong evidence for a pronounced decrease in the rate of decomposition by hydrogen peroxide at alkaline pH. Furthermore, the rate significantly decreases as the ionic strength of the solution is increased.

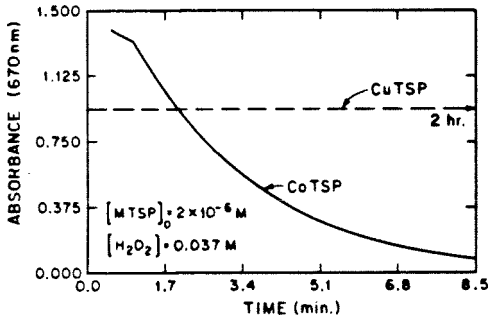

Figure 8. Optical absorption at 670 nm measured in a 10-cm cell after mixing 2×10^{-6} M $Co^{II}TSP$ with 0.037 M H_2O_2 or 2×10^{-6} M $Cu^{II}TSP$ with 0.037 M H_2O_2, respectively (aerated aqueous solutions at pH 4.6).

TABLE III: First-Order Rate Constant k for the Decomposition of $Co^{II}TSP$ by H_2O_2 at Various pH and Constant Ionic Strength (10^{-2} M)[a]

pH	k, s^{-1}
1.9	2.6×10^{-7}
4.6	3.4×10^{-7}
12.0	1.2×10^{-8}

[a] For other experimental conditions see Figure 8.

The following mechanism is suggested for the decomposition of $Co^{II}TSP$ in homogeneous solution:

$$Co^{II}TSP + H_2O_2 \rightarrow Co^{III}TSP + OH^- + OH^\bullet \quad (11)$$

$$Co^{III}TSP + OH^\bullet \rightarrow \text{decomposition products} \quad (12)$$

$$H_2O_2 + OH^\bullet \rightarrow HO_2^\bullet + H_2O \quad (13)$$

$$HO_2^\bullet \leftrightarrow O_2^{\bullet-} + H^+_{aq} \quad (14)$$

$$Co^{II}TSP + HO_2^\bullet/O_2^{\bullet-} \rightarrow \text{decomposition products} \quad (15)$$

The initial Fenton type reaction[54] produces $OH^\bullet$ radicals which could either attack the ligands of the semioxidized $Co^{III}TSP$ intramolecularly (reaction 12) or lead to the formation of superoxide $HO_2^\bullet/O_2^{\bullet-}$ [55,56] via reactions 13 and 14 which in turn destroys the parent molecule (reaction 15).[57] If, however, copper is the central atom, an initial attack via the reaction

$$Cu^{II}TSP + H_2O_2 \rightarrow Cu^{III}TSP + OH^- + OH^\bullet \quad (16)$$

is energetically unlikely. Furthermore, it is inhibited since tetragonal Cu(II) complexes with a tetradentate ligand, such as TSP, are known to be catalytically inactive.[46b] $Co^{II}TSP$, on the other hand, has two coordination sites available for the initial H_2O_2 attack. In the case of the surface complex, TiO^-–$Co^{III}TSP$–$O_2^{\bullet-}$, attack of H_2O_2 is prevented since there are no free coordination sites. The slow destruction of the hybrid catalyst by hydrogen peroxide observed at pH 0 is consistent with this explanation because of the reduced stability of the surface complex toward H_2O_2 as the TiO^- groups are protonated. The increased stability of aqueous $Co^{II}TSP$ against the destructive action of H_2O_2 at high pH (see Table III) is hence understood by the formation of the octahedral complex $(HO^-)Co^{III}TSP(O_2^{\bullet-})$ (reactions 6 and 7), whereas the formation of the dimer via

$$2Co^{II}TSP \leftrightarrow [Co^{II}TSP]_2 \quad (17)$$

should also hinder the attack by H_2O_2. Since equilibration via (17) requires the reaction of two doubly negatively charged species with each other, it is strongly favored at high ionic strength, thus explaining the marked decrease of the observed $Co^{II}TSP$ decomposition rate as the salt concentration is increased.

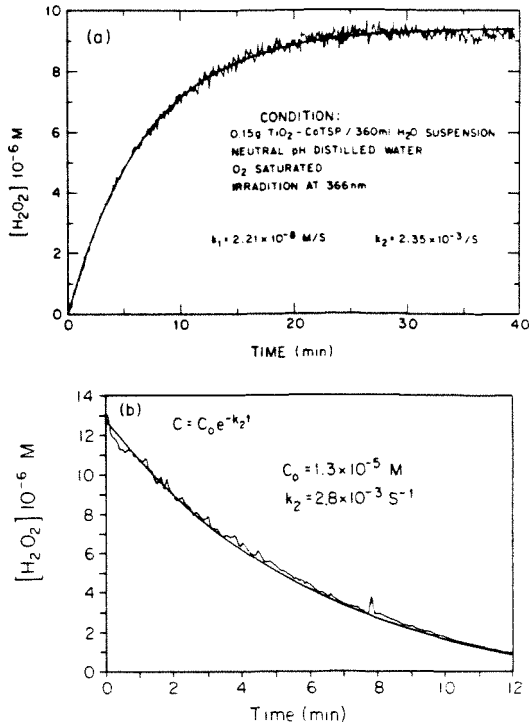

Figure 9. (a) Mathematical fit (solid curve) to the experimental H_2O_2 formation curve (Figure 4) according to the kinetic model derived in the discussion (eq 24). Parameters k_1 and k_2 yielding the best fit are shown. (b) Mathematical fit (solid curve) to the experimental H_2O_2 decay curve (Figure 5) using an exponential equation. k_2 is the parameter yielding the best fit.

The high yield and rate of H_2O_2 depletion upon the illumination of aqueous P25–TiO_2 suspensions (cf. Table II) are a striking result which can possibly be explained by a free radical mechanism.[58,59]

$$H_2O_2 + e^-_{CB} \rightarrow OH^- + OH^\bullet \quad (18)$$

$$H_2O_2 + h^+_{VB} \rightarrow H^+ + HO_2^\bullet \quad (19)$$

$$OH^\bullet + H_2O_2 \rightarrow H_2O + HO_2^\bullet \quad (20)$$

$$HO_2^\bullet + HO_2^\bullet \rightarrow H_2O_2 + O_2 \quad (21)$$

Only one photon is thus required to deplete two hydrogen peroxide molecules, leading to an efficiency of $(0.70/2) \times 100\% = 35\%$ for this process. All results with the hybrid catalyst, on the other hand, suggest that free radical intermediates are not involved in the reaction mechanism. Formation of $OH^\bullet$ and $HO_2^\bullet$ have led to the irreversible destruction of $Co^{II}TSP$,[57] but this was not observed. The stable dioxygen complex which we proposed as the active electron relay (Figure 7) only dissociates after two e^-_{CB} have been transferred via the cobalt center to the ligand, resulting in the release of H_2O_2 and OH^-, respectively, thus explaining the difference in reactivity between plain TiO_2 and the hybrid catalyst.

(c) *Kinetic Analysis.* In order to analyze the kinetic data of Figures 4 and 5, we consider all possible two-electron-transfer steps as follows:

$$O_2 + 2H^+_{aq} + 2e^-_{CB} \xrightarrow[Co^{II}TSP]{k_a} H_2O_2 \quad (22)$$

$$H_2O_2 + 2H^+_{aq} + 2e^-_{CB} \xrightarrow[Co^{II}TSP]{k_b} 2H_2O \quad (23)$$

(55) Haber, F.; Weiss, J. *Proc. R. Soc. London, Ser. A* **1934**, *147*, 332.
(56) Weinstein, J.; Bielski, B. H. J. *J. Am. Chem. Soc.* **1979**, *101*, 38.
(57) Peretz, P.; Solomon, D.; Weinraub, D.; Faraggi, M. *Int. J. Radiat. Biol. Relat. Stud. Phys., Chem. Med.* **1982**, *42*, 449.
(58) Rives-Arnau, V. *J. Electroanal. Chem.* **1985**, *190*, 279.
(59) Bielski, B. H. J.; Cabelli, D. E.; Arudi, R. L.; Ross, A. B. *J. Phys. Chem. Ref. Data* **1985**, *14*, 1041.

$$H_2O_2 + 2h^+_{VB} \xrightarrow{k_c} O_2 + 2H^+_{aq} \quad (9)$$

$$2H_2O + 2h^+_{VB} \xrightarrow{k_d} H_2O_2 + 2H^+_{aq} \quad (4)$$

(All above reactions are "overall" processes which do not imply mechanistic detail.) If the concentrations of O_2 and H^+_{aq} are taken to be constant and a steady-state concentration of e^-_{CB} and h^+_{VB} is assumed during illumination, the overall production of H_2O_2 can be described by the following kinetic equation

$$d[H_2O_2]/dt = k_1 - k_2[H_2O_2] \quad (24)$$

where k_1 is a lumped pseudo-zero-order constant reflecting the sum of eq 22 and 4 and k_2 is a lumped pseudo-first-order constant reflecting the sum of eq 23 and 9. Integration of (24) yields a best fit of the kinetic data as shown in Figure 9. The initial zero-order formation of H_2O_2 under O_2 saturation leads to $k_1 = 2.2 \times 10^{-8}$ M/s (see Figure 9a) which can be used to compute a quantum yield of $\phi_0 = 0.48$. Values of ϕ_0 are listed in Table I for different catalysts and experimental conditions and have already been discussed. At steady state ($d[H_2O_2]/dt = 0$) the depletion rate can be calculated via

$$k_2^{ss} = k_1/[H_2O_2] = 2.4 \times 10^{-3}\ s^{-1}$$

Values for k_2^{ss} do not represent "real" rate constants since they always include the photon flux into the sample. While some of the differences between various measurements (last column in Table I) are therefore simply due to different light intensities, the apparent increase from 0.9×10^{-3} to $1.7 \times 10^{-3}\ s^{-1}$ as the dioxygen concentration is decreased can be mechanistically explained. It has already been pointed out that a cobalt–superoxide complex is stable toward the attack of H_2O_2; however, reaction 23 requires that H_2O_2 enters the coordination sphere of the metal center to be significant. Reaction 25 is therefore envisioned to compete

$$TiO^-–Co^{II}TSP–H_2O + H_2O_2 \rightarrow TiO^-–Co^{III}TSP–OH + OH^- \quad (25)$$

with the uptake of O_2 in the catalytic cycle (cf. left-hand part of Figure 7) and will thus be favored at lower O_2 content. Absorption of two photons will then lead to the release of another OH^-. The absence of any complex formation with hydrogen peroxide in the dark which is strongly suggested by our results can easily be explained since the light-dependent cycle (left side in Figure 7) is a prerequisite for reaction 25.

Values for k_2 can also be calculated from the depletion rate of H_2O_2 (the solid line in Figure 9b yields $k_2 = 2.8 \times 10^{-3}\ s^{-1}$); they are listed in the last column of Table II. Even though these k_2^d values agree reasonably well with k_2^{ss} from the steady-state calculations, a quantitative comparison is not warranted since the experimental conditions differed too much.

Conclusion

It has been demonstrated that $Co^{II}TSP$ can be employed as an efficient electron relay on TiO_2 provided it is chemically bound to the semiconductor surface. The formation of octahedral cobalto complexes involving O^- groups from the oxide support is strongly indicated. This hybrid complex imparts in the high degree of chemical stability and results in efficient electron-transfer properties. The reduction of dioxygen to yield hydrogen peroxide is photocatalyzed by this hybrid catalyst upon bandgap irradiation of the TiO_2 with extremely high quantum yields. Since the superoxide adduct of $Co^{III}TSP$ is very stable, two-electron-transfer steps are strongly favored and no evidence of free radical intermediates has been observed. The formation of H_2O_2 by the oxidation of water by photogenerated holes[1-7,28-36] could not be established unambiguously. Indirect evidence in favor of this reaction stems from the formation of steady-state concentrations of H_2O_2 up to 25 μM in the absence of any detectable hole scavenger and from the observation that long-lived holes do not exist. Hydrogen peroxide and molecular oxygen were both measured as photoproducts, suggesting that surface adsorption of these molecules does not present a serious problem in the investigated systems. The polarographic method of the oxidase probe employed in this study allows the in situ observation of H_2O_2 formation and decay with a detection limit of 10^{-7} M without the addition of any interfering enzymes or chemicals. The mechanism of the photocatalytic reduction of O_2 and the depletion of H_2O_2 by use of the hybrid catalyst has been discussed in detail.

We finally like to emphasize that TiO_2–$Co^{II}TSP$ may have a considerable potential as an oxidation catalyst in oxic environments since the reduction of O_2 yields H_2O_2, which is a better oxidant, and the simultaneously formed h^+_{VB} are extremely powerful oxidants anyway. Initial experiments on the oxidation of SO_3^{2-} indeed suggest that quantum yields close to unity can be achieved reproducibly with this catalyst.[60]

Acknowledgment. We gratefully acknowledge the financial support of the U.S. EPA (Grants CR812356-01-0 and R811612-01-0), and in particular we want to thank Drs. Donald Carey and Marcia Dodge for their support. Free samples of titanium dioxide P25 from the Degussa Corp. were highly appreciated.

(60) Hong, A. P.; Bahnemann, D. W.; Hoffmann, M. R., unpublished data.

Chapter 7

Co(II) Tetrasulfophthalocyanine on Titanium Dioxide: II. The Kinetics and Mechanisms of the Photocatalytic Autoxidation of Aqueous Sulfur Dioxide

Andrew Hong, Detlef Bahnemann, Michael Hoffmann

J. of Phys. Chem., 1987, accepted

Abstract

Co(II) 4, 4', 4'', 4'''−tetrasulfophthalocyanine, Co(II)TSP, covalently linked to the surface of titanium dioxide particles, TiO_2-CoTSP, is shown to be an effective photocatalyst for the oxidation of sulfur(IV) to sulfur(VI) in aqueous suspensions. Upon band-gap illumination of the semiconductor, TiO_2, conduction band electrons and valence band holes are separated; the electrons are channeled to the bound Co(II)TSP complex resulting in the reduction of dioxygen, while the holes react with adsorbed S(IV) to produce S(VI) in the form of sulfate. The formation of S(V) radicals indicates that the reaction proceeds via successive one-electron transfers. Quantum yields in excess of unity were observed and attributed to desorption of $SO_3^{\cdot -}$ from the TiO_2 surface and subsequent initiation of a homogeneous free-radical chain reaction. Observed quantum yields between 0.5 and 300 depend on the concentration and nature of free-radical inhibitors present in the suspension. A kinetic model that integrates the photon absorption properties of the solid, the heterogeneous redox reactions on the catalyst surface, and the homogeneous reactions of S(IV), is presented.

Introduction

We have recently reported[1] the synthesis of a hybrid catalyst of Co(II) tetrasulfophthalocyanine (Co(II)TSP) covalently linked to the surface of TiO_2 (i.e., TiO_2-CoTSP) and have shown that the bound metal complex, Co(II)TSP, acts as an efficient electron relay in promoting photo-assisted redox reactions on the surface of TiO_2. The hybrid TiO_2-CoTSP catalyst appears to be highly efficient for a wide range of oxidation reactions.

The oxidation of aquated sulfur dioxide (Eq. 1) is known to proceed via either 1-electron radical or 2-electron non-radical pathways.[2-8]

$$HSO_3^- + \frac{1}{2}O_2 \longrightarrow HSO_4^- \tag{1}$$

Backström[9] proposed the following free-radical chain mechanism for metal-catalyzed autoxidation of S(IV):

$$M^{n+} + SO_3^{2-} \longrightarrow M^{(n-1)+} + SO_3^{\cdot-} \tag{2}$$

$$SO_3^{\cdot-} + O_2 \longrightarrow SO_5^{\cdot-} \tag{3}$$

$$SO_5^{\cdot-} + SO_3^{2-} \longrightarrow SO_5^{2-} + SO_3^{\cdot-} \tag{4}$$

$$SO_5^{2-} + SO_3^{2-} \longrightarrow 2SO_4^{2-} \tag{5}$$

$$2SO_3^{\cdot-} \longrightarrow S_2O_6^{2-} \tag{6}$$

This mechanism has been modified[10-13] by others to account for photolytic initiation or to include other chain carriers such as $SO_4^{\cdot-}$, $O_2^{\cdot-}$, $HO_2^{\cdot}$, and $HO^{\cdot}$. Non-radical mechanisms have also been proposed; they involve the formation of an inner-sphere complex as a prelude to 2-electron transfer oxidation of S(IV):[14,15]

$$M^{n+} + SO_3^{2-} \rightleftharpoons MSO_3^{(n-2)+} \tag{7}$$

$$MSO_3^{(n-2)+} + SO_3^{2-} \rightleftharpoons M(SO_3)_2^{(n-4)+} \tag{8}$$

$$M(SO_3)_2^{(n-4)+} + O_2 \rightleftharpoons M(SO_3)_2O_2^{(n-4)+} \tag{9}$$

$$M(SO_3)_2 \cdot O_2^{(n-4)+} \longrightarrow M^{n+} + 2SO_4^{2-} \quad (10)$$

Two-electron oxidation of S(IV) has also been observed with oxidants such as H_2O_2 [16] and O_3:[17]

$$HSO_3^- + H_2O_2 \longrightarrow H^+ + SO_4^{2-} + H_2O \quad (11)$$

$$HSO_3^- + O_3 \longrightarrow H^+ + SO_4^{2-} + O_2 \quad (12)$$

Previous studies[18,19] in this laboratory, using well-defined homogeneous catalysts such as Co(II)TSP have suggested that the metal-catalyzed reaction proceeds via a 2-electron transfer from sulfite to a preformed octahedral cobalt(III)-sulfito-superoxide complex. In general, there are large discrepancies in the reported reaction orders of the reactants and in the observed rate laws for metal-catalyzed S(IV) autoxidation.[2,3,20]

The heterogeneous photocatalytic oxidation of sulfite in a suspension of TiO_2 has been reported previously by Frank and Bard.[21] Even though they reported that TiO_2 was catalytically active, no kinetic details were given. In our study, the concentrations of S(IV), TiO_2-CoTSP, O_2, and pH were varied over a wide range in order to determine the complex reaction kinetics. We have blended together, in a model, a currently accepted homogeneous mechanism, our present and previous findings on TiO_2-CoTSP, CoTSP, and S(IV) oxidation. Our principal objectives are to provide further insight into the photochemical properties of the TiO_2-Co(II)TSP hybrid catalyst and to examine in greater detail the mechanisms for the heterogeneous photocatalytic oxidation of S(IV).

Pathways for S(IV) oxidation are currently of great interest due to the important role that SO_2 plays in cloud-, fog-, rainwater acidification.[3]

Experimental Section

In our previous paper in this series,[1] experimental details such as the quality of the water and the chemicals used, the synthesis and characterization of the hybrid catalyst, the analytical procedures used to measure H_2O_2, the illumination apparatus, the procedure for chemical actinometry, and the spectroscopic equipment were described.

Kinetic experiments were carried out in a 60 ml reactor with an optical path length of 5.5 cm equipped with quartz windows and openings for gas purging and ion selective electrodes. The incident photon flux at wavelength 366 nm was determined to be 1.3×10^{-5} M/min and remained stable over the period of the study. The hybrid catalyst was maintained in suspension by magnetic stirring. 4 μM EDTA was used in all experiments to reduce background trace-metal catalysis. Sodium phosphate, borate, and perchlorate salts were employed to maintain pH and a constant ionic strength of 0.1 M in all experiments. Sulfur(IV) concentrations during the course of the reaction were followed by withdrawing aliquot and removing the suspended solids with a 0.2 μm membrane filter; the resulting supernatant was analyzed for S(IV) according to the colorimetric method of Humphrey et al.[22] Kinetic data were obtained by following the disappearance of S(IV) as a function of time over 30 % to 80 % of the reaction. Temperature remained constant at 23 ±1 °C during all kinetic runs. The oxygen concentration was varied by continuously bubbling gas mixtures of O_2/N_2 that were regulated by Porter Model DFC-1400 digital flow controllers. The chloride concentration was measured with an Orion Model 93-17 chloride electrode connected to a Model 901 microprocessor ionalyzer. A Dionex Model 2020i ion chromatograph equipped with a mobile-phase ion chromatography (MPIC) column was used to detect the S(IV) oxidation products (i.e., SO_4^{2-} and $S_2O_6^{2-}$).[23] Titanium dioxide P25 powder (Degussa) and its surface-modified hybrid derivative (abbreviated as TiO_2-CoTSP) were used in all experiments.

Throughout this paper, the term S(IV) refers to the equilibrium species of S(IV) (i.e., $SO_2\cdot H_2O$, HSO_3^-, and SO_3^{2-}); S(V) refers to $SO_3^{\cdot-}$ and S(VI) refers to H_2SO_4 and its conjugate bases. In this paper, HSO_3^- and $SO_5^{\cdot-}$ are used in the proposed mechanism to denote principal S(IV) and dominant radical species, respectively, at slightly acidic pH (e.g., pH 5);* the involvement of appropriate conjugate forms at various pH is implied.

* The pK_{a1} and pK_{a2} for S(IV) are 1.8 and 7.2, respectively. The pK_a's for HSO_3 and $HSO_5^{\cdot}$ are < 2.[11]

Results and Discussion

A typical [S(IV)] vs. time profile for a reaction mixture containing 3 mM S(IV) and 50 mg/L TiO_2-CoTSP at pH 9.2 under illumination at 366 nm is shown in Figure 1. Sulfate was determined by ion chromatography both qualitatively and quantitatively to be the only reaction product. A very rapid disappearance of SO_3^{2-} is apparent in Fig. 1. An initial reaction rate, ν_o, which was obtained from the initial slope of this decay curve, was determined to be 4.2×10^{-4} M/min. An "initial" quantum yield, Φ, of 33 was obtained by taking the quotient of ν_o and photon flux (1.3×10^{-5} M/min) as determined by chemical actinometry. Initial rate data and quantum yields for other reaction conditions were obtained in the same manner.

Before a detailed assessment of the photocatalytic activity of the TiO_2-CoTSP hybrid was made, experiments were performed to identify possible side reactions, such as homogeneous trace metal catalysis, direct photolysis, or photocatalysis by TiO_2 or CoTSP alone. Table I provides these comparisons. Entries 1 and 2 reveal that trace metal catalysis of the sulfite oxidation still occurs, but it has been suppressed by the use of EDTA to ensure that its contribution to the overall kinetics as compared with irradiated suspensions of TiO_2-CoTSP is negligible, i.e., $\leq 5\%$. Direct photolytic initiation of chain reactions of S(IV) at 366 nm, the wavelength employed in all subsequent illumination experiments, does not occur (compare second columns of entries 1 and 2). Entries 3 and 4 indicate that homogeneous CoTSP is a very active catalyst for S(IV) oxidation, especially at high pH. However, it was found that CoTSP decomposed during these reactions, thereby limiting the usefulness of this homogeneous catalyst. The extremely high catalytic behavior of homogeneous CoTSP, which involves S(IV) as a ligand in one of the apical sites of the complex, differs from the present hybrid analog, in which the same apical site is occupied by a surface hydroxy group (compare entry 3 with entry 7). The homogeneous catalysis of CoTSP toward S(IV) oxidation has been discussed previously.[18-20] Comparison of entry 5 with entry 6, and similarly of entry 7 with entry 8, confirm that the oxidation of S(IV) in

the presence of TiO_2 as a heterogeneous catalyst proceeds primarily via a photo-assisted pathway.

It should be noted at this point that in the absence of light the background rates (i.e., the oxidation of sulfite catalyzed by trace-metal impurities of the salts used to adjust ionic strength and as buffers or by TiO_2/TiO_2-CoTSP) were examined and found to be $\leq$ 10 % of the rate when experiments were carried out under illumination (the only exception was observed at pH 12.3 and will be discussed below). The dark (ambient room light) reaction rates followed similar dependencies as those obtained when light was present; the values given in Table I for TiO_2 and TiO_2-CoTSP represent upper limits (e.g., $\nu_{dark} = 5 \times 10^{-7}$ M/min was observed when an oxygenated suspension containing 50 mg/L TiO_2-CoTSP and 0.1 mM S(IV) was illuminated). Since the error limits of the individual experiments were found to be in the order of $\pm$15 %, no attempt was made to correct mathematically the experimental data to account for the contribution of the dark reactions.

The photo-assisted oxidation of S(IV) proceeds with a quantum yield Φ greater than unity; this suggests a free radical pathway. Hayon et al.[10] proposed the following mechanism for the photo-initiated S(IV) oxidation in aqueous solution:

$$HSO_3^- \xrightarrow{h\nu} SO_3^{\cdot -} + H^+ + e_{aq}^- \tag{13}$$

$$SO_3^{\cdot -} + O_2 \xrightarrow{k_2} SO_5^{\cdot -} \tag{14}$$

$$SO_5^{\cdot -} + HSO_3^- \xrightarrow{k_3} SO_4^{\cdot -} + SO_4^{2-} + H^+ \tag{15}$$

$$SO_4^{\cdot -} + HSO_3^- \xrightarrow{k_4} SO_4^{2-} + SO_3^{\cdot -} + H^+ \tag{16}$$

$$SO_3^{\cdot -} + SO_3^{\cdot -} \xrightarrow{k_5} S_2O_6^{2-} \tag{17}$$

$$SO_4^{\cdot -} + SO_4^{\cdot -} \xrightarrow{k_6} S_2O_8^{2-} \tag{18}$$

$$SO_5^{\cdot -} + SO_5^{\cdot -} \xrightarrow{k_7} S_2O_8^{2-} + O_2 \tag{19}$$

We envision the heterogeneous photochemical processes occurring on the TiO_2-CoTSP surface as illustrated in Figure 2. Three main catalytic cycles are involved. The central cycle (steps a through e) depicts the formation and desorption of sulfite radicals by valence band holes. The reactions occurring at the metal center in the presence of molecular oxygen have been extensively studied[1] and are taken unaltered from the literature. Two SO_3^- are formed during one catalytic cycle, which involves the absorption of two photons. They can subsequently enter the solution to initialize chain reactions as indicated in reactions (14) to (19). The right cycle (steps i through k, d, e) describes the trapping and elimination of chain carrying radicals by the catalyst surface. Stabilization of radical species by surface sites of oxide materials has been documented in literature.[24-26] Ongoing research on S(IV) oxidation with colloidal TiO_2 or Fe_2O_3, both of which possess high surface areas, also indicates such a stabilizing phenomenon[27] (see also later part of the discussion). The left cycle (steps a, f through h) indicates an alternative two-electron pathway of oxidation that does not require light (dark reaction). Previous work of CoTSP supported on non-photoactive material[20,28] has shown a mode of oxidation similar to that of the homogeneous CoTSP. This is reflected by the activity of TiO_2-CoTSP under ambient light (entry 7 of Table I). The elementary reactions involved in the three cycles are summarized as follows:

a. A sulfur(IV) molecule adsorbs to a surface site replacing a water molecule while O_2 is bound to the metal center yielding cobalt(III) superoxide.

b. An electron/hole pair is created in the semiconducting solid upon absorption of a photon.

c. The conduction band electron is transferred to O_2, leading to the formation of H_2O_2. The adsorbed S(IV) meanwhile fills the separated hole with one electron and the resulting S(V) subsequently desorbs from the surface and diffuses into the bulk solution.

d, e. Absorption of a second photon generates an additional S(V) radical, and Co(III)TSP reverts to its original state.

f, g. Aqueous S(IV) is oxidized to S(VI) by bound Co(III)-superoxide via a two-electron transfer from sulfur to the cobalt center analogous to the established action of CoTSP in homogeneous solution; at the same time one electron shuttles back to the Co center.

h. The two electron process produces H_2O_2 as a by-product.

i. Intermediate sulfur radicals can compete with HSO_3^- for surface sites.

j, k. The adsorbed sulfur radicals can then be further oxidized to S(VI) by photo-generated valence band holes.

As illustrated in the center cycle of Figure 2, the process of initiating the chain carrying species, SO_3^-, involves the adsorption of S(IV) on the oxide surface, followed by the absorption of photons, and the electron transfer from S(IV) to h^+. An "intrinsic" quantum yield, ϕ, can be defined for the S(IV) $\rightarrow h^+$ electron transfer. A rate equation for S(V) initiation should reflect these processes. Assuming that adsorption of S(IV) can be described by a Langmuir isotherm and that S(IV) is the only species that is adsorbed to a significant extent, the fraction of surface site θ covered with S(IV) can be written as follows:

$$\ell + HSO_3^- \overset{K}{\rightleftharpoons} \ell\text{–}HSO_3^- \tag{20}$$

$$\ell + \ell\text{–}HSO_3^- = \ell_T \tag{21}$$

$$\theta = \frac{\ell\text{–}HSO_3^-}{\ell_T} = \frac{K[HSO_3^-]}{1 + K[HSO_3^-]} \tag{22}$$

where ℓ, ℓ-HSO_3^-, ℓ_T and K denote vacant site, S(IV) occupied site, total surface site, and S(IV) adsorption equilibrium constant, respectively. The absorption of photons is given by:

$$\text{Absorbed photon flux} = \beta\left(1 - e^{-\gamma(M)}\right) \tag{23}$$

where β denotes the incident photon flux (M/min), (M) the catalyst concentration (g/L), and γ a multiple of the apparent absorptivity of the solid (L/g). It follows that the rate equation for S(V) initiation ν_1 can be written as:

$$\nu_1 = \phi\beta\left(1 - e^{-\gamma(M)}\right)\left(\frac{K[HSO_3^-]}{1 + K[HSO_3^-]}\right) \tag{24}$$

This rate equation has the correct form and physical meaning when either (M) or [S(IV)] is very large or small. More specifically, the rate of initiation will increase as the solid content increases until it reaches a saturation limit for which all incoming photons are intercepted. After this point a further increase in solid content results in no further increase in rate. Similarly, the rate will increase with increasing [S(IV)] until all available surface sites are occupied by S(IV).

Reactions 14–16 are the proposed chain-propagating steps in the solution phase. If reaction 15 is assumed to be rate-limiting, the rate expression for the depletion of S(IV) can be written as Equation 25. And the rate equations for each of the chain carrying species are expressed as Equations 26–28:

$$\nu = k_3[SO_5^{\cdot-}][HSO_3^-] \tag{25}$$

$$\frac{d[SO_3^{\cdot-}]}{dt} = \phi\beta\left(1 - e^{-\gamma(M)}\right)\left(\frac{K[HSO_3^-]}{1 + K[HSO_3^-]}\right) - k_2[SO_3^{\cdot-}][O_2] + k_4[SO_4^{\cdot-}][HSO_3^-] \tag{26}$$

$$\frac{d[SO_4^{\cdot-}]}{dt} = k_3[SO_5^{\cdot-}][HSO_3^-] - k_4[SO_4^{\cdot-}][HSO_3^-] \tag{27}$$

$$\frac{d[SO_5^{\cdot-}]}{dt} = k_2[SO_3^{\cdot-}][O_2] - k_3[SO_5^{\cdot-}][HSO_3^-] - 2k_7[SO_5^{\cdot-}]^2 \tag{28}$$

Reaction 19 is assumed to be the chain-terminating reaction. McElroy has calculated[13] a steady-state free-radical concentration of $[SO_5^{\cdot-}]_{ss}$ that is at least 1000 times higher than all other free radical intermediates involved in the chain. As suggested (right cycle of

Figure 2), radical intermediates can be removed by further oxidation at the surface; these processes are described as follows:

$$SO_5^{\cdot -} + \ell \overset{K'}{\rightleftharpoons} \ell\text{–}SO_5^{\cdot -} \tag{29}$$

$$\ell\text{–}SO_5^{\cdot -} + h^+_{VB} \xrightarrow{k'_8} \ell\text{–}SO_3 + O_2 \tag{30}$$

$$\ell\text{–}SO_3 + H_2O \longrightarrow \ell + SO_4^{2-} + 2H^+ \tag{31}$$

where K′ is the adsorption equilibrium constant for $SO_5^{\cdot -}$. $SO_5^{\cdot -}$ is again chosen as the primary species to be oxidized because of its high steady-state concentration. The rate equation for this additional sink can be rewritten as:

$$\nu_8 = -k_8(M)[SO_5^{\cdot -}] \tag{32}$$

where k_8 ($=k'_8K'$) is a pseudo-order constant. Since $[SO_5^{\cdot -}]_{ss}$ is very low,[13] its adsorption to the surface will most likely lie in the linear portion of the adsorption isotherm (i.e., $K'[SO_5^{\cdot -}] \ll 1$.) Therefore, Equation 28 may be rewritten as:

$$\frac{d[SO_5^{\cdot -}]}{dt} = k_2[SO_3^{\cdot -}][O_2] - k_3[SO_5^{\cdot -}][HSO_3^-] - 2k_7[SO_5^{\cdot -}]^2 - k_8(M)[SO_5^{\cdot -}] \tag{33}$$

If a steady-state condition is assumed for each of the chain carriers,

$$\frac{d[SO_3^{\cdot -}]}{dt} = \frac{d[SO_4^{\cdot -}]}{dt} = \frac{d[SO_5^{\cdot -}]}{dt} = 0 \tag{34}$$

it can be shown that the following rate expression is obtained:

$$\nu' = -\frac{k_3k_8}{4k_7}(M)[HSO_3^-] + [HSO_3^-]\sqrt{\left(\frac{k_3k_8}{4k_7}\right)^2(M)^2 + \frac{k_3^2\phi\beta}{2k_7}\left(1 - e^{-\gamma(M)}\right)\left(\frac{K[HSO_3^-]}{1 + K[HSO_3^-]}\right)} \tag{35}$$

The catalytic reaction of the supported CoTSP via the 2-electron pathway (left cycle of Figure 2), and its rate expression can be written as follows:

$$Co(III)TSP(O_2^{\cdot -})_S + HSO_3^- + H_2O \xrightarrow{k'_9} Co(II)TSP(HO_2^-)_S + SO_4^{2-} + 2H^+ \tag{36}$$

$$\nu_9 = k'_9[HSO_3^-][CoTSP]_S \overset{or}{=} k'_9\alpha[HSO_3^-](M) \tag{37}$$

where α denotes the ratio of [CoTSP] to (TiO_2-CoTSP) of the hybrid catalyst. The final rate expression should be modified to incorporate these contributions as follows:

$$\nu = k_9[HSO_3^-](M) - \frac{k_3 k_8}{4k_7}(M)[HSO_3^-] + [HSO_3^-]\sqrt{\left(\frac{k_3 k_8}{4k_7}\right)^2 (M)^2 + \frac{k_3^2 \phi\beta}{2k_7}\left(1 - e^{-\gamma(M)}\right)\left(\frac{K[HSO_3^-]}{1 + K[HSO_3^-]}\right)} \tag{38}$$

$$\text{or} \quad \nu = b_1(M) + b_2\left(-(M) + \sqrt{(M)^2 + b_3\left(1 - e^{-b_4(M)}\right)}\right) \tag{39}$$

where $k_9 = k'_9\alpha$; b_1, b_2, b_3, and b_4 are lumped pseudo-order kinetic constants when [S(IV)] is held constant.

Figures 3a & b show the results of initial observed rate vs. catalyst concentration at various pH values. Figure 3a indicates a rapid increase in rate at low catalyst concentrations, followed by a gradual decrease as more catalyst is added. This behavior suggests that an increase in the solid loading results in increased absorbance of the incoming photons, which in turn provides a greater amount of valence band holes required for initiation of $SO_3^{\cdot-}$ radicals. However, the increase of absorbance eventually leads to the limit that virtually all incoming photons are intercepted and the high surface area acts only to adsorb and terminate reactive free-radical intermediates, thus shortening the chain-length of the reaction. Hence, a maximum rate is expected and it is observed around 50 mg/L. The line curves at pH 4.5 through 9.2 represent the model fit according to Equation 39. Experiments performed at high pH are consistent with the results expected for negatively charged surface* and a negatively charged adsorbate. These include reactions 20 and 29.

---

* pK_1^s (bulk-$TiOH_2^+ \rightleftharpoons$ bulk-TiOH $+H^+$) = 5.4;

pK_2^s (bulk-TiOH $\rightleftharpoons$ bulk-TiO^- + H^+) = 6.4; pH_{zpc} = 5.9 for TiO_2 as rutile.[29]

When reaction 29 is neglected (i.e., SO_5^- is repelled by the negatively charged surface) the following rate expression for high pH (e.g., pH 12.3) is obtained:**

$$\nu_{pH\,12.3} = k_9(M)[SO_3^{2-}] + k_3[SO_3^{2-}]\sqrt{\frac{\phi\beta}{2k_7}\left(1 - e^{-\gamma(M)}\right)\frac{K[SO_3^{2-}]}{1 + K[SO_3^{2-}]}} \qquad (40)$$

$$\text{or} \quad = b_1(M) + b_2\sqrt{1 - e^{-b_4(M)}} \qquad (41)$$

where b_1, b_2, and b_4 are lumped pseudo-order kinetic constants. Figure 3b now shows a rapid rise in rate at low catalyst content, followed by a first-order increase with catalyst as expected when Equation 29 no longer involves in the destruction of reactive intermediates. The overall lower reaction rate is due to the less favorable adsorption of SO_3^{2-} to the negatively charged surface (Eq. 20). The curve for pH 12.3 represents the model fit according to Equation 41.

The lumped kinetic coefficients and their definitions are listed in Table II. It should be noted that b_1, b_2, b_3 cannot be reduced to elementary rate constants. Given that $b_4 = 49$, it can be determined that, at (M) = 50 mg/L, 91 % of the photons are absorbed. With an optical path length of 5.5 cm, the catalyst's absorptivity is determined to be 3.9 L/g-cm. This value lies between 50 L/g-cm obtained for thin-film TiO_2[30] and 0.62 L/g-cm for colloidal TiO_2.[31] A lower absorptivity for the hybrid catalyst than that of the thin film value is explained by light scattering that reduces the number of available photons in the suspension. Of the several proposed pathways, it should be noted that the homogeneous chain mechanism is the major pathway for S(IV) oxidation. Calculations using the fitted b's for typical catalyst conditions (i.e., 50 mg/L) indicate that the 2-electron process illustrated on the left-hand side of Figure 2 contributes less than 0.6 % of the total rate from pH 4.5 to 9.2 and 4 % at pH 12.3.

** The dominant S(IV) species at pH 12.3 is SO_3^{2-}.

The rate expression can be rewritten to demonstrate the dependence of observed rate on [S(IV)]. When the fitted b's (e.g., at pH 4.5) together with catalyst concentration (50 mg/L) are substituted into equation 39, we see that $(M)^2 \ll b_3(1 - e^{-b_4(M)})$, $M \ll \sqrt{(M)^2 + b_3(1 - e^{-b_4(M)})}$, and $b_1(M) \ll b_2\left(-(M) + \sqrt{b_3(1 - e^{-b_4(M)})}\right)$; therefore, we can approximate Eq. 39 as:

$$\nu = \left(\frac{\phi\beta K k_3^2}{2k_7}\left(1 - e^{-\gamma(M)}\right)\right)^{0.5} [HSO_3^-]^{1.5} \qquad (42)$$

assuming $K[HSO_3^-] \ll 1$; at pH 12.3 an identical rate expression in terms of $[SO_3^{2-}]$ can be obtained from Eq. 41. Figure 4 shows the observed rate vs. [S(IV)] along with the fitted straight lines. The slopes of these van't Hoff plots indicate reaction orders of S(IV) and are 1.6, 1.3, 1.4 and 1.4 at pH 4.5, 7.0, 9.2, and 12.3, respectively. At pH 12.3 only [S(IV)] from 1 to 10 mM is fitted because, at lower concentrations, the reaction becomes so slow that the background oxidation, because of the 2-electron pathway or trace-metal catalysis, becomes significant. The presence of the 2-electron pathway will, in general, lower the observed reaction order. With this in mind, the determined reaction orders of S(IV) agree quite well with the expected value of 1.5 as predicted by Equation 42.

According to the proposed mechanisms and their resulting rate laws, the reaction rate is independent of the dissolved oxygen concentration. This prediction is confirmed by results shown in Figure 5. Very little oxidation occurs in experiments conducted under N_2. Coordinated dioxygen ($CoTSP(O_2)$) is needed to accept conduction-band electrons to make valence-band holes available for the formation of $SO_3^{\cdot-}$ radical. Molecular oxygen also reacts quickly with $SO_3^{\cdot-}$ during the chain propagation. Oxidation of S(IV) proceeds, otherwise, at constant rates over a range of $[O_2]$ 5 to 100 % saturation.

Figure 6 shows the effect of pH on the observed rate constant. A slow reaction rate is expected at high pH because of the charge repulsion of SO_3^{2-} by a negatively charged surface (pH_{zpc} for P25 $TiO_2 = 6.6$)[32]. The maximum rate occurs around pH 7. Similar pH dependencies have been noted in studies of the homogeneous photo-initiated free-radical

reactions.[10] Our observed pH dependence, which is similar to that of the homogeneous system, is consistent with the finding that chain reactions in the solution phase are the dominant pathway for S(IV) oxidation.

As shown in Figures 3, 4, and 6, $\Phi > 1$ are observed. This observation is consistent with a free-radical chain reaction pathway. To verify this mechanism, experiments have been conducted in the presence of radical scavengers such as ethanol and mannitol. Figure 7 shows that, in the presence of 1 mM ethanol, the observed quantum yield drops from 47 (see Figure 4) to 17. A further reduction to 0.57 is observed at 1 M ethanol. A theoretical quantum yield of 0.5 can be expected if one considers that 2 photons are required in order to oxidize one molecule of S(IV) to S(VI) via photo-generated valence holes and that all absorbed photons lead to a reaction. The quantum yield of 0.57 at high scavenger concentration suggests that TiO_2-CoTSP is an efficient oxidation catalyst. It should be noted that the reaction rate in the presence of 1 M ethanol reflects the oxidation of S(IV) mainly on the catalyst's surface; an identical experiment performed under ambient light shows a depletion rate less than 3 % of the illuminated one. Similar effects are seen with mannitol (see right entries of Table III).

We have proposed a photocatalytic cycle in which the photo-generated electrons and holes are channeled to the surface bound CoTSP and to the surface adsorbed S(IV) molecules, respectively. This results in the simultaneous formation of H_2O_2 from O_2 reduction and S(V) radical from S(IV) oxidation at their respective sites. To establish the activity of valence band hole, $CHCl_3$ is selected as an alternate electron donor. It has a 1-electron reduction potential of -1.4 eV[33] and therefore cannot be reduced by conduction band electrons (-0.4 eV)[34] at the CoTSP site. The only means of its transformation is through an initial oxidative attack by a valence hole (rxn 43), followed by an O_2 addition (rxn 44) and ultimately to the release of chloride ions (rxn 45).[35,36]

$$CHCl_3 + h^+_{VB} \longrightarrow CCl_3^{\cdot} + H^+ \qquad (43)$$

$$CCl_3^{\cdot} + O_2 \longrightarrow CCl_3O_2^{\cdot} \tag{44}$$

$$2CCl_3O_2^{\cdot} + 4H_2O \longrightarrow \xrightarrow{-H_2O_2} \longrightarrow 2CO_2 + O_2 + 6HCl \tag{45}$$

Figure 8a shows the release of Cl^- when suspensions of TiO_2 or the hybrid catalyst are irradiated in the presence of $CHCl_3$. While the concomitant formation of H_2O_2 (in micromolar level) during S(IV) oxidation cannot be measured because of its rapid reduction by S(IV), it can be readily detected in the case of $CHCl_3$ oxidation as shown in Figure 8b.

As reported previously,[1] H_2O_2 was photocatalytically formed and depleted during the illumination of an oxygenated suspension of TiO_2-CoTSP. A steady-state concentration of 5 μM of H_2O_2 was found. Therefore, the contribution of H_2O_2 toward the oxidation rate of S(IV) in the present study needs to be addressed. Hoffmann and Edwards[16a] have determined a second-order rate constant of 1.2×10^4 1/M-min for the reaction of H_2O_2 with S(IV) at pH 7. This value will yield a reaction rate ν_o of 1.2×10^{-6} M/min under the typical conditions of 1 mM S(IV), and 1 μM H_2O_2 ($[H_2O_2]$ is below its steady-state value in the initial period when ν_o for S(IV) oxidation is determined). Hence, the contribution of H_2O_2 toward the total rate of S(IV) oxidation (see Figure 4) is less than 1 %. At pH 12.3 where the rate of heterogeneous catalysis is minimal, the contribution of H_2O_2 is negligible because the reaction rate of H_2O_2 with S(IV) drops at least 4 orders of magnitude.

We have described the catalytic activity of the hybrid catalyst, TiO_2-CoTSP, toward S(IV) oxidation. Since the solid support, TiO_2, itself is photoactive (entry 6 of Table I), its catalytic activity needs to be addressed. A comparison of TiO_2 and TiO_2-CoTSP is given in Table III. Entry 1 indicates that TiO_2 is twice as active as TiO_2-CoTSP. However, the catalytic effect is reversed when free-radical inhibitors are present. This difference can be attributed to the different quantum efficiencies of the two catalysts. We believe that ϕ in the case of TiO_2-CoTSP is enhanced due to the effective scavenging of e^-_{CB} by CoTSP, thus leaving h^+_{VB} readily available to induce oxidation. When homogeneous free-radical pathways are suppressed, the oxidation of S(IV) or further oxidation of chain carriers by

h^+_{VB} at the catalyst's surface becomes important such that TiO_2-CoTSP will have a higher efficiency. The lower rate exhibited by TiO_2-CoTSP in the absence of radical traps is hence due to more effective termination of chain carriers. This explanation is consistent with the results of $CHCl_3$ oxidation (see Figure 8a) where TiO_2-CoTSP shows a quantum yield twice that of TiO_2. The higher ϕ of TiO_2-CoTSP compared to TiO_2 is further supported by our previous study[1] in which the hybrid catalyst showed extremely high rates of H_2O_2 formation, while TiO_2 was not effective in this regard.

As mentioned earlier, dithionate ($S_2O_6^{2-}$) and peroxodisulfate ($S_2O_8^{2-}$), which are expected chain termination products, were not observed. Long chain lengths will lower the yield of by-products resulting from recombinations of the radicals. A chain length of 50,000 has been reported[9] for the homogeneous oxidation of S(IV). This large value will produce by-products in concentrations below the detection limit of the available analytical methods. In addition, peroxodisulfate is a powerful oxidant (E° = 2.01 V, Eq. 46); its oxidation kinetics is often accelerated by metal ions and metal complexes.[37]

$$S_2O_8^{2-} + 2e^- \longrightarrow 2SO_4^{2-} \tag{46}$$

In a separate experiment we have shown that the reduced state of supported CoTSP (i.e., the yellow TiO_2-Co(I)TSP) in the absence of O_2 can be oxidized by $S_2O_8^{2-}$ as follows:

$$S_2O_8^{2-} + e^-_{CoTSP} \longrightarrow SO_4^{2-} + SO_4^{\cdot -} \tag{47}$$

Furthermore, the surface of the hybrid catalyst also contributes, as already explained, to the removal of radicals through adsorption followed by oxidation, thus leading to the formation of SO_4^{2-} rather than the dimeric chain termination products. In one extreme case when S(IV) oxidation was carried out with a high concentration of hybrid catalyst (2.3 g TiO_2-CoTSP/L) at pH 7.0, the quantum yield was found to be 0.58. This baseline quantum efficiency indicates an efficient trapping of radical intermediates, and thus a shortening of the chain-length. This latter experiment illustrates clearly the competitive

aspects of S(IV) oxidation between the solution and surface phases. It should be noted that an identical experiment performed in the absence of illumination indicates a reaction rate less than 5 % of the illuminated one. From the quantum yields (0.58) determined in experiments performed in the presence of high concentrations of scavenger, or high surface area, it is conceivable that the successive 1-electron oxidation of S(IV) at TiO_2-CoTSP surface operates at very high efficiency. Nevertheless, this mode of oxidation represents only a minor portion of the total oxidation rate under less extreme conditions (i.e., no scavenger present, or at 50 mg/L solid content). The small fraction of S(V), which leaves the surface, initiates the rapid homogeneous chain reaction with relatively long chain lengths. This results in the high initial quantum yields and the lack of detectable dithionate.

Acknowledgements:

We gratefully acknowledge the financial support of the U.S. Environmental Protection Agency (R811612-01-0). In addition, we want to thank Dr. Donald Carey for his encouragement and support. Samples of P25 TiO_2 were provided by the Degussa Corp.

References

(1) Hong, A.; Bahnemann, D.; Hoffmann, M. *J. Phys. Chem.* **1987**, *91*, 2109.

(2) Hoffmann, M.; Boyce, S. In *Advances in Environmental Science and Technology*, Vol. 12, Schwartz, S. Ed.; John Wiley & Sons: New York, 1983, p. 147.

(3) (a) Jacob, D.; Hoffmann, M. *J. Geophys. Res.* **1983**, *88*, 6611.
(b) Hoffmann, M.; Jacob, D. In *Acid Precipitation: SO_2, NO, and NO_x Oxidation Mechanisms: Atmospheric Considerations*, Calvert, J. Ed.; Butterworth: Boston, 1984; p. 101.

(4) Huss, A. Jr.; Lim, P.; Eckert, C. *J. Phys. Chem.* **1982**, *86*, 4224; *ibid*, 4229; *ibid*, 4223.

(5) Ellison, T.; Eckert, C. *J. Phys. Chem.* **1984**, *88*, 2335.

(6) Fuzzi, S. *Atmos. Environ.* **1978**, *12*, 1439.

(7) Ibusuki, T.; Barnes, H. *Atmos. Environ.* **1984**, *18*, 145.

(8) Holt, B.; Kumar, R.; Cunningham, P. *Atmos. Environ.* **1981**, *15*, 557.

(9) Backström, H. *Z. Phys. Chem.* **1934**, *25B*, 122.

(10) Hayon, E.; Treinin, A.; Wilf, J. *J. Am. Chem. Soc.* **1972**, *94*, 47.

(11) Huie, R.; Neta, P. *J. Phys. Chem.* **1984**, *88*, 5665.

(12) Huie, R.; Neta, P. *Environmental Health Perspectives*, **1985**, *64*, 209.

(13) McElroy, W. *Atmos. Environ.* **1986**, *20*, 323.

(14) Bassett, J.; Parker, W. *J. Chem. Soc.* **1951**, 1540.

(15) Freiberg, J. *Atmos. Environ.* **1975**, *9*, 661.

(16) (a) Hoffmann, M.; Edwards, J. *J. Phys. Chem.* **1975**, *79*, 2096.
(b) McArdle, J.; Hoffmann, M. *J. Phys. Chem.* **1983**, *87*, 5425.

(17) Hoffmann, M. *Atmos. Environ.* **1986**, *20*, 1145.

(18) Boyce, S.; Hoffmann, M.; Hong, A.; Moberly, L. *Environ. Sci. Tech.* **1983**, *17*, 602.

(19) Hoffmann, M.; Hong, A. *Sci. Total Environ.* **1987**, *64*, 99.

(20) Boyce, S.; Hoffmann, M.; Hong, A.; Moberly, L. In *Acid Precipitation Series*, Vol 1, Teasley, J. Ed.; Butterworth: Boston, 1984; p. 163.

(21) Frank S.; Bard, A. *J. Phys. Chem.* **1977**, *81*, 1484.

(22) Humphrey, R.; Ward, M.; Hinze, W. *Anal. Chem.* **1970**, *42*, 698.

(23) Weiss, J. *Handbook of Ion Chromatography*, Dionex Coorp., Sunnyvale, CA/USA, 1986.

(24) Lin, M.; Lunsford, J. *J. Phys. Chem.* **1975**, *79*, 892.

(25) Bahnemann, D.; Fischer, C.-H.; Janata, E.; Henglein, A. *J. Chem. Soc., Faraday Trans. 1*, accepted for publication.

(26) Bahnemann, D.; Mönig, J.; Chapman, R. *J. Phys. Chem.*, accepted for publication.

(27) Bahnemann, D.; Kern, J.; Faust, B.; Hoffmann, M. in preparation.

(28) Hong, A.; Boyce, S.; Moberly, L.; Hoffmann, M. *Environ. Sci. Tech.* **1987**, submitted.

(29) Huang, C. In *Adsorption of Inorganics at Solid-Liquid Interfaces*, Anderson, M.; Rubin, A. Ed.; Ann Arbor Science: Ann Arbor, 1981; p. 183.

(30) Bevan, H.; Dawes, S.; Ford, R. *Spectrochimica Acta*, **1958**, *13*, 43.

(31) Bahnemann, D.; Henglein, A.; Spanhel, L. *Faraday Discuss. Chem. Soc.* **1984**, *78*, 151.

(32) *Degussa Technical Bulletin Pigments*, No. 56.

(33) Wawzonek, S.; Duty, R. *J. Electrochem. Soc.* **1961**, *108*, 1135.

(34) Gerischer, H. *Topics in Applied Physics* **1979**, *31*, 121.

(35) Köster, R.; Asmus, K.-D. *Z. Naturforsch.* **1971**, *26b*, 1104.

(36) Mönig, J.; Bahnemann, K.; Asmus, K.-D. *Chem.-Biol. Interactions* **1983**, *47*, 15.

(37) Cotton F. A.; Wilkinson G. *Advanced Inorganic Chemistry*, 4th ed.; John Wiley & Sons: New York, **1980**; p. 534.

Table I: Initial Rate of S(IV) Oxidation ν_o with Different Catalysts Under Various Conditions.[a]

			ν_o (M/min) at pH		
entry	catalyst	irradiation	4.5	7.0	12.3
1	none	b		1.45×10^{-5}	
2	none	366 nm	1.28×10^{-5}	1.89×10^{-5}	3.86×10^{-6}
3	CoTSP	b		9.63×10^{-5}	$> 2.20 \times 10^{-3}$
4	CoTSP	366 nm		8.23×10^{-4}	c
5	TiO_2	b	4.79×10^{-5}	6.59×10^{-5}	7.41×10^{-7}
6	TiO_2	366 nm	4.77×10^{-4}	1.30×10^{-3}	6.99×10^{-6}
7	TiO_2-CoTSP	b	2.03×10^{-5}	4.24×10^{-5}	4.59×10^{-6}
8	TiO_2-CoTSP	366 nm	4.09×10^{-4}	5.92×10^{-4}	1.73×10^{-5}
9	TiO_2-CoTSP[d]	366 nm	4.39×10^{-4}		

[a] Concentrations were 280 mg/L for TiO_2, or TiO_2-CoTSP solid suspensions, or equivalent amount of 1.8 μM for CoTSP solution, 3 mM for S(IV), 1.2 mM for O_2.

[b] Subdued ambient room light.

[c] Reaction too fast to be accurate.

[d] No buffer used.

Table II: Lumped Kinetic Coefficients[a] for Rate Expressions of Eqs. 39 and 41 as a Function of pH.

coefficient[b]	pH 4.5	pH 7.0	pH 9.2	pH 12.3
b_1 M/(M)-min	3.88×10^{-5}	2.54×10^{-5}	4×10^{-5}	1.12×10^{-6}
b_2 M/(M)-min[c]	7.52×10^{-4}	6.22×10^{-4}	6.46×10^{-4}	1.37×10^{-5}
b_3 $(M)^2$	0.538	0.205	0.397	
b_4 1/(M)	48.7	50.8	49.0	49.0

[a] Coefficients fitted by least square regression using Gaussian-Newton method.

[b] for pH 4.5–9.2: $b_1 = k_9[HSO_3^-]$, $b_2 = \frac{k_3 k_8}{4k_7}[HSO_3^-]$, $b_3 = \frac{8k_7\phi\beta}{k_8^2}\left(\frac{K[HSO_3^-]}{1+K[HSO_3^-]}\right)$, $b_4 = \gamma$;
for pH 12.3: $b_1 = k_9[SO_3^{2-}]$, $b_2 = k_3[SO_3^{2-}]\sqrt{\frac{\phi\beta}{2k_7}\left(\frac{K[SO_3^{2-}]}{1+K[SO_3^{2-}]}\right)}$, $b_4 = \gamma$.

[c] M/min for pH 12.3.

Table III: Initial Rate of S(IV) Oxidation in the Presence of a Free Radical Scavenger.[a]

		ν_o (M/min)	
entry	[mannitol] (mM)	TiO_2	TiO_2-CoTSP
1	0	1.30×10^{-3}	5.92×10^{-4}
2	1	1.44×10^{-4}	3.18×10^{-4}
3	10	1.97×10^{-5}	4.50×10^{-5}
4	100[b]	5.47×10^{-6}	1.40×10^{-5}

[a] Concentrations were 280 mg/L for both solid suspensions, 3 mM for S(IV), 1.2 mM for O_2, and at pH 7.0.

[b] Ethanol.

Figure Captions

Figure 1. Disappearance of S(IV) ($[SO_3^{2-}]_o$ = 3 mM) on illumination (λ_{ex} = 366 nm) of an O_2-saturated aqueous suspension of TiO_2-CoTSP (50 mg/L) at pH 9.2.

Figure 2. Schematic diagram of the proposed reaction mechanism showing the photocatalytic processes of S(IV) oxidation on a TiO_2-CoTSP surface upon illumination.

Figure 3a, b. Catalyst dependence of S(IV) oxidation at various pH. The curves are mathematical fits according to the derived kinetic model (Eq. 39 and 41, see Table II for fitted parameters.) Concentrations are 3 mM for S(IV), 1.2 mM for O_2. Quantum yields are indicated.
• 1 mM for S(IV).

Figure 4. Initial rate dependence on S(IV) concentration as a function of pH. Straight lines are least-square fits with slopes indicating reaction orders in [S(IV)]. Concentrations are 50 mg/L for TiO_2-CoTSP, 1.2 mM for O_2. Quantum yields are indicated.
• 280 mg/L for TiO_2-CoTSP.

Figure 5. Initial rate dependence on O_2 concentration as a function of pH. Concentrations are 50 mg/L for TiO_2-CoTSP, 3 mM for S(IV).
• 280 mg/L for TiO_2-CoTSP, and 1 mM for S(IV).

Figure 6. Initial rate vs. pH. (a) Concentrations are 280 mg/L for TiO_2-CoTSP, 3 mM for S(IV), 1.2 mM for O_2. (b) 50 mg/L for TiO_2-CoTSP, 1 mM for S(IV).

Figure 7. Effect of ethanol on S(IV) oxidation. Concentrations are 280 mg/L for TiO_2-CoTSP, 3 mM for S(IV), 1.2 mM for O_2. Quantum yields are indicated.

Figure 8. (a) Release of Cl^- from $CHCl_3$ upon illumination of aqueous suspensions containing 280 mg/L TiO_2-CoTSP or TiO_2, 10 mM $CHCl_3$, and 0.24 mM O_2. Quantum yields are indicated. (b) The simultaneous formation of H_2O_2 in the same experiment of (a) with TiO_2-CoTSP.

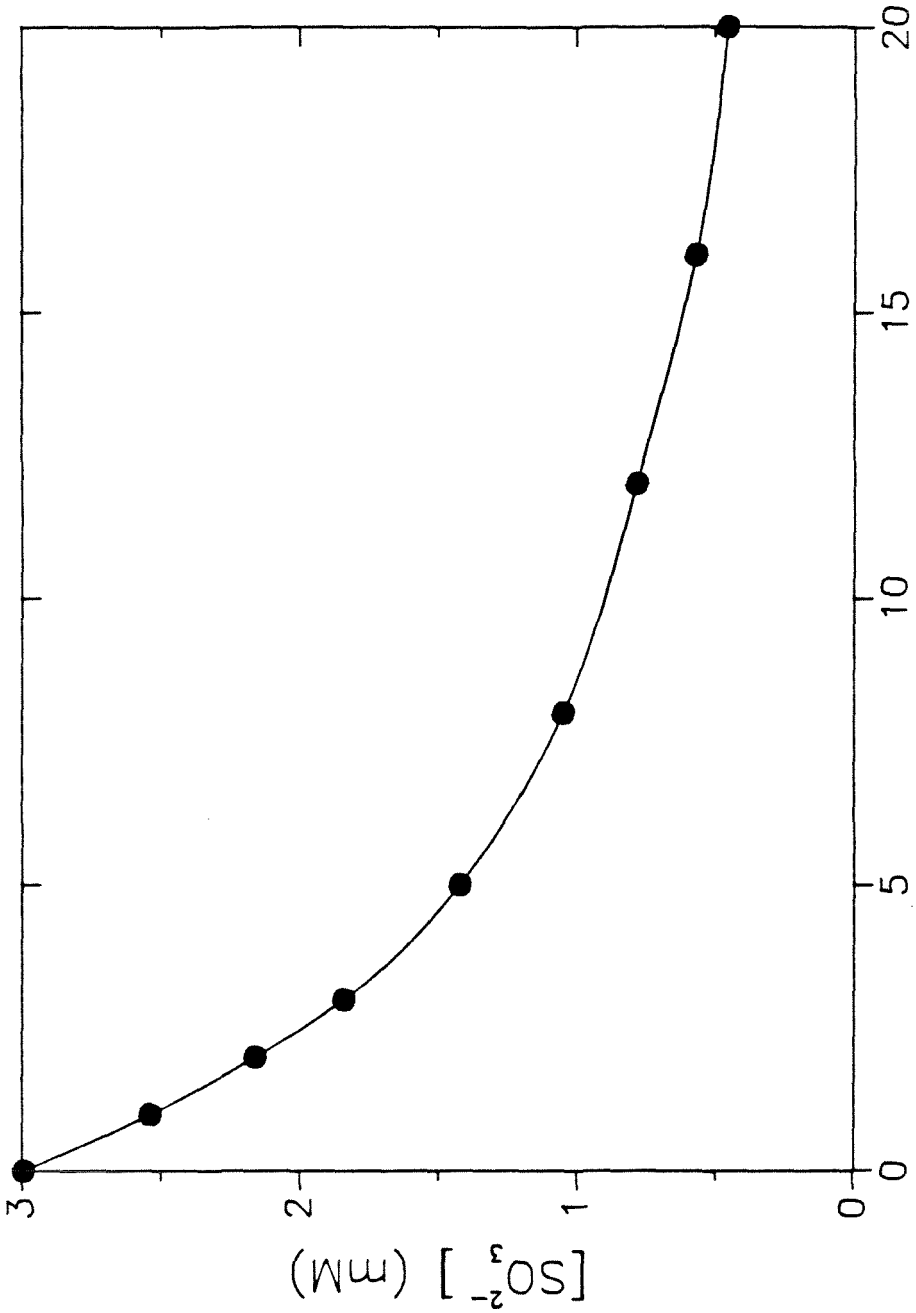

Figure 1

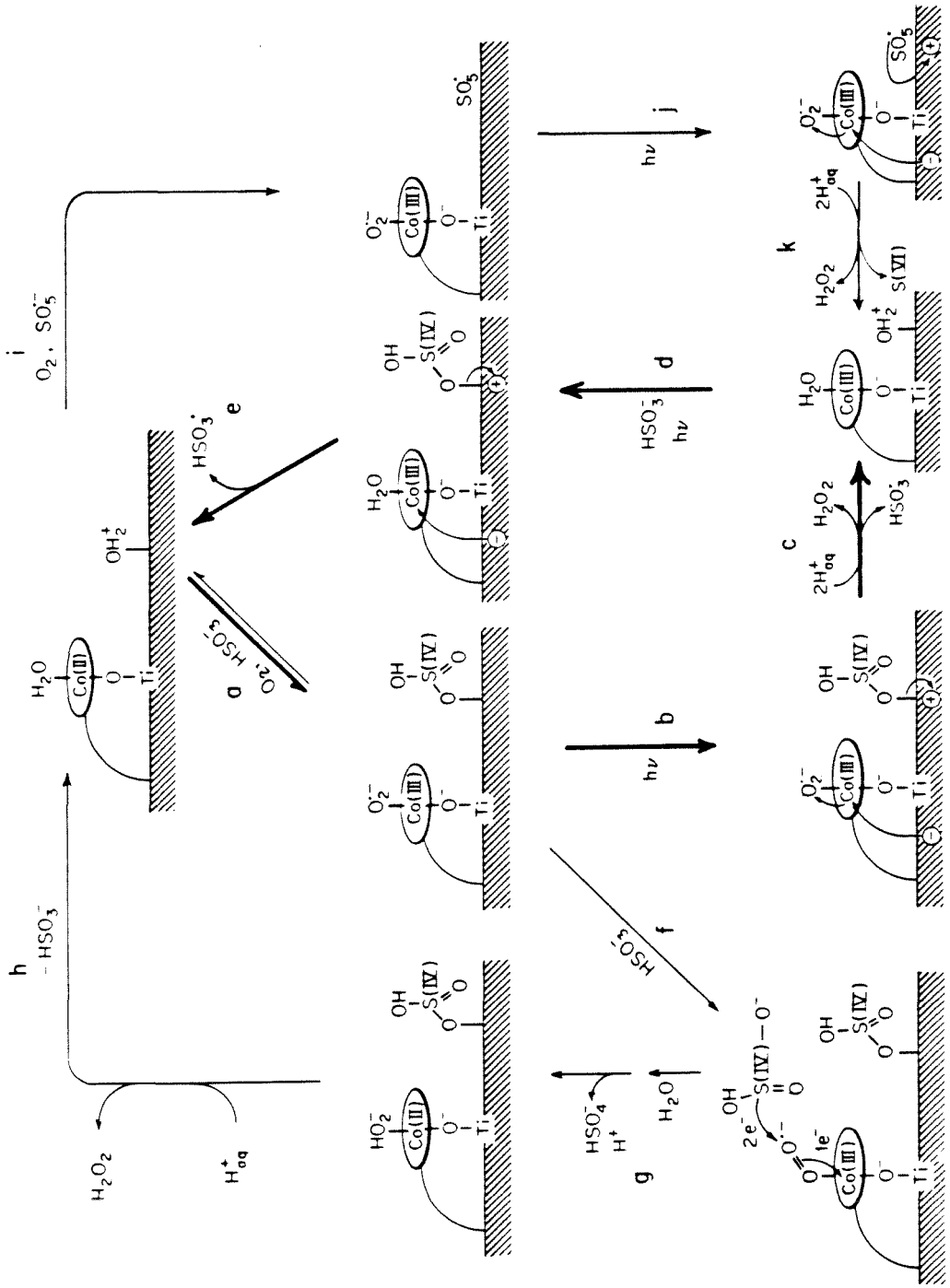

Figure 2

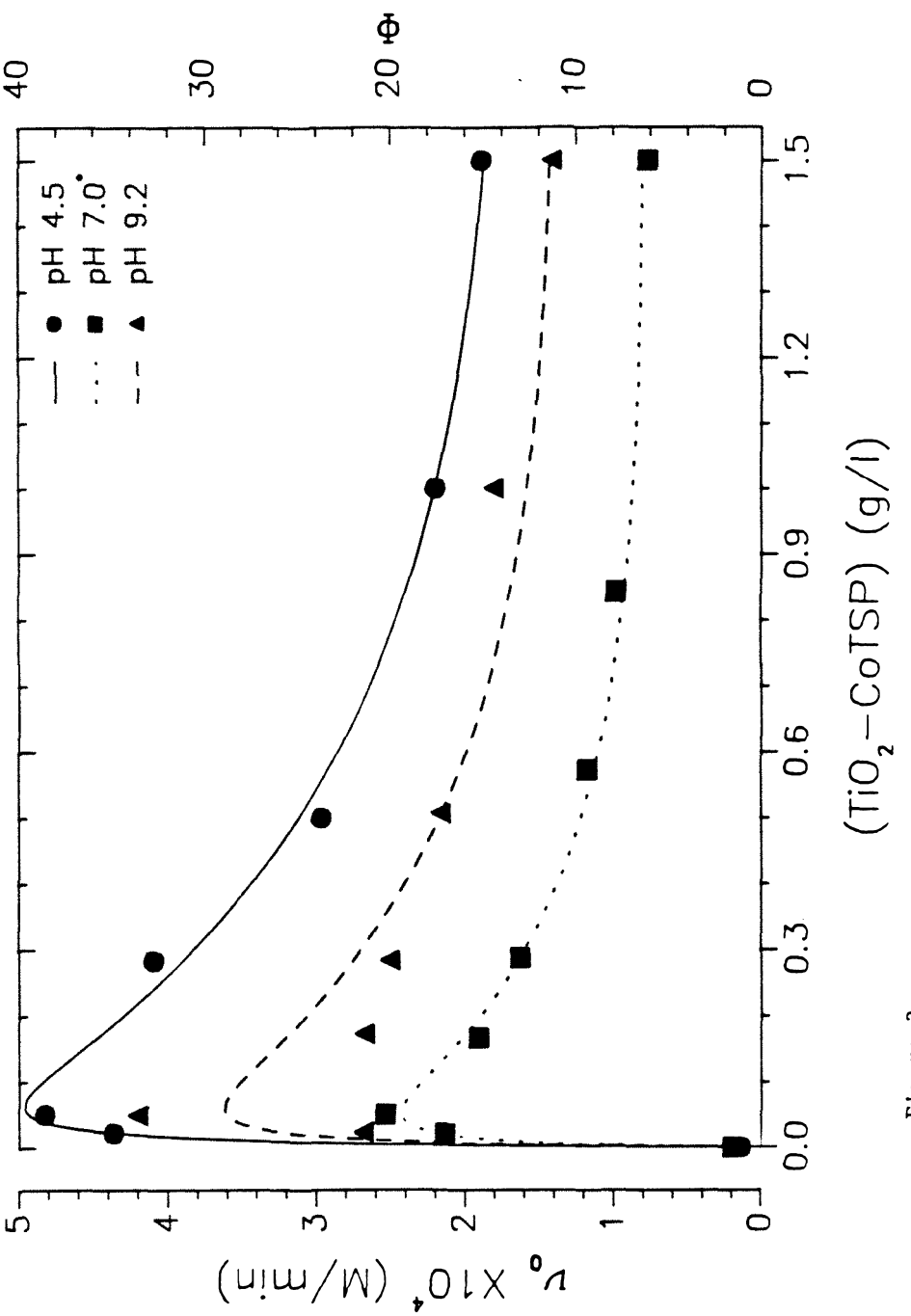

Figure 3a

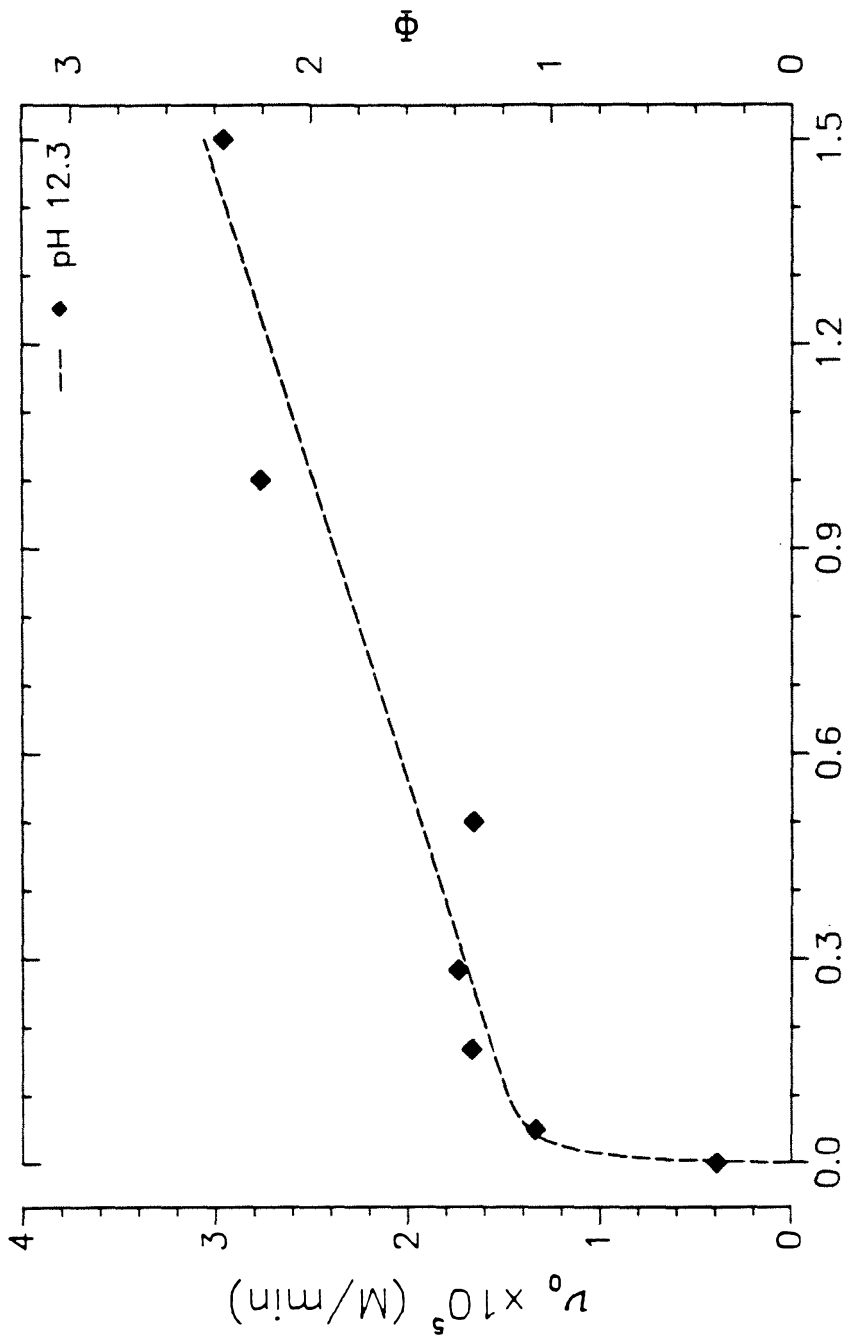

Figure 3b

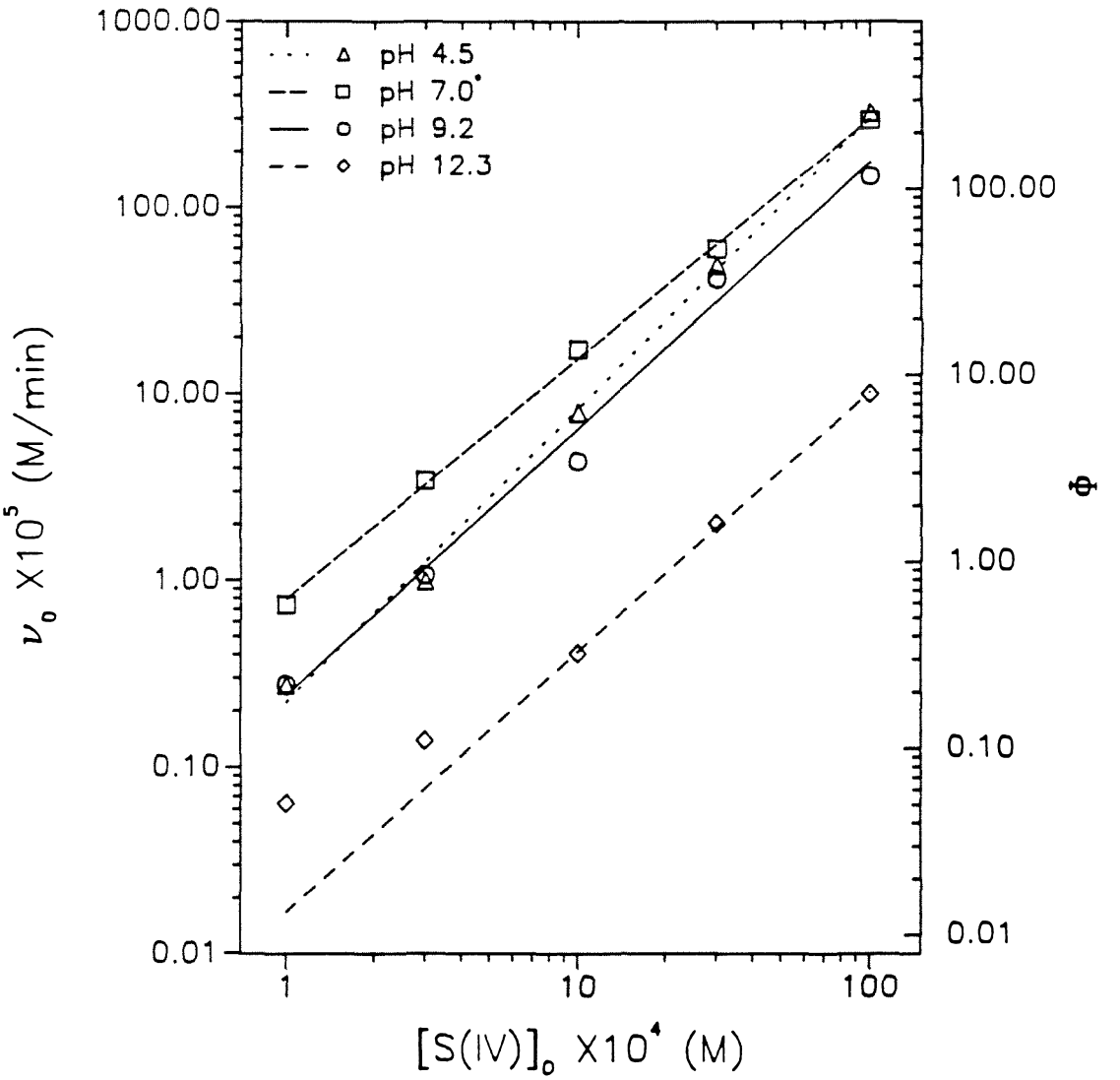
1000.00
100.00
10.00
1.00
0.10
0.01
pH 4.5
pH 7.0
pH 9.2
pH 12.3
ν_0 X10^5 (M/min)
100.00
10.00
1.00
0.10
0.01
Φ
1
10
100
[S(IV)]$_0$ X10^4 (M)

Figure 4

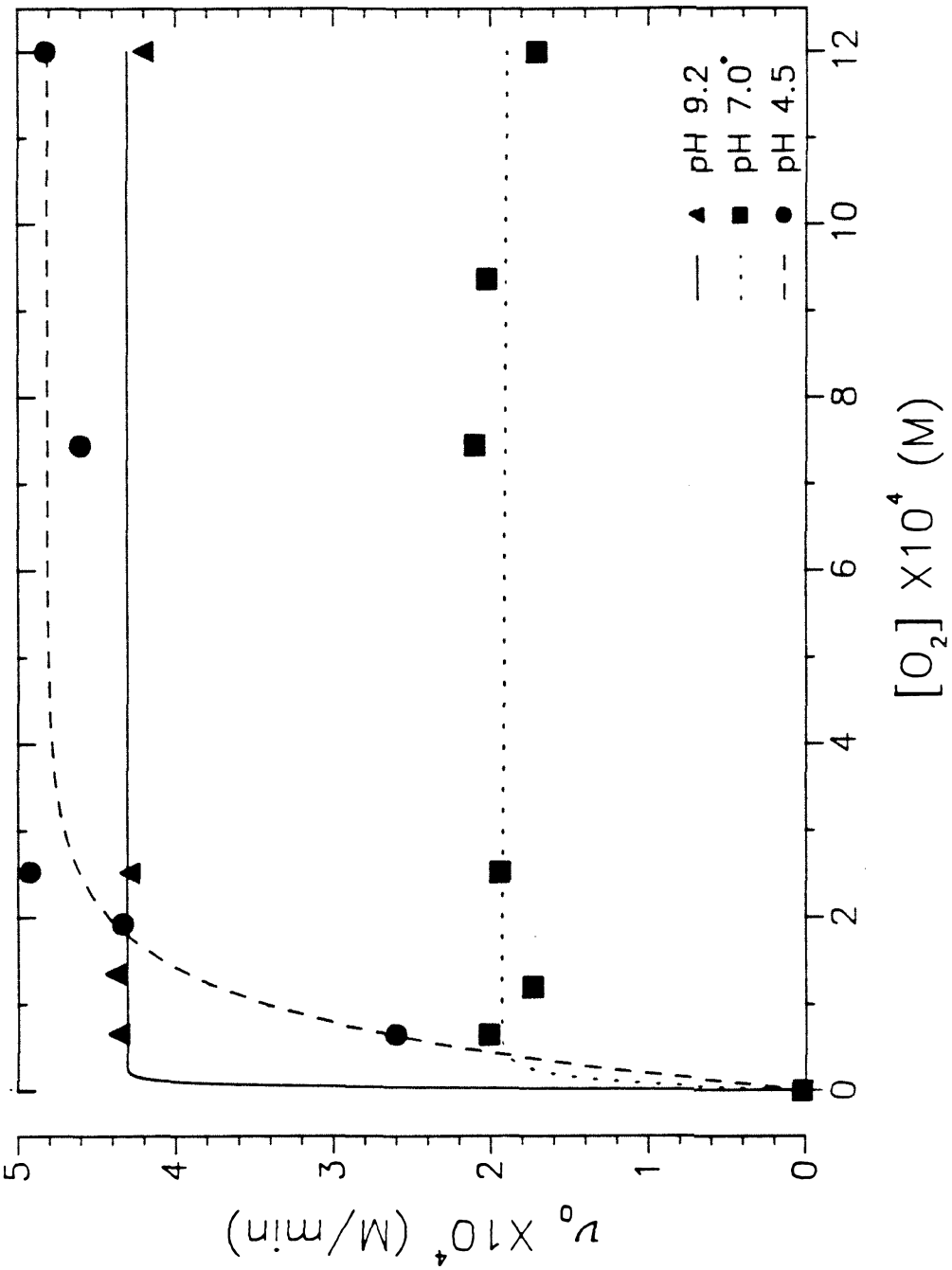

Figure 5

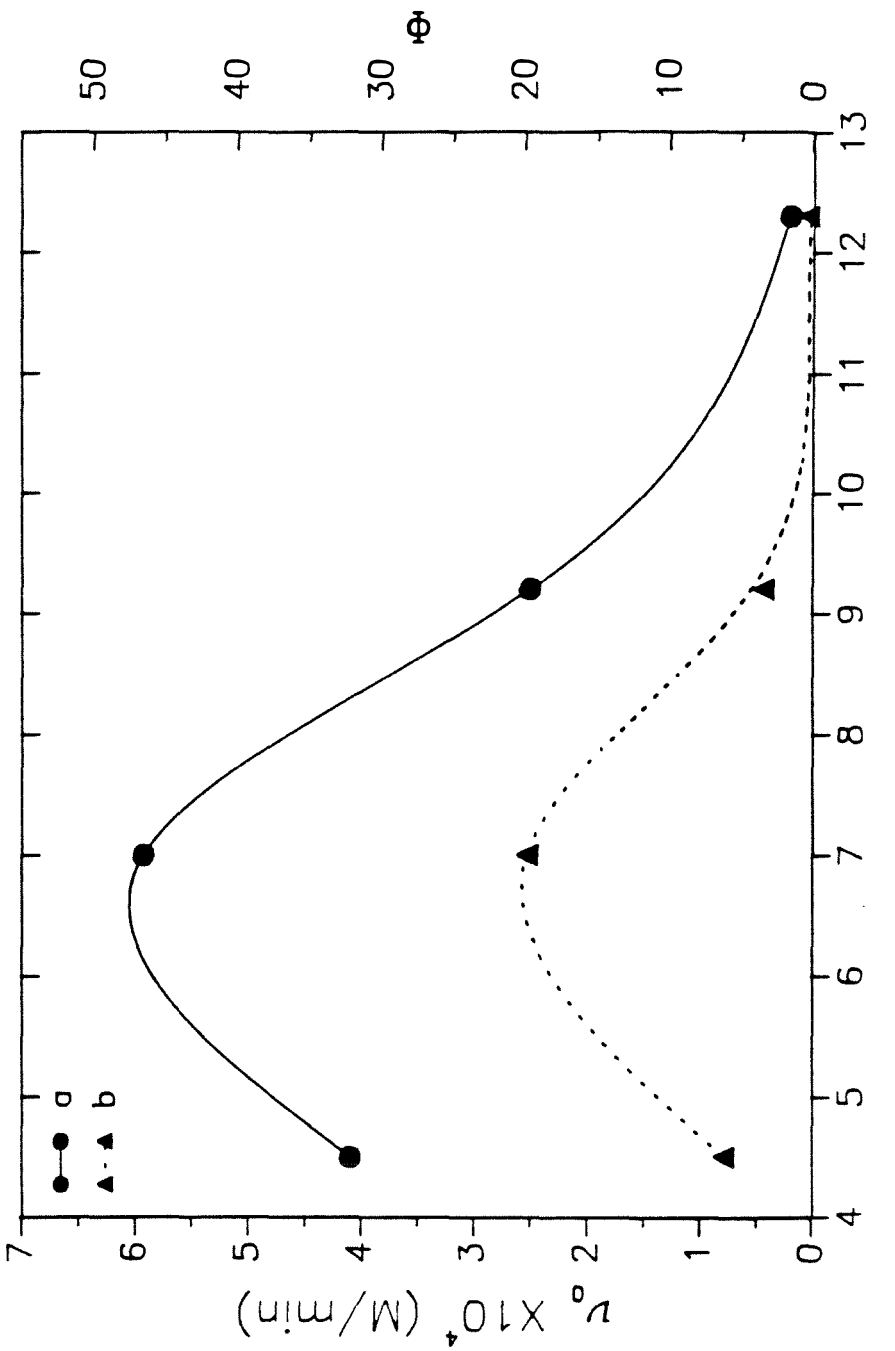

Figure 6

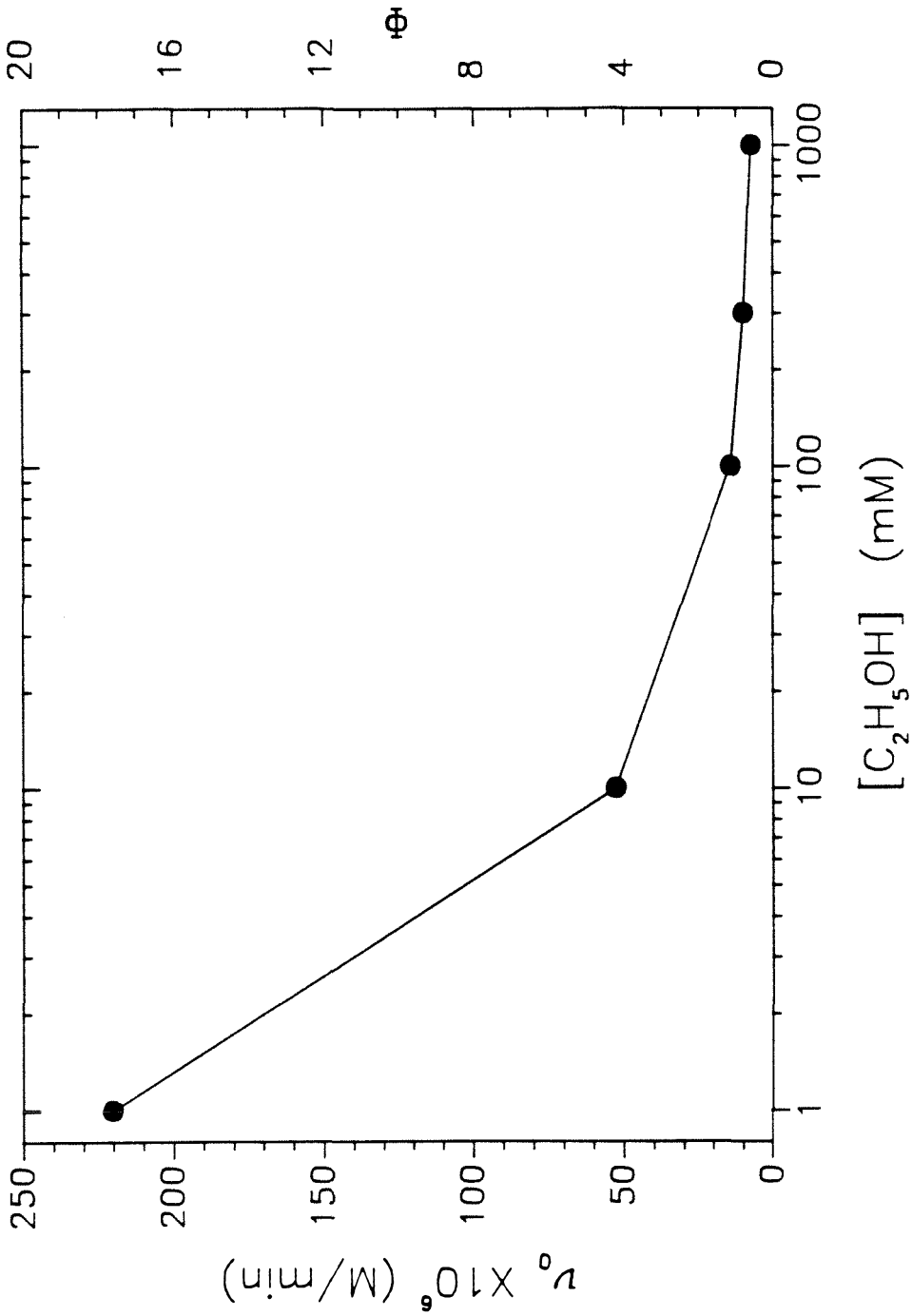
v_o X10^6 (M/min)
250
200
150
100
50
0
20
16
12
8
4
0
Φ
1
10
100
1000
[C_2H_5OH] (mM)

Figure 7

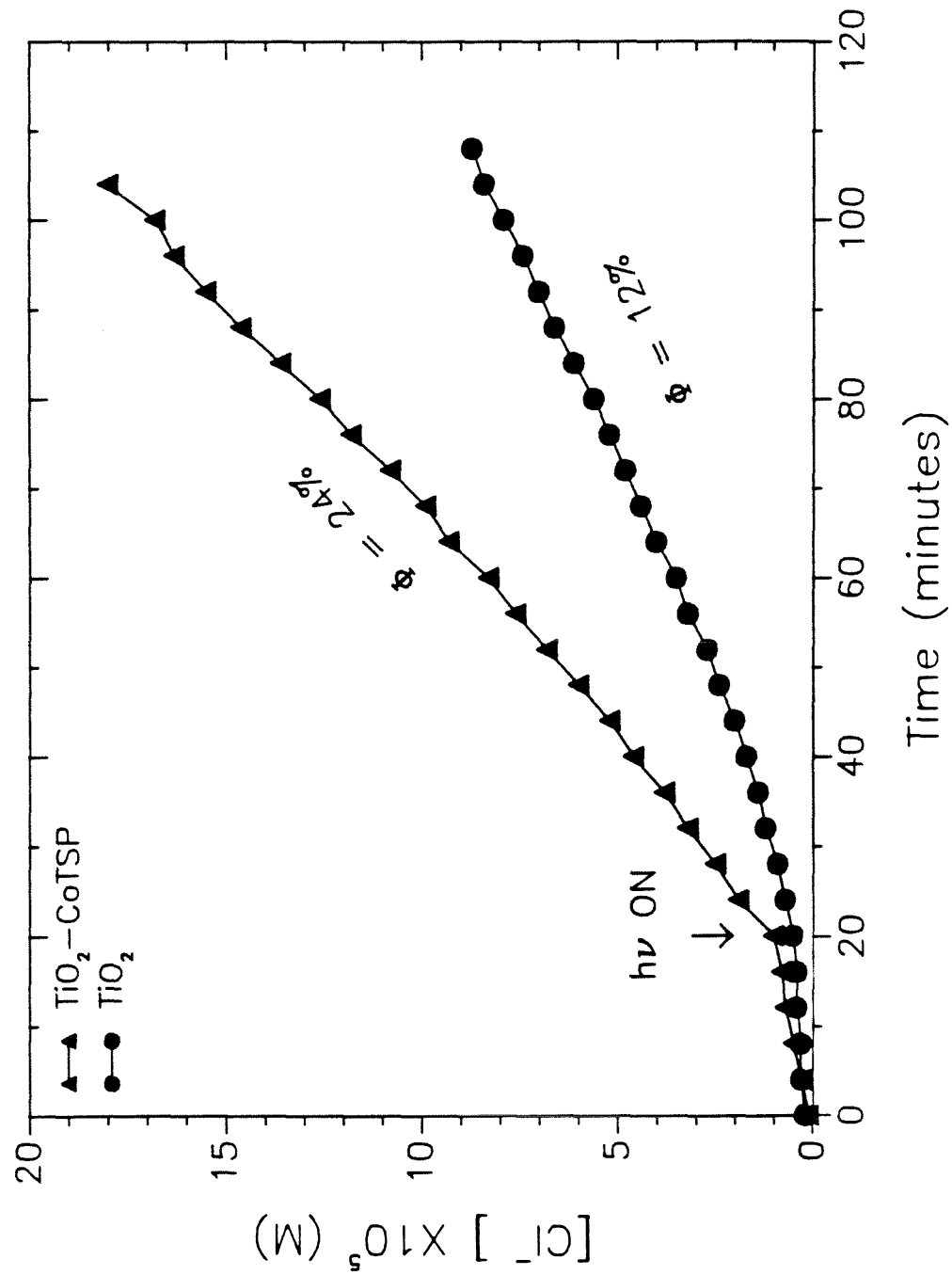
TiO_2–CoTSP
TiO_2
Φ = 24%
Φ = 12%
hν ON
[Cl⁻] X10⁵ (M)
Time (minutes)
0
5
10
15
20
0
20
40
60
80
100
120

Figure 8a

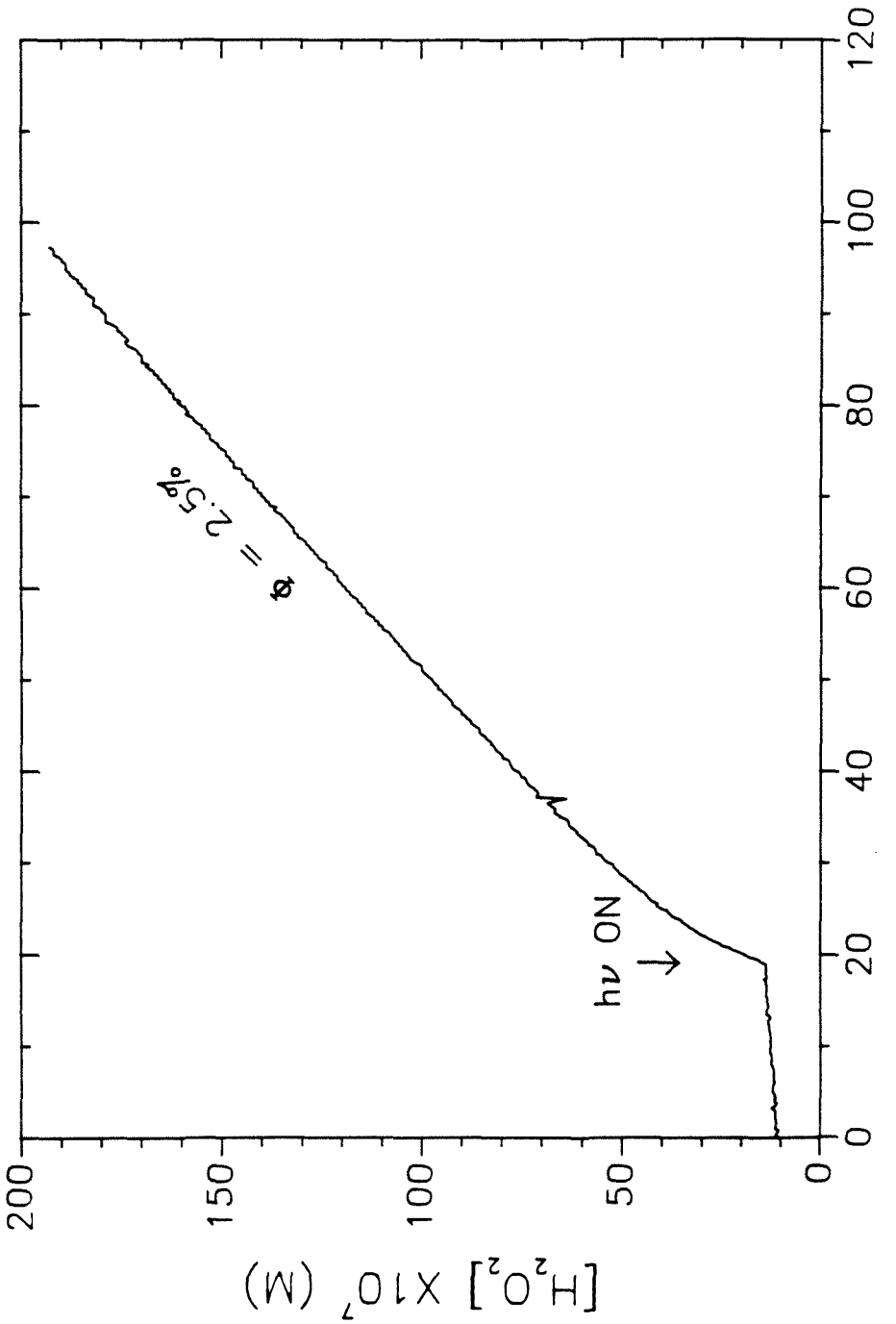
200
150
100
50
0
[H2O2] X10^7 (M)
0
20
40
60
80
100
120
Time (minutes)
hν ON
Φ = 2.5%

Figure 8b

Chapter 8

Future Research and Remarks

A. Energetic Considerations of Hybrid Catalyst Design

An electron/hole pair results when a semiconductor material is excited by radiation equal to or in excess of the band-gap energy. The immediate recombination of the e^-/h^+ pairs can be prevented by chemically attached electron donors or acceptors, by metal deposits, or by the application of external electrical fields, resulting in the prolonged life of a powerful oxidant or reductant. The redox potentials of the e^-_{CB} and h^+_{VB} are determined by the positions (relative to E_{NHE}) of the conduction and valence bands, respectively (Figure 1).[1] Since band-gap energies are material constants, a choice of materials for specific reactions may be made.

A variety of metal complexes are available as electron relays on semiconductor surfaces. The feasibility of the complex depends on its redox potential. Redox potentials for some cobalt porphyrins are listed in Table I.[2] A shift of nearly 1 V (e.g., cyanated iron mesoporphyrin at -0.23 V and platinum phthalocyanine at 0.72 V)[3] can result from factors such as central metal, peripheral groups, and coordinating ligands. From an energetic standpoint, in order for the complex to capture conduction band electron and the reduced complex to subsequently reduce a substrate, the redox potential of the relay should lie between the conduction band potential and the redox potential of the desired reaction. A hybrid Pt(IV) complex has been synthesized, and it would interesting to probe the efficiency of this relay because Pt has more accessible oxidation states than Co(II). As the Pt(IV) center is photochemically reduced by accepting e^-_{CB} successively, each subsequent

reduction step will take place at a more negative potential. Ultimately, the Pt center will be reduced to Pt(0) or higher state when it can no longer accept e^-_{CB}. Since multi-electron transfer is common in chemical reactions, the storage of more than one electron may encourage multi-electron transfer reaction at one time, which may otherwise be prohibited by kinetic barriers imposed by high-energy intermediates.

Tables II and III list the accessible one-electron redox potentials for a number of organic and inorganic compounds with respect to their reduction and oxidation, respectively.[4,5] This data compilation shows that the holes in most of the metal oxides are powerful enough to oxidize all the listed chemicals (Table III) at any given pH. The reducing capability of the conduction band and the attached complex can be selected as described above and tailored to specific needs.

B. Degradation of Hazardous Pollutants with TiO_2

Unlike its hybrid analog, plain TiO_2 offers the advantage that no pretreatments are required and is, therefore, more economical in practical applications toward pollution control. Although TiO_2 is not as active in H_2O_2 production as the hybrid case, the former demonstrates high catalytic activity toward S(IV) oxidation. This is related to the nature of reaction mechanism. TiO_2 is a good catalyst for S(IV) oxidation because the reaction involves the transfer of only one electron in the formation of a reactive intermediate; a radical-chain mechanism follows throughout the course of oxidation. This catalytic feature can be utilized in degradations of many pollutants (Table III).

A wide variety of organic compounds have been shown in the literature to be oxidized by semiconductor metal oxides. However, in-depth reports on kinetics and mechanisms are rare. TiO_2 has been shown to be active for the oxidation of $CHCl_3$ (Chapter 7). The mechanism is thought to involve an initial oxidative attack by a valence hole, followed by O_2 addition and ultimately to the release of chloride ions. Detailed kinetic and mechanistic studies are needed.

C. Atmospheric Implications

The photocatalytic formation of H_2O_2 and the photocatalytic oxidation of S(IV) have been presented in this thesis. Hydrogen peroxide and sulfur dioxide are important species in the atmosphere, ng as oxidant and acid precursor, respectively. Semiconductor materials such as Fe_2O_3 and ZnO are often found in the atmosphere. These metal oxide particles are released to the atmosphere with fly-ash during combustion processes. In a natural environment, Fe_2O_3 and TiO_2 are important constituents of desert sands.[6] Field studies have shown that desert sands can be transported over a great distance, such as from the Sahara desert to the Caribbean sea, from China to Hawaii.[7] Measurement of sand particle concentrations give an average value of 1 $\mu g/m^3$. A cloudwater suspension of 2 mg/L of sand can be calculated for a cloud liquid water content of 0.5 g/m^3. Furthermore, particle sizes larger than 25 μm are often recorded. Smaller particles are expected to have longer residence time. The presence of desert dust in the atmosphere has caused concerns over the quality and quantity of solar radiation reaching the earth's surface.[8] In the abundance of near UV radiation,

these particles that contain the semiconductor materials may provide additional surficial and photochemical pathways.

The atmosphere was once thought to be exclusively a gas-phase reactor. However, recent advances made in cloud and fog chemistry indicate that the aqueous phase plays an extremely important role in the global cycling of many elements. Research in the areas of semiconductor particles and photocatalysis may establish the role of photoactive particulate matter in atmospheric free-radical chemistry.

References

1. Gerischer, H. *Topics in Applied Physics*, **1979**, *31*, 115.

2. Durand, R. R. Jr. Ph.D. Thesis on *Catalysis of the Electroreduction of Dioxygen by Monomeric and Dimeric Cobalt Porphyrins*, Calif. Inst. of Tech., 1984, p. 59.

3. Moser, F. H.; Thomas, A. L. *The Phthalocyanines*, Vol. I, CRC Press, 1983.

4. (a) Charlot, G.; Collumeau, A.; Marchon, M. J. *Selected Constants, Oxidation-Reduction Potentials of Inorganic Substances in Aqueous Solution*, Butterworths: London, 1971.

   (b) Meisel, D.; Neta, P. *J. Am. Chem. Soc.* **1975**, *97*, 5198-5203.

   (c) Wardman, P.; Clarke, E. D. *J. C. S. Faraday Trans. I*, **1976**, *72*, 1377-1390.

   (d) Stackelberg, M. V.; Stracke, W. *Z. F. Elektrochem.* **1949**, *53*, 118-125.

   (e) Wawzonek, S.; Duty, R. C. *J. Electrochem. Soc.* **1961**, *108*, 1135-1138.

5. (a) Reference 4(a).

   (b) Suatoni, J. C.; Snyder, R. E.; Clark, R. O. *Anal. Chem.* **1961**, *33*, 1894-1897.

5. (c) Steenken, S.; Neta, P. *J. Phys. Chem.* **1979**, 83, 1134-1137.

(d) Steenken, S.; Neta, P. *J. Phys. Chem.* **1982**, 86, 3661-3667.

(e) Huie, R. E.; Neta, P. *J. Phys. Chem.* **1985**, 89, 3918-3921.

6. (a) Schrauzer, G. N.; Strampach, N.; Hui, L. N. Palmer, M. R.; Salehi, J. *Proc. Natl. Acad. Sci.* USA, **1983**, 80, 3873-3876.

(b) Schutz, L.; Rahn, K. A. *Atmos. Environ.* **1982**, *16*, 171-176.

7. Uematsu, M.; Tindale, N. W.; Duce, R. A. *EOS*, **1986**, *67*, 898.

8. Duce, R. A. *EOS*, **1986**, *67*, 898.

Table I. Redox Potential $E(Co^{III}/Co^{II})$ for Various Porphyrins

Porphyrin	E (V vs. NHE)
tetraphenylporphyrin	+0.99
tetra(p-methoxy)phenylporphyrin	+0.88
octaethylporphyrin	+0.84
tetra(p-sulfonato)phenylporphyrin	+0.74
tetra(N-methyl)pyridylporphyrin	+0.82
tetrapyridylporphyrin	+0.79
tetra(p-amino)phenylporphyrin	+0.54
tetrasulfonatophthalocyanine	+1.04

Table II. One-Electron Redox Potential, E, for the Reduction of Various Chemicals

Compound	E (V vs. NHE)	Compound	E (V)
CH_3Cl	-2.00	$C_6H_5CHCl_2$	-1.2
CH_2Cl_2	-2.10	$C_6H_5CCl_3$	-0.30
$CHCl_3$	-1.44	$(C_6H_5)_2CCl_2$	-0.47
CCl_4	-0.54	$C_6H_4Cl_2$	-2.28
CH_3Br	-1.40	C_6Cl_6	-1.21
CH_2Br_2	-1.25	$C_6H_4Br_2$	-2.09
CH_3Br_3	-0.41	C_6Br_6	-0.52
CBr_4	-0.07	$C_6H_5NO_2$	-0.49
CH_3I	-1.40	p-nitropyridine	-0.19
CH_2I_2	-0.89	p-nitroacetophenone	-0.36
CHI_3	-0.26	5-nitrouracil	-0.53
CCl_2F_2	-1.22	CH_3NO_2	-1.06

Table III. One-Electron Redox Potential, E, for the Oxidation of Various Chemicals

Compound	E (V vs. NHE)
phenol	+0.90
resorcinol	+0.81
catechol	+0.53
hydrochinone	+0.46
p-methoxyphenol	+0.60
p-aminophenol	+0.41
p-phenylendiamine	+0.73
1,2,4-trihydroxybenzene	-0.11
p-nitrophenol	+0.92
p-chlorophenol	+0.65
p-nitroaniline	+0.94
p-chloroaniline	+0.68
aniline	+0.62
2,5-dichlorophenol	+0.73
2,5-dichloroaniline	+0.90
Cl^-	+2.59
Br^-	+2.08
I^-	+1.31
SO_3^{2-}	+0.63
NO_2^-	+1.07

Figure 1. Band-gap Positions of Various Semiconductors

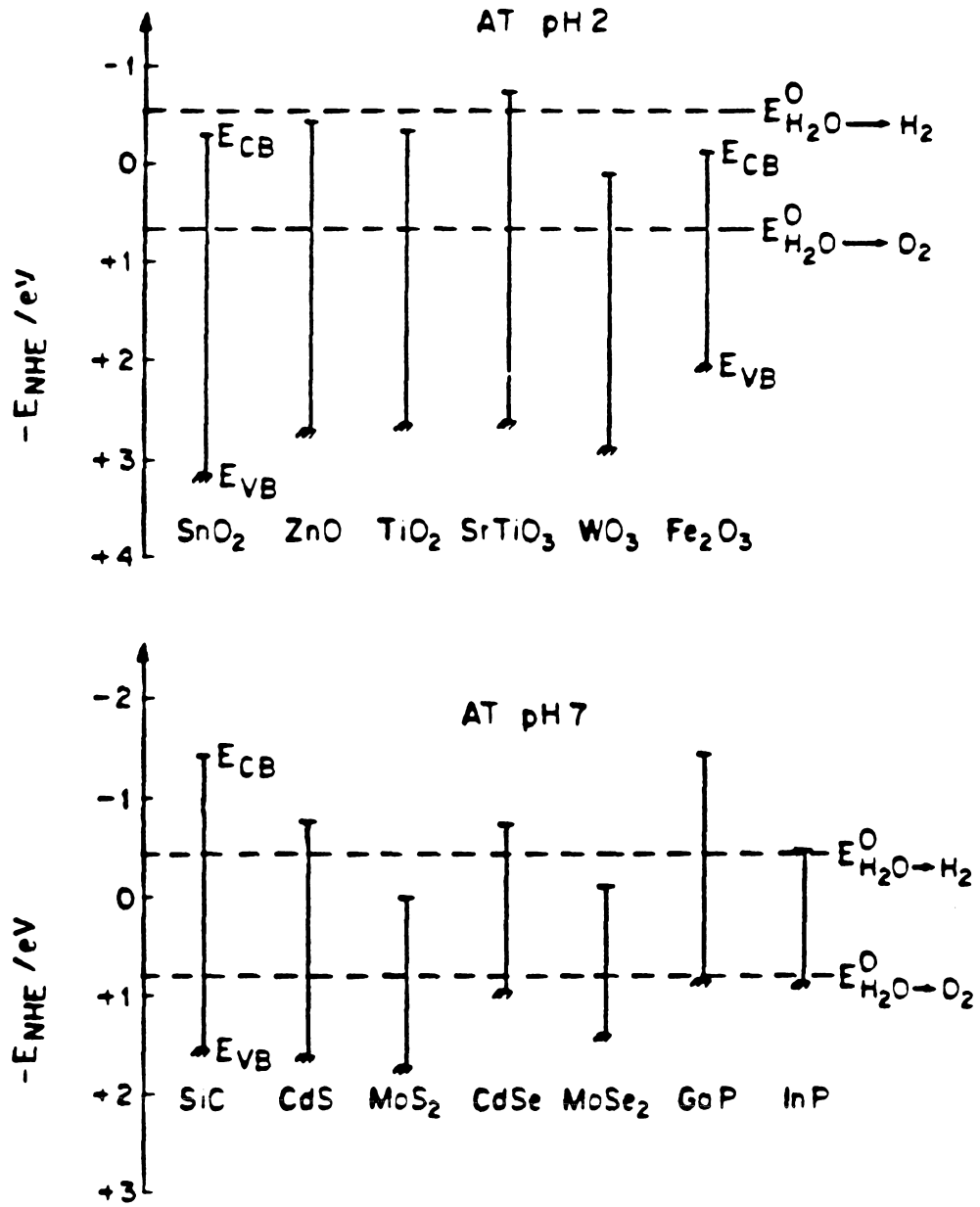

Appendix

Synthesis of Homogeneous and Heterogeneous Catalysts

This appendix summarizes various homogeneous and heterogeneous catalysts that have been prepared (Figures 1 to 5). It also describes the synthetic procedures that have not been already reported in previous chapters.

I. Homogeneous Metal-Phthalocyanines

Schematic diagrams illustrating the structures of various homogeneous phthalocyanines, phthalocyanine dimers, and one porphyrin are shown in Figures 1 and 2.

A. M-TSP (1) (M = Co^{2+}, Fe^{2+}, Mn^{2+}, Cu^{2+}, Ni^{2+}, V^{4+}, VO^{2+}, Pt^{4+})

The syntheses of various metal-tetrasulfophthalocyanines were performed by the condensation of sodium 4-sulfophthalate, ammonium chloride, urea, ammonium molybdate, and appropriate metal salts according to the procedure described in the experimental section of Chapter 2. The precursor, sodium 4-sulfophthalate, was first obtained by neutralization of 50 % 4-sulfophthalic acid (Kodak Co.) with a molar equivalent of 15 M NaOH solution. The brown solution containing sodium 4-sulfophthalate was concentrated by boiling until precipitation. The resulting solid was filtered and washed by ethanol. Various central metals, M, originated from corresponding hydrated metal sulfate salts such as $CoSO_4$, $FeCl_2$, $MnSO_4$, $VOSO_4$, etc. Pt-TSP was derived from H_2PtCl_6.

B. CoTAP (2)

Cobalt(II)-tetrasulfophthalocyanine was obtained by a modified procedure as described in the results and discussion section of Chapter 5.

C. $CoT(SO_3Na)PP$ (3)

The sodium salt of cobalt(II)tetra(p-sulfonato)phenylporphyrin was prepared by the following procedure. A mixture of meso-tetraphenylporphyrin, TPP, (2g, Aldrich) and concentrated H_2SO_4 (50 ml) in a 300 ml r-b flask equipped with a $CaCl_2$ drying tube was heated over a steam bath for 6 hours. The reaction mixture was cooled and neutralized with $NaHCO_3$, followed by dialysis in cellulose tubes (VWR) to remove inorganics. The solution was concentrated to 50 ml and filtered by fritted glass while hot. The filtrant was then evaporated to almost dryness with a rotary evaporator. A dry water-soluble product was obtained after storage in a P_2O_5 desiccator.

Cobalt was incorporated into the center $T(SO_3Na)PP$ by the following procedure. 0.23 g $CoSO_4 \cdot 7H_2O$ was added to a 60 ml aqueous solution of $T(SO_3Na)PP$ heated to gentle boiling; the reaction was allowed to proceed for 15 min. ($T(SO_3Na)PP$ solution showed an intense red fluorescence under black light; the fluorescence stopped a few minutes after the addition of the cobalt salt.) The reaction mixture was added to 500 ml water saturated with NaCl. A bluish purple solid precipitated upon cooling and was collected. This solid product was dissolved in CH_3OH (a red solution) and the solution was filtered to remove NaCl. It was then evaporated to obtain the $CoT(SO_3Na)PP$ complex.

D. Cobalt-Phthalocyanine Dimer (4-7)

The permanent dimerizations of two cobalt-phthalocyanines were performed in the following procedures. Further purification and characterization are required.

Dimer 4: $CoT(SO_2Cl)P + CoTAP \longrightarrow 4$

The preparation of $CoT(SO_2Cl)P$ was described in the results and discussion section of Chapter 6. Molar equivalent amounts (70 μmoles) of $CoT(SO_2Cl)P$ and CoTAP were dissolved in 20 ml DMSO. The solution was deoxygenated by vacuum-N_2 cycles, heated below 100°C, and stirred for 1.5 hours. Dilute aqueous HCl was added to induce precipitation. The solid was collected and repeatedly washed with HCl solution. A product that was soluble in basic solution and insoluble in acidic was obtained. It should be noted that the dimer product was linked by a sulfonamide bonding and was consistent with the solubility observations.

Dimer 5: $2CoT(SO_2Cl)P + o\text{-}C_6H_4(NH_2)_2 \longrightarrow 5$

100 μmoles $o\text{-}C_6H_4(NH_2)_2$ (MCB) dissolved in pyridine was slowly introduced to a pyridine solution containing 40 μmoles $CoT(SO_2Cl)P$. The mixture was stirred for 4 hours. A solid that formed upon addition of dilute aqueous HCl was collected and washed with dilute HCl.

Dimer 6: $2CoTAP + CHOCHO \longrightarrow 6$

Dimer 7: $2CoT(SO_2Cl)P + NH_2NH_2 \longrightarrow 7$

Dimers 6 and 7 were obtained by treatments of CoTAP with dialdehyde and $CoT(SO_2Cl)P$ with hydrazine, respectively, using pyridine as a

solvent in the aforesaid procedure for dimer 4.. Care was taken to eliminate the presence of O_2 as cobalt phthalocyanines were known to catalyze the oxidation of these employed linking reagents.

II. Hybrid Metal-Phthalocyanines

Schematic diagrams illustrating the structures of various supported phthalocyanines are shown in Figures 3, 4, and 5. Polystyrene/divinylbenzene copolymer, silica gel, and titanium dioxide powder were used as support. Complexes were linked to the surface either through direct complexation of the metal center or through covalent bonding of a peripheral group on the macrocyclic ligand.

A. Polystyrene/Divinylbenzene Copolymer as Support

IRA-93-CoTSP (8) and IRA-93-CoTAP (9) through complexation:

Amberlite IRA-93 (Rohm & Haas) is a weakly basic anion exchange resin with amino groups that can complex with metal ions. The procedure for preparing 8 was described in the results and discussion section of Chapter 5. Pyridine was used as a solvent for preparing 9 in the same procedure.

XAD-2-CoTAP (10) through covalent bonding:

$$(-CH_2CH-)_nC_6H_5 + ClCH_2OCH_3 \xrightarrow{SnCl_4} (-CH_2CH-)_nC_6H_4CH_2Cl$$

$$(-CH_2CH-)_nC_6H_4CH_2Cl + CoTAP \longrightarrow 10$$

24 g XAD-2 polystyrene resin (Rohm & Haas) was added into a r-b flask containing 100 ml $ClCH_2OCH_3$ (Aldrich). After an hour, 10 g $SnCl_4 \cdot 5H_2O$ in 50 ml $ClCH_2OCH_3$ was added. The mixture was mechanically stirred and

heated to reflux for 1.5 hours. The chloromethylated polystyrene resin was collected and washed consecutively with 800 ml THF, 800 ml THF/H_2O (3:1), 800 ml THF/HCl(3N) (3:1), 800 ml THF/H_2O (3:1), 1 L THF, and 800 ml CH_3OH. It was then dried under vacuum.

0.3 g CoTAP was added to 3 g of the treated resin suspended in 30 ml DMSO. The mixture was stirred and heated at 50°C for 5 hours. A green resin (10) was collected, washed with acetone and water.

XAD-2-CoTSP (11) through complexation:

$$(-CH_2CH-)_nC_6H_4CH_2Cl + C_3H_4N_2 \longrightarrow (-CH_2CH-)_nC_6H_4CH_2(C_3H_3N_2)$$

$$(-CH_2CH-)_nC_6H_4CH_2(C_3H_3N_2) + \text{CoTSP} \longrightarrow 11$$

0.5 g imidazole and 5 g of the chloromethylated XAD-2 were refluxed in 35 ml xylene for 5 hours. The product was collected, washed with acetone, then H_2O, until chloride free. 1 g of this solid was stirred in 50 ml of 80 μM CoTSP solution for 4 hours. The blue resin was collected and washed with H_2O.

B. Silica Gel as Support

SiO_2-$C_3H_3N_2$-CoTAP (12), SiO_2-$C_3H_3N_2$-CoTSP (13) through complexation:

The syntheses of these two silica gel-based cobalt-phthalocyanines were achieved by complexation and were reported in the results and discussion section of Chapter 5.

SiO_2-NH_2-CoTAP (14) through complexation:

Using 4-aminotriethoxysilane, $(EtO)_3Si(CH_2)_3NH_2$, as a silylation reagent for SiO_2, the preparation of this hybrid complex was parallel to the procedure for 12.

SiO_2-CoTAP (15) through covalent bonding:

The preparation of 15 was described in the results and discussion section of Chapter 5.

SiO_2-NH_2-CoTSP (16) through covalent bonding:

SiO_2 was treated with $(EtO)_3Si(CH_2)_3NH_2$ in the same manner as with $(MeO)_3Si(CH_2)_3Cl$. The treated SiO_2 was added to a $CHCl_3$ solution of $CoT(SO_2Cl)P$. The product was obtained after the rapid coupling reaction. It should be noted that the addition of untreated SiO_2 to $CoT(SO_2Cl)P$ solution also yielded a green solid; however, desorption of the complex from the surface occurred upon the addition of base.

C. Titanium Dioxide as Support

TiO_2-CoTSP (17) and TiO_2-PtTSP (18) through covalent bonding:

The synthesis of TiO_2-CoTSP was detailed in the results and discussion section of Chapter 6. The preparation of TiO_2-PtTSP from PtTSP followed a parallel procedure.

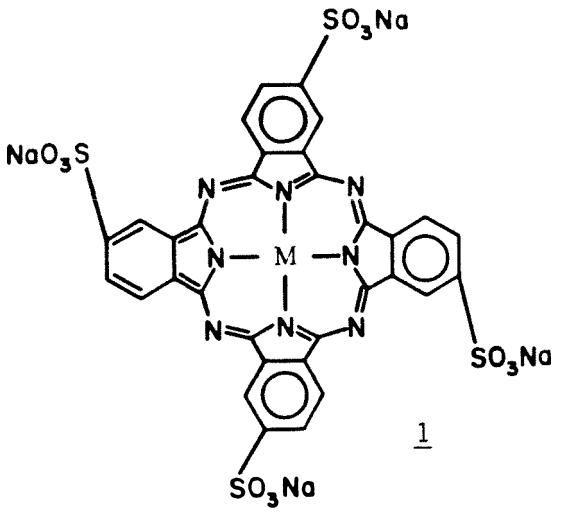

1

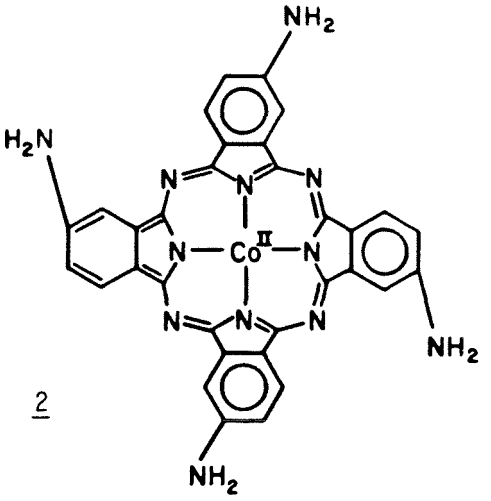

2

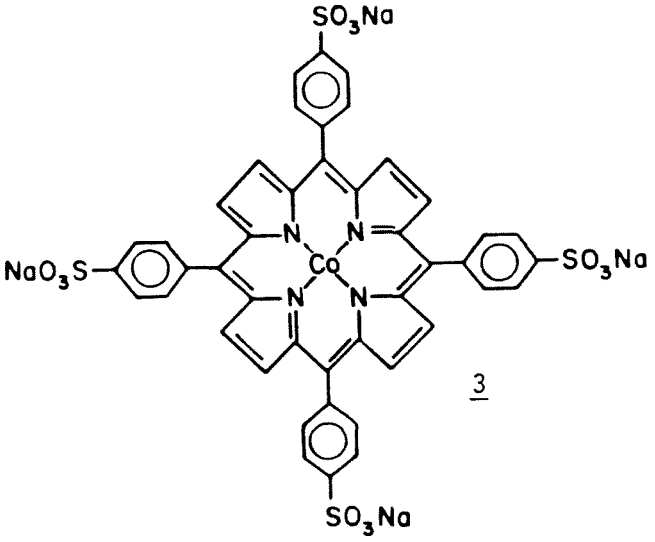

3

Figure 1. Structures of Metal Phthalocyanine and Porphyrin

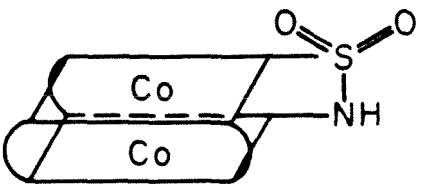

4

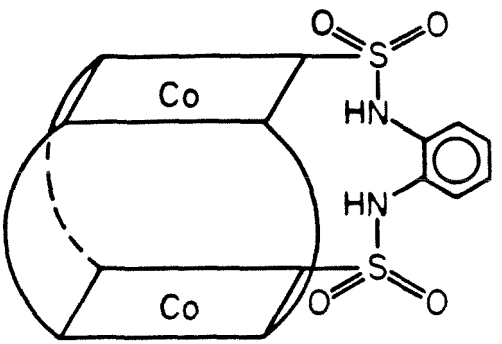

5

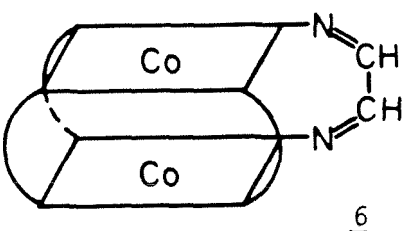

6

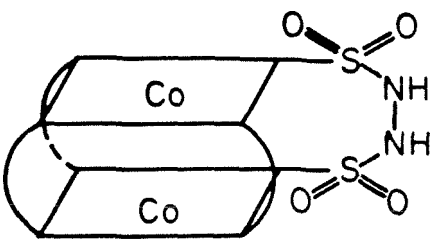

7

Figure 2. Structures of Variously Linked Dimers

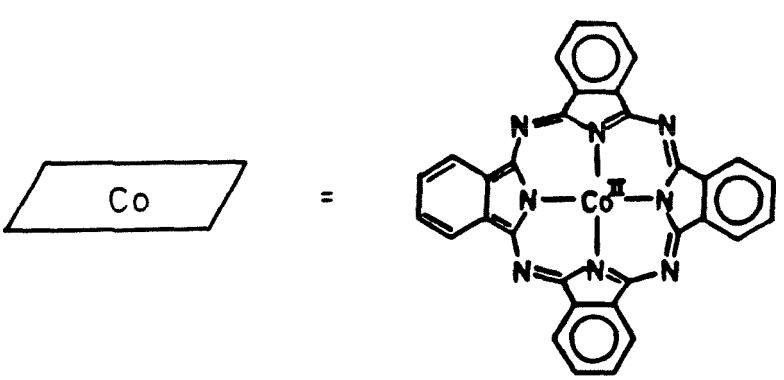

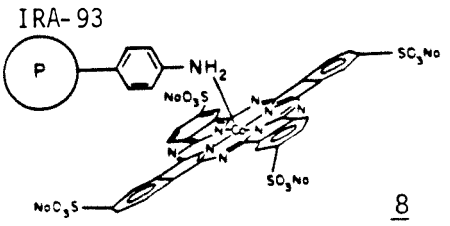

8

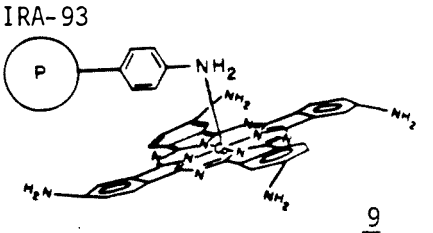

9

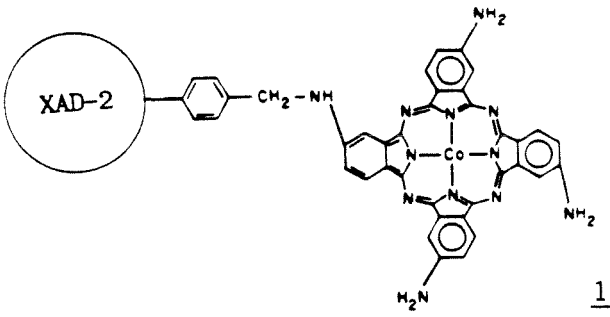

10

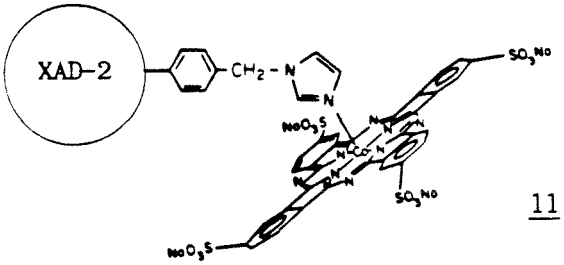

11

Figure 3. Various Polymer Supported Co(II) Phthalocyanines

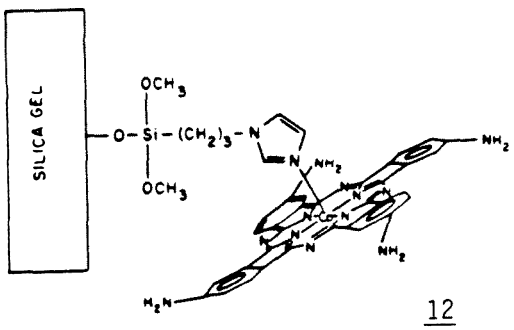

12

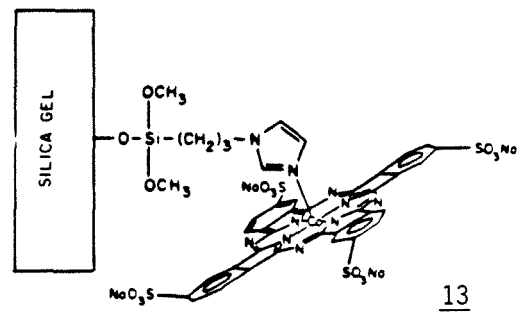

13

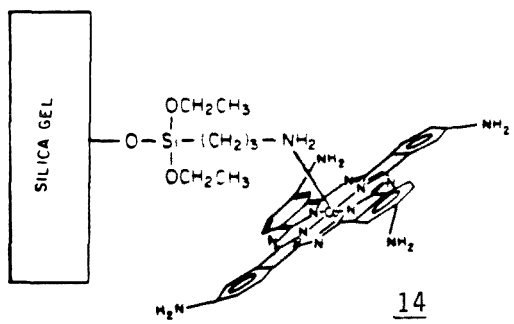

14

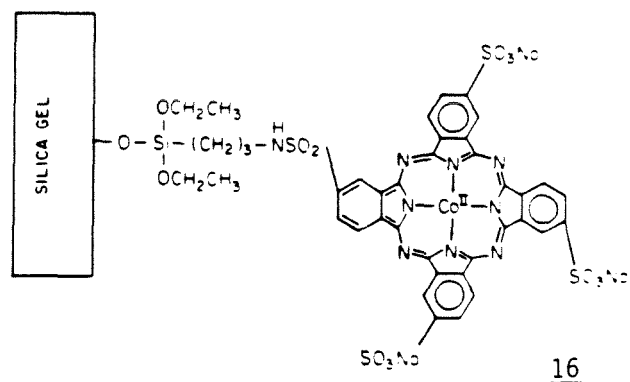

16

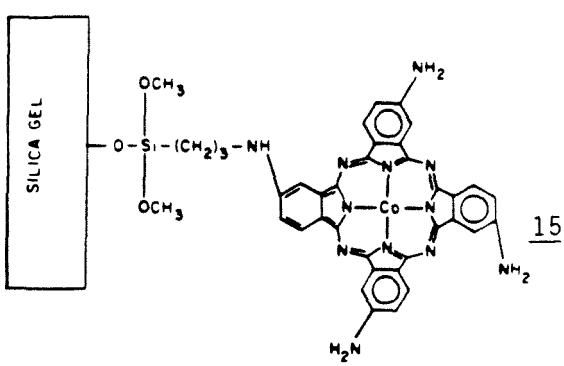

15

Figure 4. Various Silica Gel Supported Co(II) Phthalocyanines

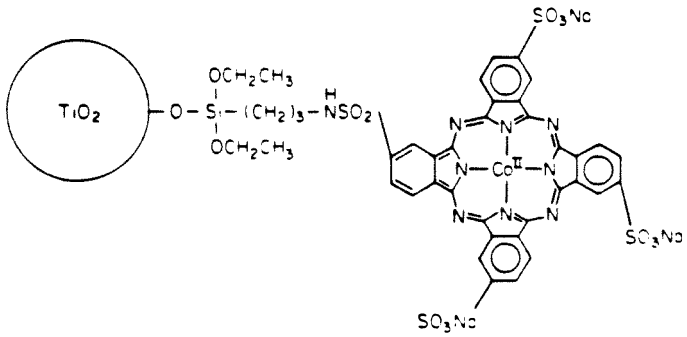

17

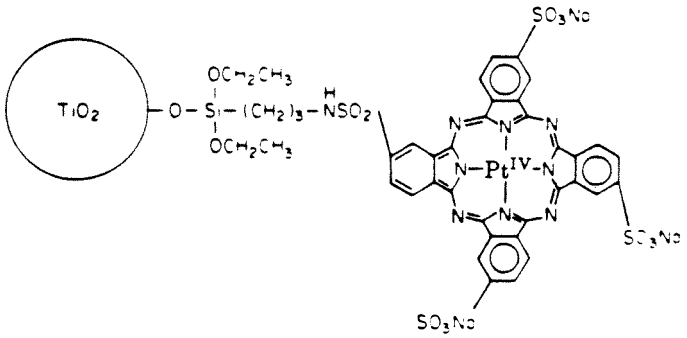

18

Figure 5. Titanium Dioxide Supported Co(II) and Pt(IV) Phthalocyanines